THE USE OF HF-ISOTOPES AND HIGH FIELD STRENGTH ELEMENTS TO CONSTRAIN MAGMATIC PROCESSES AND MAGMA SOURCES.

by

Vincentius Johannes Maria Salters

B.Sc., State University of Utrecht
(1979)
M.Sc. State University of Utrecht
(1982)

Submitted to the Department of
Earth Atmospheric, and Planetary Sciences
In Partial Fulfillment of the Requirements for the Degree of

Doctor of Philosophy

at the

Massachusetts Institute of Technology

August, 1989

Signature of Author: _____
Department of Earth Atmospheric and Planetary Sciences, MIT
August 11th 1989

Certified by: _____
Dr. Stanley R. Hart
Thesis Supervisor

Accepted by: _____
Dr. Thomas H. Jordan
Chairman, Departemental Comittee on Graduate Students.

THE USE OF HF-ISOTOPES AND HIGH FIELD STRENGTH ELEMENTS TO CONSTRAIN MAGMATIC PROCESSES AND MAGMA SOURCES.

by

Vincentius Johannes Maria Salters

Submitted to the Department of Earth Atmospheric, and Planetary Sciences on August 11th, 1989 in partial fulfillment of the requirements for the Degree of Doctor of Philosophy

ABSTRACT

The High Field Strength Elements (HFSE), Zr, Hf, Ti, Nb, and Ta in combination with Hf-isotopes are used to constrain the origin of calc-alkaline volcanism. Furthermore, Hf-isotopes are used to determine the magmatic processes and mantle sources of Mid-Ocean Ridge Basalts and Ocean Island Basalts.

CALC-ALKALINE AND ALKALINE VOLCANISM FROM THE CARPATHIANS, HUNGARY: ORIGIN AND SOURCES.

The calc-alkaline volcanism in the Carpathians predates the alkaline volcanism only by 5 Ma. Furthermore the alkali basalts contain lherzolite type xenoliths. The HFSE/REE (Rare Earth Element) ratios in the clinopyroxenes in the lherzolities are lower than the HFSE/REE of the host basalts excluding a simple cogenetic relation between the alkali basalts and the xenoliths. A simple three component mixing model can explain the trace element and isotopic variations in the calc-alkaline volcanics. One endmember is a crustal component, while the other two endmembers are located in the mantle. The xenoliths can be a mantle endmember for the calc-alkaline volcanics. The high $\Delta 7/4$ Pb of the third endmember indicates derivation from subducted sediments. Simple two component mixing can explain the range in isotopic compositons in the alkali basalts. One component in the alkali basalts is not represented in either the calc-alkaline volcanics or the xenoliths. The second component in the alkali basalts has high $\Delta 7/4$ Pb and is similar to the high $\Delta 7/4$ Pb endmember of the calc-alkaline volcanics.

TRACE ELEMENT ABUNDANCES IN LHERZOLITES; THE USE OF HFSE/REE RATIOS AS A CLUE TO MANTLE PROCESSES.

Clinopyroxenes and garnets in xenoliths from suboceanic, subcontinental and subarc xenoliths were analyzed for REE and Sr, Ti and Zr by ion microprobe. The vast majority of the mantle peridotites have trace element signatures similar to those island arc volcanics; they show HFSE depletions. These nodules, almost all anhydrous, 90%, cannot generate or be in equilibrium with mid-ocean ridge or ocean island basalt. The trace element variations in the clinopyroxenes in the peridotites are caused by a combination of some of the following processes: partial melting, melt extraction and metasomatism. The combined variations in HFSE and REE cannot be caused by a shallow level (<15GPa) mantle process and indicates fractionation of the HFSE and REE involving, most likely, perovskite as high pressure mantle phase.

THE USE OF HF-ISOTOPES TO CONSTRAIN MAGMATIC PROCESSES AND MANTLE SOURCES.

This chapter reports the results of a Hf-isotope study on island arc and oceanic basalts. Island arc basalts characteristically show depletions in HFSE compared to the REE. However, island arc basalts from oceanic regions, Aleutians, Fiji, New Britain, and Izu, have only sligthly more radiogenic $^{176}Hf/^{177}Hf$ than oceanic volcanics, indicating the HFSE depletion is at most 250 Ma. The combined Nd and Hf isotopes on the Fijian archipelago and surrounding basalts indicate the island arc basalt's mantle source is a depleted MORB-type mantle, and is not related to an OIB-type mantle.

Hf and Nd isotopes in OIB are in general well correlated indicating Sm/Nd and Lu/Hf ratios are fractionated by similar processes. Hf and Nd isotopes in MORB are not correlated and $^{176}Hf/^{177}Hf$ in MORB plot mostly below the OIB regression line for Nd-Hf isotope variations. The cause of low $^{176}Hf/^{177}Hf$ in MORB is undetermined.

Mid-Ocean Ridge Basalts have $^{176}Hf/^{177}Hf$ ratios indicating derivation from a mantle reservoir with a long term Lu/Hf ratio greater than Bulk Earth. However, the measured Lu/Hf in MORB is lower than Bulk Earth. We call this the Hf-parodox (Salters and Hart, 1989). The Lu-Hf and Sm-Nd systematics of MORBs require garnet to be a residual phase in MORB melt genesis. A sequential melting model, where melting starts in the garnet stability field(>80km, $\approx$1450°C), best explains the combined Nd and Hf isotope systematics, and is compatible with our present geophysical and geochemical knowledge of mid-ocean ridge magmatism.

Thesis supervisor: Dr. Stanley R. Hart
Professor of Geology and Geochemistry

Table of contents

List of Figures

List of Tables

Acknowledgements

In the first place I thank my advisor, Stan Hart. I consider it a privilege to be one of his students. Stan created an 11th floor haven that promotes initiative and encourages the testing of different ideas. I learned an awful lot from being allowed an insight in Stans' way of thinking and his approach to things both scientific and non-scientific. His continuous support during my residence at MIT was more then reassuring.

Nobu Shimizu is greatfully acknowledged for his willingness to be my advisor in disguise. The many hours of discussion contributed greatly to my development as a scientist. Nobu's curiousity for the unknown is contageous and his willingness to consider the unconventional is always stimulating.

Ken Burhuss is thanked for showing me what "Yankee ingenuity" is all about. Furthermore Ken is thanked for his patience and willingness to teach me "the nuts and bolts" of mass spectrometres.

George Tilton is thanked for allowing me to cook his machine for Hf-isotopes during every visit to Santa Barbara.

Mary Reid is thanked for giving me the initial excuse to visit the West Coast, and for her hospitality every time I was out there.

Samples in Chapter 2 and 3 were partly donated by: J. Gill, C. Stern, E. Jagoutz, J. Wadsworth, J. Sinton, K. Johnson, M. Barton, W. Bryan, S. Richardson, D. Weis, and J. Rubenstone for which they are thanked.

The crew of the JOIDES Resolution is thanked for keeping their good spirits during 70 days at high seas.

I thank my thesis committee for their willingness to read a thesis written by a foreigner. I learned more about English by writing this thesis, for which I thank them.

Fellow graduate students at MIT are thanked for their contributions to the MIT experience.

Brain Taras, Peter Tilke, Allen and Reneaux Kennedy, Tom Juster, Sarah Kruse, Dan Tormey, J Blusztjan, the wine tasters, the bridgeplayers are all thanked for the diversions that helped to keep my perspective and a door open to 'real' life.

My parents were always supportive of my quest to get a higher education and their unwavering encouragement is much appreciated.

Finally, I wish to thank Nancy Sampson for her love and support before and during the trying months of writing a thesis.

Introductory Note

This thesis consists out of three semi autonomous chapters. There is however a common theme to all chapters which starts with High Field Strength Elements. As such this thesis is a report of an investigation of the variations of High Field Strength Elements (HFSE), especially Hf, Zr and Ti, and the Hf isotopic composition in mantle derived melts. This study was instigated by my interest in calc-alkaline volcanics, and the possible mantle source for calc-alkaline volcanics.

Chapter 1, "Calc-alkaline and alkaline volcanism from the Carpathians, Hungary, origin and sources." is a case study of a province with calc-alkaline volcanics. The Carpathians are one of the few places where calc-alkaline and alkaline volcanism have a close spatial and temporal relationship. This relationship in addition with the composition of mantle xenoliths within the alkaline volcanics places strong constraints on the source of the Carpathian calc-alkaline volcanics. Chapter 1 is published, with S.R. Hart and G. Panto as co-authors, in a paper in the AAPG Memoir on the Carpathians.

Calc-alkaline volcanics are depleted in HFSE compared to the REE. The HFSE depletions in calc-alkaline volcanisc have long been a problem, and no conclusive origin for the HFSE depletions in calc-alkaline volcanics has been proposed. ^{176}Hf, one of the HFSE, is produced by the radiactice decay of ^{176}Lu, a REE, with $^{176}Hf/^{177}Hf$ ratio reflecting the time intergrated Lu/Hf ratio. Existence of the HFSE depletion in the source of calc-alkaline volcanics for significant geological time will lead to high $^{176}Hf/^{177}Hf$. With the analyses of the xenoliths from the Carpathians I found that HFSE depletions exist in mantle materials, and Chapter 2 ("Trace element abundances in lherzolites; the use of HFSE/REE ratios as a clue to mantle processes") describes these depletions in mantle rocks. A bit earlier, N. Shimizu found these HFSE depletions in lherzolite xenoliths from Salt Lake Crater, Hawaii. These two discoveries were the inspiration for a general quest to determine the HFSE-REE variations in mantle rocks, and led to the discovery of the ubiquitous occurrence of HFSE depleted mantle, and basically answered the question of the origin of

HFSE in calc-alkaline volcanics. This discovery was published as a letter in Geochim. Cosmochim. Acta, with N. Shimizu as co-author. Since that discovery I have analyzed many more nodules, and have found many more places where the mantle is depleted in HFSE. Furthermore, K. Johnson confirmed the occurrrence of HFSE depleted material in abyssal peridotites (Salters and Shimizu reported only 2 abyssal peridotites) confirming the HFSE-depleted mantle occurs in all different types of tectonic settings! Chapter 2 reports on the results of all the localities analyzed and also offers a model to explain the HFSE-depleted mantle material. The HFSE/REE ratios suggest that abyssal peridotite have seen the addition of an HFSE-depleted material after MORB were extracted, and that most xenoliths have a complex history with several enrichment and depletion events. Chapter 2 explains this process and suggets an origin for this HFSE depleted agent.

Chapter 3, "The use of Hf-isotopes to constrain magmatic processes and mantle sources", is concerned with the long term behavior of one of the HFSE, Hf, by investigating the $^{176}Hf/^{177}Hf$ in volcanic rocks. This investigation was started to determine the timescale of HFSE depletions in calc-alkaline source rock. However, the analyses of the $^{176}Hf/^{177}Hf$-ratio is not sufficiently precise to really put a timescale on the depletion. Because the HFSE depletion is measured relative to the REE, the $^{176}Hf/^{177}Hf$ ratio is compared to $^{143}Nd/^{144}Nd$ ratio. Thus, in Chapter 3 I also discuss the relationship between Hf and Nd isotopes for different type of volcanics and put Hf-isotopes in the framework of mantle components as described in the HAZI-papers. (Hart and Zindler, (1988), and Zindler and Hart, (1986)). This work brought as an off-spin the discovery of the Hf-paradox. This discovery and the explanation of the Hf-paradox led to strong constraints on the genesis of MORB. The Hf-paradox requires garnet as a residual phase in the MORB-source and places the onsett of melting in this source under the ridge at ≈30kbars and ≈1450°C. A paper on the Hf-paradox and its explanation is submitted, with S.R. Hart as co-author, to Nature.

Chapter 1:

Calc-alkaline and alkaline volcanism from the Carpathians, Hungary: origin and sources.

1.1 Introduction

Two different types of magmatism, alkaline and calc-alkaline, were active during the formation of the Carpathian orogenic arc. The calc-alkaline volcanism predates the alkaline volcanism and is related to subduction. The subduction was caused by the extension of the Pannonian fragment causing it to override the European plate (Royden, 1988; Stegena et al., 1975). The alkaline volcanism occurred in Pliocene to Quaternary times after cessation of extension. Earlier studies of the Carpathian magmatism indicate heterogeneity in the source of the calc-alkaline basalts (Panto, 1981; Vogl and Panto, 1983) and suggest that the calc-alkaline magmas contain a component from the subducted slab. In general the origin of the chemical characteristics of calc-alkaline volcanism is debated. The most outstanding chemical features of calc-alkaline volcanics are:

- low concentrations of High Field Strength Element (HFSE), Nb, Ta, Hf, Zr, Ti, compared to the REE (Pearce and Cann, 1973; Pearce and Norry, 1979).
- High concentrations of "mobile" elements such as Cs, Li, Be, B, Ba compared to other elements with similar incompatibility in the spinel-peridotite melt.system (Leeman, 1987; Morris and Hart, 1983)
- High concentration of Sr compared to Nd and Ce.

Different researchers have proposed essentially three different models to explain these characteristics. Stern (1982) and Morris and Hart (1983) argue that most island arc lavas are derived from an oceanic-island type source without a significant addition from the subducted slab. In a model proposed by Gill (1981), Nicholls and Ringwood (1973), and Tera et al.(1986); a slab component is an important feature in most calc-alkaline magmas. Salters and Shimizu (1988) explain the HFSE depletions in calc-alkaline volcanism as a reflection of the mantle source composition; the depletions are unrelated to the slab. Other types of magmatism do not sample this HFSE depleted mantle.

The close relationship between the alkaline and calc-alkaline volcanism in the Carpathians and the occurrence of lherzolite

xenoliths in the alkali basalts places additional constraints on the source regions in addition to those provided by geochemical techniques. Samples were selected with the aim of covering as much of the observed chemical and geographical variations as possible.

1.2 Analytical techniques.

Ba, Sr, K, Rb and Cs were separated by standard ion exchange column chromatography and concentrations were determined by isotope dilution using techniques described by Hart and Brooks (1977). Nd- isotope ratios and Sm-Nd concentrations were determined following the technique of Zindler (1980) as adapted from Richard et al. (1976). Pb-isotopic compositions were determined using the technique described by Pegram (1987) as adapted from Manhes et al (1978). U, Th and Pb concentrations were determined using techniques described by Reid (1987) Precision and normalization of the Sr, Nd and Pb isotopic data are given in Table 1. Precision for the trace element data determined by isotope dilution is better that 0.1 %, except for Ba, Rb and Cs (0.5 %). Blank levels were insignificant for the data on the volcanics reported here. Rb, Ba and K blanks can be up to 50% of the clinopyroxene separates. Sr, and Nd blanks in the clinopyroxenes are again insignificant. Zr, Nb and were determined by XRF using standard techniques. Selected volcanics were analyzed for some trace elements and REE using INAA techniques described by Ila and Frey (1986). Cr-diopsides from the lherzolite nodules in the alkali basalts were analyzed for REE and selected trace elements by ion microprobe using techniques described by Shimizu and Hart (1982).

1.3 Tectonic setting.

The Carpathians are an arcuate-shaped mountain belt forming the Eastern extension of the Alps (Fig. 1.1). The mountain belt was a zone of convergence in close spatial relationship with the Pannonian basin a back-arc-type extensional basin. Other Mediterranean

Figure 1.1:
Simplified geological map after Royden et al. (1983) showing the main geological units in the Carpathians. Horizontal striped area is molasse foredeep, Outer Carpathians. Dotted area is the Flyschnappes and the Pieniny Klippen Belt. Diagonally striped areas are Inner Carpathians. Hatched areas are the Miocene calc-alkaline volcanics.

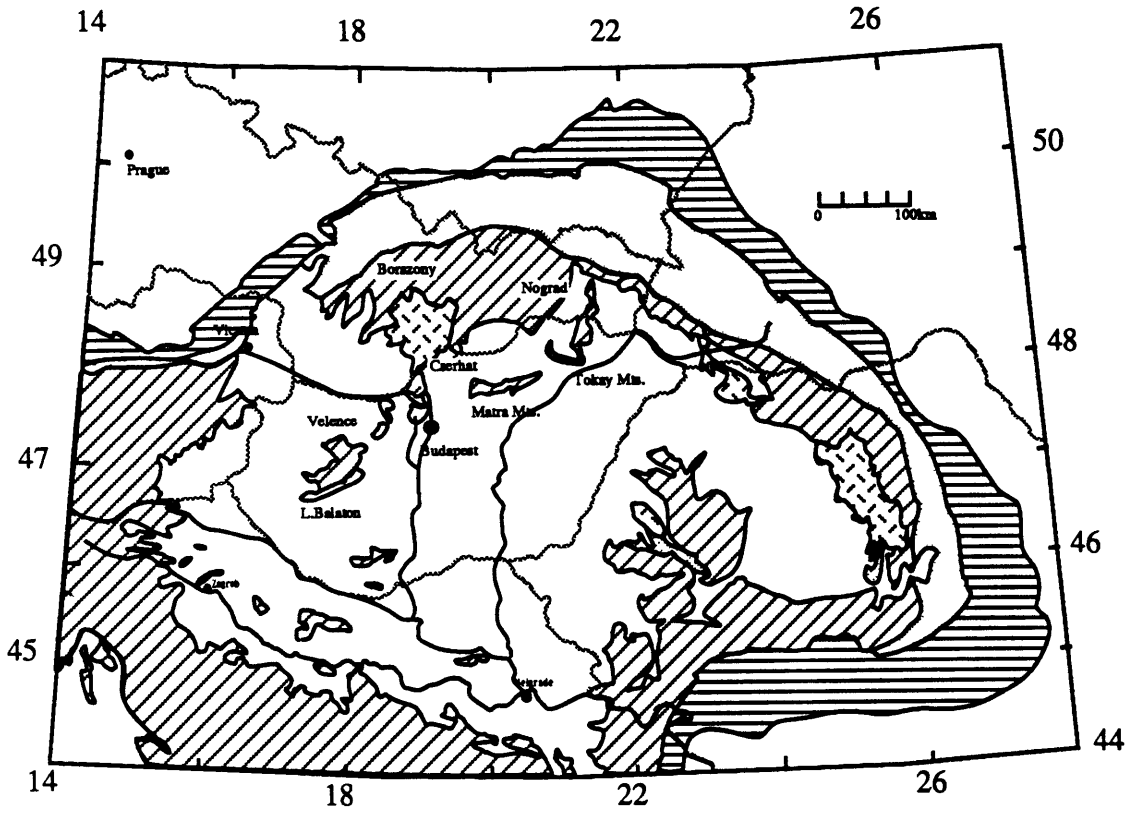
14
18
22
26
50
49
48
47
46
45
44
Prague
0
100km
Borszony
Nograd
Cserhat
Tokay Mts.
Matra Mts.
Velence
Budapest
L.Balaton

examples of this type of paired system are the Appenine-Tyrrhenian system and the Alboran-Betic Cordirella- North Africa system.

Tectonic activity in the Carpathians began in Early Cretaceous times, with outwardly thrusting and folding of the northern side of the Pannonian micro-plate. Probable southward subduction of the European platform under the northern margin of the Pannonian fragment during Paleocene and Eocene times is evidenced by a poorly developed Eocene calc-alkaline arc in the Eastern Alps and on the inner side of the West Carpathians (Burchfiel and Royden, 1982). There is no evidence for Cretaceous or Early Tertiary subduction under the eastern part of the Pannonian micro-plate. Subduction resumed during Miocene time and was, since Middle Miocene, contemporaneous with extension of the Pannonian basin; extension began about 16.5 Ma. ago (Royden, 1988). The occurrence in the accretionary prism of sediments from below the carbonate compensation depth indicates that the subducted plate was probably partly oceanic (Burchfiel, 1980; Royden, 1988). Calc-alkaline volcanism developed first in the western part of the Carpathians (Borzsony, Matra, and Cserhat mountains), then migrated eastward and southward to the Tokay mountains and the East Carpathians. This eastward migration of the calc-alkaline volcanism was accompanied by eastward migration of the thrusting in the Outer Carpathian belt. Calc-alkaline volcanism stopped 10.5 Ma ago (Poka, 1984; Royden et al., 1983).

Extension of the crust leading to the formation of the Pannonian Basin also began in in the western part of the basin during Middle to Late Miocene times. Migration of the extension seems to be in conjunction in space and time with the migration of the calc-alkaline magmatism and the thrusting in the Outer Carpathians. Active extension and faulting ended in Late Miocene times (Royden et al., 1983). Extensional tectonics was accompanied and followed by alkali basaltic magmatism. This different type of volcanic activity began in Late Miocene (10.5 Ma ago) and continued into the Quaternary, after extension had ceased (Poka, 1984; Panto, 1981). The alkali basalts can contain lherzolite xenoliths, indicating a uncontaminated, mantle origin for at least some of the basalts. The close spatial and temporal

association of the alkali basalts and the calc-alkaline volcanics allows additional constraints to be placed on the relationship between these two types of volcanism.

1.4 Results

Samples for isotopic analyses are selected from a large collection covering all three periods of magmatic activity. Selection of the samples was based on freshness and attempt to cover a large range in chemical composition, geographic position and age. In addition to the volcanics, four Cr-diopside and one amphibole separate from lherzolite nodules are analyzed for isotopic compositions. Isotopic compositions and selected trace element analyses are given in Table 1.1. A small group of volcanics are analyzed for REE and selected trace elements by INAA. Furthermore Cr-diopsides are analyzed for REE and selected trace elements by ion microprobe; the results of INAA and ion microprobe analyses are presented in Table 1.2.

The $^{87}Sr/^{86}Sr$ ratio of the alkali basalts varies from 0.703165 to 0.704204, while the $^{143}Nd/^{144}Nd$ ranges from 0.513003 to 0512700. On a Nd-Sr isotope correlation diagram all the alkali basalts fall within the field defined by oceanic volcanics (Fig. 1.2). The alkali basalts are strongly LREE enriched and show trace element patterns (Fig. 1.3) typical for oceanic alkali basalts (Clague and Frey, 1982; White et al., 1979)

Pb isotope ratios for the alkali basalts range from 18.712- 19.426 for $^{206}Pb/^{204}Pb$; 15.555- 15.721 for $^{207}Pb/^{204}Pb$; and 38.759- 39.168 for $^{208}Pb/^{204}Pb$ (Fig. 1.4). These ratios are on the high $^{207}Pb/^{204}Pb$ and $^{208}Pb/^{204}Pb$ side of the array defined by MORB.

The calc-alkaline volcanics range in composition from basaltic andesite to rhyolite. The most mafic calc-alkaline samples are medium to high-K andesites, using the definition of Gill (1981). The initial $^{87}Sr/^{86}Sr$ range from 0.70426 to 0.71125 while the $^{143}Nd/^{144}Nd$ varies from 0.512741- 0.512208. The calc-alkaline and alkaline volcanics together define a narrow array on a Nd-Sr isotope correlation diagram whereby the calc-alkaline volcanics form the low $^{143}Nd/^{144}Nd$ - high $^{87}Sr/^{86}Sr$ end of the array (Fig. 1.2). Although

Table 1.1

Trace element and isotope data for the Carpathian volcanics and xenoliths. Precision of the Sr and Nd isotopic ratios is better than 0.005% (2σ); $^{87}Sr/^{86}Sr$ values are relative to 0.70800 for E&A standard, and $^{143}Nd/^{144}Nd$ are relative to 0.51262 for BCR-1; $^{143}Nd/^{144}Nd$ is normalized to $^{146}Nd/^{144}Nd=0.71290$. Pb isotopes have been normalized to the NBS 981 standard; the precision is better than 0.05% per amu. The trace element ratios were all determined by isotope dilution (see text). Sr-isotope initial ratios were calculated assuming ages of 40 m.y.(#68, #77), 18 Ma.(Borzsony), 16 m.y.(Matra, Cserhat) and 15 Ma. (Tokaj). Age corrections are insignificant for Nd-isotopes. Except for Zr and Nb all trace element are determined by isotope dilution. For rock types, AB= alkali basalts; A= andesite; D=dacite and R= rhyolite.

Table 1.1
Trace element concentrations (in ppm) and isotopic compositions for the Carpathian volcanics and associated mantle xenolith minerals

Sample	Szt-1002	Bo-1022	147 nod	148 nod	Amph	147	148	118	99	103	116	134	55	57	107
Locality	Nograd	Nograd	Nograd	Nograd	Balaton	Nograd	Nograd	Nograd	Nograd	Balaton	Balaton	Sarospatak	Borzsony	Borzsony	Borzsony
Rocktype	Diopside	Diopside	Diopside	Diopside	Kaersutite	AB	AB	AB	AB	AB	AB	AB	A	A	A
87/86 Sr	0.703094	0.703482	0.705122	0.702791	0.703086	0.703256	0.703165	0.703199	0.704030	0.704204	0.703310	0.705950	0.707958	0.708103	0.708140
87/86 Sr i	-	-	-	-	-	-	-	-	-	-	-	-	0.70786	0.70798	0.70799
143/144 Nd	0.513638	0.512373	0.512901	0.513209	0.512835	0.513003	0.512941	0.512915	0.512762	0.512700	0.512889	0.512546	0.512384	0.512400	0.512469
206/204 Pb	-	-	-	-	18.78	19.183	19.161	19.426	18.875	18.712	19.158	19.018	18.855	18.901	18.918
207/204 Pb	-	-	-	-	15.60	15.555	15.573	15.643	15.613	15.648	15.647	15.721	15.668	15.658	15.689
208/204 Pb	-	-	-	-	38.53	38.759	38.803	39.168	38.788	38.842	39.055	39.279	38.942	38.947	39.038
K	28.64	40.7	153.5	648	16415	14827	21080	19961	18809	16319	16491	29093	19476	19324	15001
Rb	0.0076	0.001	0.275	2.56	10.62	64.88	85.2	67.9	64.1	50.5	58.2	133.5	87.2	88.9	71.9
Cs	0.0012	0.0019	0.106	0.025	0.0235	0.911	1.118	0.74	1.25	1.1	1	1.04	4.89	4.07	4.06
Sr	25.53	63.8	32.45	39.61	498.4	786.2	964.2	841.2	937.4	621.4	622.9	375.4	630.2	527.3	344.1
Ba	0.516	0.681	1.388	1.51	432	827	941.2	788	836	531	562	547	1292	1031	308
Nd	1.493	4.06	2.42	2.6	15.6	37.57	41.32	42.48	44.64	29.73	32.27	18.83	26.3	22.91	17.55
Sm	0.832	1.23	0.402	0.798	4.47	6.94	7.36	7.81	8.2	6.11	6.47	3.97	4.96	4.6	3.98
U	-	-	-	-	-	1.99	2.31	2.08	2.13	1.4	1.61	-	-	3.64	1.99
Pb	0.084	0.132	-	-	0.5	3.05	4.23	3.78	6.23	5.38	4.2	-	9	25.56	12.47
Nb	-	-	-	-	-	75.2	79.6	81.5	68.8	39	60.7	13.2	4.1	5.4	6
Zr	7	5.2	27.8	27.4	-	241	255	290	351	217	260	125	127	141	139
K/Cs	23867	21421	1448	25920	698511	16276	18855	26974	15047	14835	16491	27974	3983	4748	3695
K/Rb	3768	40700	558	253	1546	229	247	294	293	323	283	218	223	217	209
Rb/Sr	0.000	0.000	0.008	0.065	0.021	0.083	0.088	0.081	0.068	0.081	0.093	0.356	0.138	0.169	0.209
Sm/Nd	0.557	0.303	0.166	0.307	0.287	0.185	0.178	0.184	0.184	0.206	0.200	0.211	0.189	0.201	0.227
Sr/Nd	17.10	15.71	13.41	15.23	31.95	20.93	23.33	19.80	21.00	20.90	19.30	19.94	23.96	23.02	19.61
Zr/Zr*	0.43	0.16	1.88	1.34	0.00	1.01	0.98	1.08	1.24	1.10	1.23	0.99	0.75	0.94	1.15

Sample	113	77	68	61	92	87	91	128	132	126
Locality	Borzsony	Velence	Matra	Matra	Matra	Cserhat	Cserhat	Tokaj	Tokaj	Tokaj
Rocktype	A	A	A	A	A	A	A	D	D	R
87/86 Sr	0.708915	0.707505	0.704464	0.709175	0.707936	0.706488	0.708016	0.709667	0.707364	0.713521
87/86 Sr i	0.70865	0.70680	0.70426	0.70894	0.70778	0.70619	0.70789	0.70935	0.70703	0.71125
143/144 Nd	0.512338	0.512527	0.512741	0.512308	0.512380	0.512516	0.512417	0.512264	0.512420	0.512208
206/204 Pb	19.414	18.897	18.938	18.694	18.799	18.782	18.910	18.729	18.838	18.786
207/204 Pb	15.631	15.675	15.657	15.659	15.673	15.658	15.675	15.663	15.692	15.721
208/204 Pb	39.123	39.154	38.964	38.861	38.931	38.856	39.114	38.997	39.092	39.279
K	25278	20253	11712	18461	13005	17778	12626	19463	27226	35203
Rb	116.4	77.4	69.8	91.6	63.9	102.7	49.7	98.5	122.9	161.8
Cs	6.11	1.55	9.9	9.56	5.47	8.4	2.91	4.3	4.1	5.22
Sr	326.5	317.8	562	253.4	271.4	225.7	267.1	189.2	225.3	43.9
Ba	776	533	548	377	230	247	256	374	608	781
Nd	18.58	26.76	25.01	25.5	15.83	17.82	26.76	22.54	28.53	30.36
Sm	2.93	5.35	4.58	5.6	3.73	4.33	4.41	-	5.62	6.76
U	46	2.11	2.75	1.86	1.49	2.5	-	2.08	3.45	3.05
Pb	38.18	10.11	10.21	14.77	10.39	14.83	-	16.67	19.57	25.58
Nb	5.9	13.6	14.1	8.6	6.2	8.2	7.4	7.5	16.2	9.8
Zr	83	186	91	148	154	183	158	162	229	85
K/Cs	4137	13066	1183	1931	2378	2116	4339	4526	6640	6744
K/Rb	217	262	168	202	204	173	254	198	222	218
Rb/Sr	0.357	0.244	0.124	0.361	0.235	0.455	0.186	0.521	0.545	3.686
Sm/Nd	0.158	0.200	0.183	0.220	0.236	0.243	0.165		0.197	0.223
Sr/Nd	17.57	11.88	22.47	9.94	17.14	12.67	9.98	8.39	7.90	1.45
Zr/Zr*	0.74	1.06	0.57	0.86	1.39	1.45	0.97	-	1.23	0.41

Table 1.2.

Trace element data of selected samples from the Carpathians. Cs, Rb, Th, Sr, Ba, Pb are isotope dilution data. For the volcanics Zr, Nb, and Ti are XRF data and rest is INAA. For the xenoliths elements were determined by ion micro probe except for those mentioned under isotope dilution. Norm is column with normalizing values used. Data essentially from Anders and Grevesse (1989).

Table 1.2:
Trace element concentrations (in ppm) for Carpathian igneous rocks

		Xenoliths					Alkali basalts					Calc-alkaline	
Sample #	Norm.	Szt 1002	Bo-1002	147 nod	148 nod	Amph	147	148	116	103	99	68	57
Cs	0.0045	0.00	0.00	0.11	0.03	0.02	0.91	1.12	1.00	1.10	1.25	9.90	4.07
Rb	0.22	0.01	0.00	0.28	2.56	10.62	64.9	85.2	58.2	50.5	64.1	69.8	88.9
Pb	0.06	0.08	0.13	-	-	0.50	3.05	4.23	4.20	5.38	6.23	10.21	25.56
Ba	2.34	0.52	0.68	1.39	1.51	432	827	941	562	531	836	548	1031
Th	0.0294	-	-	-	-	-	6.60	7.87	5.38	4.77	7.21	6.80	12.60
U	0.0081	-	-	-	-	-	6.94	7.36	6.47	1.40	2.13	2.75	3.64
K	100	28.6	40.7	153.5	648	16514	14827	21080	16491	16319	18809	11712	19324
Ta	0.0142	-	-	-	-	-	5.01	5.70	3.70	2.51	4.26	0.70	0.54
Nb	0.246	-	-	-	-	-	75.2	79.6	60.7	39.0	68.8	14.1	5.4
La	0.235	-	-	-	-	4.94	50.0	57.8	36.4	32.8	52.5	31.1	30.1
Ce	0.603	1.17	3.20	2.16	7.88	16.85	92.3	106.9	72.7	66.0	103.4	60.3	58.7
Sr	7.4	25.5	63.8	32.5	39.6	498.0	786.2	964.2	622.9	621.4	937.4	562.0	527.3
Nd	0.452	1.23	3.11	1.92	5.03	15.6	34.8	39.8	32.0	28.2	42.5	24.9	23.5
Hf	0.1024						4.57	4.97	4.73	4.31	6.02	2.37	3.82
Zr	3.94	7.0	5.2	27.8	27.4	50.0	241	255	260	217	351	91	141
Sm	0.147	0.60	0.89	0.94	1.53	4.47	6.82	7.32	6.47	6.11	8.20	4.82	4.60
Eu	0.056	0.26	0.36	0.44	0.62	1.62	2.20	2.33	2.10	1.95	2.50	1.37	1.38
Ti	436	1570	113	2006	2529	26300	11205	11859	13472	10987	13865	4029	5406
Tb	0.0363	-	-	-	-	-	0.89	0.91	0.80	0.79	0.93	0.54	0.73
Dy	0.245	1.59	1.62	2.13	2.35	2.78	-	-	-	-	-	-	-
Er	0.1603	1.10	0.16	1.42	1.65	1.25	-	-	-	-	-	-	-
Yb	0.162	1.16	0.10	1.18	1.34	0.44	2.18	2.37	2.01	1.72	2.12	1.98	2.70
Lu	0.0243	-	-	-	-	-	0.31	0.35	2.97	0.27	0.32	0.32	0.46

Cs, Rb, Th, U, K, Ba, Pb and Sr are isotope dilution data. For the volcanics Zr, Nb and Ti are XRF data and rest is INAA. For the xenoliths trace elements were determined by ion microprobe, except for those mentioned under istope dilution.
Norm is normalization values from Anders and Grevesse, (1989), with added in house values for the volatile elements.

Figure 1.2:
$^{143}Nd/^{144}Nd$ versus $^{87}Sr/^{86}Sr$ for the Carpathian volcanics and xenoliths, also indicated is the field for oceanic volcanics, taken from Zindler and Hart (1986). Also indicated are fields for the Banda Arc Morris (1984); Whitford and Jezek (1979), Lesser Antilles (Davidson, 1983; Davidson, 1986), and Italy (Hawkesworth and Vollmer 1979).

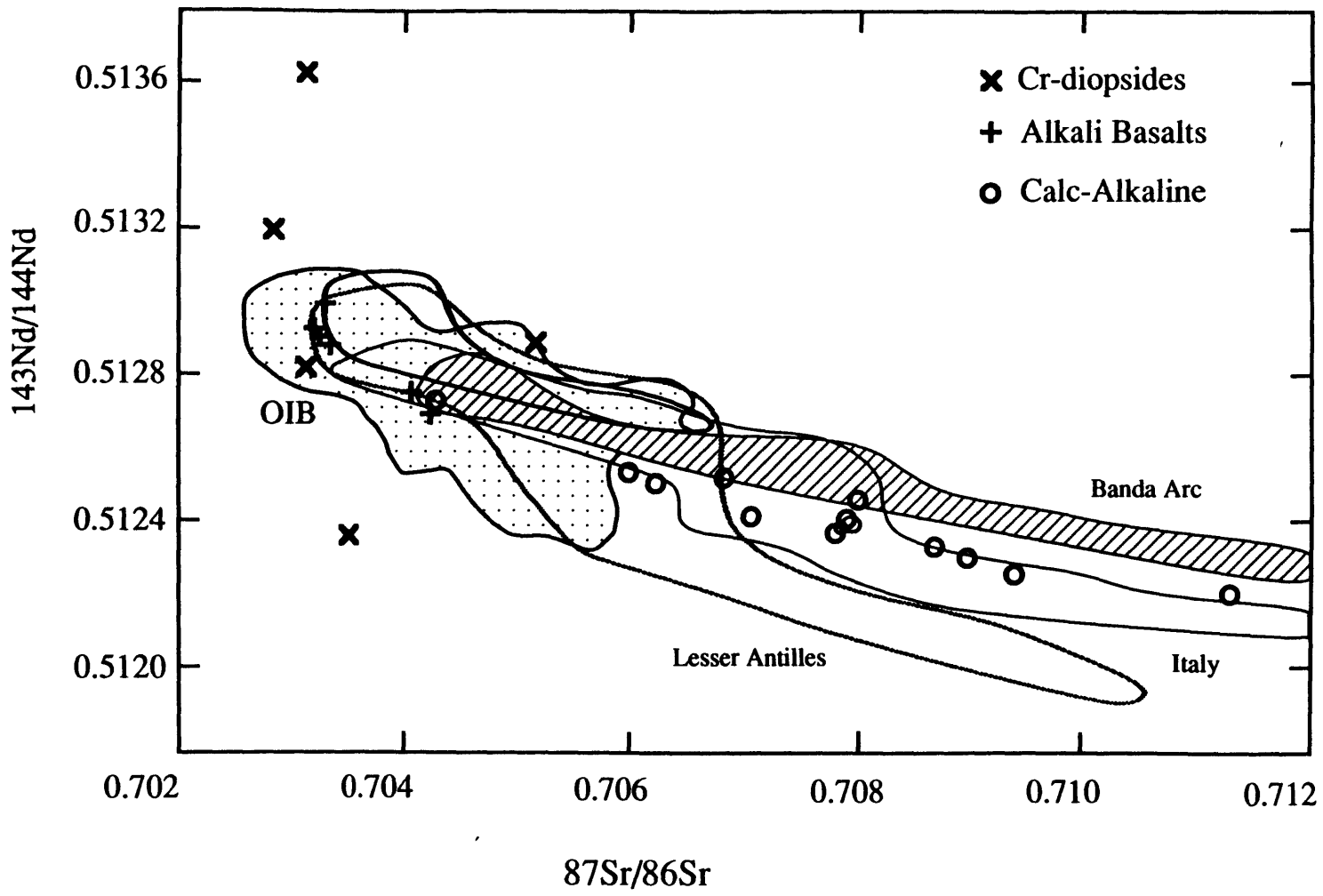
Cr-diopsides
Alkali Basalts
Calc-Alkaline
OIB
Banda Arc
Lesser Antilles
Italy
0.5136
0.5132
0.5128
0.5124
0.5120
143Nd/144Nd
0.702
0.704
0.706
0.708
0.710
0.712
87Sr/86Sr

Figure 1.3:

A. Spidergrams for lherzolites. Normalizations are from Anders and Grevesse (1989), with small adaption for Sr and Hf as to achieve consistency between the different isotopic systems. Normalization values are tabulated in Table 1.2.

B. Spidergrams for alkali basalts

C. Spidergrams for calc-alkaline volcanics

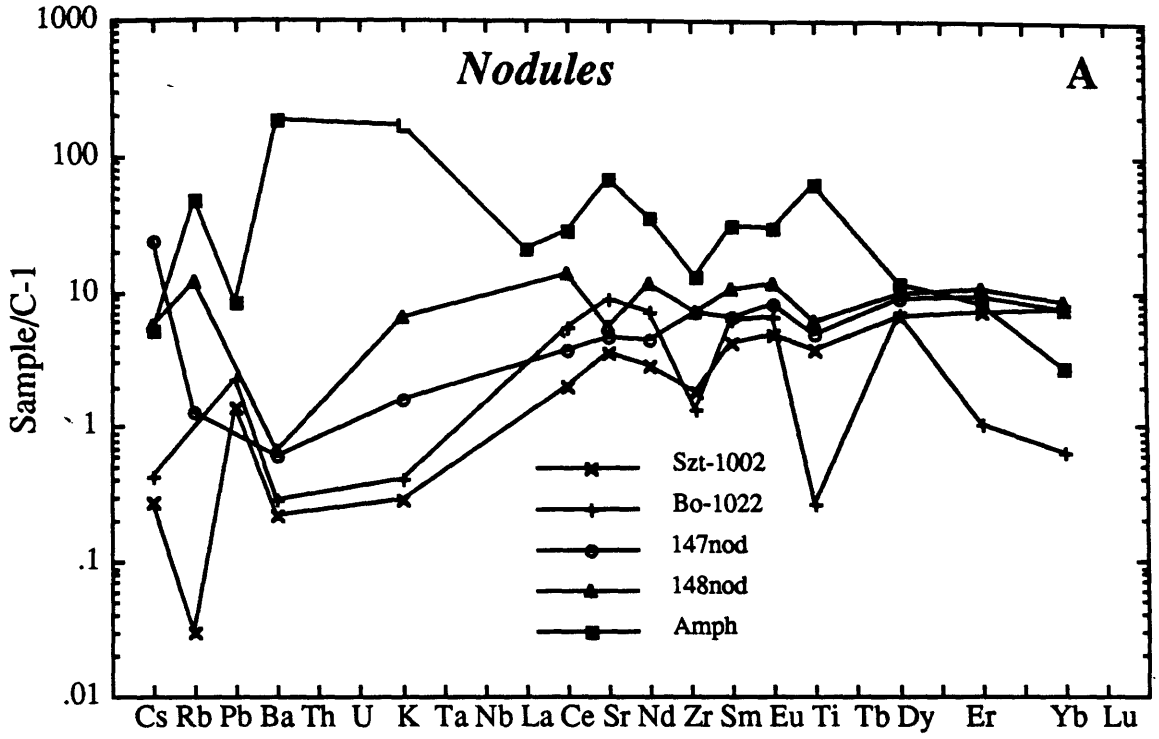
Nodules
A
1000
100
10
1
.1
.01
Sample/C-1
Szt-1002
Bo-1022
147nod
148nod
Amph
Cs Rb Pb Ba Th U K Ta Nb La Ce Sr Nd Zr Sm Eu Ti Tb Dy Er Yb Lu

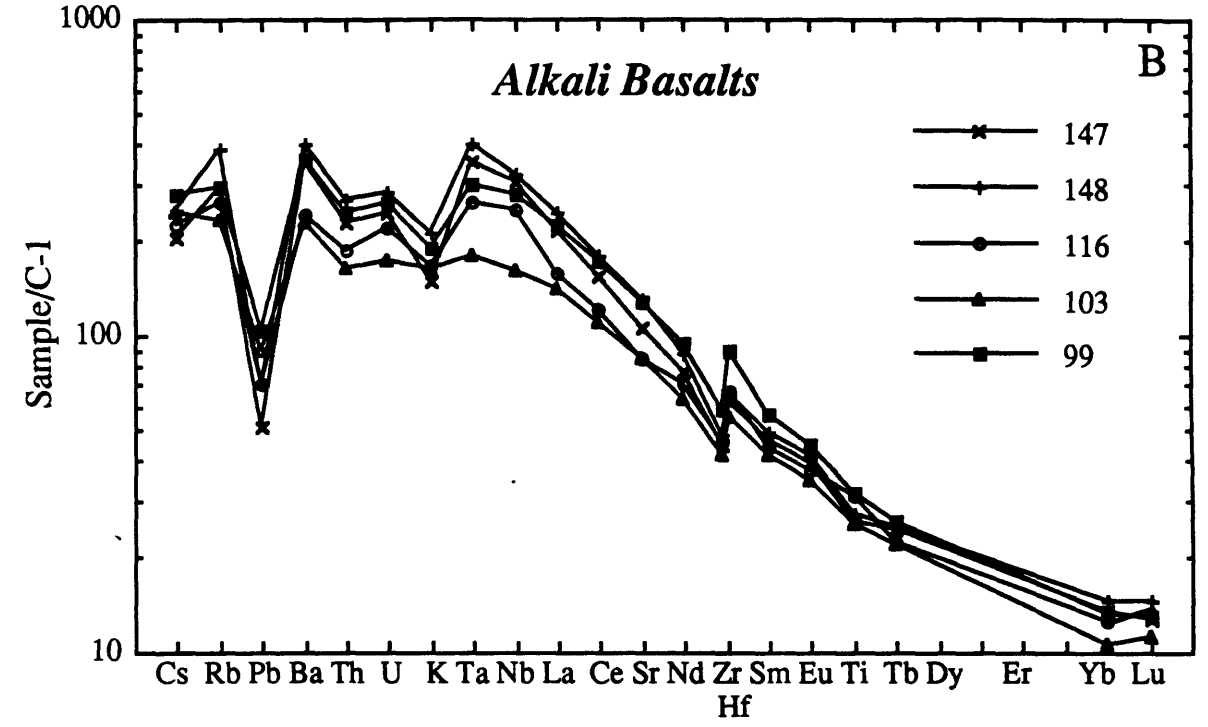
Alkali Basalts
B
147
148
116
103
99
Sample/C-1
1000
100
10
Cs Rb Pb Ba Th U K Ta Nb La Ce Sr Nd Zr Sm Eu Ti Tb Dy Er Yb Lu
Hf

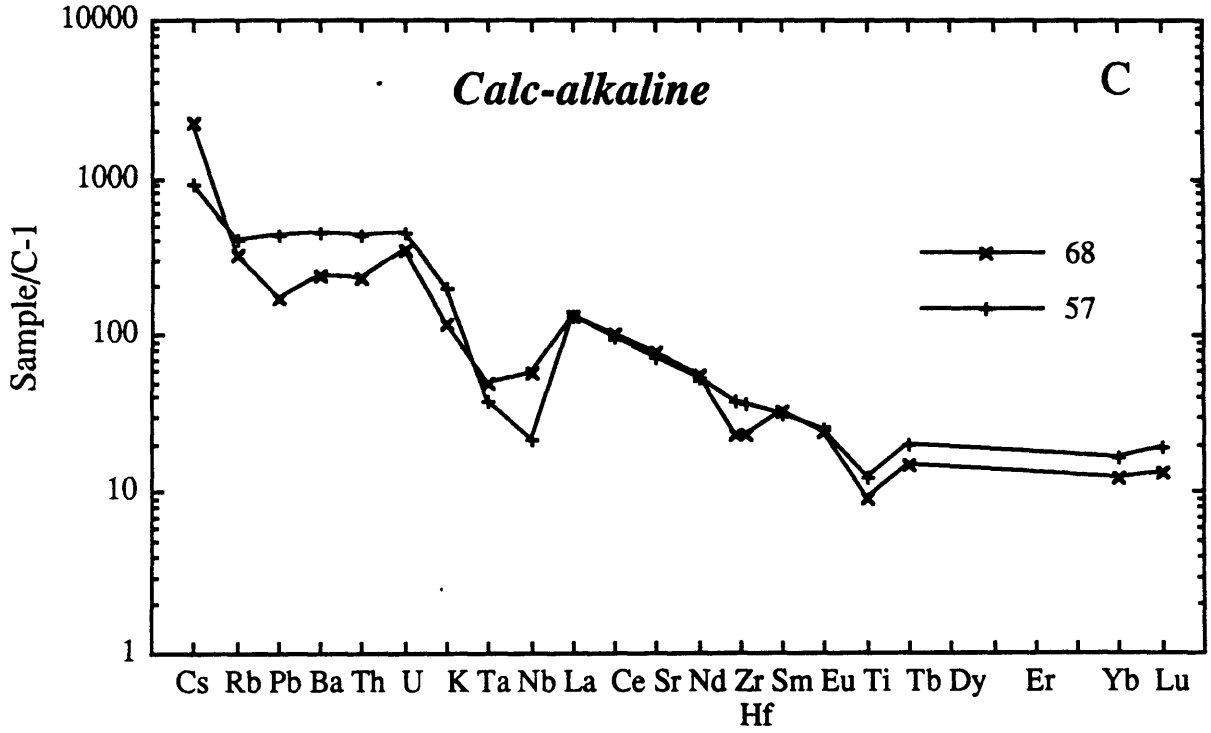
Calc-alkaline
C
68
57
Sample/C-1
10000
1000
100
10
1
Cs Rb Pb Ba Th U K Ta Nb La Ce Sr Nd Zr Sm Eu Ti Tb Dy Er Yb Lu
Hf

Figure 1.4:
$^{207}Pb/^{204}Pb$ and $^{208}Pb/^{204}Pb$ versus $^{206}Pb/^{204}Pb$ for the Carpathian volcanics compared with other localities. Circles are calc-alkaline volcanics, plusses are alkali basalts and cross is the kaersutite vein. Field for oceanic basalts from Zindler and Hart (1986) and references therein, field for Banda from Morris (1984), for Martinique, Lesser Antilles (Davidson, 1983; Davidson, 1986), for Turkey (Gulen, 1984). Field for pelagic sediments as from Salters et al. (1988).

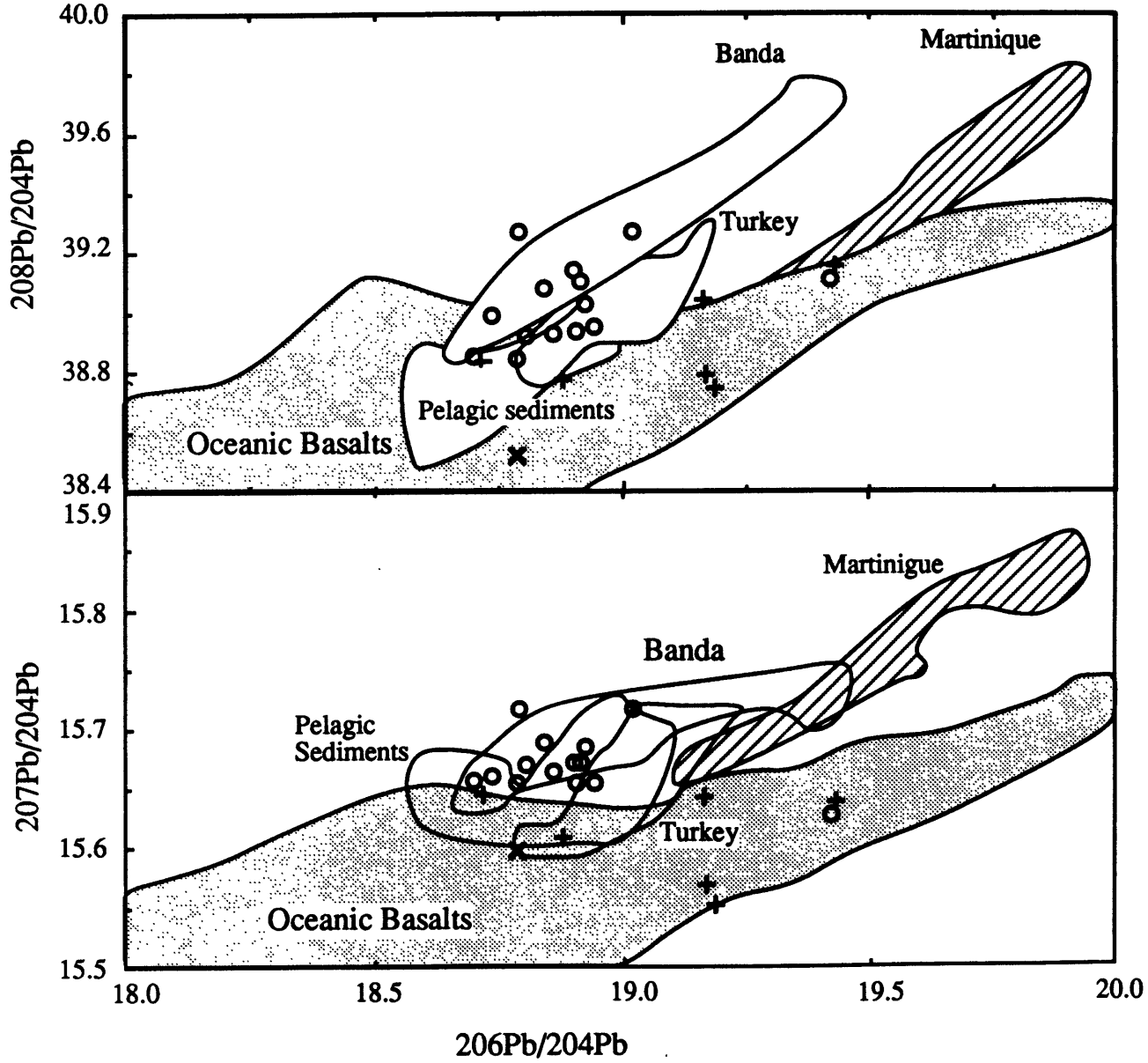
40.0
39.6
39.2
38.8
38.4
208Pb/204Pb
Banda
Martinique
Turkey
Pelagic sediments
Oceanic Basalts
15.9
15.8
15.7
15.6
15.5
207Pb/204Pb
Martinigue
Banda
Pelagic
Sediments
Turkey
Oceanic Basalts
18.0
18.5
19.0
19.5
20.0
206Pb/204Pb

Figure 1.5:
$^{87}Sr/^{86}Sr$ versus SiO_2 and Zr/Zr* for the Carpathian volcanics and mantle xenoliths. Symbols as in Fig. 1.2. See text for explanation.

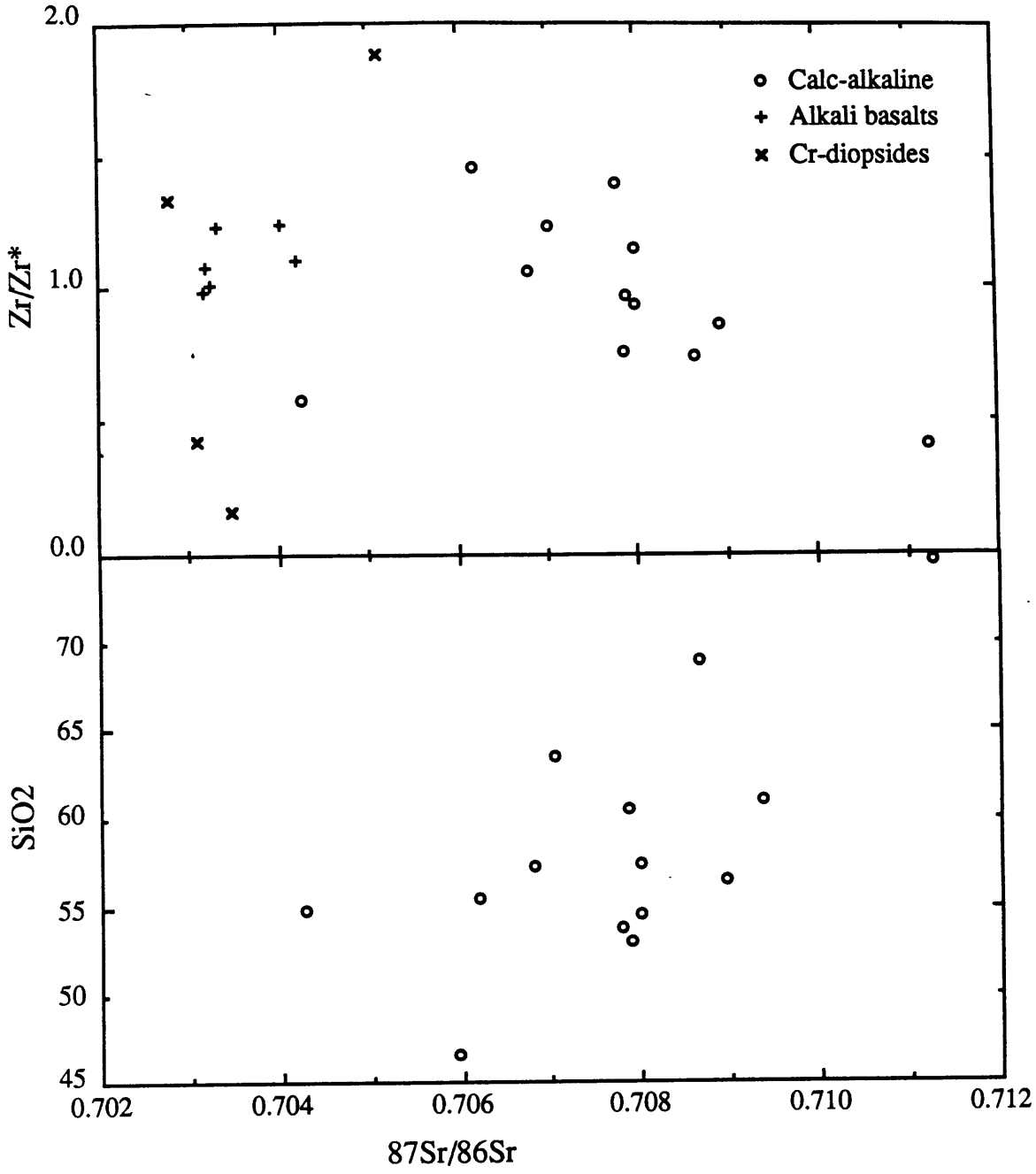
Calc-alkaline
Alkali basalts
Cr-diopsides
Zr/Zr*
2.0
1.0
0.0
SiO2
70
65
60
55
50
45
0.702
0.704
0.706
0.708
0.710
0.712
87Sr/86Sr

showing some scatter, the calc-alkaline volcanic suite displays correlations between $^{87}Sr/^{86}Sr$ and Zr/Zr* (negative) and SiO_2 (positive) (Fig 1.5).

With the exception of sample 113, the calc-alkaline volcanics are more limited in $^{206}Pb/^{204}Pb$ (18.694- 18.918) than the alkali basalts. $^{207}Pb/^{204}Pb$ ratios of the calc-alkaline volcanics varies from 15.631 to 15.761 and $^{208}Pb/^{204}Pb$ varies from 38.816 to 39.154. $^{207}Pb/^{204}Pb$ and $^{208}Pb/^{204}Pb$ of the calc-alkaline volcanics are in general higher than the range displayed by the alkali basalts. The calc-alkaline lavas straddle the high $^{207}Pb/^{204}Pb$ boundary of the MORB field and are clustered close to the field of pelagic sediments. As a consequence, all the calc-alkaline lavas show positive Δ7/4 Pb.

The calc-alkaline and alkaline volcanics have different K/Cs and Rb/Cs ratios, reflecting the enrichment in Cs in the calc-alkaline volcanics, as is typical for subduction-related volcanics (Morris and Hart, 1983). Except for sample 134, the two different types of volcanics have non-overlapping $^{87}Sr/^{86}Sr$ ratios as well. Although neither the alkaline nor the calc-alkaline volcanics show consistent trends in major or trace element (x vs y) variation diagrams, on spidergrams the volcanics show patterns typical for their type of magmatism (Fig. 1.3).

Sample 134 is anomalous in its isotopic and trace element characteristics. Based on its occurrence (from a drill hole overlying calc-alkaline volcanics) it was originally correlated with the younger alkali basalts suite elsewhere in Hungary (Panto, 1981). However, except for its K/Cs and Rb/Cs ratio, the trace element and Sr and Nd isotopic characteristics of Sample 134, are like the other calc-alkaline volcanics; this includes low the Ti and Zr content of Sample 134.

The four clinopyroxenes seperates from lherzolite xenoliths in alkali basalts show a large variation in Nd isotopes, ε_{Nd}=-4.8 to +19.7, while restricted in Sr-isotopes. The sample Szt-1022, with ε_{Nd}=19.7, has the highest ε_{Nd} yet measured in mantle Cr-diopsides and can be considered as an endmember. The HFSE/REE ratios of the Cr-diopsides are too low to be in equilibrium with the host basalts, (see also Salters and Shimizu (1988)). However, the lherzolites are possible source rocks for the calc-alkaline lavas. The kaersutite has

Sr and Nd isotope characteristics similar to the depleted end of the array formed by the Carpathian volcanics, and has Pb isotopes close to one end of the alkali basalt range.

1.5 Discussion

Although the Carpathian alkaline and calc-alkaline samples represent a large compositional variation, a geographical extent of over 500km, and an age spread of over 30 Ma, the lavas form a remarkably narrow array on a Nd-Sr isotope correlation diagram. This well-defined trend in Nd and Sr isotopes led us to attempt to explain the chemical variations without making an a priori distinction between the alkaline and calc-alkaline suite of lavas. The tightness of the array is even more remarkable considering the large variation in Nd-isotopes in the clinopyroxenes from the lherzolite xenoliths. Similarly large ranges and highly correlated Sr and Nd - isotopic compositions are observed for the Lesser Antilles (Davidson, 1983), the Banda Arc, Indonesia (Morris, 1984), and the Italian volcanic province (Hawkesworth and Vollmer, 1979; Taylor et al., 1979). In all three cases, the variations are explained crustal contamination. The high Sr and low Nd isotope ratios are typical for crustal materials and the increase of $^{87}Sr/^{86}Sr$ with SiO_2 (Fig. 1.5) leads to the conclusion that the observed isotopic variation in Nd and Sr isotopes was caused by crustal contamination, possibly accompanied by crystal fractionation. Due to the concave shape of the Nd-Sr array, the $^{143}Nd/^{144}Nd$ of the crustal endmember is well constrained (Langmuir et al., 1978). However, simple mixing of the two extreme samples of the array, alkali basalt #118 and #148 on the one end, and rhyolite #126 on the other end, produces an array markedly more concave than the observed array. Given the observed Sr, Nd concentrations, and Nd isotopic composition of the endmembers, simple mixing with $^{87}Sr/^{86}Sr$ in the crustal endmember as a free parameter cannot generate the observed array. The flatness of the observed array can be caused by a higher Sr/Nd ratio of the mantle endmember of the calc-alkaline suite than the

Table 1.3:
Endmembers for mixing calculations

	Upper Crust	Mantle 2	Mantle 1
Sr	350	498.4	791
Nd	29	15.6	39
Pb	8	0.5	3
87Sr/86Sr	0.7155	0.703086	0.702791
143Nd/144Nd	0.51204	0.512835	0.513209
206Pb/204Pb	18.66	18.78	20

Figure 1.6

Three component mixing model for the Carpathian volcanics and associated xenoliths. Large circles symbolize the endmembers. Endmembers are listed in Table 3. Symbols for volcanics and xenoliths as in Fig. 1.2. Numbers on the curves are the percentages of an endmember needed.

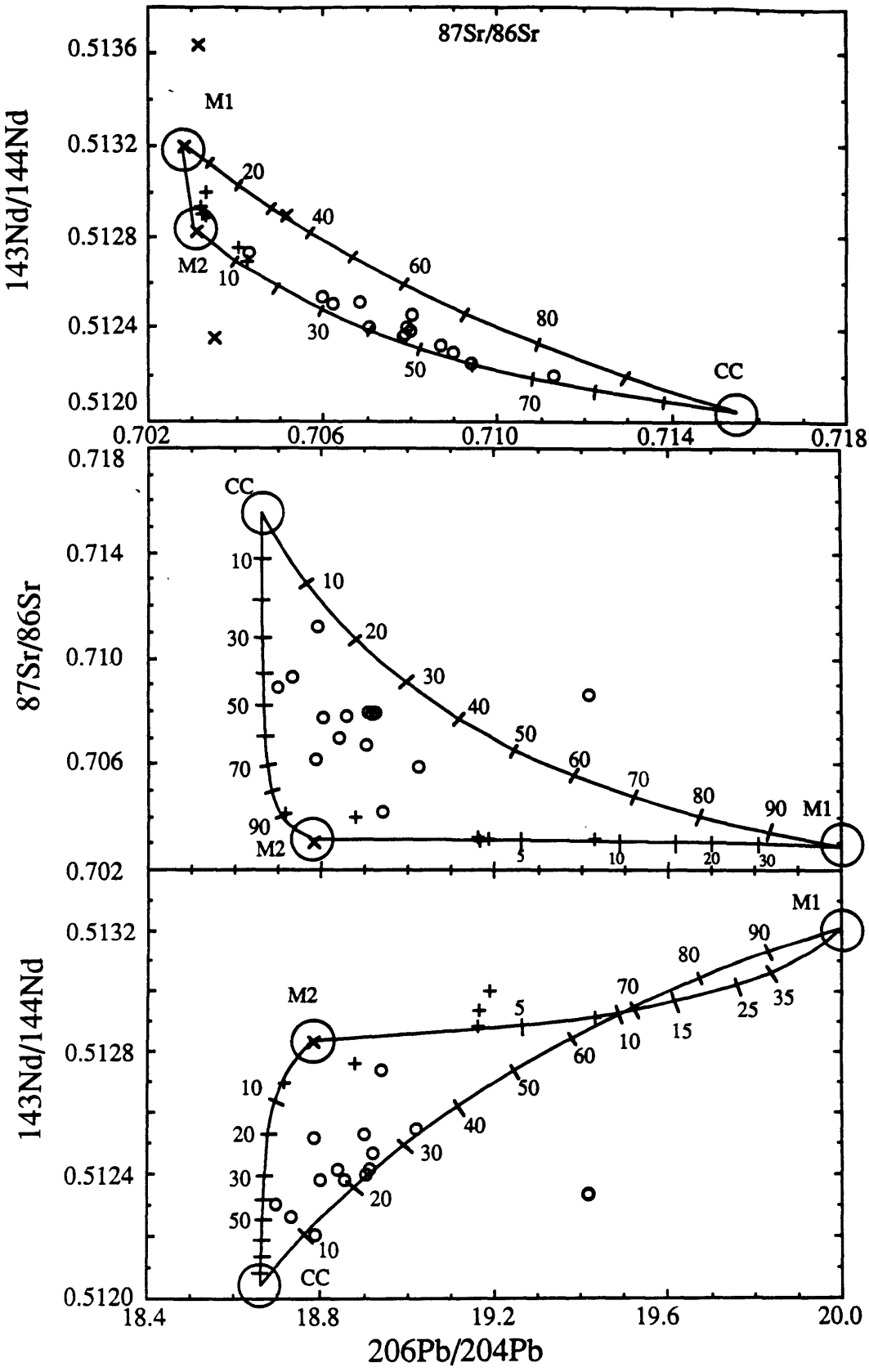
87Sr/86Sr
143Nd/144Nd
0.5136
0.5132
0.5128
0.5124
0.5120
0.702
0.706
0.710
0.714
0.718
M1
M2
CC
87Sr/86Sr
143Nd/144Nd
206Pb/204Pb
18.4
18.8
19.2
19.6
20.0

Sr/Nd of the alkali basalts. Calc-akaline volcanics in general have higher Sr/Nd ratios than alkali basalts (Hickey et al., 1986), and see also Fig 1.6. On the other hand, the flatness of the array can indicate that the contamination of the basaltic magmas with silicic magmas is accompanied by fractional crystallization. In a combined fractional crystallization and assimilation model, as described by Allegre and Minster (1978) and DePaolo (1982), the observed Sr-Nd array can be modelled with the observed endmembers. However, this model requires the calculated mass of assimilated material to be large and consequently the amount crystallized is large. Although this explains the Sr/Nd ratios, since it leads to unrealistically high Nd concentrations, this model must be rejected.

Fig. 1.4 shows the variation of the Pb-isotopic compositions of the Carpathian volcanics. The field occupied by the volcanics is changed from an array to a triangular-shaped field, and thereby rules out simple two component mixing as a model to explain the observed isotopic variations. At least three components are nessecary to explain the observed variation. In modelling the trace element and isotopic variations I tried to keep the characteristics of the endmembers as similar as possible to measured trace element and isotopic composition in samples, and as such the mixing models are melt-mixing models.

Simple three component mixing, with the samples extreme in composition as endmembers, cannot explain the observed variations. The resulting field will not contain the low $^{143}Nd/^{144}Nd$, high $^{206}Pb/^{204}Pb$ calc-alkaline volcanics. Although highly unconstrained, mixing and fractional crystallization combined, as described by Allegre and Minster (1978), DePaolo (1982), with the corners of the field of the volcanics as the endmembers will not produce the observed variations either. The above models fail to model the Pb isotopes and concentrations especially, and the Pb characteristics are thus crucial parameters in the calculations. Extending the allowed compositions of the endmembers to compositions of the clinopyroxenes in the xenoliths is hampered by our lack of knowledge of the Pb-isotopic compositions of the lherzolites nodules. The variability of the mantle below the Carpathians, as evidenced by

the variability in the clinopyroxenes from the lherzolite xenoliths, allows a large range of possible mantle endmembers. However, sample 148nod is the only sample that can be used as a single endmember. This endmember has an assumed $^{206}Pb/^{204}Pb$=20.0. A combination of the other lherzolites would also be able to serve as an endmember in the mixing models.

If the Sr, Nd and Pb concentrations and isotopic compositions are to be explained by three component mixing then the endmembers as listed in Table 1.3 are necessary. The low $^{206}Pb/^{204}Pb$, $^{207}Pb/^{204}Pb$ and $^{208}Pb/^{204}Pb$ makes the amphibolite vein a possible endmember, mantle endmember M2 in Fig. 1.6, for the mixing models. All isotopic and trace element characteristics for Sample Amph fit the mixing model, making Amph endmember M2. This is in agreement with the conclusion of Salters et al. (1988) that mixing in or near the source region was an important process in generating the isotopic variability in the alkali basalts. M1 is a composite endmember: by lack of the Pb isotopic compositions of the lherzolites, a.chosen $^{206}Pb/^{204}Pb$= 20.0 is needed to obtain the Pb-isotopic variations in the alkali basalts and calc-alkaline volcanics. Sr and Nd isotopic composition of nod148, and Sr-Nd-Pb trace element ratios from alkali basalt 147 are used for endmember M1. Fig.1.6 shows the mixing model for the Carpathian volcanics. The upper crust contaminant, endmember CC, is taken from Salters et al. (1988), except for the Pb concentration which is taken as in sample 126.

Although the models can explain the isotopic variability, the other trace element characteristics have to be modelled too. Relating the trace element characteristics of Cr-diopsides to basalts requires knowledge of the crystal-melt distribution coefficients (D's). The D's used to constrain the melting process and the justification for the choice of Ds for the different phases are given in Chapter 2 (see Fig. 2.5 and Table 2.1), and will not be repeated here.

Some of the trace element characteristics of the clinopyroxenes from the mantle xenoliths exclude the possibility of the alkali basalts and the clinopyroxenes being related by a simple one stage melting process. In general the Cr-diopsides in the Carpathian nodules are too depleted in High Field Strength Elements (HFSE) to be related to the

alkali basalts. This HFSE depletion is a general characteristic of spinel peridotites (Salters and Shimizu, 1988a). Fig. 1.3A shows the short spidergram for the Cr-diopsides and for the kaersutite vein. Based on the distribution coefficients, none of the nodules can be in equilibrium with the alkali basalts. However, the mantle as observed in the clinopyroxenes can serve as source material for the calc-alkaline volcanics. The HFSE/REE ratios prohibit the derivation of the alkali basalts out of the lherzolite xenoliths.

1.6 Origin of the observed components

Based on the trace element and isotopic variations of the xenoliths and the volcanics, the mantle beneath the Carpathians is extremely heterogeneous. Isotopic heterogeneity of paired calc-alkaline and alkaline volcanism, is less extreme for Fiji (Gill, 1984) and Turkey (Gulen, 1984)), or equal, as in the case of Patagonia (Skewes and Stern, 1979; Stern et al., 1986). Two mantle components are needed to explain the low $^{87}Sr/^{86}Sr$ end of the calc-alkaline field of the Carpathians. These two components have to differ in Pb-isotopes and be similar in Sr and Nd isotopes. Again Sample nod148 can be one of the endmembers, although no Pb data exists for this sample. The kaersutite vein is the other possible mantle endmember of the calc-alkaline suite.

The calc-alkaline volcanics lie outside the field of oceanic basalts indicating, addition of the sediment/crustal component to the calc-alkaline magmas (Fig.1.7). The Pb isotopes in the alkali basalts indicate several of these basalts also contain a sediment component. The Pb isotopes of the kaersutite are on the edge of the field for pelagic sediments, indicating this component might have a modest slab (sediment) component as compared to the other end member. Pb isotopes are indeed very good indicators of the presence of a sediment component (Hickey et al., 1986). The trace element signature of the kaersutite vein, allows it to be a component in the arc magmatism. Furthermore, the $^{143}Nd/^{144}Nd$ combined with the low Sm/Nd ratio of the kaersutite vein is consitent with derivation from a depleted type mantle, possibly subducted oceanic lithosphere.

Figure 1.7:

Δ7/4 versus Δ8/4 for the Carpathian volcanics. Field for other volcanics as from references in Fig. 1.4. Symbols as in Fig1.2. ΔPbs are the deviation in $^{207}Pb/^{204}Pb$ and $^{208}Pb/^{204}Pb$ from the Northern Hemisphere Reference Line(NHRL). Equations for the NHRL are:

$(^{207}Pb/^{204}Pb)_{NHRL}=0.1084(^{206}Pb/^{204}Pb)_m+13.491$

$(^{208}Pb/^{204}Pb)_{NHRL}=1.209(^{206}Pb/^{204}Pb)_m+15.62$

which are the $^{207}Pb/^{204}Pb$ and $^{208}Pb/^{204}Pb$ ratios of the NHRL for a measured $^{206}Pb/^{204}Pb$ ratio.

$\Delta^{207}Pb/^{204}Pb=\{(^{207}Pb/^{204}Pb)_m-(^{207}Pb/^{204}Pb)_{NHRL}\}*100$

$\Delta^{208}Pb/^{204}Pb=\{(^{208}Pb/^{204}Pb)_m-(^{208}Pb/^{204}Pb)_{NHRL}\}*100$

are the deviations from the NHRL according to Hart (1984). Field for Aleutians are from Kay et al. (1978) and Morris and Hart (1983). Field for Fiji from Gill (1984).

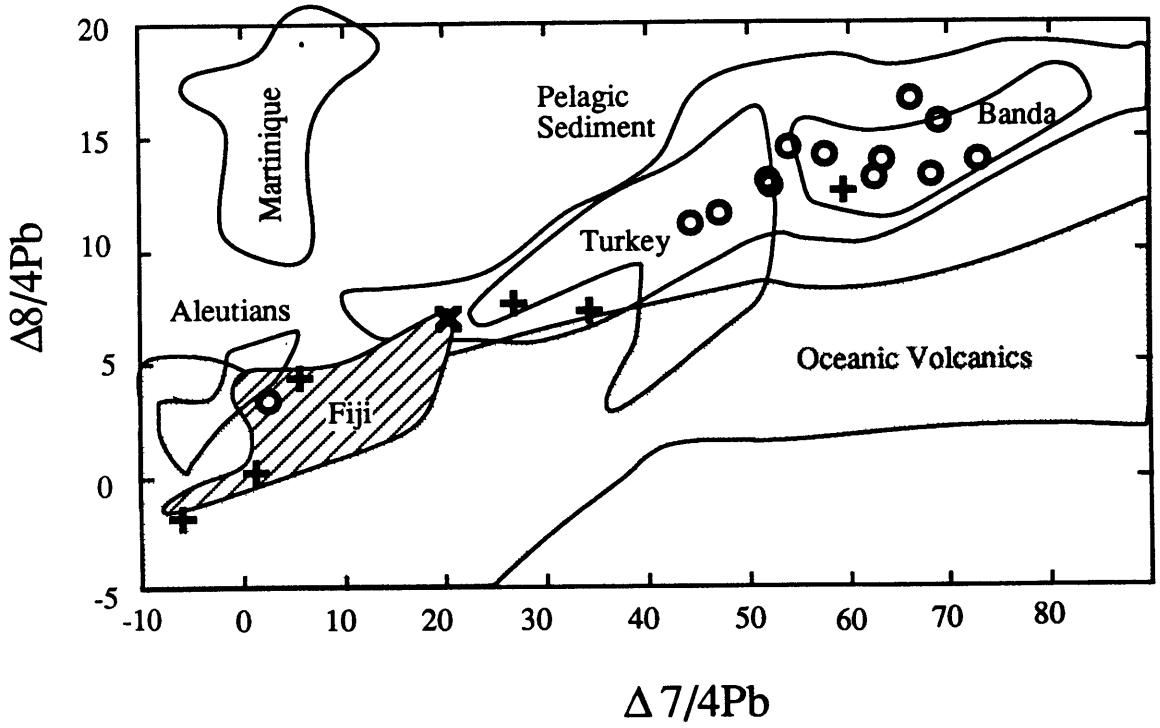
Martinique
Pelagic
Sediment
Banda
Turkey
Aleutians
Fiji
Oceanic Volcanics
Δ8/4Pb
Δ7/4Pb
20
15
10
5
0
-5
-10
0
10
20
30
40
50
60
70
80

It is proposed that the two mantle endmembers of the calc-alkaline volcanics are samples nod148 and Amph, since both the isotopic and trace element signatures are consistent with them being parents to the calc-alkaline volcanics. Since $^{87}Sr/^{86}Sr$ ratios of the calc-alkaline volcanics are higher than those of the proposed mantle endmembers, the choice of these two endmembers also implies that the calc-alkaline volcanics are mixtures of crustal and mantle. None of the endmembers is observed in a pure form in the volcanics. The high $\Delta 7/4Pb$ and $\Delta 8/4Pb$ in all the calc-alkaline volcanics requires positive ΔPb values for nod148.

In general, it is perceived that alkali basalts are formed by low degrees of melting of a source enriched in trace elements (Basaltic Volcanism Study Project, 1981). Salters et al. (1988) argued that the decoupling of isotopes and trace elements in the alkali basalts is caused by a recent enrichment event. The lack of HFSE depletions in the alkali basalts indicates a radically different source for the alkali basalts than for the calc-alkaline volcanics. None of the likely mantle phases have the distribution coefficients that allow generation of magmas both depleted in HFSE/HFSE* and magmas with HFSE/HFSE*≈1. However, the occurrence of lherzolite type xenoliths in the alkali basalts strongly suggests that ascent to the surface left minimal time for modification by crustal components. The Pb-isotopic characteristics, combined with the HFSE/REE ratios, distinguish the alkali basalts from the calc-alkaline volcanics. The HFSE/REE ratios also distinguish the alkali basalts from the lherzolites. The HFSE/REE ratios are considered to be unaffected by crystal fractionation and thus indicate different source materials. As a consequence, the high $^{206}Pb/^{204}Pb$ end of the alkali basalt-array is not present in the lherzolite nodules. The alkali basalts inherited their trace element characteristics from a mantle different than the nodules they are transporting. This adds another mantle component to the two already needed for the calc-alkline volcanics. The calc-alkaline and alkaline volcanics can share the kaersutite vein as a component.

The calc-alkaline and alkaline volcanics are either generated from different types of mantle or from a mantle that was significantly

modified after generation of the calc-alkaline magma. If the alkaline volcanics are from a modified calc-alkaline source, then at least the Sr and Nd isotopic composition is relatively unchanged. However, it seems more likely that the calc-alkaline and alkaline volcanism are generated from their 'own' sources. In light of the upcoming chapters, it also seems likely that the calc-alkaline mantle source is a depleted-type mantle, which underwent addition of a slab component before or during melting. The alkali basalts come from a 'deeper' source and just sample this modified mantle on their way to the surface.

1.7 Conclusions

1) The mantle beneath the Carpathians consists out of at least 3 components, two OIB-type component, in order to generate the range in $^{206}Pb/^{204}Pb$ in the alkali basalts, and a 'calc-alkaline' component, i.e. a component with low HFSE/REE ratios..
2) The occurrence of HFSE depletions in the clinopyroxenes in the xenoliths argues strongly for the HFSE depletions in the calc-alkaline volcanics to be a mantle characteristic.
3) The $^{87}Sr/^{86}Sr$ of thecalc-alkaline volcanics indicate these lavas are all modified to some extend by a crustal component.
4) Based on the $^{143}Nd/^{144}Nd$ of the clinopyroxenes in the xenoliths, the calc-alkaline type (HFSE depleted) mantle is extremely heterogeneous in Nd-isotopes.

1.8 References

Allegre, C.J. and Minster, J.-. (1978). Quantative models of trace element behaviour in magmatic processes. Earth Plan. Sci. Lett. **38**: 1-25.

Anders, E. and Grevesse, N. (1989). Abundances of the elements: Meteoritic and solar. Geochim. Cosmochim. Acta. **53**: 197-214.

Basaltic Volcanism Study Project. (1981). Basaltic Volcanism on the terrestrial planets. New York, Pergamon Press.

Burchfiel, B.C. (1980). Eastern European alpine system and the Carpathian orocline as an example of collision tectonics. Tectonophysics. **63**: 31-36.

Burchfiel, B.C. and Royden, L. (1982). Carpathian foreland fold and trust belt and its relation to Pannonian and other basins. AAPG Bull. **66**: 1179-1195.

Clague, D.A. and Frey, F.A. (1982). Petrology and trace element chemistry of the Honolulu volcanics, Oahu: Implication for the oceanic mantle below Hawaii. J. Petrol. **23**: 447-504.

Davidson, J.P. (1983). Lesser Antilles isotopic evidence of the role of subducted sediment in island arc magma genesis. Nature. **306**: 253-256.

Davidson, J.P. (1986). Isotopic and trace element constraints on the petrogenesis of subduction-related lavas from Martinique, Lesser Antilles. J. Geophys. Res. **91**: 5943-5962.

DePaolo, D.J. (1982). Trace element and isotopic effects of combined wallrock assimilation and fractional crystallization. Earth Plan. Sci. Lett. **53**: 189-202.

Fujimaki, H., Tatsumoto, M. and Aoki, K. (1984). Partition coefficients of Hf, Zr and REE between phenocrysts and groundmasses. J. Geophys.Res. **89**: 662-672.

Gill, J.B. (1981). Orogenic andesites and plate tectonics. Berlin, Springer Verlag.

Gill, J.B. (1984). Sr-Pb-Nd isotopic evidence that both MORB and OIB sources contribute to oceanic island arc magmas in Fiji. Earth Plan. Sci. Lett. **68**: 443-458.

Gulen, L. (1984). Sr, Nd, Pb isotope annd trace element geochemistry of calc-alkaline and alkaline volcanics, eastern Turkey. MIT PhD.

Hart, S.R. (1984). The DUPAL anomaly: A large scale isotopic mantle anomaly in the Southern Hemisphere. Nature. **309**: 753-757.

Hart, S.R. and Brooks, C. (1977). The geochemistry and evolution of the early precambrian mantle. Contrib. Mineral. Petrol. **61**: 109-128.

Hawkesworth, C.J. and Vollmer, R. (1979). Crustal contamination versus enriched mantle: $^{143}Nd/^{144}Nd$ and $^{87}Sr/^{86}Sr$ evidence from the Italian volcanics. Contrib. Mineral. Petrol. **69**: 151-165.

Hickey, R.L., Frey, F.A. and Gerlach, D.C. (1986). Multiple sources for basaltic arc rocks from the southern volcanic zone of the Andes (34^{o}-41^{o}S): Trace element and isotopic evidence for contributions from subducted oceanic crust, mantle and continental crust. J. Geophys.Res. **91**: 5963-5983.

Irving, A.J. and Frey, F.A. (1984). Trace element abundances in megacrysts and their host basalts: Constaints on partition coefficients and megacryst genesis. Geochim. Cosmochim. Acta. **48**: 1201-1221.

Kay, R.W., Sun, S.S. and Lee-Hu, C.N. (1978). Pb and Sr isotopes in volcanic rocks from the Aleutians and Pribilof Isalnds, Alaska. Geochim. Cosmochim. Acta. **42**: 263-273.

Langmuir, C.H., Voche, R.D., Jr, Hanson, G.N. and Hart, S.R. (1978). A general mixing equation with applications to Icelandic basalts. Earth Plan. Sci. Lett. **37**: 380-392.

Leeman, W.P. (1987). Boron geochemistry of volcanic arc magmas: evidence for recycling of subducted oceanic lithosphere. EOS, Abstr. **68**: 462.

Manhes, G., Minster, J.-. and Allegre, C.J. (1978). Comparative uranium-thorium-lead and rubidium-strontium of St. Severin amphoterite: Concequences for early solar system chronology. Earth Plan. Sci. Lett. **39**: 14-24.

Morris, J.D. (1984). Enriched geochemical signatures in Aleutian and Indonesian arc lavas: An isotopic and trace element investigation. Massachusetts Institute of Technology, Cambridge PhD.

Morris, J.D. and Hart, S.R. (1983). Isotopic and incompatible element constraints on the genesis of island arc volcanics: Cold Bay and Amak Islands, Aleutians. Geochim. Cosmochim. Acta. **47**: 2015-2030.

Nicholls, I.A. and Ringwood, A.E. (1973). Effect of olivine stability in tholeiites and the production of silica undersaturated magmas in the island arc environment. J.Geol. **81**: 285-300.

Panto, G. (1981). Rare earth element geochemical pattern of the Cenozoic volcanism in Hungary. Earth Evolution Series. **3-4**: 249-256.

Pearce, J.A. and Cann, J.R. (1973). Tectonic setting of basic volcanic rocks determined using trace element analyses. Earth Plan. Sci. Lett. **19**: 290-300.

Pearce, J.A. and Norry, M.J. (1979). Petrogenetic implications of Ti, Zr, Y and Nb variations in volcanic rocks. Contrib. Mineral. Petrol. **69**: 33-47.

Pegram, W.J. (1986). Geochemical processes in the sub-continental mantle and the nature of crust mantle interaction: Evidence from the Mesozoic Appalachian Tholeiite Province. Massachusetts Institute of Technology, Cambridge, Massachusetts PhD.

Richard, P.N., Shimizu, N. and Allegre, C.J. (1976). $^{143}Nd/^{144}Nd$, a natural tracer: An application to oceanic basalts. Earth Plan. Sci. Lett. **31**: 269-278.

Royden, L.H. (1988). Late Cenozoic Tectonics of the Pannonian basin system. AAPG Memoir. Tulsa, Oklahoma, AAPG and Hungarian Geological Society.

Royden, L., Horvath, F. and Rumpler, J. (1983). Evolution of the Pannonian basin system, 1. Tectonics. **2**: 63-90.

Salters, V.J.M., Hart, S.R. and Panto, G. (1988). Origin of late Cenozoic volcanic rocks from the Carpathian Arc, Hungary, Ch. 19. Pannonian Basin: a study in basin evolution. Tulsa, Oklahoma, AAPG and Hungarian Geol. Soc.

Salters, V.J.M. and Shimizu, N. (1988a). HFSE depletions in peridotites, local variations and possible origin (abstr.). V.M. Goldschmidt Conference.

Salters, V.J.M. and Shimizu, N. (1988b). World-wide occurrence of HFSE-depleted mantle. Geochim. Cosmochim. Acta. **52**: 2177-2182.

Shimizu, N. and Hart, S.R. (1982). Appplications of the ion micro-probe to geochemistry and cosmochemistry. Ann. Rev. Earth Plan. Sci. **10**: 483-526.

Skewes, M.A. and Stern, C.R. (1979). Petrlogy and geochemistry of alkali basalts and ultramafic inclusions from the Palei-Aike volcanic field min southern Chile and the origin of Patagonian plateau lavas. J. Volc. Geotherm. Res. **6**(3-25):

Stegena, L., Geczy, B. and Horvath, F. (1975). Late Cenozoic evolution of the Pannonian basin. Tectonophysics. **26**: 71-90.

Stern, C.R., Saul, S., Futa, K. and Skewes, M.A. (1986). Nature and evolution of the subcontinental mantle lithosphere below southern South America and implications for Andean magmatism. Revista Geologica de Chile. **27**: 41-53.

Stern, R.J. (1982). Strontium isotopes from circum-pacific intra-oceanic island arcs and marginal basins:Regional variations and implications for magma genesis in island arcs. Geol. Soc. Am. Bull. **93**: 477-486.

Taylor, H.P., Jr, Giannetti, B. and Turi, B. (1979). Oxygen isotopes geochemistry of the potassic igneous rocks from the Roccamonfina volcano, Roman comagmatic region, Italy. Earth Plan. Sci. Lett. **46**: 81-106.

Tera, F., Brown, L., Morris, J.D., Sacks, I.S., Klein, J. and Middleton, R. (1986). Sediment incorporation in island-arc magmas: Inferences from ^{10}Be. Geochim. Cosmochim. Acta. **50**: 535-550.

Vogl, M. and Panto, G. (1983). Geochemistry of young alkaline basaltic volcanism in Hungary. :

White, W.M., Tapia, M.D.M. and Schilling, J.-. (1979). The petrology and geochemistry of the Azores Islands. Contrib. Mineral. Petrol. **69**: 201-213.

Whitford, D.J. and Jezek, P.A. (1979). Origin of Late Cenozoic lavas from the Banda arc, Indonesia: Trace element and Sr isotope evidence. Contrib. Mineral. Petrol. **68**: 141-150.

Zindler, A. (1980). Geochemical processes in the earth's mantle and the nature of crust-mantle interactions: Evidence from studies of Nd and Sr isotope ratios in mantle derived igneous rocks and lherzolite nodules. Massachusetts Institute of Technoloy, Cambridge, Massachusetts PhD.

Zindler, A. and Hart, S.R. (1986). Chemical Geodynamics. Ann. Rev. Earth Plan. Sci. **14**: 493-571.

Chapter 2:

Trace element abundances in lherzolites; the use of HFSE/REE ratios as a clue to mantle processes.

2.1 Introduction

This chapter discusses Rare Earth Element (REE), Sr and High Field Strength Element (HFSE) variations in diopsides and garnets from mantle xenoliths. Lherzolite xenoliths are solid samples from the upper mantle of which the major mineral phases are unaffected by the eruption process. As such, they are important in understanding mantle processes. Furthermore, our present knowledge of the trace element characteristics of mantle-derived melts, combined with our knowledge of solid melt partition coefficients, allows comparison of peridotites with basalts and assessment of their relationship.

The results of previous major, trace element and isotopic studies on peridotite xenoliths and massifs indicate a mantle history with relative few (1 or 2) depletion or enrichment events (Frey et al., 1985; Jagoutz et al., 1980; Menzies et al., 1987b; Roden et al., 1988). For instance, the depleted Mid Ocean Ridge Basalt (MORB) reservoir is thought to be formed by extracting melt which formed continental crust. Isotopic investigations indicate that this depleted MORB mantle is between 1.5-2.0 Ga in average age (Allegre et al., 1983a; Allegre et al., 1983b; Hofmann, 1988; Tatsumoto, 1978; Zindler and Hart, 1986), and is thought to be relatively undisturbed since the depletion. On the other hand, peridotite xenoliths found in kimberlites in S. Africa are thought to have first undergone melt extraction, causing depletion, followed by metasomatism causing Light (L)REE enrichment and modal metasomatism (Nixon and Boyd, 1979). As a third example, some peridotites have major and trace element characteristics similar to the initial Bulk Earth (BE) composition 4.5 Ga ago, and these peridotites could represent pristine mantle material (Hart and Zindler, 1986; Jagoutz et al., 1979a; Jagoutz et al., 1979b). The combination of the REE and the HFSE is useful in constraining the history of peridotites, and in assessing the relationship between the peridotites and the major types of volcanism. The focus of this chapter will be determining the trace element variations, REE and HFSE especially, of clinopyroxenes in peridotites and the relationship between clinopyroxenes in lherzolites and melts.

Throughout this chapter I will be using the terms enriched and depleted. These enrichments and depletions are measured compared to Bulk Earth (BE) values. X_n is defined as the concentration of element X divided by the BE concentration of element X. "Enrichment" is defined as $X_n/Y_n>1$, whereby element X partitions into the melt over the solid more than element Y, $D_X<D_Y$. D_X is the solid-melt distribution coefficient of element X. "Enriched" material looks like it experienced melt addition, although melt addition as a physical process is not specifically required. "Depleted" material looks like it experienced melt extraction compared to BE, i.e., $X_n/Y_n<1$. Furthermore, I will be using the term "High Field Strength Element depletions". Samples with HFSE/REE ratios lower than BE values are classified as HFSE depleted.

Much of the work on peridotites in recent years is focussed on modally metasomatized xenoliths; since the concentrations of trace elements in these xenoliths are high and relatively easy to measure (for review, see Menzies et al. (1987), and Erlank et al. (1987)). Anhydrous spinel peridotites are much more difficult to analyze for trace elements. Consequently, good studies on anhydrous peridotites are scarce; Zindler and Jagoutz (1988), and Stosch et al. (1986) are examples.

The present study of anhydrous lherzolites presents data obtained with the ion microprobe. The ion-microprobe allows in situ analyses on individual grains for selected trace elements and REE. The method of analysis was first described by Shimizu et al. (1978) and further documented by Shimizu and Hart (1982). Mass interferences of complex molecules are eliminated by use of energy filtering. Since this is an in-situ technique, we avoid possible contamination with reagents; furthermore this technique is much less labour intensive than any other techniques.

Frey and Prinz (1978), classified mantle xenoliths from San Carlos, Arizona, into two groups based mainly on their Mg#. Group I is the group with high Mg#, high Cr contents, and Cr-diopside as the main Ca-bearing mineral. This group is considered to be a representative of either 'unmelted' peridotite, or peridotite residual after melting. Group II xenoliths are characterized by low Mg# and a

lower Ca/Al ratio, and are thought to represent mantle material that has seen addition of melt, or addition of phases that crystallized from a melt.

Menzies et al. (1987), divide, partly based on the mineralogy, modal metasomatism in two classes:

- K-metasomatism, leading to modal mica and richterite bearing peridotite. These xenoliths have elevated concentrations of Rb, K, LREE and Ti and are thought to be altered by a hydrous fluid (Erlank et al., 1987).
- Fe-Ti metasomatism, leading to kaersutite veining and to addition of pargasite. This metasomatism is thought to be caused by addition of basanitic melts resulting in an increase in trace element contents and a decrease in the Mg# and the Ca/Al ratio. This Fe-Ti metasomatism leads to lherzolites belonging to Group II of Frey and Prinz (1978).

Both types of metasomatism are modal and result in the presence of H_2O-bearing phases. Almost all of the xenoliths I have analyzed are anhydrous. If metasomatism caused any of the variations presented in the upcoming section, then this metasomatism either had to be followed by a dehydration process (since the metasomatism is cryptic), or the metasomatism took place outside the stability field of any of the hydrous phases. However, the kind of trace element variations caused by metasomatism still needs to be known.

This chapter discusses trace element variations in mostly anhydrous lherzolites, harzburgites, and few hydrous lherzolites. Whenever hydrous lherzolites are included in the group they will be specially mentioned. The trace element variation in the clinopyroxenes of the hydrous group can be used to determine the character of hydrous metasomatism. It is a general notion that samples more depleted in major elements than BE have experienced a melt extraction event. The estimate for BE of Hart and Zindler (1986) is used to determine whether a peridotite is depleted in major elements such as Ca, Al.

In this chapter I will be using the ratios Zr/Zr* and Ti/Ti* to quantifying the HFSE depletion compared to the REE. Zr* is the chondrite-normalized average of the RE elements neighboring Zr on a

so-called spidergram; see Fig. 2.1 for an example. Thus $Zr^*=(Nd_n+Sm_n)/2$ and $Ti^*=(Eu_n+Tb_n)/2$. In the ratios Zr/Zr*, and Ti/Ti*, Zr and Ti are the C-1 normalized concentrations. In most cases Tb was not measured, but interpolated from Eu and Dy. HFSE/HFSE* ratios <1 indicate depletions in HFSE compared to the REE.

2.1.1 Are diopsides representative of the bulk rock lherzolite?

I have analyzed mostly diopsides from anhydrous lherzolites. It is, to some degree, important to assert whether the clinopyroxene is an adequate representative of the bulk rock (i.e. 4 phase spinel lherzolite) in trace element ratios. For REE this has been argued by numerous authors (Downes and Dupuy, 1987; Roden et al., 1984a; Stosch and Seck, 1980). Fig. 2.1 compares the Sr, REE, and some HFSE abundances for clinopyroxenes and bulk rock anhydrous four phase spinel lherzolites. Fig. 2.1 supports the general assumption that HFSE/REE ratios in Cr-diopsides are approximately the same as in the bulk rock. Since a significant part of the LREE content of lherzolites can be located on grain boundaries (Zindler and Jagoutz, 1988), the clinopyroxenes may have a somewhat lower Sm/Zr or Nd/Zr than the bulk rock.

I tried to analyze spinels from spinel lherzolites, but failed due to the low concentration of REE and HFSE in spinel. As a consequence, I believe that spinel cannot significantly contribute to the HFSE-REE budget in lherzolites. The Ti-depletions in the diopsides in Fig. 2.1 are somewhat larger than the depletions in the bulk rock. Orthopyroxene is a phase which can contain measurable amounts of Ti. I determined the effect of orthopyroxene for two xenoliths from Salt Lake Crater, all 11% Cr-diopside and 25-28% orthopyroxene, and concluded that at most 10% of the Ti budget of the whole rock can be in the orthopyroxene. The lack of any correlation, between Ti/Ti* and Zr/Zr* and modal diopside/enstatite ratio, indicates that enstatite does not contain the complement of the HFSE budget.

The existence of a Ti-rich accessory phase (i.e. sphene or Fe-Ti ilmenite) can be rejected on the basis that, although they are hard to find, I have not observed any. Furthermore, Ti saturation is needed

Figure 2.1

Incompatibility diagram. Elemental concentrations are normalized to C-1 chondrites (Anders and Grevesse, 1989) for the refractory elements See Table 1 for values. Open symbols are whole rocks. Filled symbols and crosses are clinopyroxenes. Diamonds are for Dreiser Weiher, Germany (Jagoutz et al., 1979a; Jagoutz et al., 1979b). Other samples are from Ronda, whole rock data, and sample# from Frey et al. (1985). Clinopyroxenes clearly mimic their whole rock in trace element ratios. Triangles are sample R238, plusses and crosses are R717, and squares are R855.

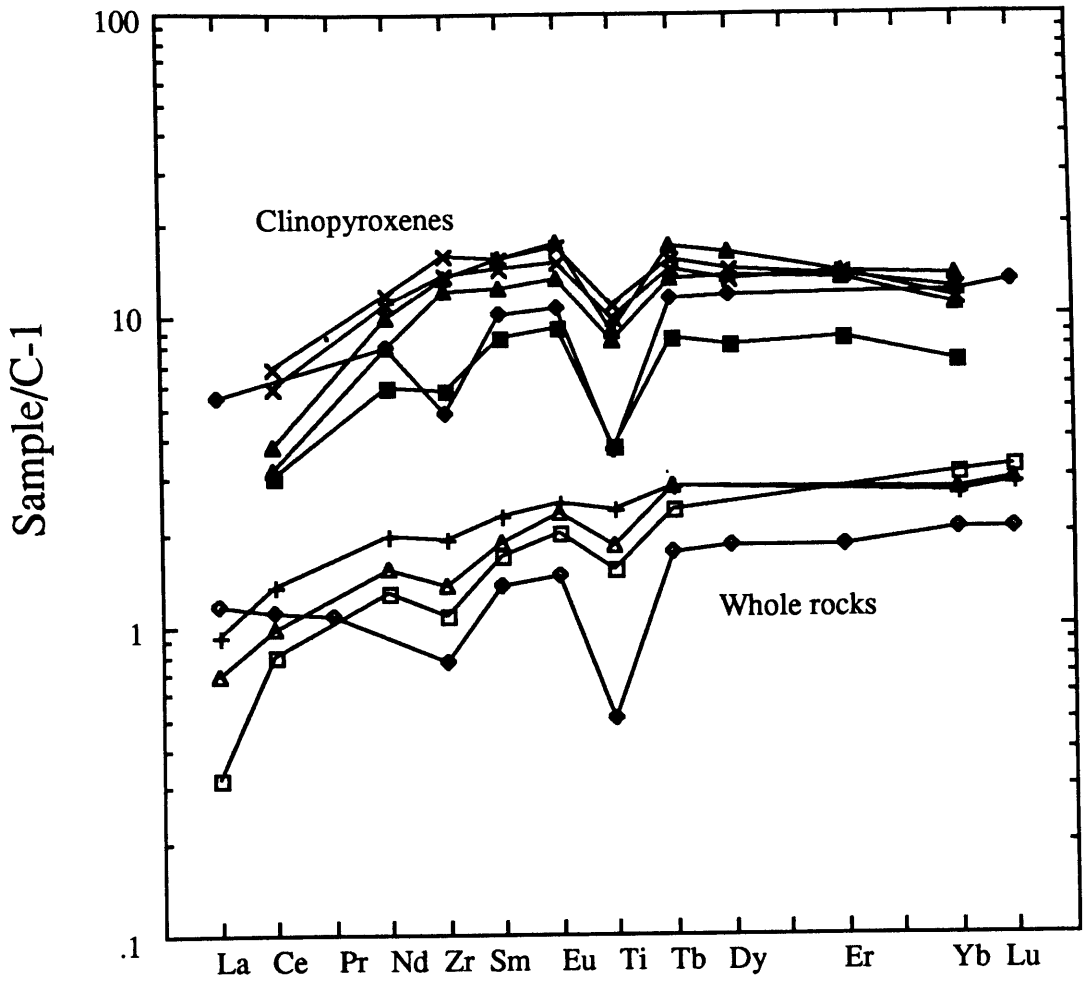
100
10
1
.1
Sample/C-1
Clinopyroxenes
Whole rocks
La Ce Pr Nd Zr Sm Eu Ti Tb Dy Er Yb Lu

in order to stabilize a Ti-rich phase. I expect Ti saturation to cause enrichment of Ti compared to the REE and not depletion. A formal treatment of the budget of the HFSE and REE is hampered by the lack of sufficient data on both bulk rock and mineral phases for the HFSE.

From the above discussion it can be concluded that REE/HFSE ratios in the diopsides are an accurate representation of the bulk rock REE/HFSE ratios. However, to relate these clinopyroxenes to a melt, only knowledge of the appropriate clinopyroxene/melt distribution coefficients is needed. A bulk rock lherzolite without any HFSE depletions in its whole rock pattern can contain Cr-diopsides with HFSE depletions. For instance, in garnet lherzolites, with smooth bulk rock spidergram pattern, the clinopyroxene will have a Zr depletion and Ti enrichment. The partition pattern for Cr-diopside is smooth (see next section). Consequently, melt in equilibrium with the Cr-diopside will mimic the pattern of the Cr-diopside, and in the above case the melt will have Zr depletions and Ti enrichments. The trace element ratios of the melt are determined by knowledge of the trace element ratios of the Cr-diopside and the distribution coefficients only. This is not a new concept, but just a consequence of the partition laws. Equally, the Mg# of olivine determines the Mg# of the liquid in equilibrium with this olivine. Furthermore, the use of a "bulk rock" pattern is a dangerous concept since xenoliths are most times coarse grained materials. The large grain size makes it hard to obtain a representative sample of bulk rock material, especially since a large number of xenoliths are fist size or smaller! Furthermore, the occurrence of zonation, found more and more often in xenoliths, makes the bulk rock concept even more difficult. Given the distribution coefficients, measuring clinopyroxene determines what a melt in equilibrium with this clinopyroxene should look like.

2.2. Trace element distribution coefficients and normalization values.

Crucial to our understanding of mantle processes is the knowledge of the partition coefficients; i.e. knowledge of the capability of the different mantle phases to fractionate trace element ratios. Here I discuss two ways to obtain information on the

distribution coefficients (D's) of the different phases. One is actual measurement; either by experiments or by phenocryst-matrix analyses. The other way is to study the integrated trace element pattern of a melt in the form of a spidergram (Sun et al., 1979; Wood, 1979). The spidergram provides information on the relative compatibility of the elements in a bulk rock sense (assuming a source composition), and does not lead to information on the absolute distribution coefficients.

I will restrict myself to the REE, Zr, Ti and Sr, thus the position of the non-RE elements with respect to the REE on a spidergram and the normalization values of the REE and non REE need to be determined. A large amount of data is available on the distribution of trace elements between clinopyroxene and liquid, using a wide variety of techniques and a large range in compositions. A large range in distribution coefficients is observed, and this is partly explained by the effect of differences in bulk composition on the D's (Green and Pearson, 1985). In selecting the distribution coefficients, I considered studies on natural basalts only. These D's are carefully examined, realizing that lack of equilibrium in the experiments or incomplete separation of the phases will generally lead to higher distribution coefficients for the incompatible elements (closer to unity). Experimental data are rejected when either run duration changed the D's (Shimizu, 1980; Shimizu et al., 1982), or clinopyroxene and matrix were not well separated (Tanaka and Nishizawa, 1975), or crystals were demonstrably zoned in trace elements (Nicholls and Harris, 1980). Furthermore, very few data are available for Zr or Hf and the REE combined; essentially only three studies consider these elements together (Dunn, 1987; Fujimaki et al., 1984; Irving and Frey, 1984). In Dunn's experiments, D_{Lu}/D_{Hf} varies only from 1.73-1.92, while Fujimaki's experiment finds D_{Lu}/D_{Hf} of 1.67. Irving and Frey measured megacryst host pairs, and Fujimaki et al. (1984) measured phenocryst-matrix pairs. These three studies strongly suggest that D_{Hf} in clinopyroxene is intermediate between D_{Sm} and D_{Nd}. Fig. 2.2 shows distribution coefficient pattern from the different studies, and my preferred values. My preferred data set is chosen from the

Figure 2.2

A: Clinopyroxene-melt distribution coefficients.

Shaded area is range reported for megacrysts, and plusses are the preferred values of Irving and Frey (1984). Hatched area is range of D's obtained in experiments by Grutzeck et al. (1974). Triangles are experiments reported by Dunn (1987). Squares are D_{Zr} reported by McCallum and Charrette (1978). Crosses are from an experiment reported by Fujimaki et al. (1984). Heavy solid line is my preferred set.

B. Garnet-melt distribution coefficients.

Circles are the average of garnet-melt data reported by Irving and Frey (1978). Plusses are megacrysts and crosses are experimental data from Fujimaki et al. (1984). Triangles are experimentally determined Ds by Shimizu and Kushiro (1975). Heavy solid line is my preferred set; see also Table 2.1.

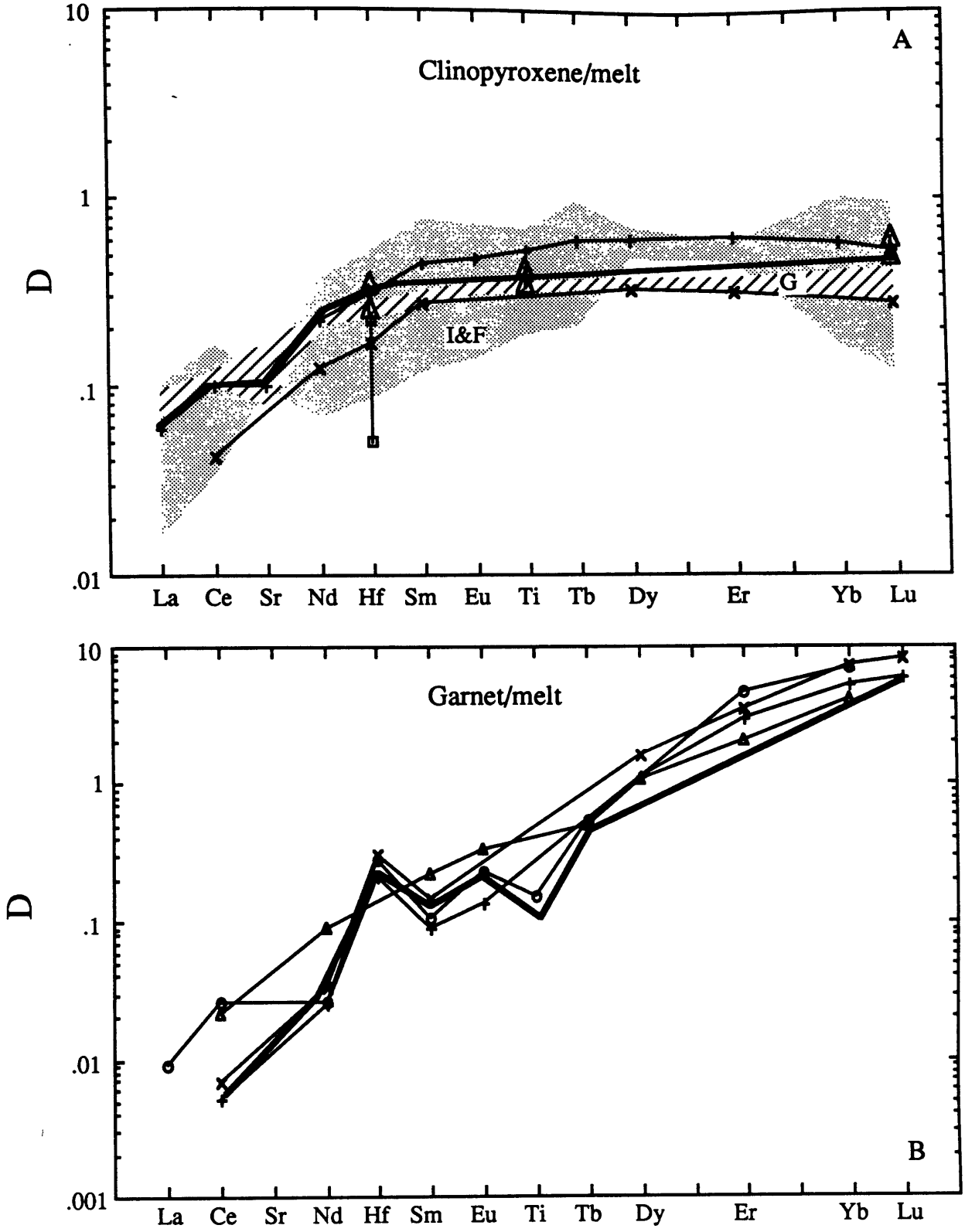
10
1
.1
.01
D
A
Clinopyroxene/melt
G
I&F
La Ce Sr Nd Hf Sm Eu Ti Tb Dy Er Yb Lu
10
1
.1
.01
.001
D
Garnet/melt
B
La Ce Sr Nd Hf Sm Eu Ti Tb Dy Er Yb Lu

Table 2.1
Chondrite normalization values (in ppm) and mineral/melt distribution coefficients for the REE and the HFSE

	C-1	Diopside	Garnet	Amphibole
La	0.235			
Ce	0.603	0.1	0.004	0.26
Sr	7.4	0.08	0	0.64
Nd	0.452	0.18	0.03	0.44
Hf	0.1024	0.28	0.23	0.38
Zr	3.94	0.28	0.23	0.38
Sm	0.147	0.28	0.13	0.76
Eu	0.056	0.31	0.2	0.88
Ti	436	0.34	0.1	2.1
Tb	0.0363	0.35	0.4	0.83
Dy	0.245	0.36	0.7	0.78
Er	0.1603	0.39	1.7	0.68
Yb	0.162	0.44	4.5	0.59
Lu	0.0243	0.45	5.5	0.51

Figure 2.3

Hofmann diagrams for MORB and OIB. OIB data from Basaltic Volcanism Study Project (1981), Clague and Frey (1982), Dupuy et al. (1987), García et al. (1986), Lanphere and Frey (1987), Liotard et al. (1986), White et al. (1979). Large squares are for averages of the Hawaiian volcanoes as reported by Leeman et al. (1980), except for the square lowest in Sm and Nd. This square is average N-MORB mantle as reported by Hofmann (1988). MORB dataset from Clague et al. (1981), Dosso et al. (1988), Frey et al. (1980), Frey and Green (1974), Langmuir et al. (1977), Pearce et al. (1985), Price et al. (1986), Puchelt and Emmermann (1983), Rhodes et al. (1978), Wood et al. (1979). The slightly positive correlation between Nd/Zr and Nd combined with the slightly negative to flat correlation between Sm and Sm/Zr indicates the incompatibility of Zr is intermediate between Nd and Sm in the MORB-OIB-anhydrous peridotite system.

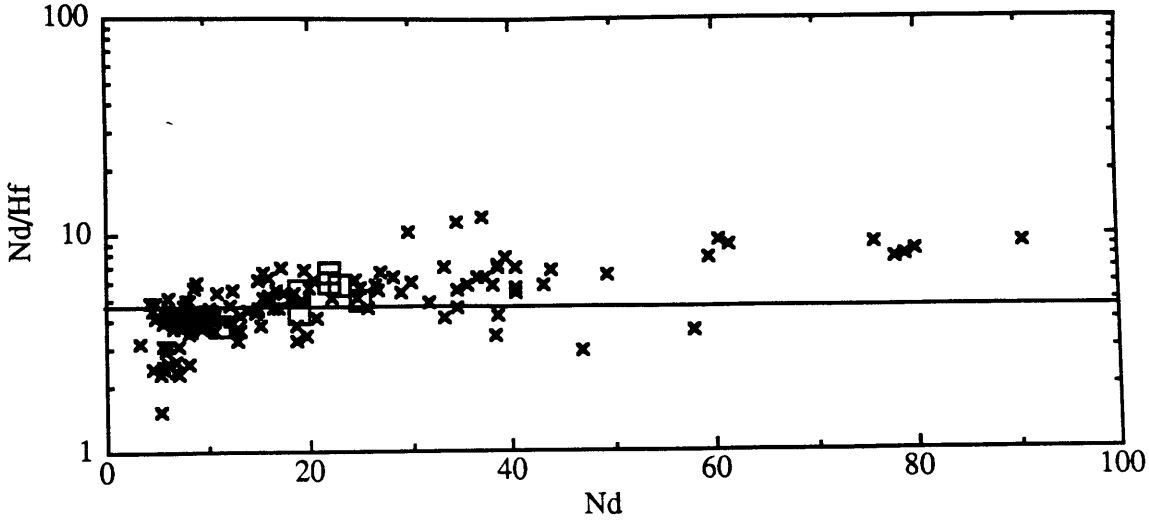
100
10
1
Nd/Hf
0
20
40
60
80
100
Nd

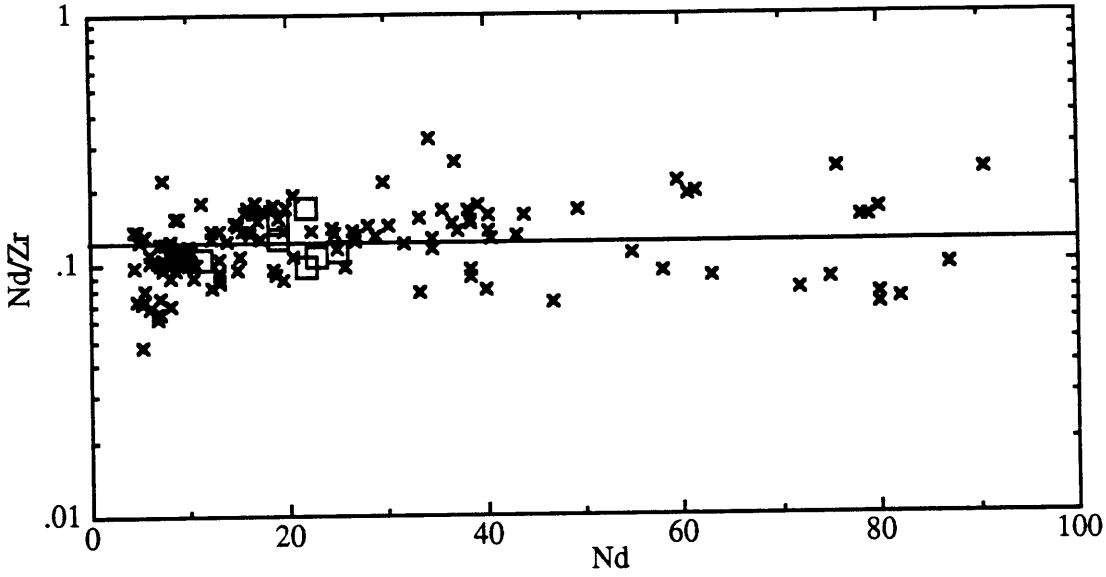
1
.1
.01
Nd/Zr
0
20
40
60
80
100
Nd

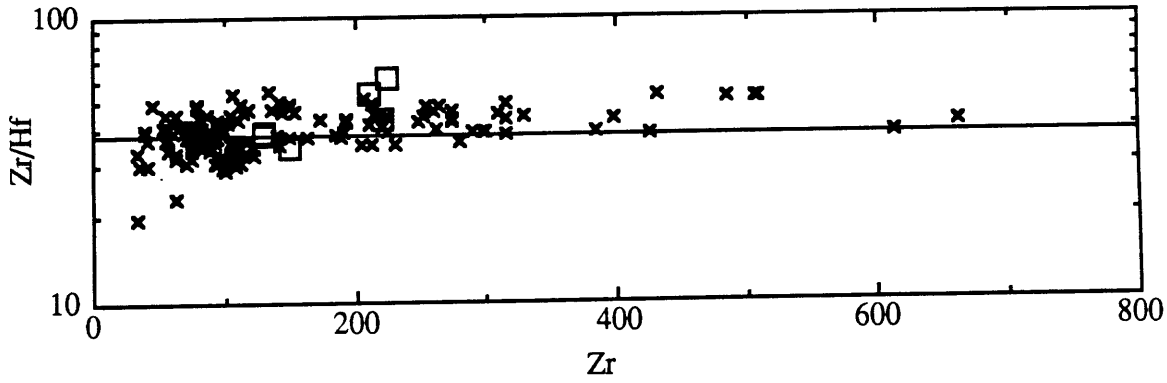
100
10
Zr/Hf
0
200
400
600
800
Zr

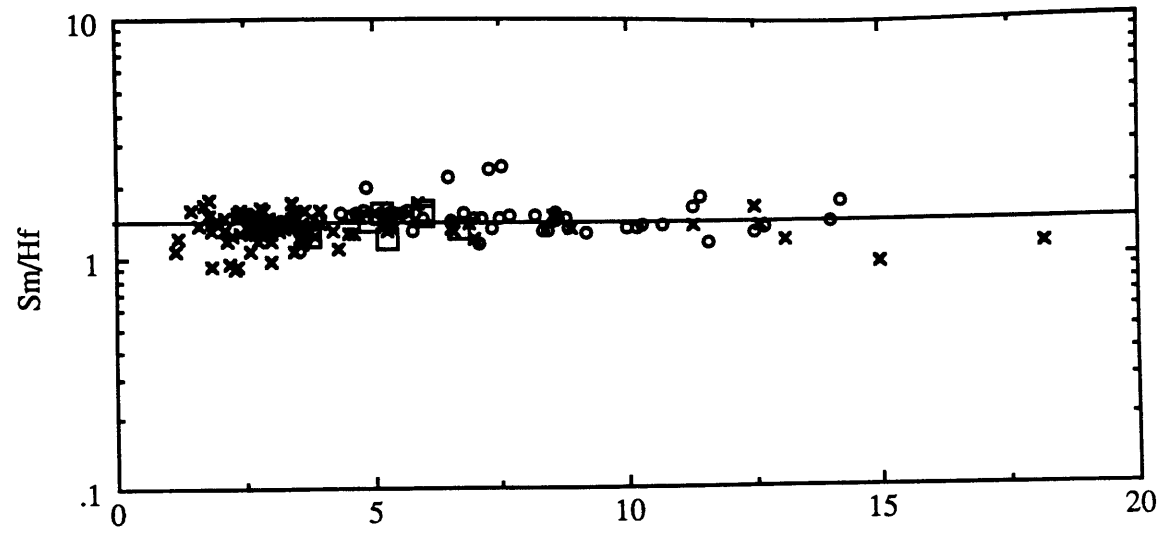
10
1
.1
Sm/Hf
0
5
10
15
20
Sm

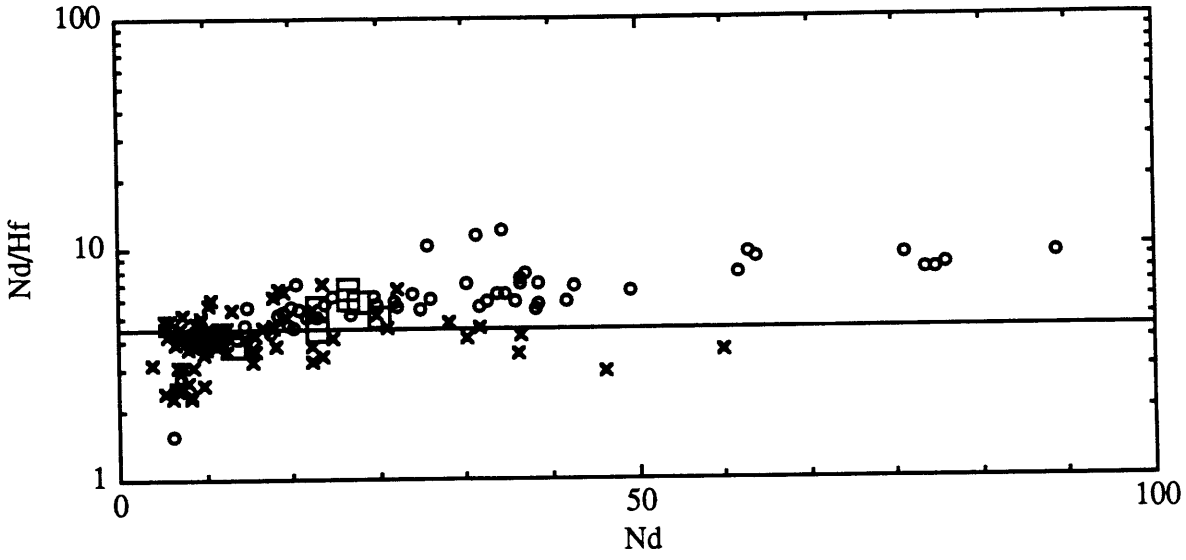
100
10
1
Nd/Hf
0
50
100
Nd

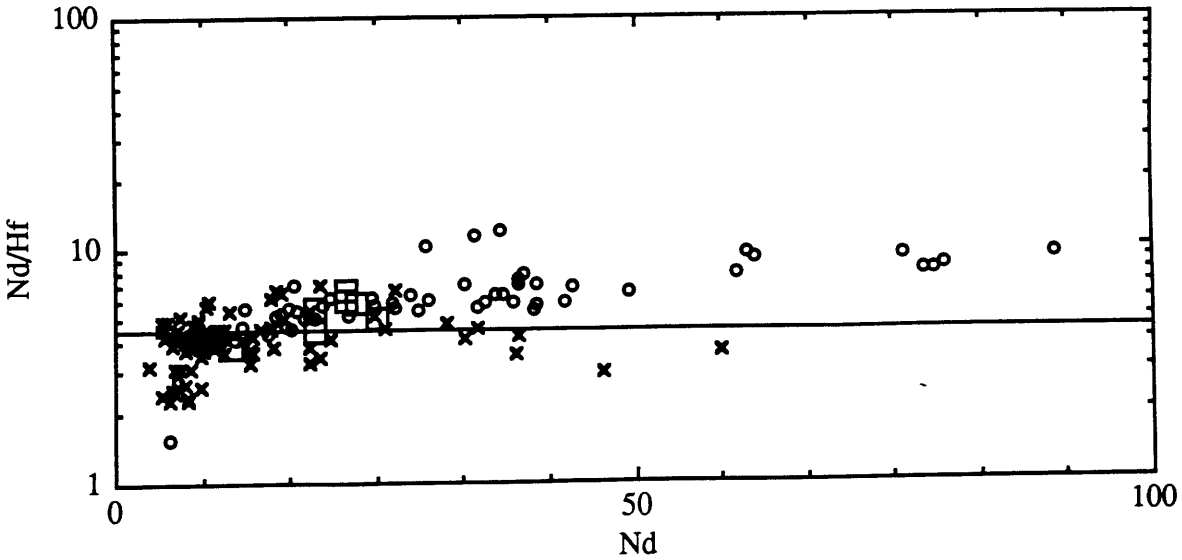
100
10
1
Nd/Hf
0
50
100
Nd

average data set of Irving and Frey (1984), Schnetzler and Philpotts (1970), the experimental data of Dunn (1987), Fujimaki et al. (1984), and Grutzeck et al. (1974). For Ti the above data sets are used combined with the average of the D's derived from the experimental data of Grove and Bryan (1983), Huebner et al. (1976), and Tormey et al. (1987). I contend that, while the absolute value of the D's can be off by more than 20%, the ratio of distribution coefficients for two different elements is essentially constant. As a consequence, trace element ratios constrain the models better than concentrations, and I will thus restrict my discussion largely to trace element ratios.

The second way of determining relative distribution coefficients is with so-called spidergrams. The spidergram approach was pioneered by Sun et al. (1979) and Wood (1979). On a spidergram, the elements are arranged according to increasing compatibility (to the right) in the system anhydrous spinel lherzolite-melt; and the order is such that MORBs form a fairly smooth pattern on a spidergram. A smooth pattern is defined as a pattern without any local minima and maxima, i.e., the third derivative of the trace element pattern always equals zero. A simpler and more straight forward method was explained by Hofmann (1988), using what I propose to call Hofmann-diagrams. These type of diagrams plot concentration of element X versus the concentration ratio of incompatible elements X and Y for MORB and OIB (Hofmann, 1988; Newsom et al., 1986). A horizontal line on this diagram is interpreted to mean similar incompatibilty for element X and Y in the system peridotite-melt over a wide range of melt fractions (Hofmann, 1988). Fig. 2.3 shows that in MORB and OIB Zr and Hf are intermediate in incompatibility between Sm and Nd. Using this method Zr and Hf plot between Sm and Nd, Ti between Eu and Tb, and Sr between Ce and Nd on a.spidergram. This order is the same as the order of Pegram (1986) and Sun et al. (1979). Within the limits of the analytical precision, Zr and Hf behave similarly and I will plot Zr and Hf at the same position on a spidergram. I will use the one element as a substitute for the other wherever necessary.The normalization values are also an important factor in the determining the shape of the trace elements pattern, and a large number of normalizations and element order is in current use (Pegram, 1986;

Saunders, 1987; Sun et al., 1979; Tarney et al., 1981; Thompson et al., 1983; Wood, 1979). Since the order of elements is determined (with Hofmann diagrams), the normalization can be independent of the order of the elements. I choose the simplest normalization possible: average C-1 chondrite. The advantage of this normalization is that it invokes the least number of assumptions. Furthermore, the trace element ratios of this estimate are similar to our best current estimate of BE satisfying a large range of geochemical parameters (Hart and Zindler, 1988). Any deviation observed on a spidergram is a deviation from C-1 and is then assumed to be a fractionation (differentiation) process that happened in the last 4.55 Ga. The C-1 normalization factors are those published by Anders and Grevesse (1989), with slight changes for Hf and Sr. For Hf the Lu/Hf ratio of Beer et al. (1984) is used, with Lu=0.0243 ppm (Anders and Grevesse, 1989). For Sr an average of Anders and Grevesse (1989) and Beer et al. (1984) is taken. Both evaluations have their merit. These C-1 normalizing values are tabulated in Table 2.1. In this chapter I will discuss the variations and differences between sample sets, thereby reducing the importance of the normalization.

For MORBs, which are thought to be formed by melting of anhydrous spinel lherzolite (Dick and Fisher, 1984; Elthon, 1988; Falloon and Green, 1987), any deviation from a smooth pattern on a spidergram indicates either non-smooth source characteristics or different residual phases (i.e. different from 4-phase spinel lherzolite).

2.2.1 Garnet distribution coefficients.

Only three studies of garnet-melt distribution coefficients for REE are known: Fujimaki et al. (1984), Irving and Frey (1978) and Shimizu and Kushiro (1975). The Patagonian data set, which includes garnet lherzolites and eclogites, allows assessment of the distribution coefficients between garnet and clinopyroxene of the REE and HFSE (Fig. 2.4). Since clinopyroxene-melt D's are known, garnet-melt D's can then be calculated. Compared with the data of Shimizu (1975) and Shimizu and Allegre (1978) on coexisting garnets and

Figure 2.4

Garnet- clinopyroxene distribution coefficients from garnet lherzolites and eclogites from Pali, Aike, Patagonia. A. D's for garnet bearing xenoliths. B. D's for garnet bearing xenoliths including eclogites.

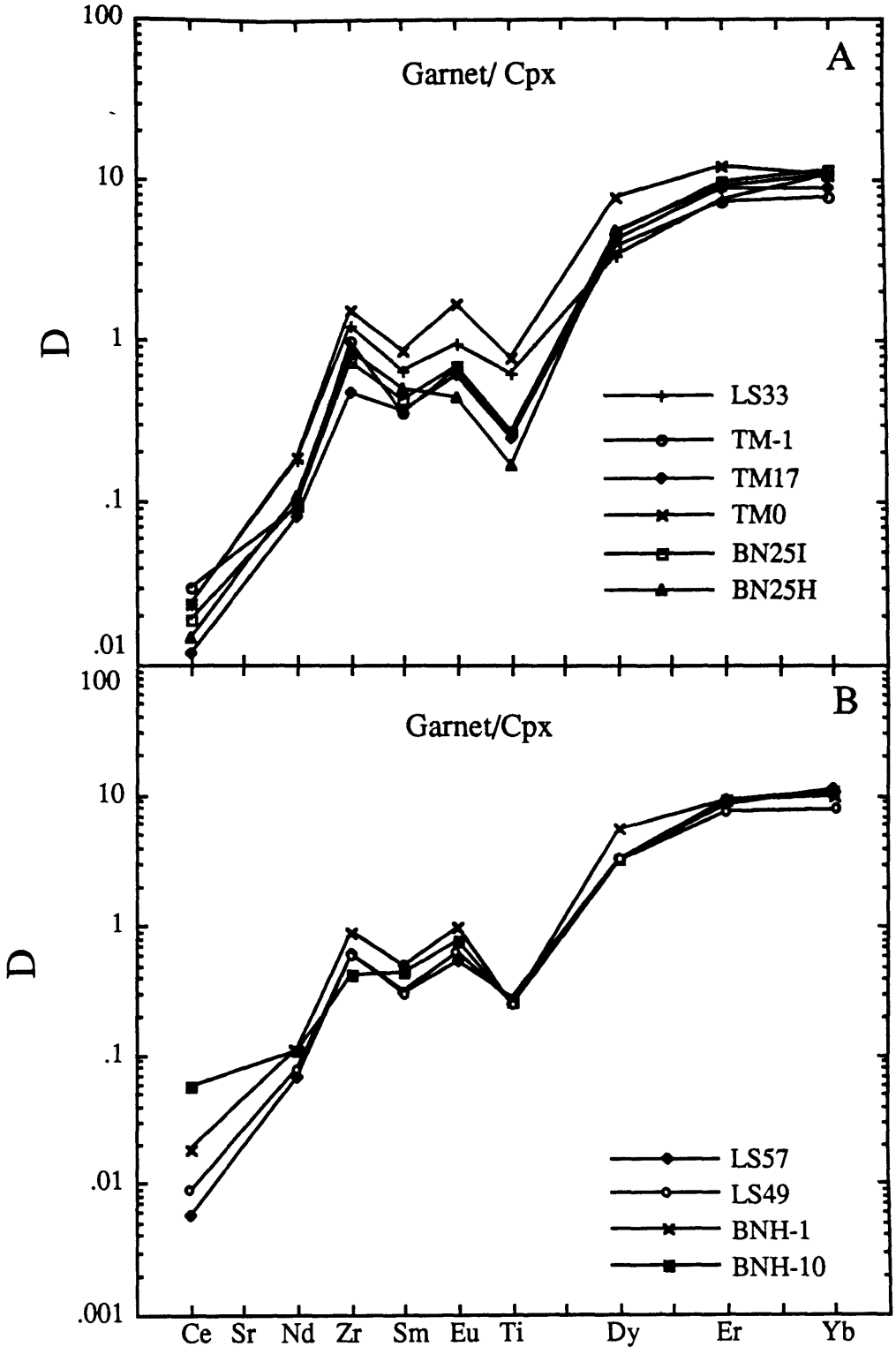
A
Garnet/ Cpx
D
100
10
1
.1
.01
LS33
TM-1
TM17
TM0
BN25I
BN25H
B
Garnet/Cpx
D
100
10
1
.1
.01
.001
LS57
LS49
BNH-1
BNH-10
Ce
Sr
Nd
Zr
Sm
Eu
Ti
Dy
Er
Yb

Figure 2.5
Mineral-melt distribution coefficient patterns based on the available data. Pattern for amphibole taken from Irving and Frey (1984).

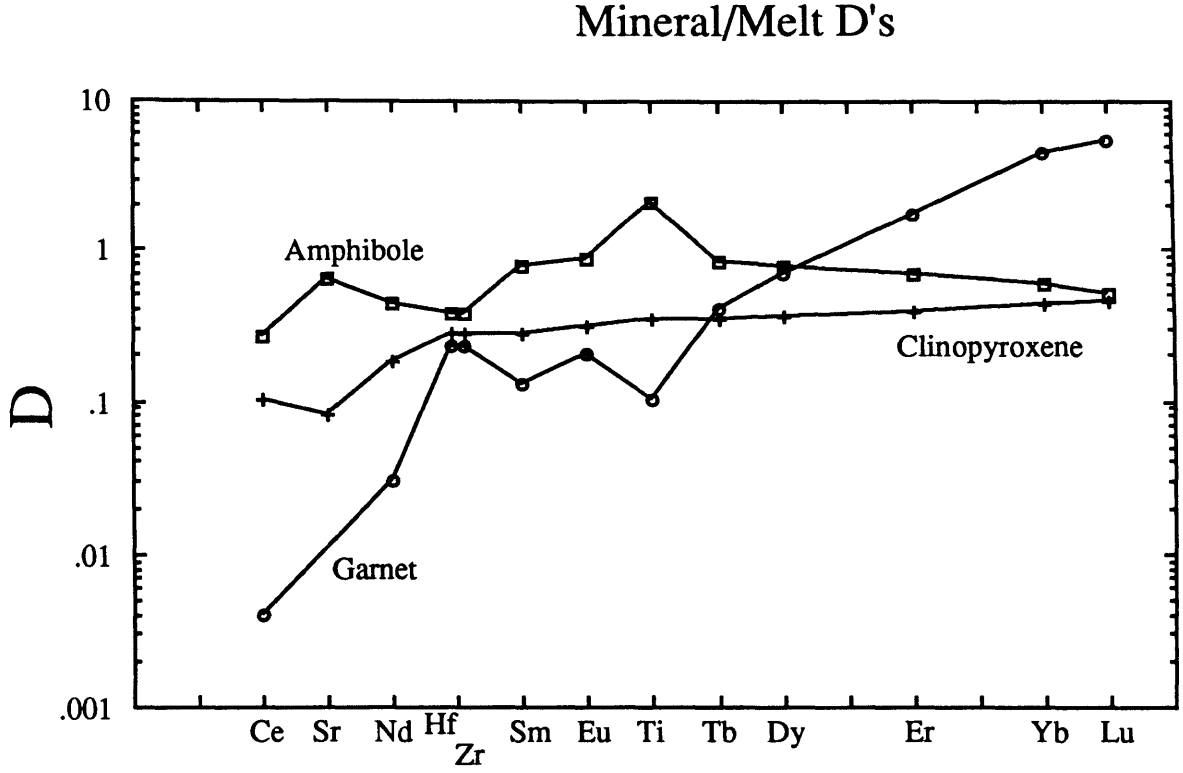
Mineral/Melt D's
10
1
.1
.01
.001
D
Amphibole
Clinopyroxene
Garnet
Ce
Sr
Nd
Hf
Zr
Sm
Eu
Ti
Tb
Dy
Er
Yb
Lu

clinopyroxenes, the Patagonian garnet/cpx D's are generally lower. Except for Ti, however, the distribution coefficient patterns display parallel patterns. The Ti distribution in garnet is important for the generation of HFSE depletions or enrichments. The Patagonian data set indicates, $D_{Ti}<D_{Eu}$ and D_{Dy}, while Shimizu's data set indicates $D_{Ti}>D_{Eu}$ and $D_{Ti}\approx D_{Dy}$. A literature survey on coexisting garnets and clinopyroxenes in mantle nodules leads to a confused picture (Ehrenberg, 1979; Harte et al., 1987; MacGregor, 1979; Reid et al., 1975; Shee and Gurney, 1979). D_{Ti} between garnet and clinopyroxene varies between 0.1 to 4. No obvious correlation between Mg#, P, T or other characteristics is found. The occurrence of zonation and inhomogeneity between grains (Boyd and Finger, 1975; Shimizu and Allegre, 1978; Smith and Boyd, 1987) in some of the South African xenoliths add another complexity in the assessment of the distribution data. The homogeneity of Patagonian samples allows assessment of the garnet-cpx D's. The calculated garnet-melt distribution coefficients, are in agreement with the data of Fujimaki et al. (1984) and Irving and Frey (1978) (Fig. 2.2). The Patagonian data set is taken as equilibrium garnet-clinopyroxene partitioning, and is the only natural data available.

Fig. 2.4 shows the garnet-clinopyroxene partition coefficients. The patterns of the individual samples are parallel, although the total variation is approximately a factor of 3. The data do not allow assessment of the absolute levels of D's; however partition coefficient ratios can be derived accurately. With the use of the clinopyroxene-melt D's from Table 2.1 the garnet/melt D-pattern in Fig. 2.2 was constructed. The D's obtained agree well with the data of Fujimaki and with other estimates of garnet-melt D's for the REE (Frey et al., 1978).

Based on the above D's, garnet can significantly fractionate the REE from the HFSE. The capability of garnet to fractionate the LREE from the HREE is well known and is also reflected in the Patagonian data set. Melt generated in the garnet stability field has lower Zr/Zr* than its source and a higher Ti/Ti*. Good correlations between Zr/Zr* and Ti/Ti* and Ce/Yb are thus expected if garnet is one of the major phases fractionating HFSE from REE. Of the known high pressure

major mantle phases, majorite and perovskite (Ringwood, pers. comm; Kato et al., 1987; Kato et al., 1988) also appear capable of fractionating the HFSE from the REE, and these high pressure phases prefer Zr, Hf, and Ti over REE. Fig. 2.5 compares the D's for garnet, clinopyroxene, and amphibole, showing their effect on spidergrams.

2.3 Individual localities.

First I will describe and present the data for the different xenolith localities. In selecting the different localities, I tried to cover as wide a range of tectonic situations as possible. Tectonic setting is determined by the location of the xenolith field, and not inferred from the chemical characteristics of the xenoliths. The data presented in the tables are the averages of analyses of 3-4 different grains in each sample. I was unable to detect either zoning or large differences within the anhydrous samples. Some of the H_2O-bearing samples do show variations in REE and trace element content. These variations are always correlated with differences in concentration of all the trace elements, while the shape of the pattern on a spidergram for the different spot analyses remains the same. It must be stressed that the majority (90%) of the samples in this study are homogeneous. The data presented in Tables 2.2 through 2.8 and Fig. 2.6 through 2.16 represent the results of analyses of over 400 individual spots.

2.3.1 Carpathians.

A detailed discussion of the tectonic setting may be found in Chapter 1 and references therein. The data for the clinopyroxenes of Carpathian xenoliths are shown in Table 2.2 and Fig. 2.6A. The xenoliths are hosted by alkali basalts, which are at most 10 Ma younger than a previous episode of calc-alkaline volcanism. The close spatial and temporal relationship between the alkaline and calc-alkaline volcanism indicates the xenoliths are from a sub-arc type mantle. The xenoliths, all from Nograd county, are small (1-2cm), all anhydrous and contain at most 8% of modal diopside. Samples 147

Table 2.2
Trace element data for clinopyroxenes from the Carpathians, Hungary.
Concentrations are in ppm

Sample	Szt-1002	Bo-1002	147	148
Abundances				
Ce	1.17	3.20	2.16	7.88
Sr	25.5	63.8	32.5	39.6
Nd	1.23	3.11	1.92	5.03
Hf				
Zr	7.0	5.2	27.8	27.4
Sm	0.60	0.89	0.94	1.53
Eu	0.26	0.36	0.44	0.62
Ti	1570	113	2006	2529
Tb				
Dy	1.59	1.62	2.13	2.35
Er	1.10	0.16	1.42	1.65
Yb	1.16	0.10	1.18	1.34
Normalized abundances				
Ce	1.94	5.31	3.58	13.07
Sr	3.45	8.62	4.39	5.35
Nd	2.72	6.88	4.25	11.13
Hf	0.00	0.00	0.00	0.00
Zr	1.78	1.32	7.06	6.95
Sm	4.08	6.05	6.39	10.41
Eu	4.64	6.43	7.86	11.07
Ti	3.60	0.26	4.60	5.80
Tb	0.00	0.00	0.00	0.00
Dy	6.49	6.61	8.69	9.59
Er	6.86	1.00	8.86	10.29
Yb	7.16	0.62	7.28	8.27
Zr/Zr*	0.522	0.204	1.326	0.646
Ti/Ti*	0.685	0.040	0.565	0.548

Figure 2.6
Spidergrams for clinopyroxenes from lherzolite xenoliths Carpathians (A) and from Nunivak, Alaska (B).

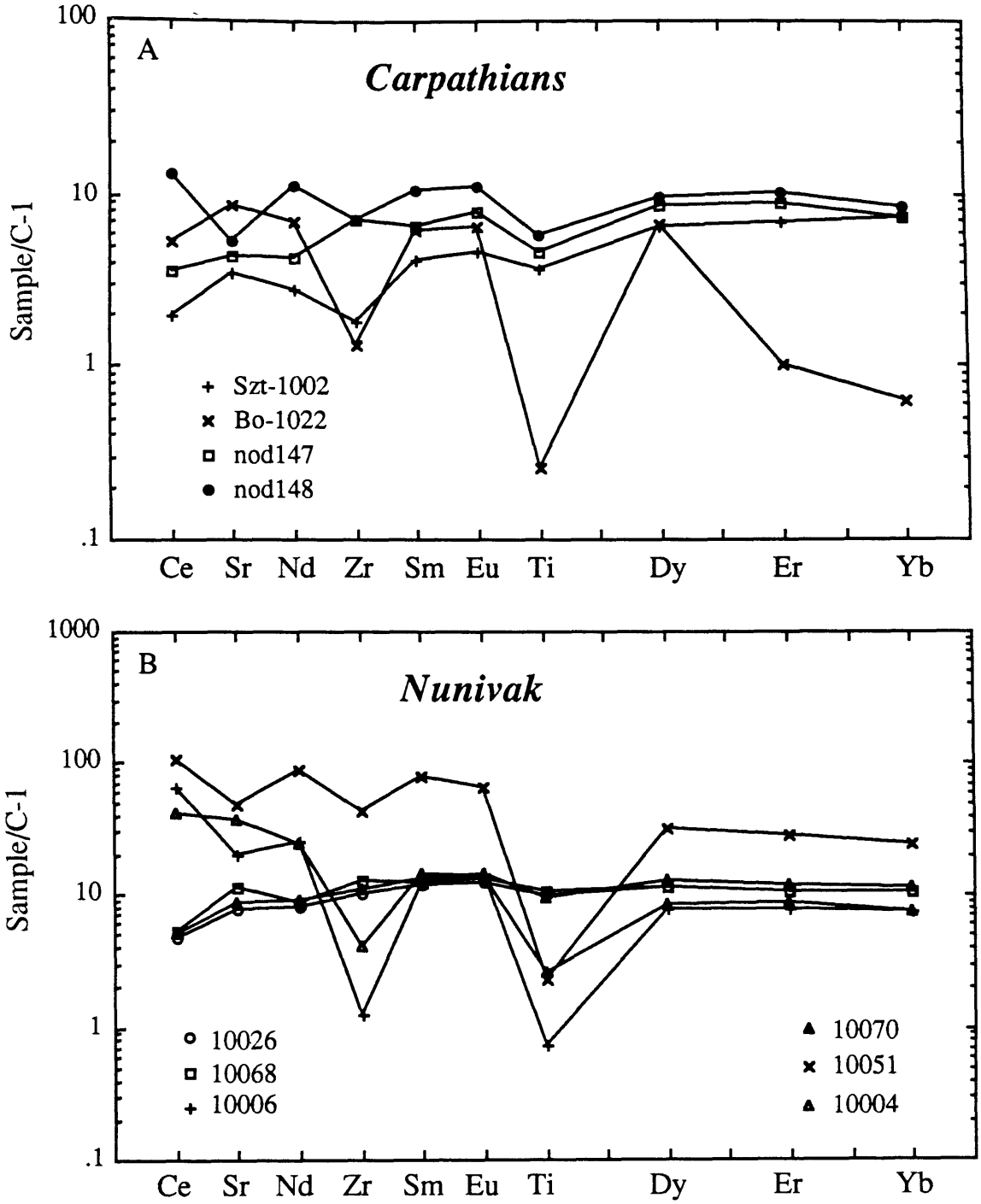
A
Carpathians
Sample/C-1
100
10
1
.1
+ Szt-1002
× Bo-1022
□ nod147
● nod148
Ce Sr Nd Zr Sm Eu Ti Dy Er Yb
B
Nunivak
Sample/C-1
1000
100
10
1
.1
○ 10026
□ 10068
+ 10006
▲ 10070
× 10051
▲ 10004
Ce Sr Nd Zr Sm Eu Ti Dy Er Yb

Table 2.3
Trace element analyses for clinpyroxenes from lherzolites from Nunivak, Alaska

Sample	10026	10068	10070	10004	10051*	10006*
Abundances in ppm						
Ce	2.87	3.15	3.06	24	64	38.685
Sr	57	83	63	272	351	146.3
Nd	3.53	3.94	3.96	10.8	40	11.1
Zr	40	49	42	16	170	4.9
Sm	1.69	1.77	1.95	2.07	11.6	1.76
Eu	0.69	0.73	0.78	0.76	3.60	0.78
Ti	4186	4524	4020	1090	1003	318
Dy	2.73	2.76	3.13	2.03	7.67	1.89
Er	1.69	1.66	1.84	1.38	4.42	1.23
Yb	1.71	1.70	1.80	1.21	3.86	1.18
Normalized abundances						
Ce	4.8	5.2	5.1	40	105	64
Sr	7.7	11.2	8.6	37	47	20
Nd	7.8	8.7	8.8	24	88	25
Zr	10.1	12.4	10.7	4.0	43	1.24
Sm	11.5	12.0	13.3	14.1	79	12.0
Eu	12.2	13.0	14.0	13.5	64	14.0
Ti	9.6	10.4	9.2	2.5	2.3	0.7
Dy	11.2	11.2	12.8	8.3	31	7.7
Er	10.5	10.3	11.5	8.6	28	7.7
Yb	10.5	10.5	11.1	7.5	24	7.3
Zr/Zr*	1.048	1.198	0.972	0.212	0.516	0.068
Ti./Ti*	0.846	0.855	0.743	0.254	0.053	0.076

* means xenolith contains amphibole

and 148 contain 4 and 2% modal diopsides and are harzburgites. Three of the 4 xenoliths have Zr/Zr*<1 and all have Ti/Ti*<1. The Carpathian xenoliths show positive correlations of Ti/Zr with Ti/Ti*, and Sr/Nd with Zr/Zr*. Zr/Zr* and Ti/Ti* are not correlated, indicating decoupling of Ti and Zr.

2.3.2 Nunivak.

Six samples, donated by M.F. Roden from Nunivak were analyzed. Results are in Table 2.3 and are shown in Fig. 2.6B. Nunivak basanites are sampling subcontinental mantle; their location close to the Aleutian arc allows the interpretation that the xenoliths are from a sub-arc mantle. Samples are described by Roden (1982). Samples 10051 and 10006 contain amphibole. Trace element patterns in the lherzolites are flat to LREE enriched and 3 lherzolites show large HFSE depletions. The trace elements of the 6 samples from Nunivak show reasonably good correlations between Ce/Yb and Ti/Zr and Sm/Nd. Ti/Ti* and Zr/Zr* are also coupled, whereby the two clinopyroxenes from the hydrous samples have the lowest Zr/Zr* and Ti/Ti* and high Ce/Yb. The variations in trace elements have been attributed to hydrous fluid metasomatizing the mantle beneath Nunivak (Roden et al., 1984a). The Nunivak data indicate that hydrous metasomatism will have Ti/Ti*<1 and Zr/Zr*<1 while being LREE enriched. The range in isotopic compositions of Nunivak Island basalts is smaller than the range in isotopic compositions of the clinopyroxenes in the lherzolite xenoliths (Roden et al., 1984a).

2.3.3 Kilbourne Hole and Potrillo Maar.

Fifteen samples were analyzed from Potrillo Maar and Kilbourne Hole, New Mexico. Samples are on loan from E. Jagoutz. Analyses are listed in Table 2.3 and shown in Fig. 2.7 A, B. Potrillo Maar and Kilbourne Hole are located in the Rio Grande rift area. The xenoliths are from sub-continental lithosphere which is undergoing extension. All the analyzed samples are anhydrous harzburgites and lherzolites. In general, Kilbourne Hole is known for its large percentage of fertile

Table 2.4A
Trace elements abundances for diopsides from lherzolites from Kilbourne Hole, New Mexico.

Sample	KBH 17	KBH 24	KBH 26	KBH 40	KBH 138	KBH8/80	KBH 8/81	KBH 9/48
Abundances in ppm								
Ce	1.98	0.84	1.23	2.65	2.40	6.50	13.2	1.73
Sr	31.0	20.6	28.5	54.0	32.3	53.4	87.8	39.0
Nd	2.11	1.96	2.65	3.61	3.75	6.12	8.41	2.55
Zr	23.8	18.8	24.4	38.5	32.2	30.2	30.0	15.0
Sm	1.00	1.27	1.52	1.64	1.95	2.33	2.77	1.44
Eu	0.40	0.56	0.71	0.78	0.89	0.80	0.97	0.64
Ti	1824	3126	3532	3226	3662	3319	3139	3083
Dy	1.91	2.48	3.01	3.11	3.19	2.58	3.16	2.54
Er	1.26	1.48	2.03	2.10	1.92	1.43	2.02	1.49
Yb	1.25	1.47	1.81	1.73	2.02	1.51	1.83	1.55
Normalized abundances								
Ce	3.29	1.39	2.04	4.39	3.98	10.8	21.9	2.87
Sr	4.19	2.78	3.85	7.30	4.36	7.22	11.9	5.27
Nd	4.67	4.34	5.86	7.99	8.30	13.5	18.6	5.64
Zr	6.04	4.77	6.20	9.77	8.17	7.66	7.61	3.81
Sm	6.78	8.62	10.34	11.16	13.3	15.9	18.8	9.76
Eu	7.09	9.95	12.68	13.93	15.9	14.3	17.3	11.4
Ti	4.18	7.17	8.10	7.40	8.40	7.61	7.20	7.07
Dy	7.78	10.1	12.3	12.7	13.0	10.5	12.9	10.4
Er	7.84	9.26	12.7	13.1	12.0	8.94	12.6	9.30
Yb	7.72	9.07	11.2	10.7	12.5	9.34	11.3	9.57
Zr/Zr*	1.055	0.737	0.765	1.020	0.758	0.522	0.406	0.494
Ti/Ti*	0.572	0.717	0.646	0.547	0.562	0.582	0.454	0.638

Table 2.4B
Trace element analyses for Potrillo Maar, New Mexico

Sample	POT 31	POT 36	POT 91	Pot108	POT 149	POT 124	POT 136
Abundances in ppm							
Ce	5.86	21.68	3.70	5.89	2.81	20.1	2.28
Sr	64.6	1.8	0.4	37.4	29.9	62.3	37.5
Nd	3.49	17.96	4.20	3.85	1.71	16.59	3.02
Zr	35.2	74.4	60.7	22.0	7.1	61.8	30.7
Sm	1.39	5.50	1.92	1.59	0.57	4.96	1.59
Eu	2.94	2.12	0.86	0.60	0.21	1.86	0.67
Ti	2947	16481	6671	1557	831	9461	5188
Dy	2.18	5.93	2.57	2.39	0.75	4.78	2.65
Er	1.22	3.60	1.36	1.56	0.35	2.77	1.55
Yb	1.17	3.34	1.24	1.55	0.36	2.43	1.64
Normalized abundances							
Ce	9.71	36.0	6.14	9.77	4.65	33.4	3.78
Sr	8.73	0.24	0.05	5.05	4.04	8.41	5.07
Nd	7.72	39.7	9.29	8.52	3.79	36.7	6.68
Zr	8.93	18.9	15.4	5.58	1.80	15.7	7.79
Sm	9.43	37.4	13.1	10.8	3.85	33.7	10.8
Eu	52.5	37.9	15.4	10.6	3.68	33.2	12.0
Ti	6.76	37.8	15.3	3.57	1.91	21.7	11.9
Dy	8.88	24.2	10.5	9.75	3.07	19.5	10.8
Er	7.64	22.5	8.48	9.75	2.16	17.3	9.67
Yb	7.20	20.6	7.65	9.58	2.20	15.0	10.1
Zr/Zr*	1.042	0.489	1.378	0.579	0.472	0.445	0.891
Ti/Ti*	0.178	1.135	1.114	0.346	0.549	0.758	1.027

Figure 2.7
Spidergrams for clinopyroxenes from anhydrous spinel lherzolites from Kilbourne Hole (A) and Potrillo Maar (B).

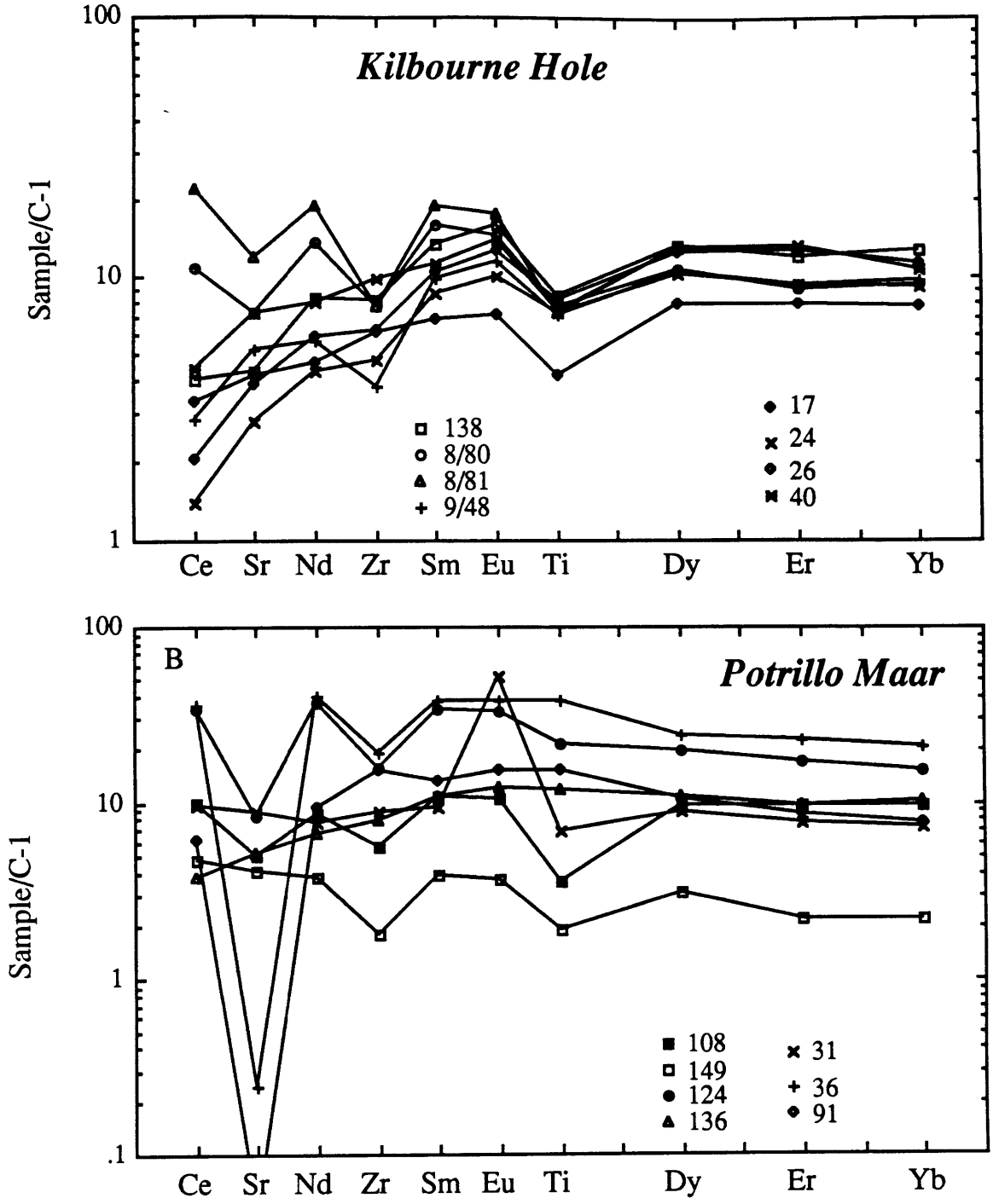
Kilbourne Hole
Sample/C-1
100
10
1
138
8/80
8/81
9/48
17
24
26
40
Ce Sr Nd Zr Sm Eu Ti Dy Er Yb
B
Potrillo Maar
Sample/C-1
100
10
1
.1
108
149
124
136
31
36
91
Ce Sr Nd Zr Sm Eu Ti Dy Er Yb

lherzolites (Carter, 1970). Some of the lherzolites are similar in composition to primitive mantle (Hart and Zindler, 1986; Jagoutz et al., 1979b), which initiated our interest in the Kilbourne Hole xenoliths. Lherzolites from both Kilbourne Hole and Potrillo Maar are brought to the surface by alkali basalts. Except for two samples, all Kilbourne Hole samples are slightly LREE depleted, i.e., $Ce_n/Yb_n<1$. All samples do show Ti/Ti*<1, and 4 out of the 9 samples have Zr/Zr*<1. The occurrence of HFSE depleted compositions at Kilbourne Hole was also reported by Roden et al. (1988). Samples from Potrillo Maar have more or less flat REE patterns. Samples POT31, POT36, and POT124 belong to Group II lherzolites (Frey and Prinz, 1978). All Potrillo Maar samples are anhydrous, 4 out of 7 have Zr/Zr*<1, and only three are depleted in Ti. Some samples show extreme depletion in Sr, down to 0.4ppm!

Kilbourne Hole xenoliths display a larger variation in the LREE than in the HREE. Potrillo Maar xenoliths show similar variations in LREE and HREE, and the spider patterns are roughly parallel. The clinopyroxenes in both Potrillo Maar and Kilbourne Hole show a positive correlation of Sr/Nd with Zr/Zr*. High Sr/Nd ratios, and Zr/Zr*<1 are characteristics of subduction related, calc-alkaline lavas (Gill, 1981; Hickey et al., 1986; Salters, 1987). The Kilbourne Hole and Potrillo Maar samples show a correlation in Sr/Nd with Zr/Zr* which is opposite to that of calc-alkaline lavas. High Sr/Nd might be caused by addition of a slab component (Tera et al., 1986). The variations in the New Mexico xenoliths indicate that the depletions in HFSE are not simply related to the subduction process (Salters, 1987). In general Kilbourne Hole and Potrillo Maar samples show an increase in Ti/Ti* with increasing Ti/Zr and Ti content. Also, the LREE depleted samples have lower Zr/Zr* than the LREE enriched samples. The combination of these variations cannot be explained by simple melt depletion processes.

2.3.4 Patagonia.

A large number of xenoliths from Patagonia (collected by C.R. Stern) have been analyzed for major and trace elements. However, a

Figure 2.8

Map with sample localities of xenolith occurrence in southern South America, as adapted from Stern et al. (1986).

1= Comallo, Argentina; 2= Praguaniyue, Argentina; 3= Lago Colhue Huapi; 4= Meseta Buenos Aires; 5= Mesata de la Muerte; 6= Meseta Las Viscaches; 7= Pali Aike. Numbers for the sample localities are the same as the numbers occurring in Table 2.5.

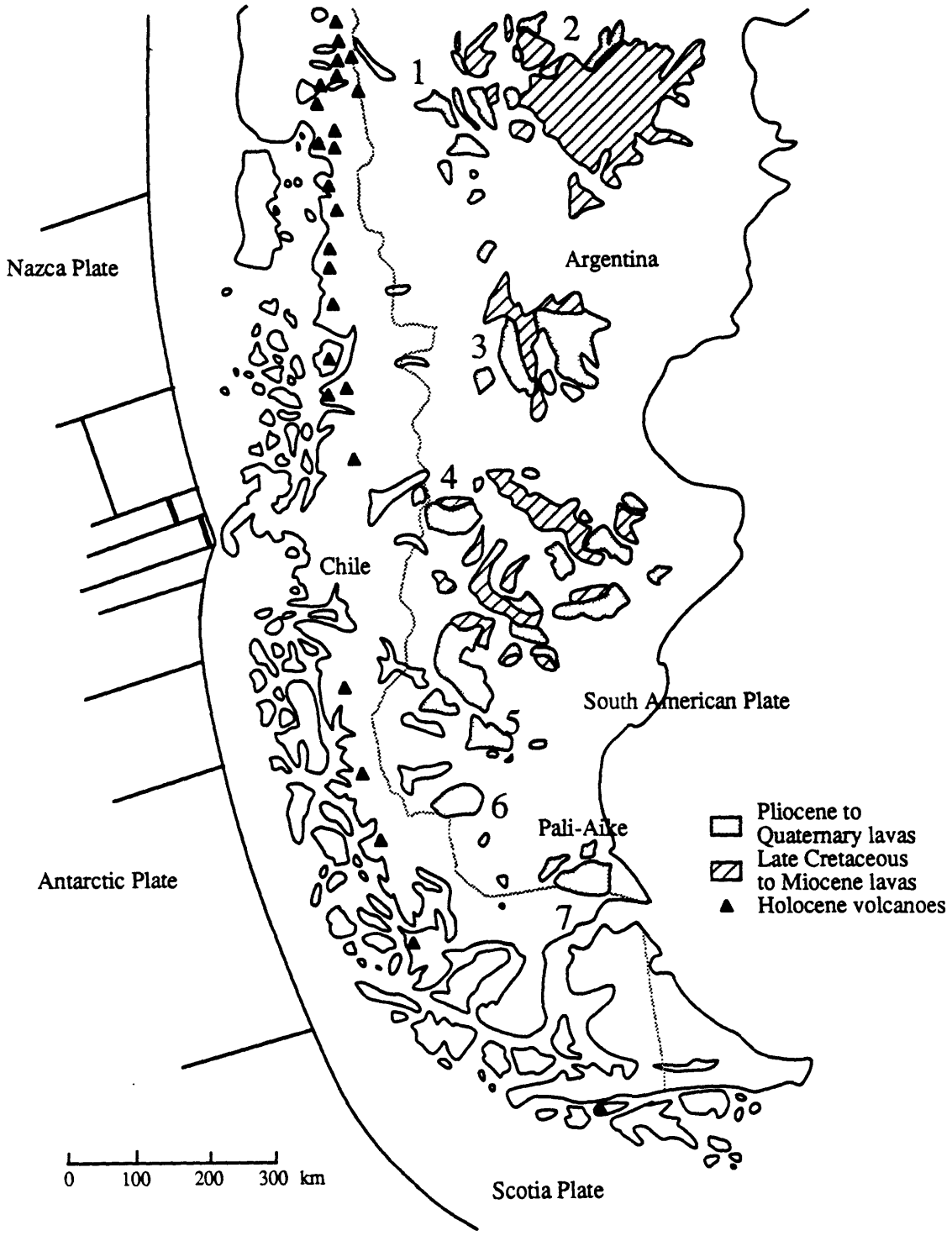
1
2
3
4
5
6
7
Nazca Plate
Argentina
Chile
South American Plate
Pali-Aike
Antarctic Plate
Scotia Plate
Pliocene to Quaternary lavas
Late Cretaceous to Miocene lavas
Holocene volcanoes
0 100 200 300 km

Table 2.5
Trace element abundances in garnet and clinopyroxene from garnet bearing xenoliths from Patagonia, Chili.

Sample	LS33 Cpx	LS33 Gar	LS57Cpx	LS57Gar	LS49 Cpx	LS49 Gar	TM-1Cpx	TM-1Gar	TM17 Cpx	TM17 Gar
Abundances in ppm										
Ce	3.79	0.090	3.61	0.020	6.85	0.060	1.71	0.050	5.16	0.060
Sr	75.5		82.0		67.6		71.4		41.1	
Nd	3.58	0.630	6.32	0.420	6.78	0.520	3.55	0.320	3.95	0.320
Zr	23.4	28.5	68.0	41.5	70.1	41.7	59.9	58.2	24.7	11.3
Sm	1.24	0.783	2.01	0.616	2.34	0.753	1.46	0.513	1.38	0.500
Eu	0.435	0.413	0.704	0.379	0.739	0.462	0.542	0.355	0.510	0.310
Ti	2472	1543	3244	915	4415	1147	4264	1070	2229	544
Dy	0.927	3.13	1.24	3.95	1.168	3.73	0.915	3.48	0.870	3.65
Er	0.308	2.30	0.376	3.18	0.250	2.28	0.325	2.40	0.330	2.87
Yb	0.252	2.72	0.345	3.83	0.220	2.31	0.344	2.69	0.370	3.28
Normalized abundances										
Ce	6.29	0.15	5.99	0.03	11.4	0.10	2.84	0.08	8.56	0.10
Sr	10.2		11.1		9.14		9.65		5.55	
Nd	7.92	1.39	14.0	0.93	15.0	1.15	7.85	0.71	8.74	0.71
Zr	5.94	7.23	17.3	10.5	17.8	10.6	15.2	14.8	6.26	2.88
Sm	8.40	5.33	13.7	4.19	15.9	5.12	9.90	3.49	9.39	3.40
Eu	7.77	7.38	12.6	6.77	13.2	8.25	9.68	6.34	9.11	5.54
Ti	5.67	3.54	7.44	2.10	10.1	2.63	9.78	2.45	5.11	1.25
Dy	3.78	12.8	5.07	16.1	4.77	15.2	3.73	14.2	3.55	14.9
Er	1.92	14.3	2.35	19.8	1.56	14.2	2.03	15.0	2.06	17.9
Yb	1.56	16.8	2.13	23.6	1.36	14.3	2.12	16.6	2.28	20.2
Mode in %	15	10	15	10	70	30	10	15	20	10

Table 2.5 cont'd

Sample	TM0 Cpx	TM0 Gar	BN25ICpx	BN25IGar	BN25HCpx	BN25HGar	BNH-1Cpx	BNH-1Gar	BNH10Cpx	BNH10Gar
Abundances										
Ce	5.5	0.130	3.44	0.064	4.15	0.061	7.26	0.136	3.36	0.190
Sr	46.5		32.7		38.5		64.7		25.7	
Nd	4.20	0.780	3.52	0.331	3.32	0.351	5.22	0.595	4.34	0.473
Zr	20.8	31.9	107	77.6	121	103	12.1	10.9	155	65.1
Sm	1.500	1.260	1.504	0.642	1.42	0.699	1.356	0.666	2.24	0.960
Eu	0.540	0.890	0.672	0.452	1.15	0.507	0.438	0.418	0.859	0.666
Ti	2509	1934	6448	1765	5690	943	2592	656	5102	1260
Dy	0.920	7.13	1.146	5.33	1.05	5.01	0.517	2.79	1.814	5.62
Er	0.340	4.11	0.434	4.27	0.615	5.67	0.202	1.840	0.680	5.06
Yb	0.390	4.20	0.455	5.11	0.639	6.80	0.200	1.950	0.761	5.80
Normalized abundances										
Ce	9.07	0.22	5.70	0.11	6.88	0.10	12.0	0.23	5.57	0.32
Sr	6.28		4.42		5.21		8.75		3.47	
Nd	9.29	1.73	7.78	0.73	7.35	0.78	11.6	1.32	9.61	1.05
Zr	5.27	8.09	27.1	19.7	30.7	26.1	3.06	2.76	39.2	16.5
Sm	10.2	8.57	10.2	4.37	9.68	4.76	9.23	4.53	15.3	6.53
Eu	9.64	15.9	12.0	8.08	20.5	9.05	7.82	7.46	15.3	11.9
Ti	5.75	4.44	14.8	4.05	13.0	2.16	5.94	1.50	11.7	2.89
Dy	3.76	29.1	4.68	22.	4.29	20.5	2.11	11.4	7.40	22.9
Er	2.12	25.6	2.71	27.	3.84	35.4	1.26	11.5	4.24	31.6
Yb	2.41	25.9	2.81	32.	3.95	42.0	1.23	12.0	4.70	35.8
Mode in %	15	15	1	20	2	25	50	10	30	2

Table 2.6
Trace element abundances (ppm) in Patagonian lherzolites, harzburgites, eclogites and pyroxenites

Sample#	LS33	LS57	TM-1	TM17	TM0	BN25I	BN25H	BNH10	53	BN46	BNH-3	TM16
Rocktype	GL	GL	GL*	GL	GL	GHa	GHa	GHa	GOp	GOp	GOp	SpL*
Cpx in %	15	15	15	20	15	1	2	2	-	-	-	15
Abundances												
Ce	2.31	2.17	0.714	3.46	2.80	0.225	0.363	3.16	0.037	0.099	0.061	15.2
Sr	45.3	49.2	28.6	27.4	23.2	1.6	2.9	24.1				96
Nd	2.40	3.96	1.61	2.74	2.49	0.483	0.571	4.10	0.355	0.338	0.387	9.35
Zr	25	57	59	20	26	79	104	149	161	11	113	50
Sm	1.054	1.455	0.890	1.087	1.380	0.683	0.753	2.162	0.639	0.589	0.515	2.42
Eu	0.426	0.574	0.430	0.443	0.715	0.463	0.554	0.847	0.446	0.459	0.373	0.847
Ti	2100	2312	2348	1668	2222	1988	1295	4862	1520	587	1615	3692
Dy	1.808	2.33	2.45	1.797	4.03	5.13	4.72	2.051	4.79	4.07	3.07	1.369
Er	1.104	1.496	1.568	1.177	2.23	4.08	5.29	0.953	3.21	3.00	2.61	0.578
Yb	1.240	1.739	1.749	1.340	2.30	4.89	6.34	1.076	3.49	3.25	3.48	0.549
Normalized abundances												
Ce	3.83	3.61	1.18	5.74	4.64	0.37	0.60	5.24	0.06	0.16	0.10	25.3
Sr	6.12	6.65	3.86	3.70	3.14	0.21	0.39	3.25		0.00	0.00	12.95
Nd	5.31	8.76	3.57	6.06	5.51	1.07	1.26	9.08	0.78	0.75	0.86	20.7
Zr	6.46	14.57	14.94	5.13	6.68	20.1	26.5	37.8	40.8	2.85	28.8	12.66
Sm	7.17	9.90	6.06	7.39	9.39	4.65	5.12	14.70	4.35	4.01	3.50	16.47
Eu	7.61	10.25	7.68	7.92	12.77	8.26	9.90	15.13	7.96	8.19	6.67	15.13
Ti	4.82	5.30	5.38	3.82	5.10	4.56	2.97	11.15	3.49	1.35	3.70	8.47
Dy	7.38	9.49	10.01	7.33	16.43	20.9	19.26	8.37	19.57	16.60	12.53	5.59
Er	6.89	9.33	9.78	7.34	13.88	25.5	33.0	5.95	20.01	18.68	16.25	3.61
Yb	7.65	10.73	10.79	8.27	14.17	30.2	39.2	6.64	21.57	20.07	21.45	3.39
Zr/Zr*	1.035	1.562	3.106	0.763	0.896	7.015	8.294	3.179	15.881	1.198	13.198	0.682
Ti/Ti*	0.639	0.531	0.637	0.495	0.364	0.365	0.228	0.866	0.295	0.122	0.430	0.709
Locality	7	7	7	7	7	7	7	7	7	7	7	7

*means hydrous phase is present
For xenoliths that contain both clinopyroxene and garnet the value reported in this table is the weighted average value for garet and clinopyroxene combined
Numbers in the locality row correspond with the locality numbers in fig.8

Table 2.6 cont'd

Sample#	TM15	MC-1	BN72	LS71	LLS-1	X-3	V8	V9	V11	V13	MBA-1	CH-5
Rocktype	SpL*	SpL*	SpL*	Ha	Ha	Ha*	SpL	SpL	SpL	SpL	SpL	SpL
Cpx in %	15		10	<5	5	<5	<10	<10	<10	<10	10	15
Abundances												
Ce	7.44	8.15	2.72	2.16	3.52	4.23	12.7	0.56	0.03	0.28	7,60	3.62
Sr	47	84	62	59	65.9	81	298	11.9	0.6	4.1	111	49.4
Nd	4.36	5.34	6.249	3.200	4.460	5.317	7.39	0.71	0.16	0.26	3.90	2.900
Zr	71	32	48	28	57	49	72	4.7	0.7	0.9	18	21
Sm	1.707	2.118	2.133	1.219	1.722	1.732	2.60	0.32	0.30	0.22	0.847	1.164
Eu	0.646	0.863	0.779	0.413	0.665	0.603	0.91	0.12	0.15	0.11	0.288	0.525
Ti	2850	3594	1143	475	324	381	3391	221	778	724	671	1917
Dy	1.161	2.32	1.254	0.697	1.067	1.119	3.48	0.41	1.27	0.87	1.103	2.039
Er	0.470	1.017	0.519	0.126	0.438	0.487	1.89	0.26	0.96	0.58	0.642	1.215
Yb	0.473	0.922	0.605	0.153	0.480	0.506	1.90	0.30	1.04	0.68	0.723	1.289
Normalized abundances												
Ce	12.33	13.52	4.51	3.58	5.84	7.01	21.1	0.93	0.05	0.46	12.60	6.00
Sr	6.36	11.34	8.33	8.01	8.90	10.88	40.2	1.61	0.08	0.55	15.00	6.68
Nd	9.64	11.81	13.83	7.08	9.87	11.76	16.35	1.57	0.35	0.58	8.63	6.42
Zr	18.09	8.15	12.11	7.08	14.35	12.32	18.35	1.19	0.18	0.24	4.44	5.28
Sm	11.61	14.41	14.51	8.29	11.71	11.78	17.69	2.18	2.01	1.50	5.76	7.92
Eu	11.53	15.41	13.91	7.38	11.87	10.77	16.25	2.14	2.68	1.96	5.14	9.38
Ti	6.54	8.24	2.62	1.09	0.74	0.87	7.78	0.51	1.78	1.66	1.54	4.40
Dy	4.74	9.45	5.12	2.84	4.35	4.57	14.20	1.67	5.20	3.55	4.50	8.32
Er	2.93	6.34	3.24	0.79	2.73	3.04	11.79	1.62	5.97	3.62	4.00	7.58
Yb	2.92	5.69	3.74	0.94	2.96	3.13	11.73	1.85	6.43	4.20	4.46	7.96
Zr/Zr*	1.702	0.621	0.854	0.921	1.330	1.046	1.078	0.633	0.150	0.228	0.617	0.737
Ti/Ti*	0.705	0.614	0.239	0.186	0.079	0.100	0.500	0.255	0.507	0.666	0.312	0.487
Locality	7	7	7	7	7	7	6	6	6	6	4	3

GL=Garnet lherzolite
GOp=Garnet pyroxenite
SpL=Spinel Lherzolite
Ha=Harzburgite
Ec=Eclogite
Web= Websterite
GA=garnetharzburgite

Sample#	BN36C	BN96	TL-6	P12	C-5	BNH-1	LS49	BNH-7	BNC-6	LS-3	BN47	BN07
Rocktype	SpL*	SpL	SpL	SpL	SpL	Ec	Ec	Web	Web	Web	Web	Web
Cpx in %			10	10	15	50	70	60	50	50	80	80
Abundances												
Ce	6.62	3.19	0.728	46.8	26.9	6.07	4.81	10.18	15.03	8.07	0.706	13.54
Sr	65	56	13	246	177	54	47	85	72	60	9	166
Nd	5.93	2.94	1.387	39.5	16.18	4.45	4.90	9.33	3.50	6.21	0.532	11.159
Zr	70	28	7.7	127	74	12	62	66	22	37	2.3	121.2
Sm	2.15	1.297	0.848	11.47	3.90	1.241	1.860	3.13	1.021	2.254	0.332	3.989
Eu	0.756	0.584	0.356	3.72	1.286	0.434	0.656	1.102	0.457	0.863	0.198	1.399
Ti	3507	2139	1406	878	543	2269	3435	2824	2948	2611	557	7302
Dy	1.425	2.492	1.597	5.19	2.17	0.895	1.936	1.911	3.14	2.27	1.248	2.93
Er	0.398	1.568	1.058	2.21	1.058	0.475	0.860	0.738	1.904	1.041	0.886	1.244
Yb	0.361	1.668	1.138	2.55	1.031	0.491	0.847	0.757	1.818	1.023	0.826	1.285
Normalized abundances												
Ce	10.98	5.29	1.21	77.6	44.7	10.07	7.98	16.88	24.9	13.38	1.17	22.5
Sr	8.81	7.55	1.78	33.3	24.0	7.29	6.39	11.47	9.78	8.08	1.16	22.4
Nd	13.12	6.50	3.07	87.4	35.8	9.85	10.85	20.64	7.74	13.74	1.18	24.7
Zr	17.79	7.01	1.94	32.2	18.73	3.01	15.63	16.62	5.54	9.35	0.58	30.8
Sm	14.62	8.82	5.77	78.0	26.6	8.44	12.66	21.30	6.94	15.33	2.26	27.1
Eu	13.50	10.43	6.37	66.4	23.0	7.76	11.71	19.68	8.16	15.41	3.54	25.0
Ti	8.04	4.91	3.22	2.01	1.25	5.20	7.88	6.48	6.76	5.99	1.28	16.75
Dy	5.82	10.17	6.52	21.2	8.85	3.65	7.90	7.80	12.83	9.28	5.09	11.95
Er	2.48	9.78	6.60	13.77	6.60	2.96	5.36	4.61	11.88	6.49	5.53	7.76
Yb	2.23	10.30	7.02	15.74	6.37	3.03	5.23	4.67	11.22	6.31	5.10	7.93
Zr/Zr*	1.283	0.914	0.440	0.389	0.601	0.329	1.330	0.793	0.754	0.643	0.340	1.187
Ti/Ti*	0.735	0.474	0.502	0.039	0.068	0.815	0.754	0.412	0.696	0.448	0.315	0.812
Locality	7	7	5	2	1	7	7	7	7	7	7	7

PAGES (S) MISSING FROM ORIGINAL

Page 90 is missing.

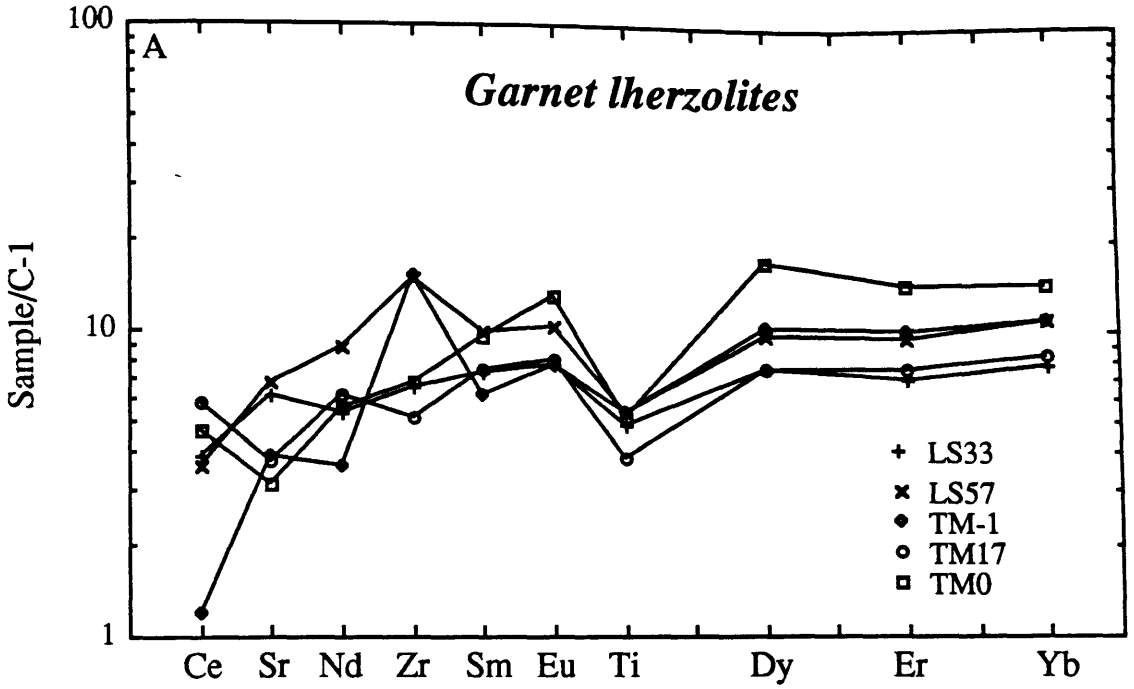
A
Garnet lherzolites
Sample/C-1
100
10
1
Ce Sr Nd Zr Sm Eu Ti Dy Er Yb
LS33
LS57
TM-1
TM17
TM0

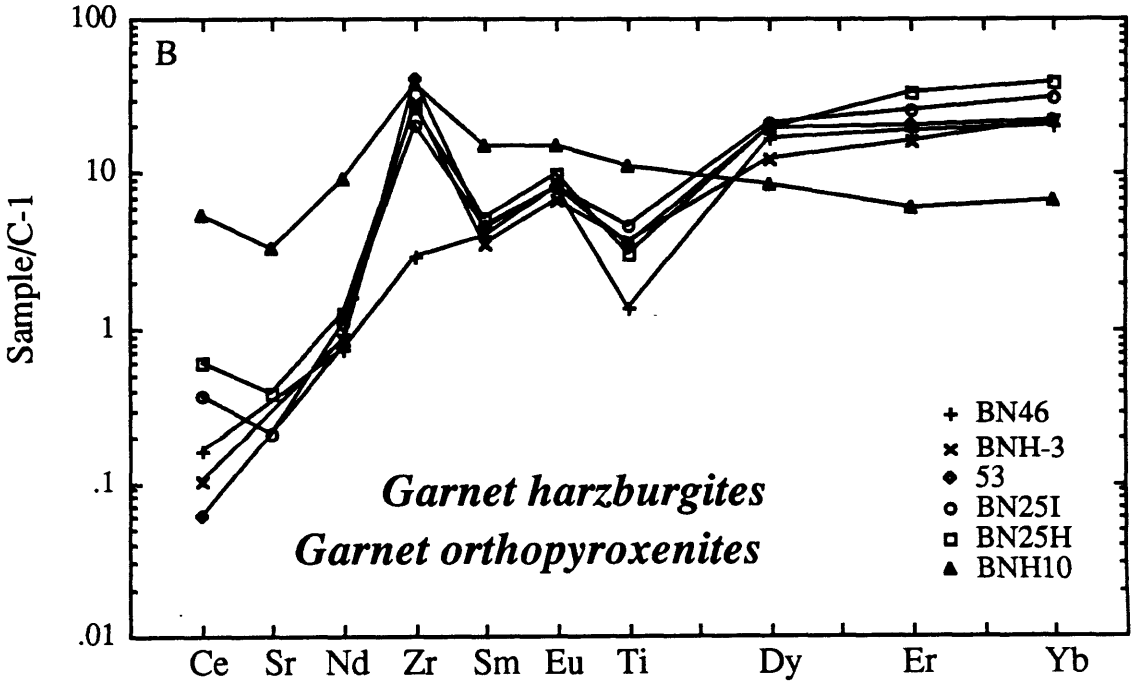
B
Garnet harzburgites
Garnet orthopyroxenites
Sample/C-1
100
10
1
.1
.01
Ce Sr Nd Zr Sm Eu Ti Dy Er Yb
BN46
BNH-3
53
BN25I
BN25H
BNH10

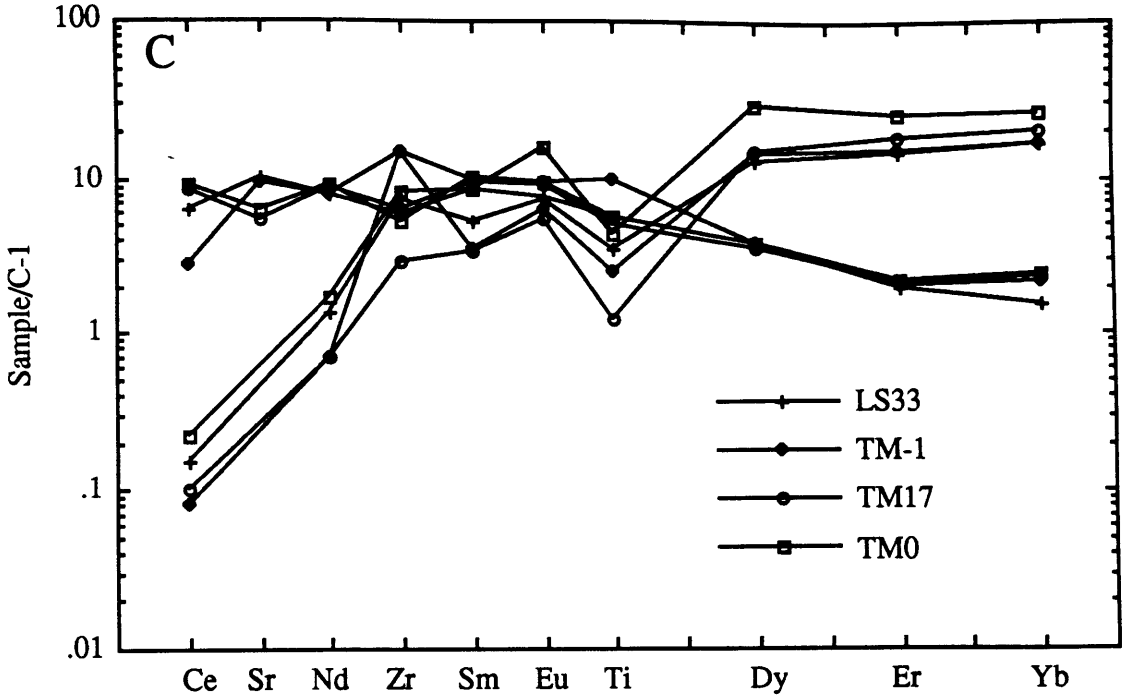
C
100
10
1
.1
.01
Sample/C-1
LS33
TM-1
TM17
TM0
Ce
Sr
Nd
Zr
Sm
Eu
Ti
Dy
Er
Yb

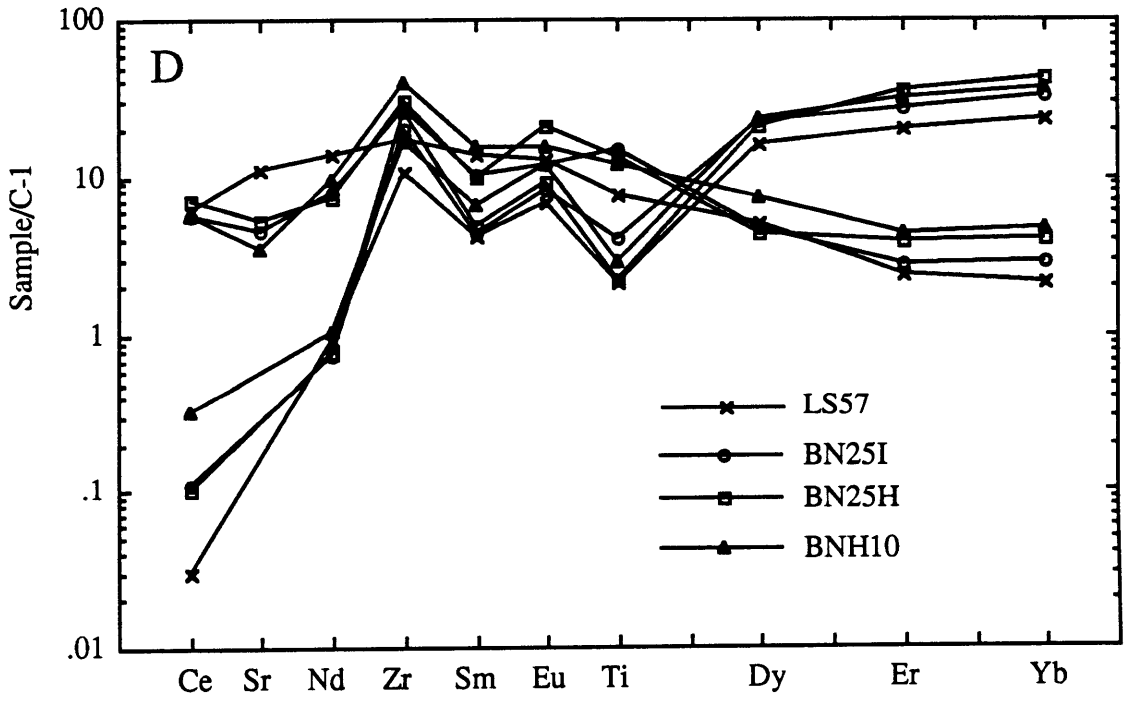
D
100
10
1
.1
.01
Sample/C-1
LS57
BN25I
BN25H
BNH10
Ce
Sr
Nd
Zr
Sm
Eu
Ti
Dy
Er
Yb

Figure 2.10 and 2.11
Spidergrams for Patagonian spinel lherzolites.

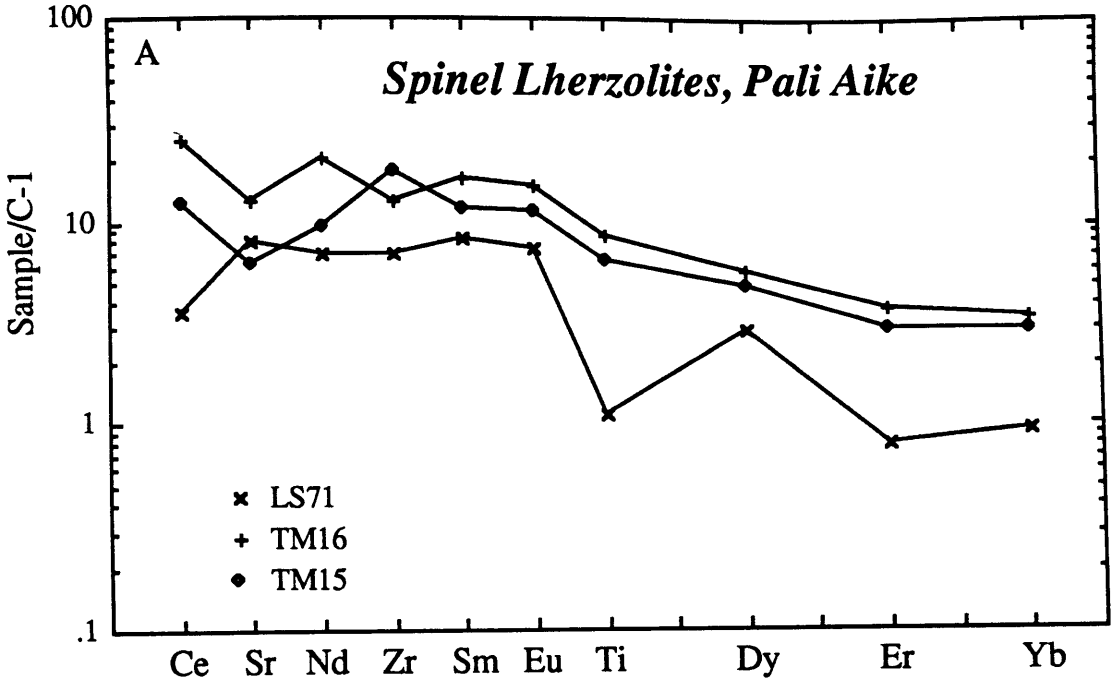
A
Spinel Lherzolites, Pali Aike
Sample/C-1
100
10
1
.1
LS71
TM16
TM15
Ce
Sr
Nd
Zr
Sm
Eu
Ti
Dy
Er
Yb

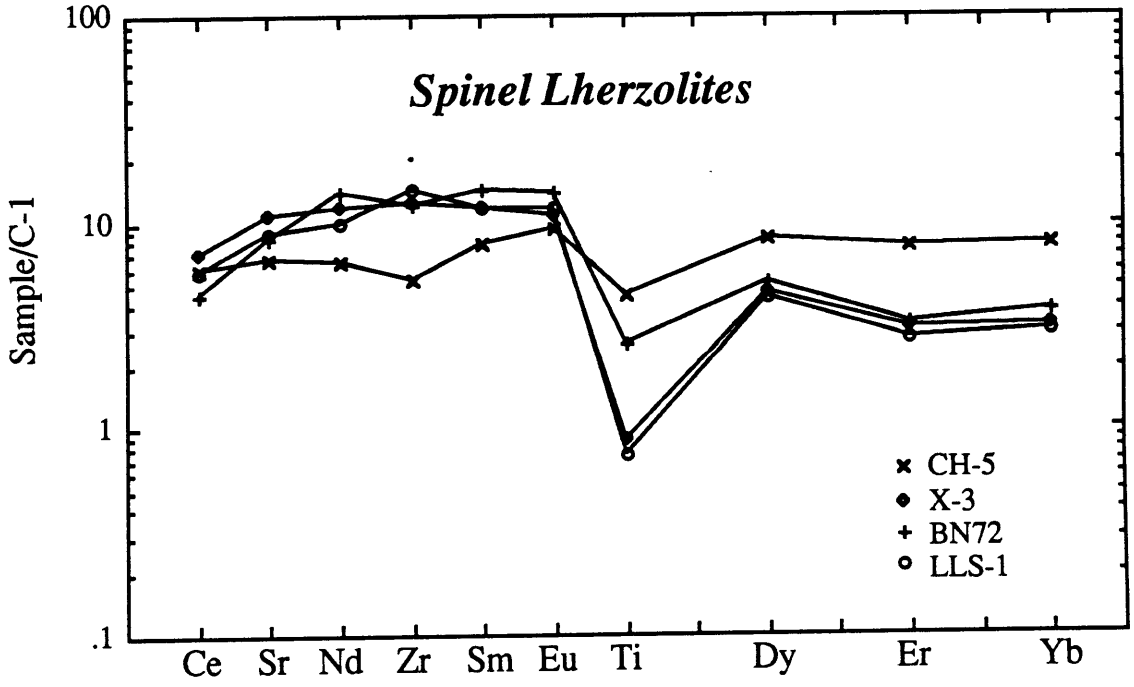
Spinel Lherzolites
Sample/C-1
100
10
1
.1
CH-5
X-3
BN72
LLS-1
Ce
Sr
Nd
Zr
Sm
Eu
Ti
Dy
Er
Yb

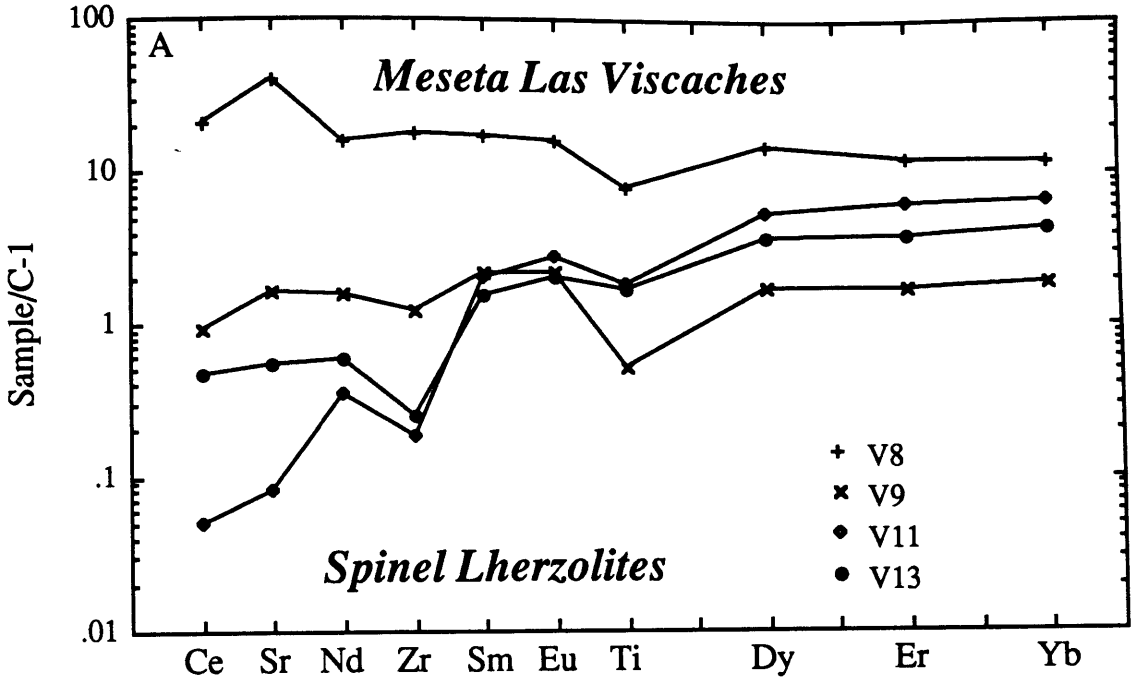
A
Meseta Las Viscaches
Spinel Lherzolites
V8
V9
V11
V13
Sample/C-1
100
10
1
.1
.01
Ce Sr Nd Zr Sm Eu Ti Dy Er Yb

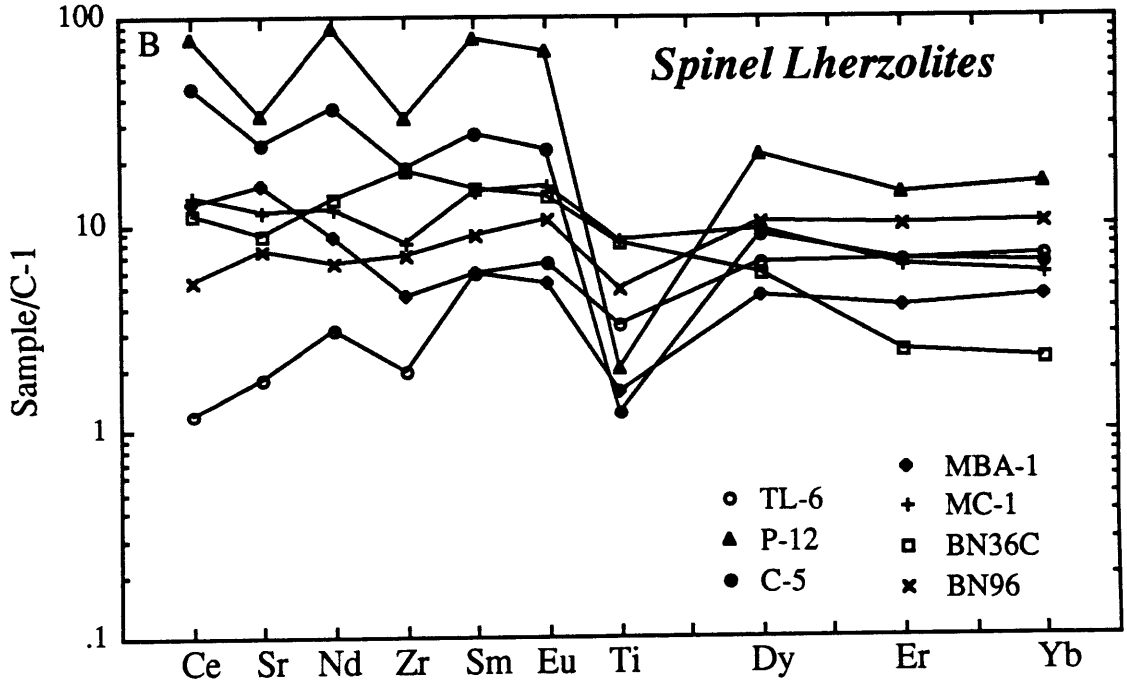
B
Spinel Lherzolites
TL-6
P-12
C-5
MBA-1
MC-1
BN36C
BN96
Sample/C-1
100
10
1
.1
Ce Sr Nd Zr Sm Eu Ti Dy Er Yb

Figure 2.12

Spidergrams for Group II-type xenoliths from Pali Aike. In B composite patterns as in Fig. 2.9 are shown. Figure C shows the trace element patterns of the individual phases of the xenoliths. LREE depleted patterns are the garnets.

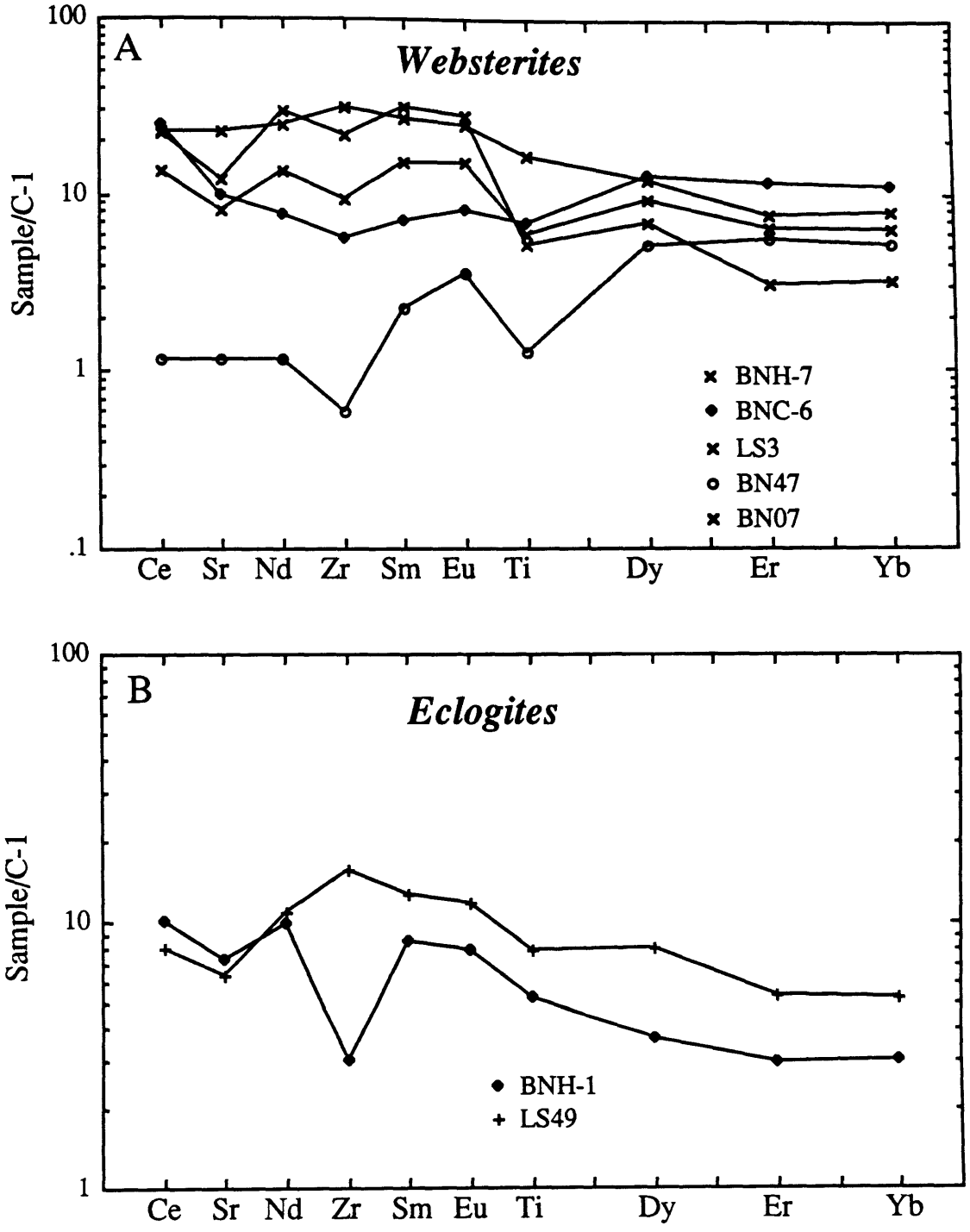
A
Websterites
100
10
1
.1
Sample/C-1
Ce Sr Nd Zr Sm Eu Ti Dy Er Yb
BNH-7
BNC-6
LS3
BN47
BN07
B
Eclogites
100
10
1
Sample/C-1
Ce Sr Nd Zr Sm Eu Ti Dy Er Yb
BNH-1
LS49

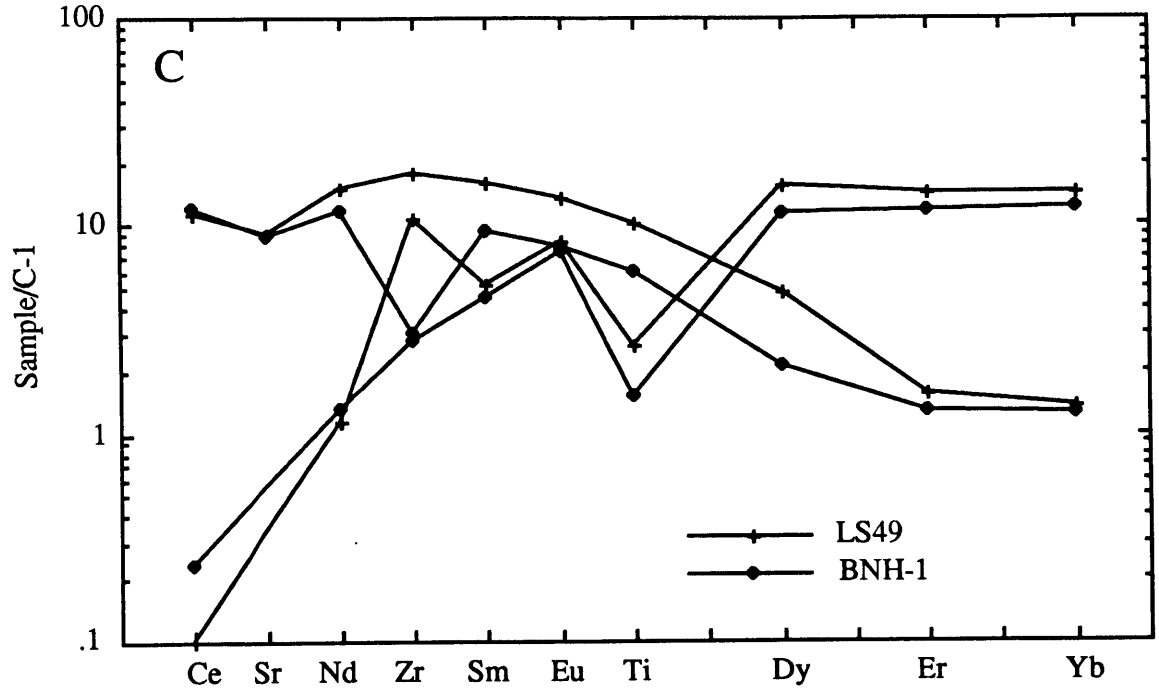
C
100
10
1
.1
Sample/C-1
Ce
Sr
Nd
Zr
Sm
Eu
Ti
Dy
Er
Yb
LS49
BNH-1

Figure 2.13
Zr/Zr* and Ti/Ti* versus Mg# and CaO/Al_2O_3 for Patagonian samples. Major element data is unpublished data of Stern.

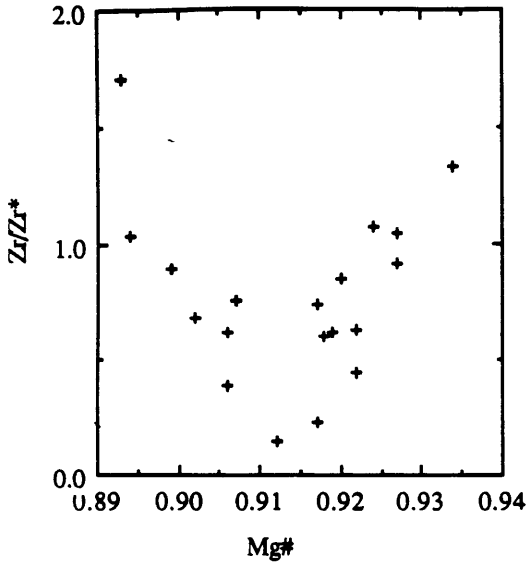
2.0
1.0
0.0
Zr/Zr*
0.89
0.90
0.91
0.92
0.93
0.94
Mg#

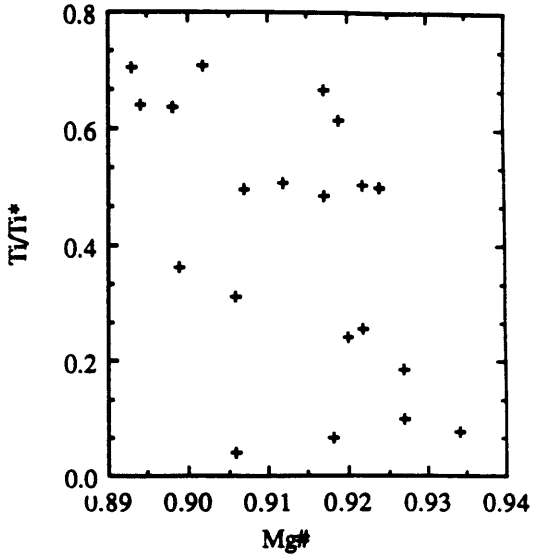
0.8
0.6
0.4
0.2
0.0
Ti/Ti*
0.89
0.90
0.91
0.92
0.93
0.94
Mg#

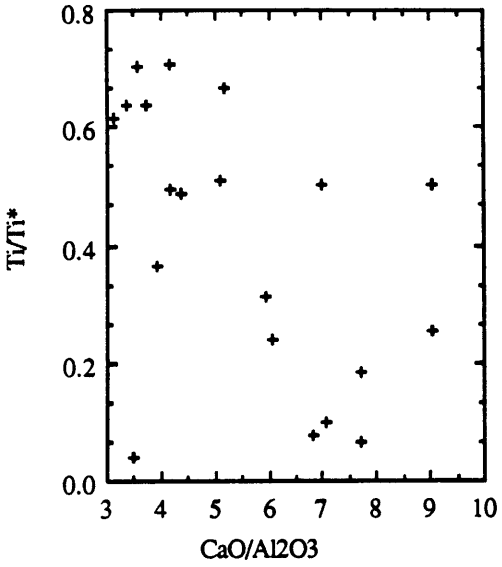
0.8
0.6
0.4
0.2
0.0
Ti/Ti*
3
4
5
6
7
8
9
10
CaO/Al2O3

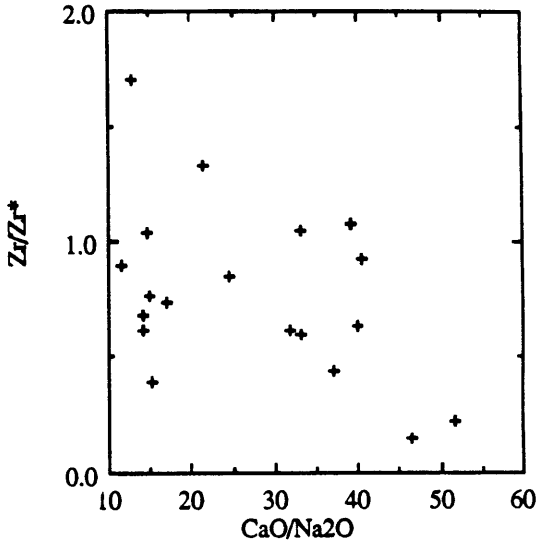
2.0
1.0
0.0
Zr/Zr*
10
20
30
40
50
60
CaO/Na2O

complete data set for the Patagonian nodules is not available yet; especially some key major element data still need to be collected. This report on the Patagonian samples is an interim report on the research of this nodule suite. Work on the samples is still in progress. Fig. 2.8 is a location map of the xenolith occurrences. Xenoliths occurrences are numbered and the location numbers can be found in Table 2.6. All the trace element mineral data are displayed in Fig. 2.9 through 2.12 and are listed in Table 2.5 and 2.6. Samples are arranged according to their petrology. Details of the petrology can be found in Stern et al. (1989). Most of the samples are from Pali-Aike, one of the largest xenolith fields of southern South America. All samples are brought to the surface by alkali basalts. Pali Aike is one of the few occurrences in the world where garnet lherzolites are hosted by alkali basalts. The garnet lherzolites equilibrated at pressures between 19 and 23 kbars, (TM1 and LS33 respectively), which is on the low pressure end of the garnet stability field. Temperature estimates for the garnet lherzolites are between 950°C and 1100°C. The garnet lherzolites contain up to 35% combined diopside and garnet. Pali Aike is the only known locality with hydrous lherzolites on the Patagonian Plateau. Xenoliths from the Patagonian Plateau are unzoned and homogeneous within a sample. The different xenoliths show a large range in trace element compositions among xenoliths from one locality and between different localities. At Meseta Las Viscaches, (MLV) especially, the clinopyroxenes of the different xenoliths show large variations. At MLV Ce/Yb ranges from 6.7 to 0.029, which is one of the largest ranges observed at one locality. The lowest Ce/Yb samples are low in Zr/Zr* and high in Mg#. Currently work is in progress to determine the isotopic compositions of clinopyroxenes from MLV to constrain the isotopic variability, possibly the age of the heterogeneity, and to investigate the relationship among MLV xenoliths.

A large number of the spinel peridotites are depleted in both Ti and Zr compared to the REE. Garnet lherzolites are all depleted in Ti and have variable Zr-content. The garnets in the garnet orthopyroxenites, except for BNH-10, have Ti depletions, Zr

enrichments, and LREE depletions, mimicking the garnet-melt D-pattern.

The garnet peridotites contain up to 35% modal diopside plus garnet. The clinopyroxenes of the garnet peridotites have CaO/Na_2O ratios<16, indicating a major element chemistry close to BE, or even more enriched in melt components than BE. Ti-REE variations in the garnet peridotites, however, are consistent with melt extraction with garnet as the main residual phase. However, the Zr/Zr* vs. Ce/Yb variations in the garnet lherzolites are inconsistent with the involvement of garnet. Stern et al. (1986) and Stern et al. (1989) interpreted the xenoliths as representing MORB type mantle, based on the radiogenic Nd and unradiogenic Sr isotopic compositions of the garnet lherzolites. The major element characteristics of the garnet lherzolites imply a more fertile mantle than depleted MORB-type mantle.

The Patagonian xenoliths as a group show a positive correlation between Zr/Zr* and Ti/Ti* on the one hand, and Mg# and CaO/Al_2O_3 on the other hand (Fig. 2.13). This indicates that the processes leading to the HFSE depletions are related to processes causing the variations in the major element chemistry.

Of the group II type xenoliths (Fig. 2.12), 5 of the 7 xenoliths have diopsides with Zr/Zr*<1, and all xenoliths have Ti/Ti*<1, indicating none of the clinopyroxenes could have been in equilibrium with the host basalt. Affinity of the Group II clinopyroxenes to an arc-type magma, i.e. a magma with HFSE depletions and Sr-enrichments, is not likely since the clinopyroxenes miss the characteristic Sr-enrichment of island-arc type lavas.

2.3.5 North East Queensland.

The Mingela and Arthurs Peak samples belong to the Mingela alkali basalt province, 75 mile NW of Townsville, Queensland. The alkali basalts range in age from 41-44 Ma and crop out as plugs and dikes (Stephenson et al., 1980). The alkali basalts plugs are surrounded by partly consolidated alluvium, sands and clays. The exposures are formed due to recent (<50 Ka) uplift and preferential erosion of the

Table 2.7
Trace element abundances in clinopyroxenes from lherzolites from NE Queensland, Australia

Sample	LE-2	LE-3	LE-4	M1-8	M2-7	AP16	AP10	Y-7	Y-8	Y-9	Y-10	Y-11
Abundances in ppm												
Ce	2.09	0.55	1.44	9.57	3.53	0.14	0.32	24.4	6.40	0.13	0.045	0.063
Sr	28.9	8.5	16.7	99.4	64.2	2.9	3.2	87.1	62.0	4.20	0.398	0.998
Nd	1.546	1.466	1.398	5.05	2.40	1.27	0.36	6.98	5.23	0.36	0.484	0.694
Zr	10.5	8.6	11.4	16.7	19.9	6.6	1.9	10.3	63.4	5.00	2.00	3.80
Sm	0.86	1.02	0.57	1.37	1.10	1.09	0.39	2.19	2.26	0.39	0.65	1.62
Eu	0.386	0.477	0.211	0.558	0.479	0.535	0.197	0.682	0.913	0.212	0.336	0.373
Ti	2292	2404	1736	2323	3139	2772	1215	1705	3248	1951	2530	2451
Dy	1.826	2.293	1.048	2.20	2.04	2.67	1.389	2.362	2.772	1.319	2.18	2.16
Er	1.104	1.418	0.757	1.375	1.184	1.814	0.939	1.436	1.489	0.890	1.470	1.367
Yb	1.164	1.460	0.850	1.407	1.267	1.889	1.008	1.501	1.610	1.022	1.490	1.376
Normalized abundances												
Ce	3.47	0.913	2.38	15.87	5.86	0.232	0.538	40.5	10.61	0.213	0.075	0.105
Sr	3.91	1.152	2.26	13.43	8.68	0.398	0.433	11.78	8.37	0.568	0.054	0.135
Nd	3.42	3.24	3.09	11.16	5.30	2.80	0.803	15.44	11.58	0.802	1.071	1.536
Zr	2.67	2.19	2.88	4.24	5.04	1.67	0.483	2.61	16.09	1.269	0.508	0.964
Sm	5.87	6.92	3.86	9.33	7.46	7.41	2.68	14.92	15.36	2.67	4.39	11.05
Eu	6.90	8.51	3.77	9.97	8.56	9.55	3.52	12.18	16.30	3.79	6.00	6.66
Ti	5.26	5.51	3.98	5.33	7.20	6.36	2.79	3.91	7.45	4.47	5.80	5.62
Dy	7.45	9.36	4.28	9.00	8.34	10.90	5.67	9.64	11.31	5.39	8.90	8.81
Er	6.89	8.85	4.72	8.58	7.38	11.32	5.86	8.96	9.29	5.55	9.17	8.53
Yb	7.19	9.01	5.25	8.68	7.82	11.66	6.22	9.27	9.94	6.31	9.20	8.50
Zr/Zr*	0.575	0.431	0.829	0.414	0.790	0.327	0.277	0.172	1.194	0.731	0.186	0.153
Ti/Ti*	0.742	0.627	1.010	0.553	0.848	0.636	0.658	0.345	0.509	1.035	0.833	0.762

LE = Lake Eachem
M= Mingela
AP= Arthurs Peak
Y= Yangaburro

Figure 2.14

Spidergrams for clinopyroxenes in anhydrous lherzolites from north east Queensland. LE= Lake Eachem, M= Mingela, AP= Arthurs Peak, same volcanic province as Mingela, and Y= Yangaburro, same volcanic province as Lake Eachem.

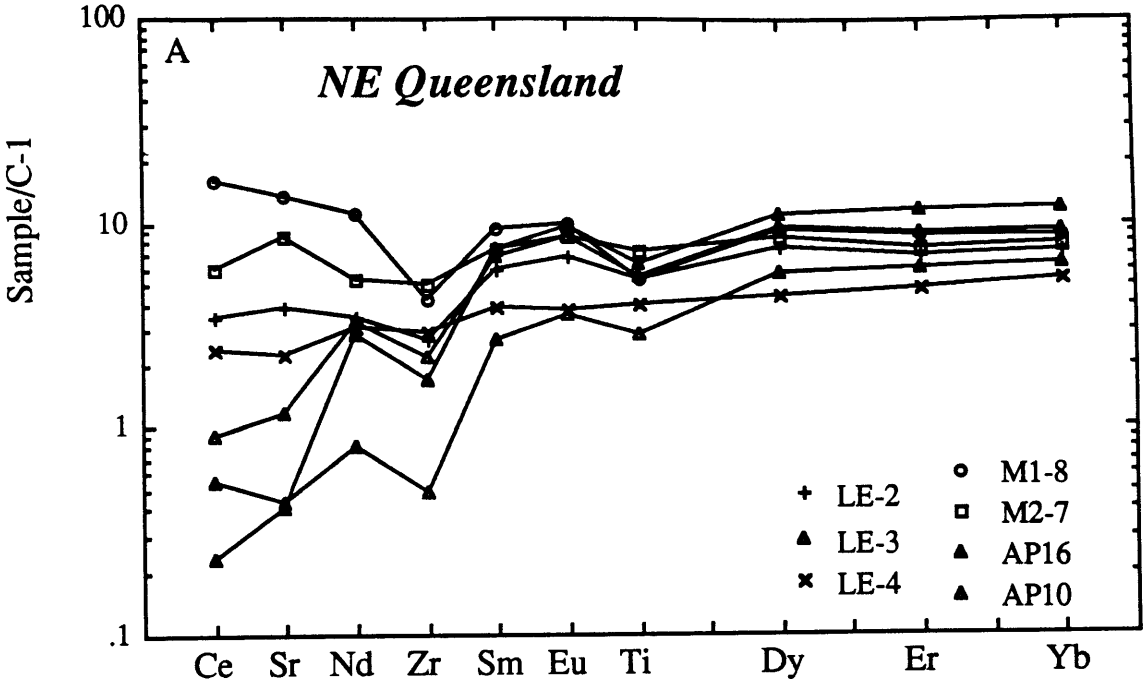
A
NE Queensland
Sample/C-1
100
10
1
.1
Ce
Sr
Nd
Zr
Sm
Eu
Ti
Dy
Er
Yb
LE-2
LE-3
LE-4
M1-8
M2-7
AP16
AP10

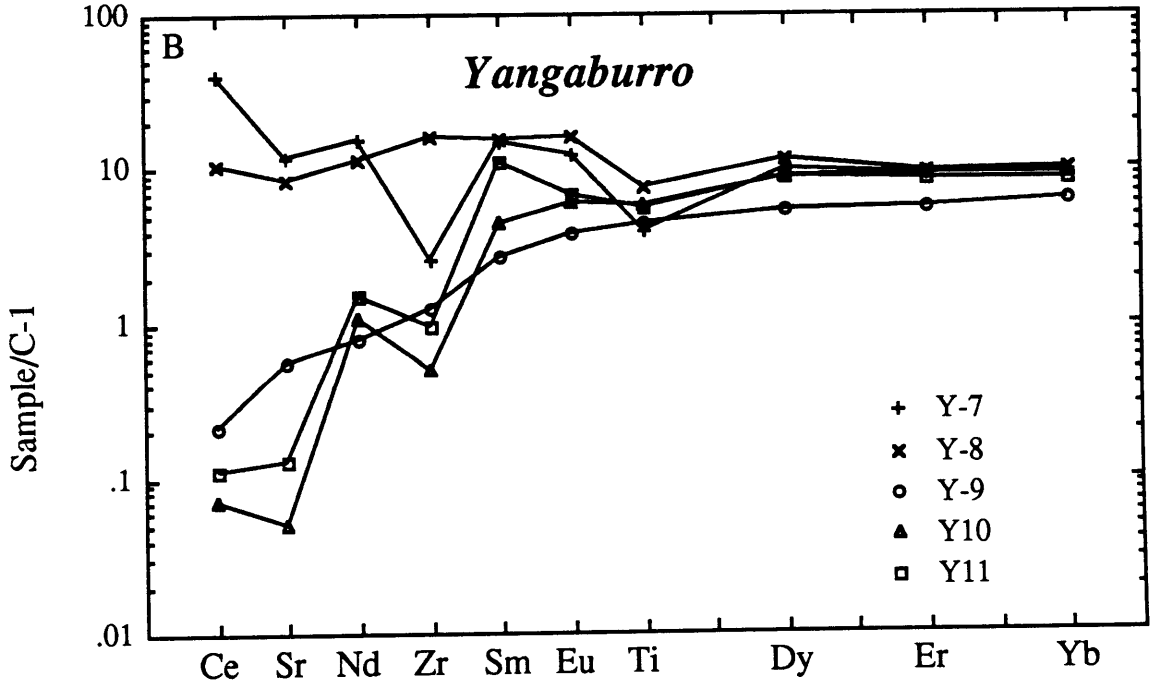
B
Yangaburro
Sample/C-1
100
10
1
.1
.01
Ce
Sr
Nd
Zr
Sm
Eu
Ti
Dy
Er
Yb
Y-7
Y-8
Y-9
Y10
Y11

surrounding sediments. The volcanic products thus form the topographic highs in the landscape. Samples from Mingela province are all harzburgitic, and small (<1cm).

The Lake Eachem and Yangaburro samples belong to the Atherton province (Stephenson et al., 1980), just SW of Cairns. The xenoliths are brought to the surface by alkali basalts 3 Ma-10 Ka in age. The Atherton peridotites are more fertile xenoliths than the Mingela ones: >15% diopside, and are fist size at Lake Eachem, while at Yangaburro they range from 2-30 cm in diameter. The Yangaburro occurrence is extremely rich in xenoliths, with over 99% of the outcrop consisting of peridotite material. Occasionally, the xenoliths have a partial, 2-3 mm rind of basalt. Although the extent of the peridotite horizon is unknown, the landscape suggests that a hill 400m in diameter and 30m high is a solid xenolith deposit. (The peridotite is mined as rocks for aquaria and rock gardens). Trace element data are listed in Table 2.7 and shown in Fig. 2.14. Although the composition of the clinopyroxenes in the individual xenoliths from Yangaburro is homogeneous, the samples show large inter-xenolith variation. These five xenoliths come from an outcrop area of about $0.3m^2$. Again most xenoliths show HFSE depletions, and the size of the Ti and Zr depletions is not correlated.

2.3.6 Suboceanic localities.

Twentyone samples of sub-oceanic lithosphere were analyzed. Analyses are listed in Table 2.8. The trace element patterns are shown in Fig. 2.15 and 2.16. All samples are anhydrous spinel lherzolites or harzburgites, typically small (1-2cm in diameter) with less that 3% modal diopside (except for SA17 with 8% modal clinopyroxene). The ion microprobe is the best technique available for determining REE concentrations in these small samples. Samples 3994A and 3860 are garnet-bearing harzburgites. The garnet has not yet been analyzed. The range of Sr, REE, and HFSE contents in clinopyroxenes from these suboceanic peridotites is larger than the range found in oceanic lavas. Based on the REE and HFSE content most of these clinopyroxenes cannot be in equilibrium with oceanic

Table 2.8
Trace elements in clinopyroxenes from lherzolites from oceanic localities

	Western Samoa						Cape Verdes		Comores		
Sample	SA3-6	S2-2-1	UP1-1V	UP1-4	SA17	SA3-2	85-LI20-1	85-LI20-2	AJ319C	AJ310	AJ319f
Abundances in ppm											
Ce	7.44	0.04	49.4	46.3	69.7	40.8	27.9	35.4	0.005	95	112
Sr	5.67	0.32	246	87.8	190	162	200	147	0.8	214	401
Nd	0.611	0.018	18	39	26	24	23	16	0.033	46.1	36.6
Zr	0.033	4.57	45	147	45	67	19	4	3.5	41	253
Sm	0.058	0.008	3.12	12.28	3.94	6.04	6.96	3.99	0.048	10.864	7.484
Eu	0.019	0.005	1.13	4.12	1.09	1.74	2.38	1.37	0.018	3.025	5.072
Ti	42.2	43	865	1821	1310	512	4361	3936	371	400	1426
Dy	0.050	0.044	1.396	10.32	1.584	2.88	4.22	2.83	0.355	9.078	5.031
Er	0.087	0.080	0.704	4.61	0.666	1.079	1.86	1.37	0.272	4.724	2.45
Yb	0.146	0.170	0.730	4.97	0.676	0.991	1.95	1.39	0.342	4.701	2.275
Normalized abundances											
Ce	12.34	0.07	81.9	76.7	115.6	67.6	46.3	58.7	0.008	157.8	186.5
Sr	0.77	0.04	33.3	11.87	25.7	21.9	27.0	19.85	0.108	29.0	54.1
Nd	1.35	0.04	40.0	87.3	56.6	52.6	51.1	35.8	0.073	102.0	80.9
Zr	0.01	1.16	11.46	37.2	11.31	17.02	74.4	14.52	0.888	10.48	64.1
Sm	0.39	0.06	21.2	83.5	26.8	41.1	47.3	27.2	0.327	73.9	50.9
Eu	0.34	0.09	20.1	73.5	19.42	31.2	42.6	24.4	0.321	54.0	90.6
Ti	0.10	0.10	1.98	4.18	3.01	1.17	10.00	9.03	0.851	0.92	3.27
Dy	0.20	0.18	5.70	42.1	6.46	11.76	17.23	11.53	1.449	37.1	20.5
Er	0.55	0.50	4.39	28.8	4.15	6.73	11.60	8.56	1.697	29.5	15.28
Yb	0.90	1.05	4.50	30.7	4.17	6.12	12.03	8.58	2.11	29.0	14.04
Zr/Zr*	0.010	24.589	0.374	0.435	0.271	0.363	1.512	0.461	4.447	0.119	0.972
Ti/Ti*	0.221	0.545	0.086	0.044	0.133	0.032	0.195	0.299	0.814	0.013	0.032

Table 2.8 cont'd

	Malaita				Galapagos	Ascension	Kerguelen	Azores	MIOR	Romanche
Sample	3860	3994A	3540	3568	E98-i		K29a			
Abundances in ppm										
Ce	10.46	3.41	2.13	5.44	17.46	4.25	18.39	15.30	0.034	1.29
Sr	73.4	57.5	18.5	39.5	121	9	36	149	0.34	2.5
Nd	10.9	4.2	2.8	4.3	11.9	3.7	12.8	6.7	0.116	4.82
Zr	45.3	30.8	16.3	19.6	36.4	22.6	16.8	49.0	0.35	35.0
Sm	3.014	1.136	1.629	1.975	3.51	1.4	3.4	1.32	0.267	2.93
Eu	0.982	0.329	0.709	0.733	1.2	0.53	1.24	0.48	0.143	1.04
Ti	6758	571	3220	3782	2664	2494	3283	1818	886	3657
Dy	1.144	0.389	3.102	2.17	2.72	2.40	2.95	1.112	1.51	4.92
Er	0.29	0.071	1.944	1.056	1.379	1.573	1.405	0.68	1.24	2.64
Yb	0.299	0.041	2.077	0.964	1.14	1.323	1.167	0.555	1.17	2.02
Normalized abundances										
Ce	17.34	5.66	3.53	9.02	29.0	7.05	30.5	25.4	0.056	2.14
Sr	9.92	7.77	2.50	5.34	16.29	1.24	4.85	20.1	0.046	0.34
Nd	24.07	9.33	6.29	9.54	26.33	8.12	28.3	14.87	0.257	10.66
Zr	11.50	7.82	4.14	4.97	9.24	5.75	4.26	12.43	0.089	8.88
Sm	20.5	7.73	11.08	13.44	23.9	9.52	23.1	8.98	1.82	19.93
Eu	17.54	5.88	12.66	13.09	21.4	9.46	22.1	8.57	2.55	18.57
Ti	15.50	1.31	7.39	8.67	6.11	5.72	7.53	4.17	2.03	8.39
Dy	4.67	1.59	12.66	8.84	11.08	9.80	12.04	4.54	6.16	20.08
Er	1.81	0.44	12.13	6.59	8.60	9.81	8.76	4.24	7.74	16.47
Yb	1.85	0.25	12.82	5.95	7.04	8.17	7.20	3.43	7.22	12.47
Zr/Zr*	0.516	0.917	0.476	0.433	0.368	0.651	0.166	1.043	0.086	0.581
Ti/Ti*	0.780	0.196	0.389	0.495	0.227	0.398	0.267	0.385	0.361	0.293

Figure 2.15
Spidergram for clinopyroxenes in xenoliths from Samoa (A) and from Cape Verde and Comores (B).

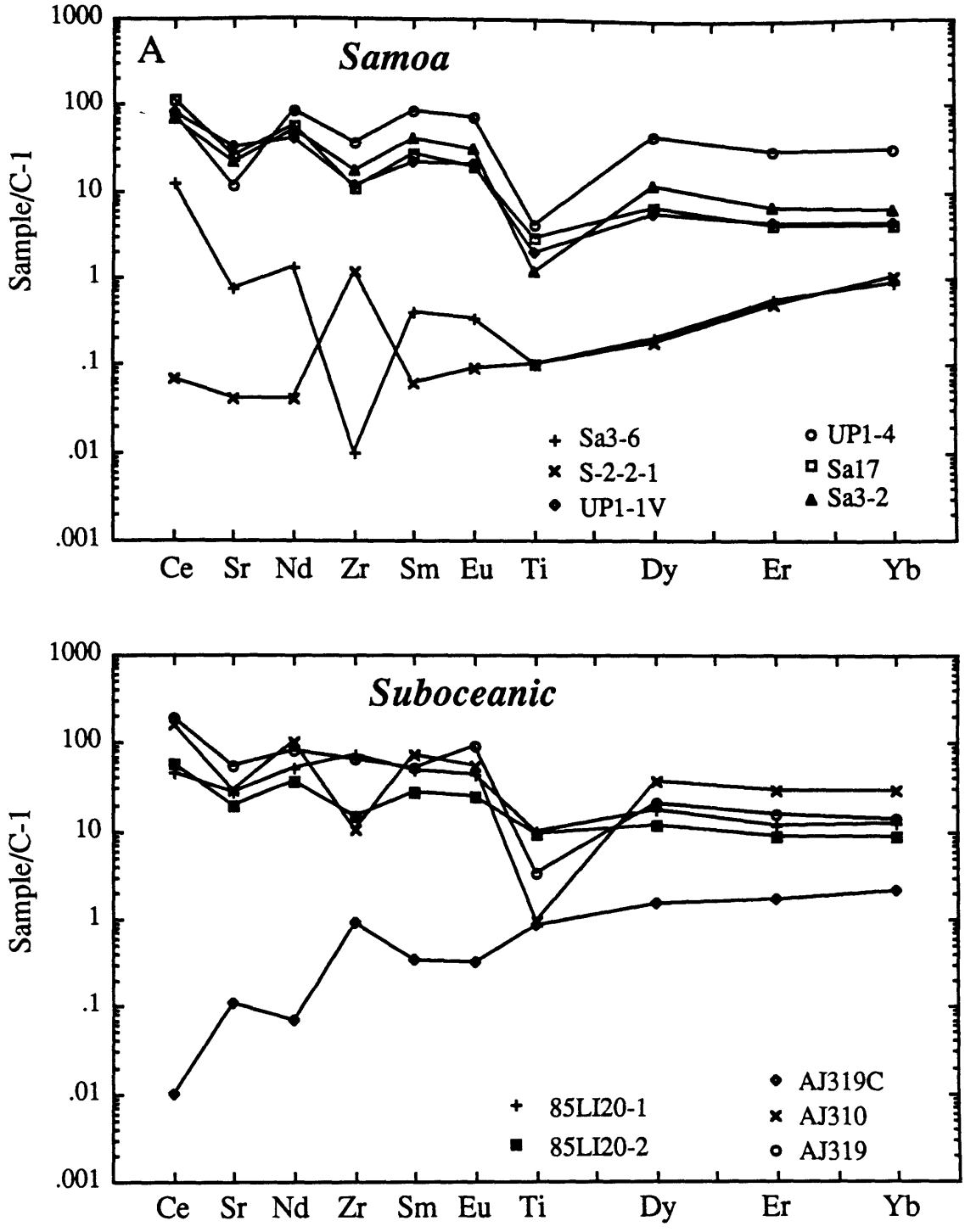
A
Samoa
Sample/C-1
1000
100
10
1
.1
.01
.001
Ce Sr Nd Zr Sm Eu Ti Dy Er Yb
+ Sa3-6
× S-2-2-1
◆ UP1-1V
○ UP1-4
□ Sa17
▲ Sa3-2
Suboceanic
Sample/C-1
1000
100
10
1
.1
.01
.001
Ce Sr Nd Zr Sm Eu Ti Dy Er Yb
+ 85LI20-1
■ 85LI20-2
◆ AJ319C
× AJ310
○ AJ319

Figure 2.16
Spidergrams for xenoliths from Malaita (A). (B) displays some lherzolites from ocean islands and two abyssal peridotites: Central Indian Ridge and Romanche.

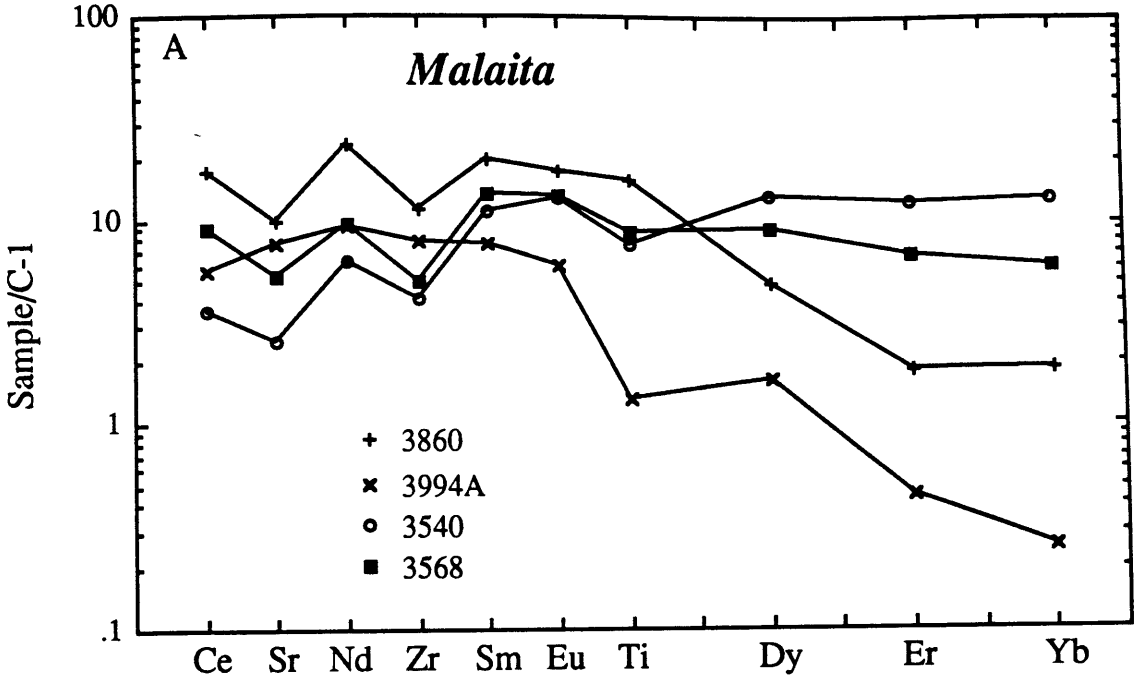
A
Malaita
100
10
1
.1
Sample/C-1
3860
3994A
3540
3568
Ce
Sr
Nd
Zr
Sm
Eu
Ti
Dy
Er
Yb

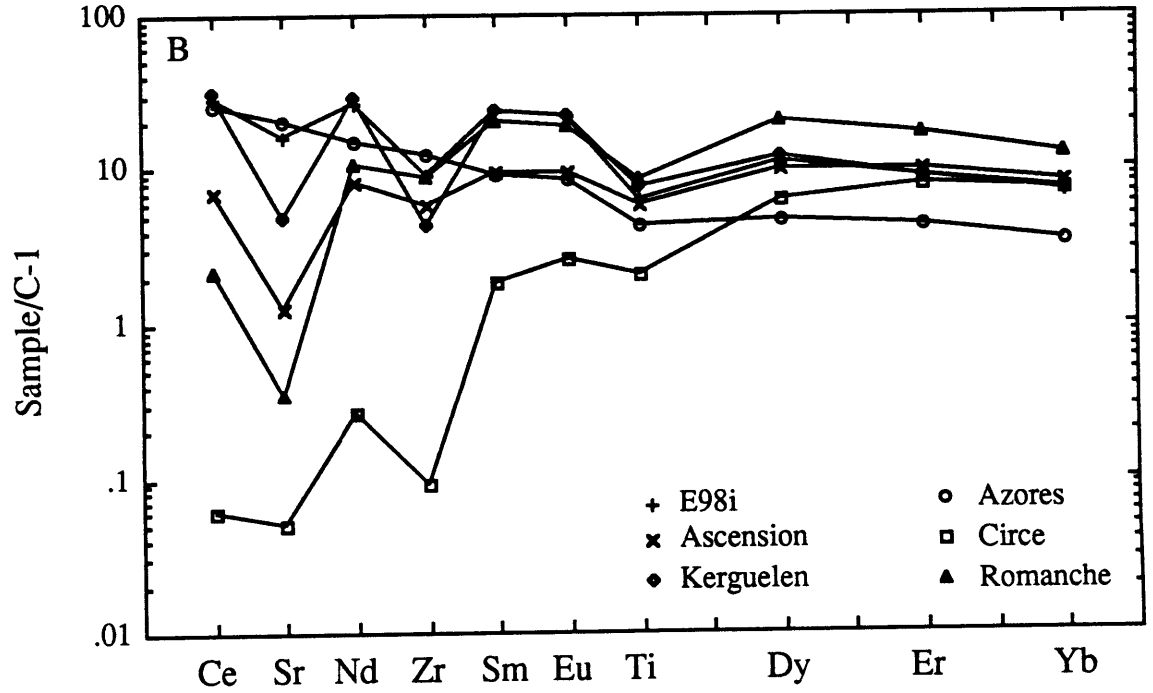
B
100
10
1
.1
.01
Sample/C-1
E98i
Ascension
Kerguelen
Azores
Circe
Romanche
Ce
Sr
Nd
Zr
Sm
Eu
Ti
Dy
Er
Yb

lavas. Specifically, the majority of the clinopyroxenes are depleted in Ti and Zr. In addition, some samples from Samoa, Comores and one sample from Cape Verde have very high concentrations of REE with Ce/Yb ≈100. In contrast, other samples from these islands contain extremely depleted clinopyroxenes. The two abyssal peridotites, one from the Romanche Fracture Zone and one from the Central Indian Ocean Ridge (Shimizu and Hart, 1974), are depleted in LREE but also display HFSE depletions.

2.4 First order consequences of HFSE depletions.

The extent of HFSE depletions in the analyzed clinopyroxenes exceeds that found in OIB and MORB (Fig. 2.17). The data for clinopyroxenes from peridotites include samples in this paper (Table 2.2 to Table 2.8) data for abyssal peridotites (Johnson et al., 1989), data for xenoliths from Central Europe (Blusztjan and Shimizu, 1988), unpublished data from Shimizu on spinel lherzolites from Salt Lake Crater, Hawaii, and published data (see figure caption for references). The whole rock data for xenoliths from S. Africa (Nixon and Boyd, 1979) were added because these xenoliths are metasomatized by a hydrous phase. Consequently they define enrichments caused by hydrous metasomatism. Although the data set is substantially larger than the data set of Salters and Shimizu (1988), the general characteristics of Fig. 2.17 are the same as Fig. 4 of Salters and Shimizu. Approximately 80% of the clinopyroxenes in peridotites, both in the subcontinental and in the suboceanic(!) environment, have larger HFSE depletions than MORB and OIB. Since clinopyroxene-melt partition coefficients do not exhibit HFSE anomalies, MORB and OIB with HFSE/HFSE*≈1, can not be in equilibrium with these clinopyroxenes.

Several workers (Dick and Fisher, 1984; Prinzhofer and Allegre, 1985; Shibata and Thompson, 1986) contend that abyssal peridotites are related o MORB by simple melting processes. The occurrence of HFSE depletions in abyssal peridotites precludes a simple relationship between MORB and the present mineral compositions in the abyssal peridotites. A more complex melting model, in which

Figure 2.17

Ti/Ti* versus Zr/Zr* for peridotites and the three major types of basalts. Added to the peridotite data of this chapter are the data of Blusztjan and Shimizu (1988), Frey et al. (1985), Jagoutz et al. (1979a), Jagoutz et al. (1979b), Johnson et al. (1989), Melson et al. (1972), Nixon et al. (1981), Roden et al. (1984b), Shimizu (1987) Data sources for the MORB and OIB as in Fig. 2.5. Data sources for IAB from(Basaltic Volcanism Study Project (1981), Dupuy et al. (1982), Fujimaki (1986), Gerlach (1986), Morris (1984). Solid square is average N-type MORB from Hofmann (1988).

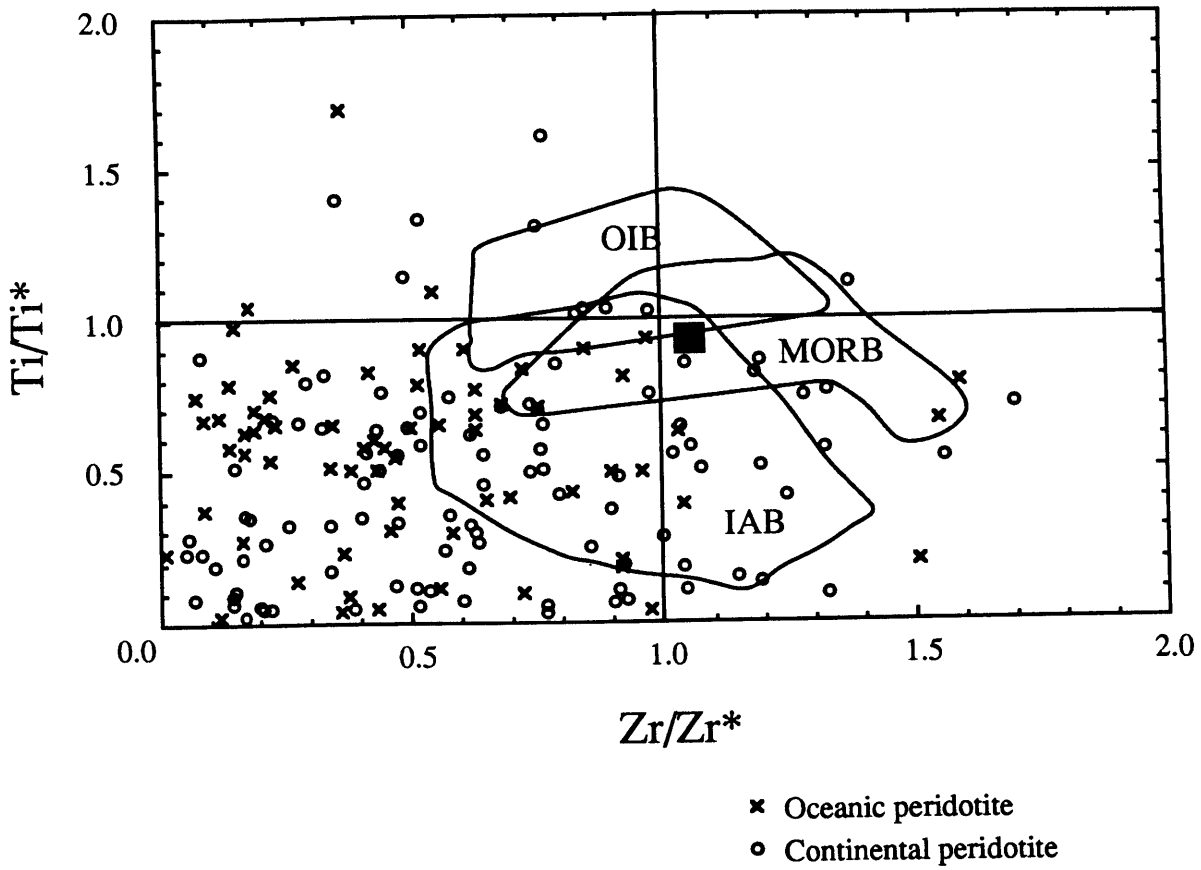
2.0
1.5
1.0
0.5
0.0
0.5
1.0
1.5
2.0
Ti/Ti*
Zr/Zr*
OIB
MORB
IAB
Oceanic peridotite
Continental peridotite

garnet is a residual phase during MORB genesis, has been proposed by Johnson et al. (1989) and Langmuir et al. (1977), and will also be discussed in Chapter 3. However, the existence of both Ti and Zr depletions is inconsistent with garnet as the only cause for HFSE depletions in abyssal peridotites, because with garnet residual $Zr/Zr^*>1$ is expected for the metamorphic clinopyroxene. In addition, the widespread occurrence of HFSE-depleted peridotites and the predominance of this type over other peridotites at all known occurrences suggest that the HFSE depleted peridotite is either a volumetrically significant part of the suboceanic mantle or that the mantle samples occurring on the ocean floor and at ocean islands are not representatives of the bulk of the upper mantle.

On the other hand, island arc magmas characteristically exhibit depletions in HFSE, and HFSE depleted peridotites may be in equilibrium with island arc lavas. The HFSE depletion is one of the most characteristic features of island arc basalts and has been used to determine the paleo-tectonic environment (Pearce and Cann, 1973; Pearce and Norry, 1979). Although many island arc magmas have Sm/Hf ratios similar to oceanic lavas (White and Patchett, 1984), the Nd/Hf and Sm/Nd ratios in island arc lavas are typically different from Nd/Hf and Sm/Nd in oceanic lavas. This illustrates the usefulness of the extended REE diagram and the purpose of the HFSE* notation. With the extended REE diagram the HFSE* notation can be used to quantify the HFSE depletion independent of the slope of the REE pattern.

The ubiquity of the HFSE-depleted peridotites in the shallow mantle (Fig. 2.17) strongly suggests that the HFSE depletions in island arc lavas are a characteristic of the mantle source. Thus, there is no need to require either a Ti-rich residual phase (Green, 1981; Morris and Hart, 1983) or a slab component enriched in alkaline, alkaline earth and rare earth elements and depleted in HFSE (Gill, 1981; Kay, 1980; Nicholls and Ringwood, 1973) to explain the HFSE depletions. Island arc lavas may still have a slab component; however, this slab component need not have HFSE depletions. High Sr/Nd ratios are another characteristic of island arc lavas. Assuming the Sr/Nd ratio in IAV reflects slab involvement, the lack of correlation between

Figure 2.18

Variations of the trace element depletions with Sr/Nd ratios. Sr/Nd ratios can be used as indicator for subduction characteristics. Crosses are oceanic peridotites, open circles are continental peridotites. Additional data sources for peridotites as in Fig. 2.17. Lines are bulk earth values for Sr/Nd and Ti/Ti*.

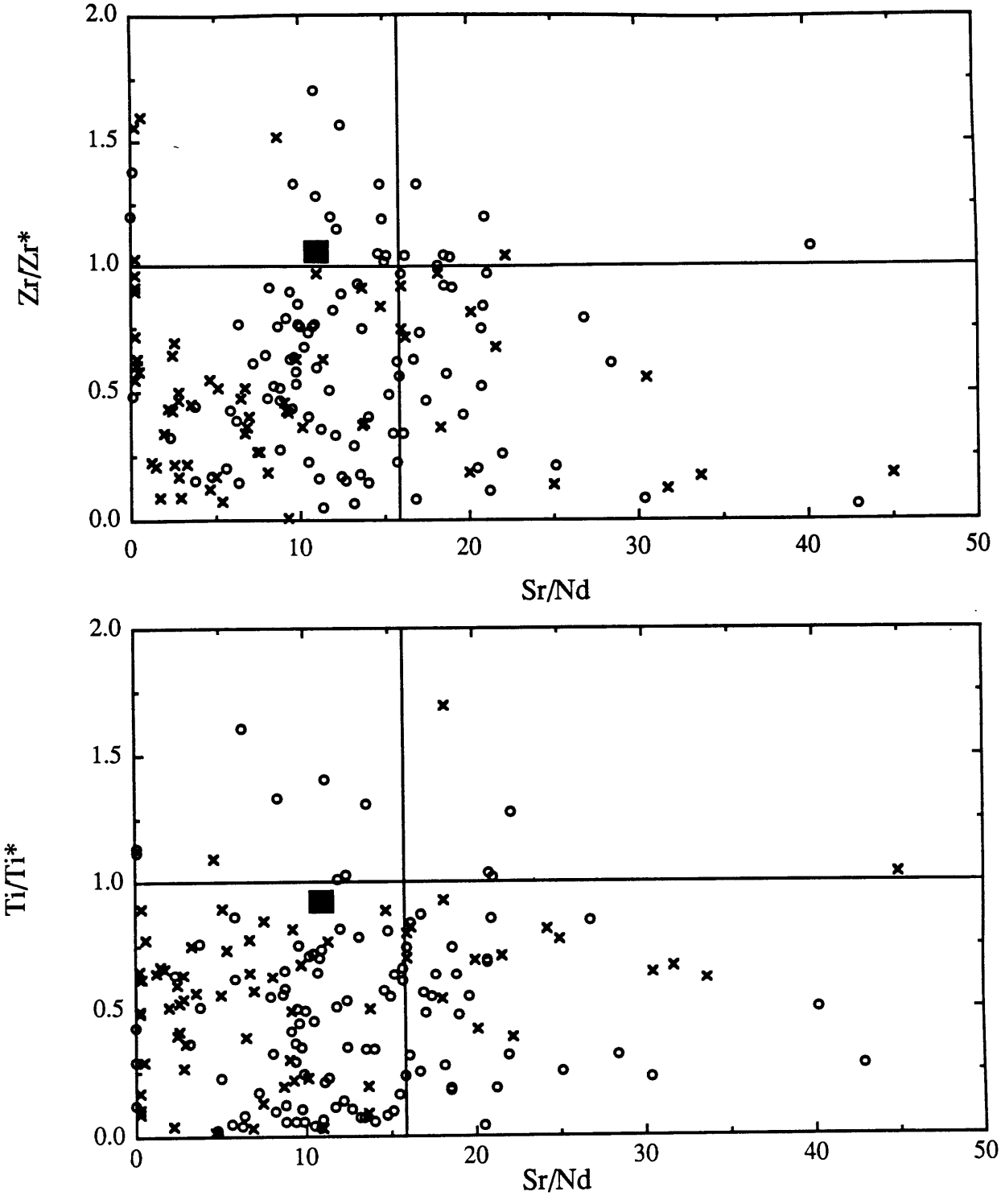
2.0
1.5
1.0
0.5
0.0
Zr/Zr*
0
10
20
30
40
50
Sr/Nd
2.0
1.5
1.0
0.5
0.0
Ti/Ti*
0
10
20
30
40
50
Sr/Nd

Sr/Nd and either Zr/Zr* or Ti/Ti* (Fig. 2.18) and the occurrence of HFSE-depleted sub-oceanic mantle suggests that the slab component is not the component creating the HFSE depletion. Furthermore, the lack of correlation between Zr/Zr* and Ti/Ti* indicates that more than one process can cause HFSE depletions. It seems plausible that island arc volcanism is the only type of volcanism that consistently samples the HFSE depleted mantle. Strictly speaking, the HFSE depleted mantle is only observed in the shallow part of the mantle, i.e., in IAV, which come from the mantle wedge above the subducted slab, and in mantle xenoliths from a maximum depth of 100-150km. OIB and MORB originate deeper in the mantle (>200km) and in general, they do not show pronounced HFSE depletions. These HFSE-depleted peridotites can reside only in the upper part (top 200km) of the mantle, at temperatures below their peridotite solidus. In an arc setting, the slab component fluxes the overlying HFSE depleted mantle wedge by adding alkaline, earth alkaline, and volatile elements, thereby decreasing the solidus temperature and causing melting.

2.5 Trace element variations in peridotites; general considerations.

Figs. 2.18 through 2.23 show the trace element variations of a selected groups of samples, with emphasis on the HFSE-REE variations. Only localities with six or more analyzed samples are used. Hydrous peridotites, only present in the Patagonian and S.African data sets, are also plotted, because these samples indicate the effect of metasomatism on the trace element ratios. Data in the figures are restricted to Group I peridotites.

The purpose of the next section is to attempt to explain the observed general trends. The details of the variations are ignored but will be discussed in separate papers for the individual localities, where the trace element data will be combined with modal data and major element data. The range in trace element content of the peridotite data set, and especially the variability in trace element ratios at the different localities, is larger than the observed ranges and variability in the host basalts. The heterogeneity of trace

Figure 2.19- 2.23

Trace element variations of clinopyroxenes in peridotites. Different symbols are for different datasets: crosses are oceanic xenoliths, filled diamonds are Meseta Las Viscaches, open diamonds are other Patogonian lherzolites (garnet-bearing samples are plotted as calculated trace element contents as presented in Fig. 2.9), circles are NE Queensland, squares are Potrillo Maar and Kilbourne Hole all from this study. Triangles are abyssal peridotites (Johnson et al., 1989), plusses are Salt Lake Crater spinel lherzolites (Shimizu, 1987), small squares are SE Poland lherzolites (Blusztjan and Shimizu, 1988), and stars are South African whole rock data from (Nixon et al., 1981). The South African data is the only whole rock data. All other data is ion microprobe data on clinopyroxenes. Numbers 1, 2 and 3 represent the three extreme groups of xenoliths that are at the end of the trends. Arrows indicate in what direction the residual mantle will change if a melt was extracted. A stands for amphibole, C means clinopyroxene, and G means garnet. Arrows with M means the direction in which the mantle will change if a metasomatic fluid/melt is added. Boxes in Fig. 2.23 indicate the range in MORB and OIB. Horizontal and vertical lines indicate the bulk earth values for the relavant trace element ratio.

Figure 2.19 Ce/Yb versus Zr/Zr* and Ti/Ti* for peridotites

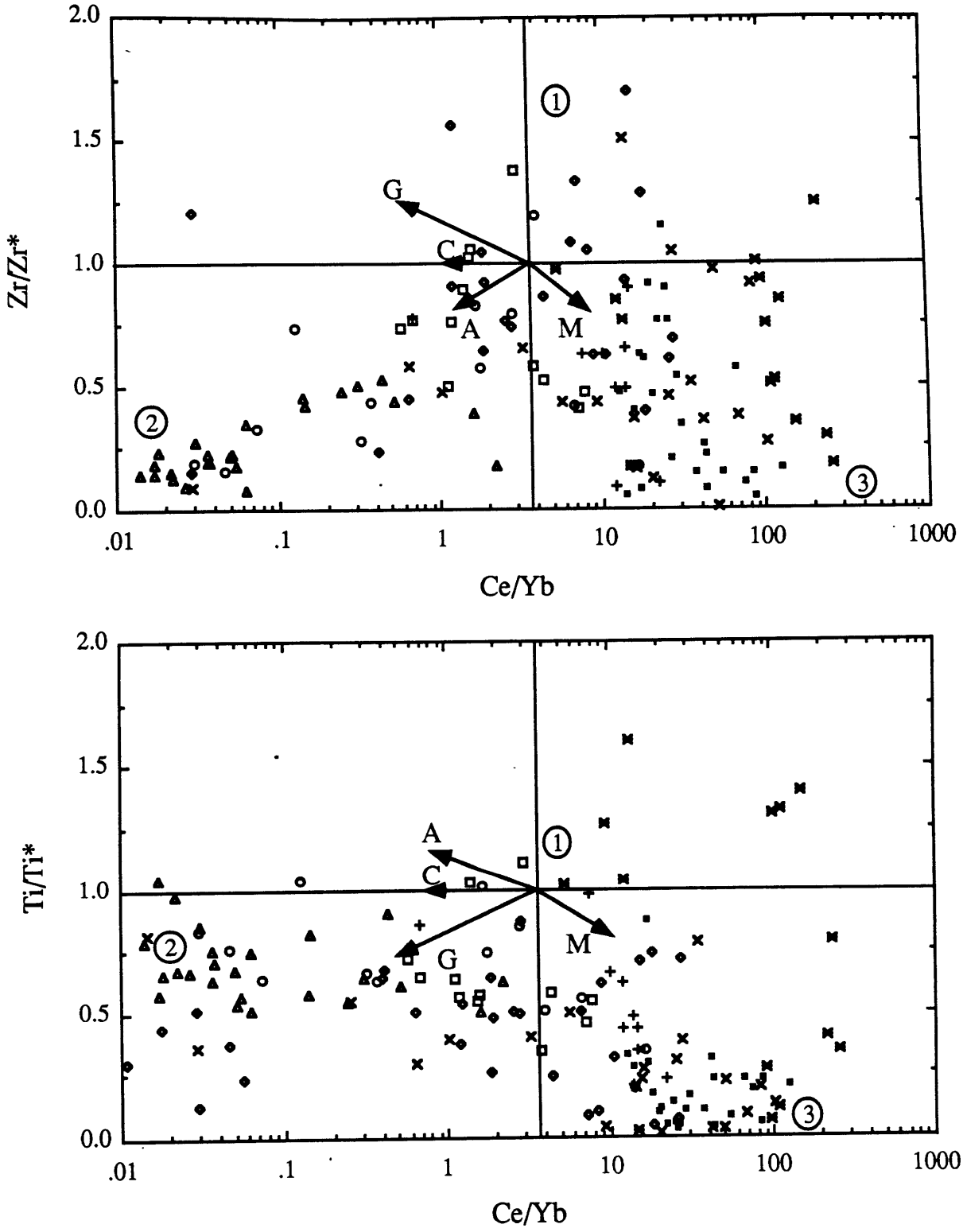

Figure 2.20 Sm/Nd versus Zr/Zr* and Ti/Ti* for peridotites

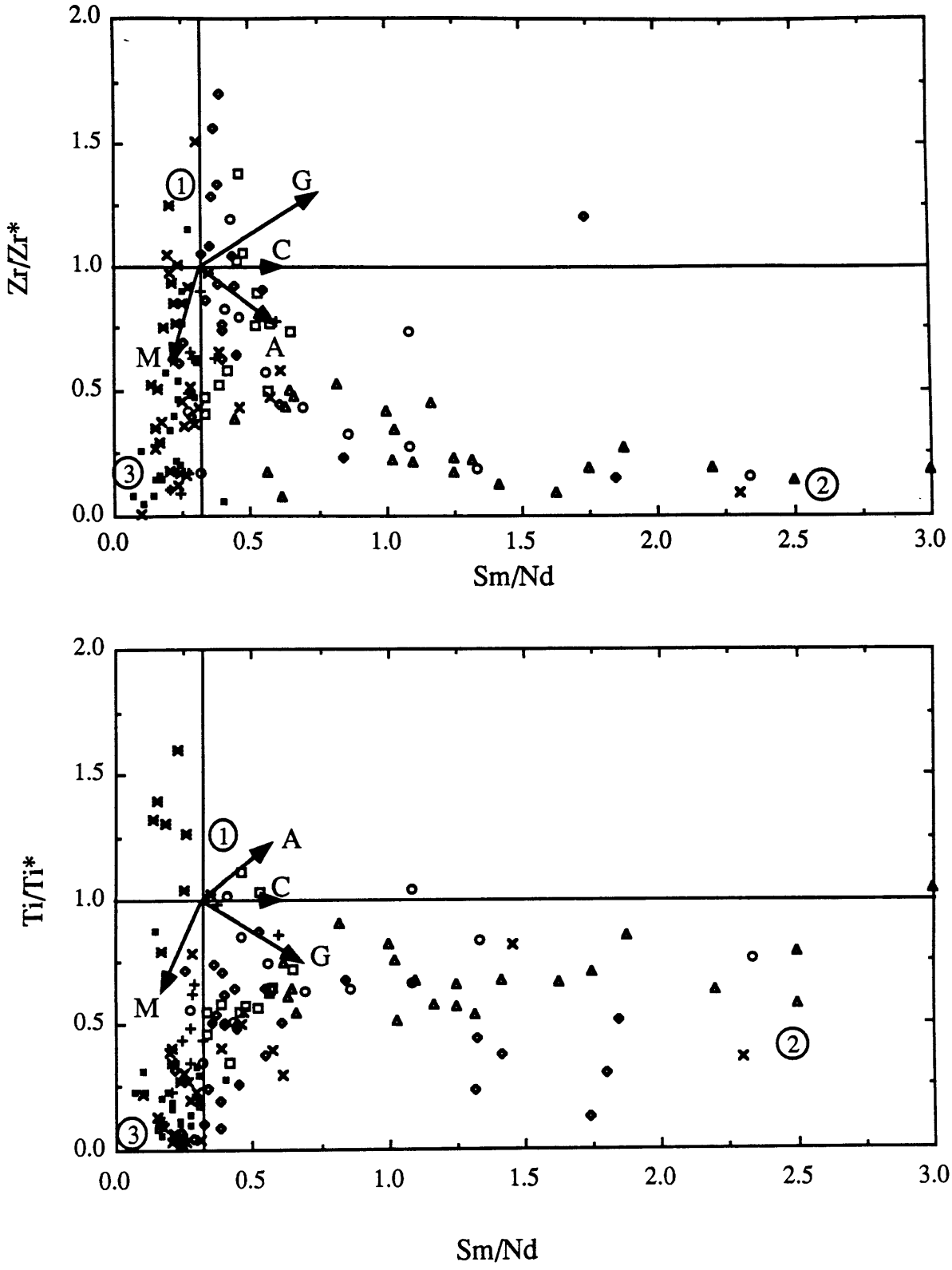

Figure 2.21 Ce/Yb versus Sm/Nd and Ti/Zr for peridotites

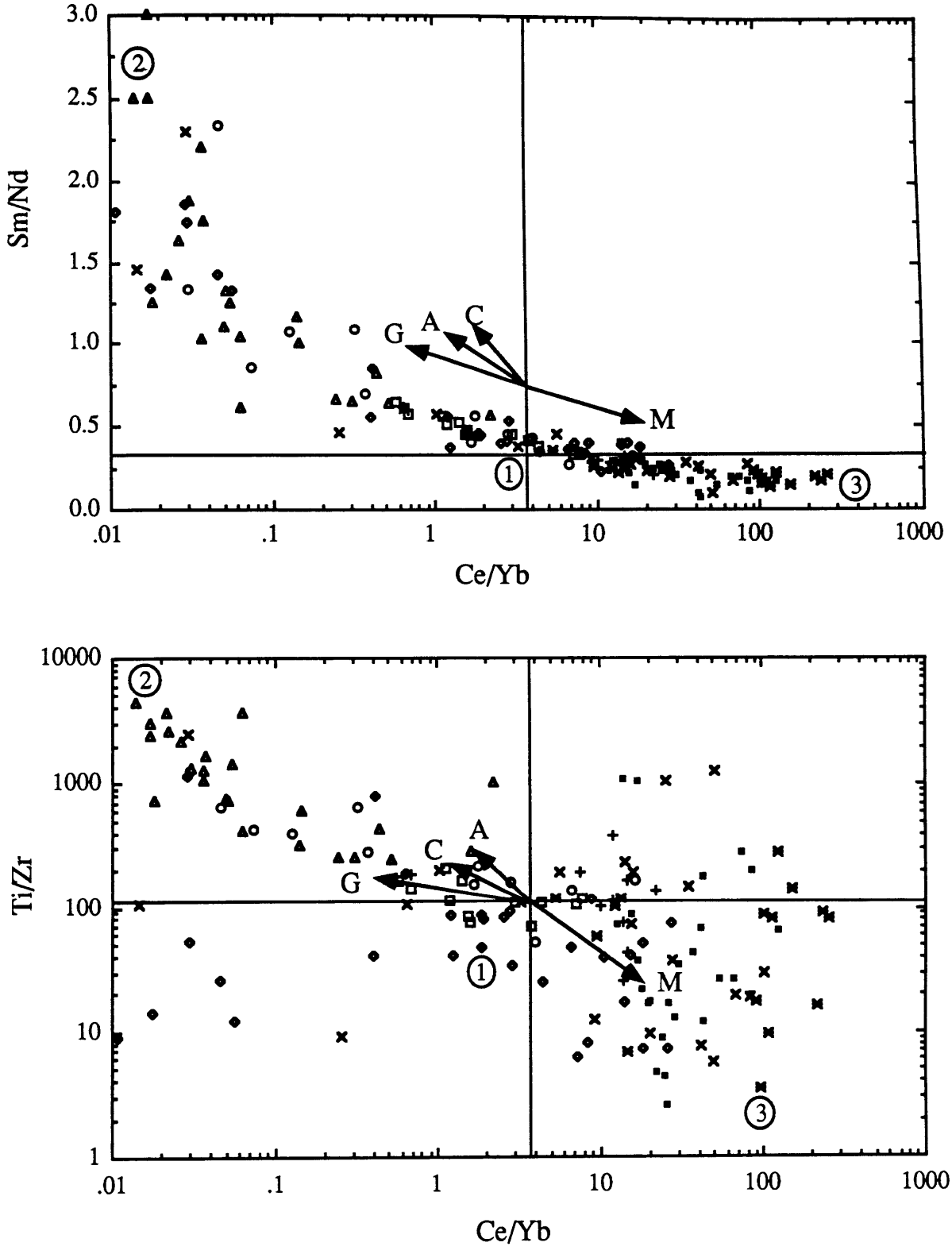

Figure 2.22 Ti/Zr versus Zr/Zr* and Ti/Ti* for peridotites

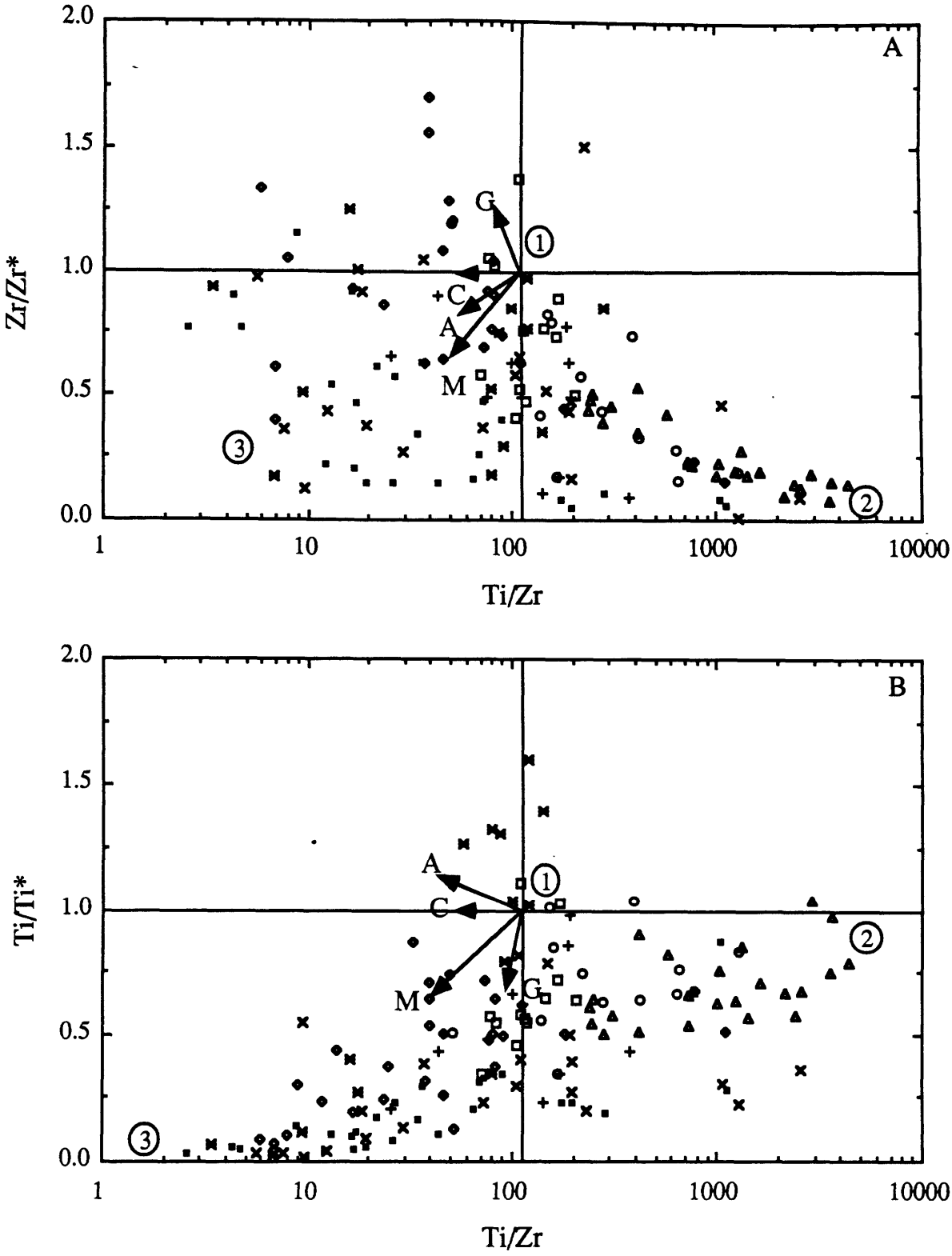

Figure 2.23 Zr verus Zr/Zr* and Ti versus Ti/Ti* for peridotites

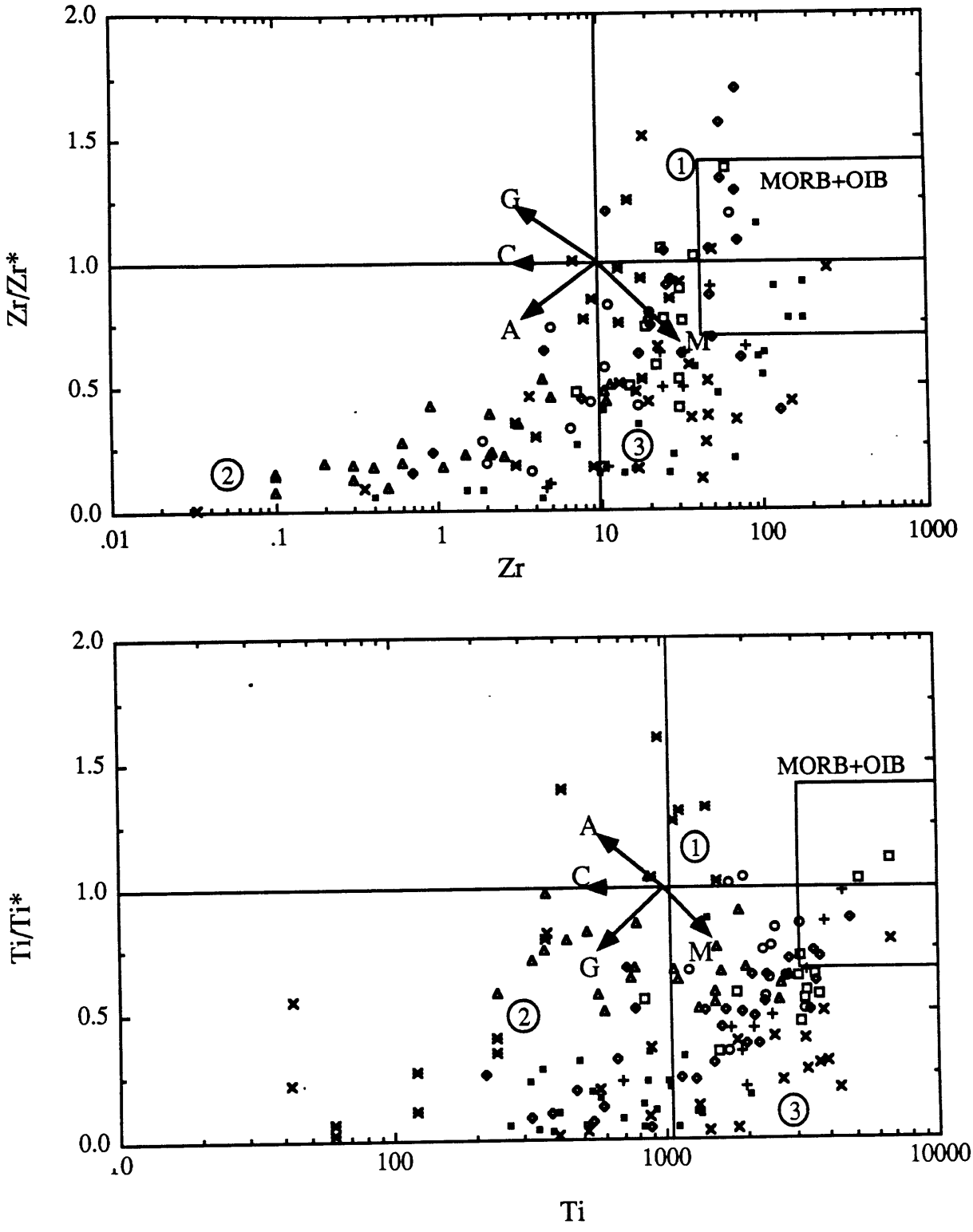

element ratios and isotopes in suites of peridotite xenoliths is well established (Downes and Dupuy, 1987; Press et al., 1986; Roden et al., 1988; Song and Frey, 1989; Stern et al., 1989; Stosch et al., 1986). Most of the lherzolites are depleted in a basaltic component; i.e., the mineralogy and major elements indicate they have undergone melting compared to a fertile, BE-type mantle. Although the range in isotopic compositions of xenoliths is larger than the range in basalts (Menzies and Hawkesworth, 1987) the isotopic compositions combined with the trace elements indicate this depletion is a young process (<2Ga) (Galer and O'Nions, 1988; Roden et al., 1988; Stosch and Lugmair, 1986; Zindler and Jagoutz, 1988). Melting has to be an important process in fractionating the trace elements, and a removal of melt is often invoked to explain the trace element depletions; e.g. see Frey et al. (1985) as an example. Mixing of individual batches of melt from a heterogeneous mantle is considered to cause the more restricted range in trace element compositions of magmas. I will consider both melting and metasomatism as possible processes fractionating the trace elements. Menzies et al. (1987a), in reviewing modally metasomatized xenoliths, define two observed metasomatic processes: a Fe-Ti-enrichment process, which is melt related, and a K-LREE enrichment process, which is fluid metasomatism related. I considered melting with garnet, amphibole or clinopyroxene as the major residual phases. The directions in the rosette on each diagram indicate the direction in which coexisting clinopyroxene will change by removal of a melt with one of the three phases as the major residual phase. Addition of this melt would have the opposite effect. The fourth direction in the rosette is a hypothetical metasomatic process. This metasomatic process causes LREE enrichment, and enrichment in REE relative to both Ti and Zr. Addition of this metasomatic component will lead to a decrease in Ti/Ti*, Zr/Zr*, and Ti/Zr. This type of metasomatic process can be observed in xenoliths from S.Africa (Erlank et al., 1987; Nixon and Boyd, 1979). Carbonatites are another example of material sometimes extremely enriched in REE and low in Zr and Ti. Thus, the proposed existence of a process creating HFSE depletions while creating LREE enrichment is plausible and observed.

Figs. 2.18 through 2.23 show again most clinopyroxenes in lherzolites are depleted in the HFSE compared to REE. As a first approximation the field for peridotites has a boomerang shape in Fig. 2.19. The top of the boomerang is formed by material which is close in BE for Ce/Yb and Sm/Nd, but has both Ti/Ti* and Zr/Zr*>1. The group of samples with these characteristics is labeled (1). One end of the boomerang is formed by samples that have in general a depleted LREE pattern; the extreme end of this group is labeled (2). A number of oceanic xenoliths fall on the BE-(2) arm of the boomerang and a major part of the trend is formed by abyssal peridotites. Abyssal peridotites are interpreted as being the residues of sequential partial melting in the garnet stability field (Johnson et al., 1989). Furthermore, the samples showing an extreme range in Ce/Yb at one locality (Yangaburro and Mechetas Las Viscaches) lie on this trend. The other arm of the boomerang is formed by some of the other Patagonian samples, lherzolites from SW Poland, and the some of the South African lherzolites.

The complexity of the observed variations is illustrated by considering the arm of the boomerang from (2) to BE in Fig. 2.19. On Fig. 2.19A (and in Figs. 2.20A, 2.21A, B, and 2.23A) this trend is parallel to the amphibole vector and approximately perpendicular to the direction for garnet melting or metasomatism. In Fig. 2.19B (and Figs. 2.20B, and 2.23B) the BE-(2) trend is parallel to the garnet vector and almost perpendicular to the amphibole vector. Ti behaves as if garnet is the major phase controlling it, and for Zr, amphibole seems to be the major phase controlling it.

The BE-(3) trend is roughly parallel to the metasomatism vector in every diagram except for Fig. 2.23. However, the sample groups within the BE-(3) trend have different directions within the array on Fig. 2.20B, and if this hypothetical metasomatism was indeed a major process, then there should be a good correlation between Ti/Ti* and Zr/Zr*, which is clearly not true (see Fig. 2.17). The samples lying towards (1) in the diagrams represent a component which is also hard to reconcile with the proposed processes. In essence, Ti and Zr behave again opposite to each other for the proposed phases. Tracking one individual group of closely related samples always

Figure 2.24

Potential range in isotopes for clinopyroxenes in xenoliths if the xenoliths were left undisturbed for 2by. Data taken from Table 2.1-2.8. For the Hf-isotope ratio it was assumed that the chondrite normalized Ce/Yb equals the chondrite normalized Lu/Hf. Field for oceanic basalts is also indicated, but hardly visible.

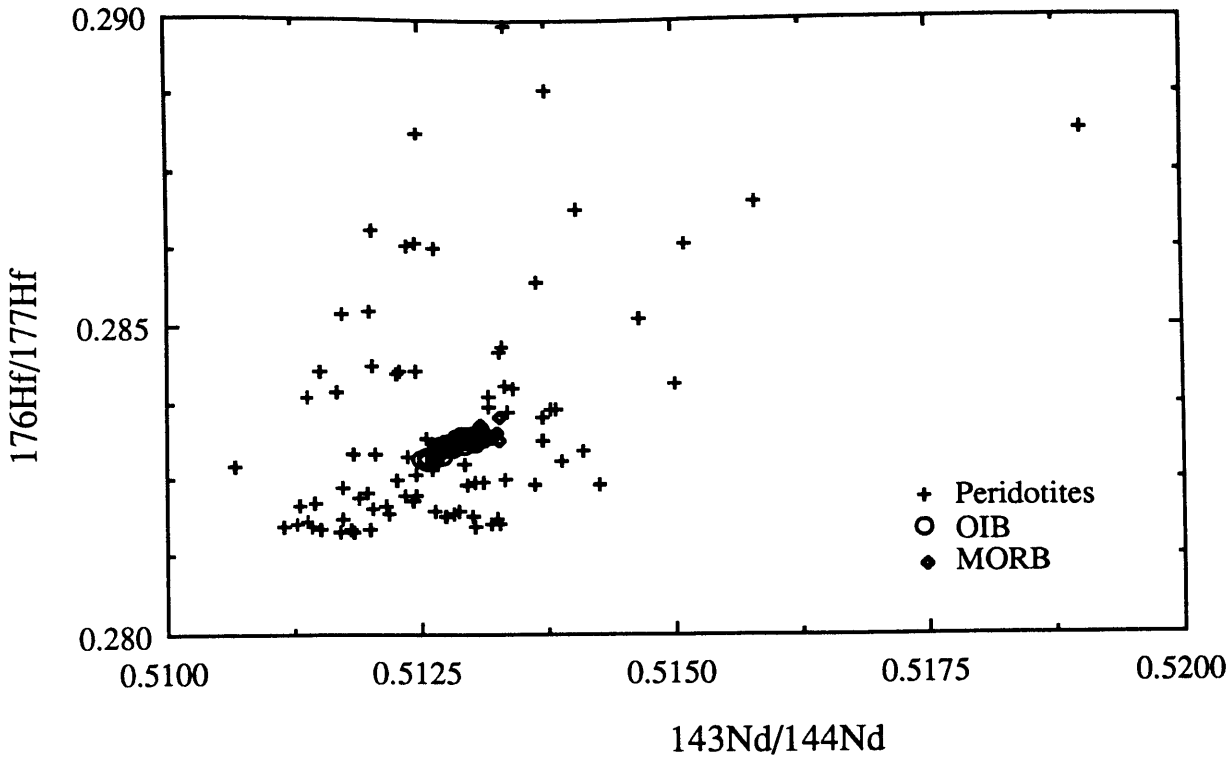
0.290
0.285
0.280
176Hf/177Hf
0.5100
0.5125
0.5150
0.5175
0.5200
143Nd/144Nd
Peridotites
OIB
MORB

breaks down at some point on a HFSE-REE variation, and some phase fractionating the REE from the HFSE is necessary. In Fig. 2.21A and B, all 4 fractionation processes are roughly parallel, but still substantial variation in Ti/Zr is observed, as well as variation in Sm/Nd at the low Ce/Yb end of the array. Also, Fig. 2.23 shows the field for oceanic lavas, and clearly these lavas are not complementary to, or in equilibrium with, the majority of the observed mantle samples. From the above observations it can be concluded that simple depletion/enrichment events using the observed phases are not able to explain the trace element variations in peridotites. Furthermore, even when continental lavas are included, variations in Ti/Ti* and Zr/Zr* in basalts are limited. In some cases, continental volcanic rocks have HFSE depletions (Ormerod et al., 1988; Pegram, 1986) and in very rare cases (Leucite Hills, Wyoming) HFSE enrichments are observed. But oceanic and continental volcanic rocks show very limited variations in trace element ratios and, except for IAB, have Zr/Zr* and Ti/Ti* close to unity. Clinopyroxenes with Ti/Ti*<1 and Zr/Zr*<1 cannot be in equilibrium with or generate MORB, OIB or the majority of continental volcanic rocks.

Fig. 2.24 shows the potential isotopic variability of the xenoliths assuming the observed trace element ratios exist for 2 Ga. The calculated potential variations are extremely large, indicating that either the trace element variations are all very young, or the magmas do not sample this type of peridotite as melts, or the isotopic heterogeneities are small scale compared to the region magma samples. Based on direct isotopic evidence from xenoliths the trace element variations are young (<1Ga) (Galer and O'Nions, 1988; Richardson et al., 1985; Salters, 1987; Stosch and Lugmair, 1986; Stosch et al., 1986; Zindler and Jagoutz, 1988).

The notion that likely depletion/enrichment processes cannot explain the trace element variations in these peridotites, plus their obvious failure to be an equilibrium residue for common basalts, suggests the existence of an additional process. The existence of HFSE-depleted material, especially as a ubiquitously sampled sub-oceanic mantle component, is obvious and has to be explained.

Since no shallow level process (<100km deep) is capable of producing the HFSE depletion as observed in peridotites, I propose, almost by default, that most HFSE-depletions are generated in the deeper mantle. Preliminary data on majorite and perovskite (Kato et al., 1987; Kato et al., 1988) indicate that these phases, together with garnet, are able to fractionate the REE from the HFSE and allow for the decoupling of Ti and Zr during solid-melt partitioning. I suggest these high pressure phases play a role in the creation of the HFSE depletions. Generation of the HFSE depletions in the lower mantle then brings up a problem of how to transport these characteristics to shallow levels in the mantle without significantly fractionating MORB and OIB HFSE/REE ratios. If Zr/Hf ratio is not fractionated by magmatic processes (see Chapter 3 and Section 2.2 on D's for justification), then the small range in the isotopic compositions of OIB and MORB compared with the potential range in peridotites indicates the observed HFSE/REE ratios are young.

From a tectonic point of view, it seems almost impossible for abyssal peridotites not to be the residue of MORB genesis. For the same tectonic reason, xenoliths collected from ocean islands must have seen melt extraction leading to either MORB or OIB. Whether this relationship between peridotites is the result of simple melting (Dick and Fisher, 1984; Prinzhofer and Allegre, 1985; Shibata and Thompson, 1986), or more complex melting (Johnson et al., 1989), at some point, either in the spinel or in the garnet stability field, these peridotites were in equilibrium with melt. The HFSE/HFSE* ratios in abyssal peridotites indicate that if these peridotites are residual to MORBs, then the melt extraction was not the last process these peridotites have seen. In order to solve these apparent contradictions, I propose the following explanation. A cartoon of the process is given in Fig. 2.25. The first step is completely arbitrary. It is postulated that in the deeper mantle, at the root zone of the upwelling limb of a convection cell, the mantle is metasomatized by small degrees of melt. This melt was in equilibrium with perovskite and majorite and as such developed HFSE depletions. The melt is frozen in at depth and has both Zr and Ti depletions, almost no Sr, and low Ce/Yb. The rising limb of the convection cell then becomes

Figure 2.25

Cartoon of a ridge. Solid horizontal line indicates beginning of melting. Dashed line indicates possible depth of the garnet-spinel transition. No scale is implied. Curves with fishhook arrows indicate mantle flowlines. Lines with solid arrows indicate melt movement.

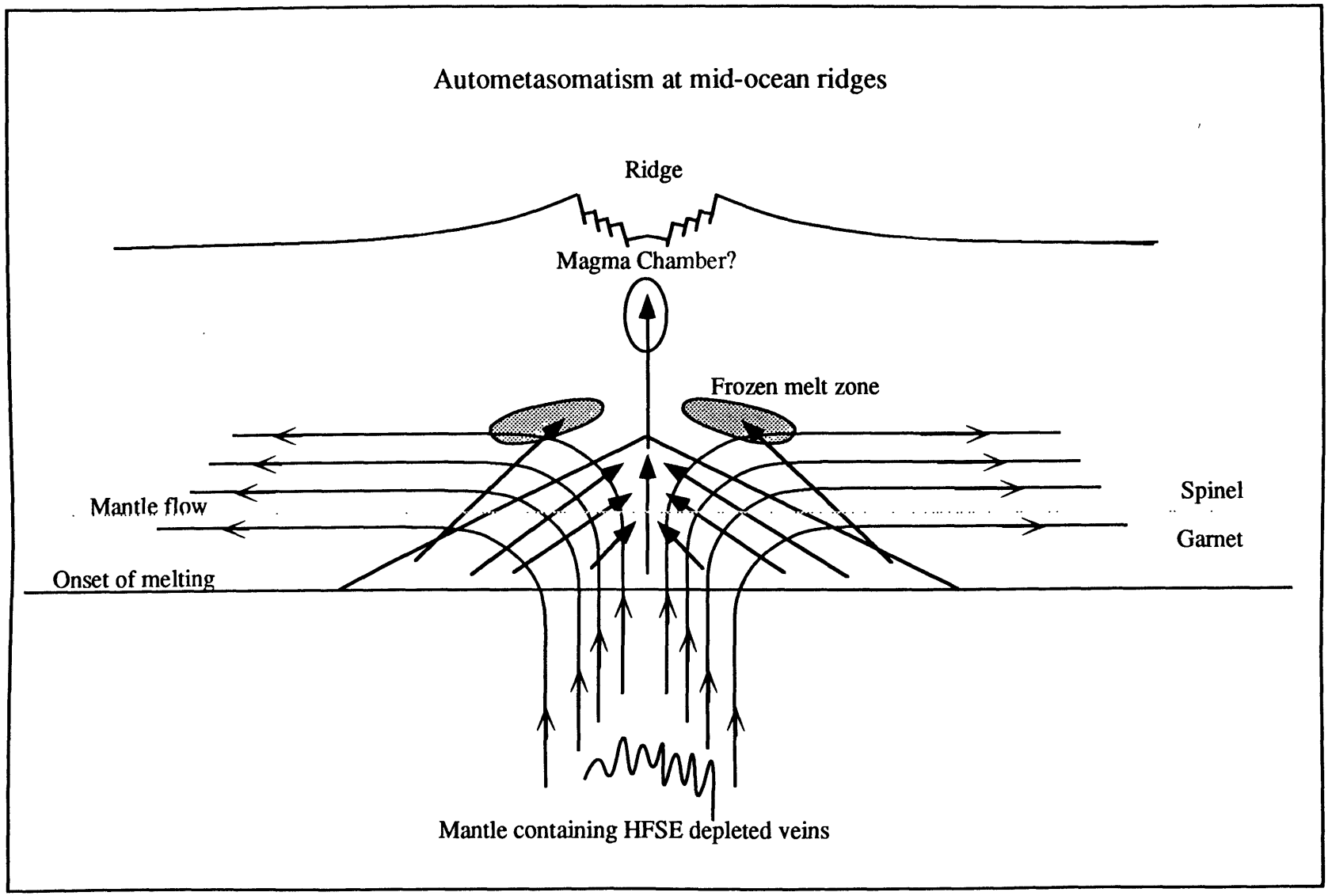
Autometasomatism at mid-ocean ridges
Ridge
Magma Chamber?
Frozen melt zone
Mantle flow
Spinel
Garnet
Onset of melting
Mantle containing HFSE depleted veins

the vehicle that transports this newly created HFSE depleted vein to the upper parts of the mantle. When the mantle rises and undergoes decompression melting, the first material to melt is this HFSE-depleted vein material. In an attempt to explain the observations, I propose that the MORB melting process (Fig. 2.25) is not completely efficient, but is instead autometasomatic. Recent models for mantle and magma flow beneath the mid-ocean ridges indicate magma collection is not necessarily 100% efficient (Phipps Morgan, 1987; Phipps Morgan and Forsyth, 1988; Scott and Stevenson, 1989). Melt generated at the edge of the melting regime can have a path more vertical than the path needed to reach the ridge axis. This edge-melt percolates through a mantle which has seen 10-15% melt extraction on ridge to generate MORB. The edge-melt is depleted in HFSE and is trapped and frozen into this depleted mantle. Since the mantle, that freezes in the "edge-melts", is highly depleted, it will take on the trace element signature of this metasomatic melt. Recent calculations on melt flow indicate that the collection process is less efficient at a ridge-transform intersection (Cordery and Phipps Morgan, 1989; J. Phipps Morgan, pers.comm). At a ridge-transform intersection this extra uncollected melt is capable of infiltrating the abyssal mantle. Abyssal peridotites are only sampled at transform faults. MORB represents a larger degree of melting, and thereby the trace element signature of the small fraction of vein material is swamped by the overall signature of the mantle melts. It has been well documented that the chemistry of MORB changes from representing high degrees of melting at the center of a ridge segment, to lower degrees of melting near a transform fault (Klein et al., 1988; Langmuir et al., 1986). As a consequence, abyssal peridotites contain more information on the transform fault effect than on the melting that occurs at the center of the ridge. I require that the metasomatizing agent deep in the mantle be depleted in LREE and Sr while having $Zr/Zr<1$ and $Ti/Ti^*<1$ and consequently high Ti/Zr. Although majorite fractionates the REE less strongly then garnet, still both majorite and perovskite have $D_{LREE}<D_{HREE}$ (Kato et al., 1987; Kato et al., 1988; Ohtani et al., 1988). However, more experiments on garnet, and other high pressure phases are needed to more accurately determine the

D's. Island arc basalts sample the frozen in HFSE-depleted mantle (see above). Thus island arc basalts are most likely generated from a source with characteristics similar to MORB. This refractory type mantle, when fluxed with a component from the subducted slab, is able to generate IAB.

2.6 CONCLUSIONS

1) HFSE/REE of clinopyroxenes from anhydrous spinel peridotites and of the bulk rock are similar.
2) Peridotite xenoliths show extreme variations in trace element concentrations and ratios.
3) Trace elements ratios in a single xenolith occurrence can cover a large part of the range observed for the world wide variation.
4) Ti and Zr, although both a HFS, behave differently during mantle fractionation processes.
5) HFSE depletions in island arc basalts are reflecting source characteristics. IABs are probably generated from a depleted mantle source.
6) Abyssal peridotites are most likely the results of melt extraction to generate MORB followed by a small degree of metasomatism. The abyssal peridotites related to transform faults are not representative of a residual MORB mantle.
7) HFSE-REE variations as observed in clinopyroxenes in peridotite cannot be explained with metasomatism or melting in equilibrium with garnet, amphibole and diopside. Part or all of the HFSE depletions indicate equilibration of melts with 'deep' mantle phases such as perovskite and majorite.

2.7 References

Allegre, C.J., Hart, S.R. and Minster, J.F. (1983a). Chemical structure and evolution of the mantle and the continents determined by inversion of Nd and Sr isotopic data, I. Theoretical models. Earth Plan. Sci. Lett. **66**: 177-190.

Allegre, C.J., Hart, S.R. and Minster, J.F. (1983b). Chemical structure and evolution of the mantle and the continents determined by inversion of Nd and Sr isotopic data, II. Numerical experiments and discussion. Earth Plan. Sci. Lett. **66**: 191-213.

Anders, E. and Grevesse, N. (1989). Abundances of the elements: Meteoritic and solar. Geochim. Cosmochim. Acta. **53**: 197-214.

Basaltic Volcanism Study Project. (1981). Basaltic Volcanism on the terrestrial planets. New York, Pergamon Press.

Beer, H., Walter, G., Macklin, R.L. and Patchett, P.J. (1984). Neutro capture cross sections and solar abundances of ^{160,161}Dy, ^{170,171}Yb, ^{175,176}Lu and ^{176,177}Hf for the *s*-process analysis of the radionuclide ^{176}Lu. Phys. Rev. **C30**: 464-478.

Blusztjan, J. and Shimizu, N. (1988). The trace element variations in clinopyroxenes from spinel peridotite xenoliths from S.W. Poland. V.M. Goldschmidt Conference. 30.

Boyd, F.R. and Finger, L.W. (1975). Homogeneity of minerals in mantle rocks from Lesotho. Carnegie Inst. Wash. Yearb. **74**: 519-525.

Carter, J.L. (1970). Mineralogy and chemistry of the Earth's upper mantle based on the partial fusion- partial crystallization model. Geol. Soc. Am. Bull. **81**: 2021-2034.

Clague, D.A. and Frey, F.A. (1982). Petrology and trace element chemistry of the Honolulu volcanics, Oahu: Implication for the oceanic mantle below Hawaii. J. Petrol. **23**: 447-504.

Clague, D.A., Frey, F.A., Thompson, G. and Rindge, S. (1981). Minor and trace element geochemistry of volcanic rocks dredged from the Galapagos spreading center: role of crystal fractionation and mantle heterogeneity. J. Geophys. Res. **86B**: 9469-9482.

Cordery, M.J. and Phipps Morgan, J. (1989). Melt migration at ridge-transform intersections. preprint. :

Dick, H.J.B. and Fisher, R.L. (1984). Mineralogical studies of the residuals of mantle melting: abyssal and alpine-type peridotites. Kimberlites II: The mantle and crust-mantle relationships. Amsterdam, Elsevier.

Dosso, L., Bougault, H., Beuzart, P., Calvez, J.Y. and Joron, J.L. (1988). The geochemical structure of the south-east Indian ridge. Earth Plan. Sci. Lett. **88**: 47-59.

Downes, H. and Dupuy, C. (1987). Textural, isotopic and rare earth variations in spinel peridotites xenoliths, Massif Central, France. Earth Plan. Sci. Lett. **82**: 121-135.

Dunn, T. (1987). Partioning of Hf, Lu, Ti and Mn between olivine, clinopyroxene and basaltic liquid. Contrib. Mineral. Petrol. **96**: 476-484.

Dupuy, C., Dostal, J., Marcelot, G., Bougault, H., Joron, J.L. and Treuil, M. (1982). Geochemistry of basalts from central and southern New Hebridesarc: Implication for their source rock composition. Earth Plan. Sci. Lett. **60**: 207-225.

Dupuy, C., Vidal, P., Barsczus, H.G. and Chauvel, C. (1987). Origin of basalts from the Marquesas Archipelago (south central Pacific

Ocean); isotope and trace elemnt constraints. Earth Plan. Sci. Lett. **82**: 145-152.

Ehrenberg, S.N. (1979). Garnetiferous ultramafic inclusions in minette from the Navajo volcanic field. The mantle sample: Inclusions in kimberlites and other volcanics. Washington DC, American Geophysical Union.

Elthon, D. (1988). The petrogenesis of primary mid-ocean ridge basalts. Critical. Rev. Marine Sci. **in press**:

Erlank, A.J., Waters, F.G., Hawkesworth, C.J., Haggerty, S.E., Allsopp, H.L., Rickard, R.S. and Menzies, M.A. (1987). Evidence for mantle metasomatism in peridotite nodules from the Kimberley pipes, South Africa. Mantle Metasomatism. London, Academic Press.

Falloon, T.J. and Green, D.H. (1987). Anhydrous partial melting of MORB pyrolite and other peridotite compositions at 10 kbar: Implications for the origin of primitive MORB glasses. Min. Petrol. **37**: 181-219.

Frey, F.A., Dickey, J.S., Thompson, G., Bryan, W.B. and Davies, H.L. (1980). Evidence for heterogeneous primary MORB and mantle sources, NW Indian ocean. Contrib. Mineral. Petrol. **74**: 387-402.

Frey, F.A. and Green, D.H. (1974). The mineralogy, geochemisty and origin of lherzolite inclusions in Victorian basanites. Geochim. Cosmochim. Acta. **38**: 1023-1059.

Frey, F.A., Green, D.H. and Roy, S.D. (1978). Integrated models for basalt petrogenesis: a study of quartz tholeiites to olivine melilitites from south eastern Australia utilizing geochemical and experimental petrological data. J. Petrol. **19**: 463-513.

Frey, F.A. and Prinz, M. (1978). Ultramafic inclusions from San Carlos, Arizona: petrological and geochemical data bearing on their petrogenesis. Earth Plan. Sci. Lett. **38**: 129-176.

Frey, F.A., Suen, J. and Stockman, H.W. (1985). The Ronda high temperature peridotite: Geochemistry and petrogenesis. Geochim. Cosmochim. Acta. **49**: 2469-2491.

Fujimaki, H. (1986). Fractional crystallization of the basaltic suite of the Usu volcano, southwest Hokkaido, Japan, and its relationships with the associated felsic suite. Lithos. **8**: 129-140.

Fujimaki, H., Tatsumoto, M. and Aoki, K. (1984). Partition coefficients of Hf, Zr and REE between phenocrysts and groundmasses. J. Geophys.Res. **89**: 662-672.

Galer, S.J.G. and O'Nions, R.K. (1988). Chemical and isotopic studies of ultramafic inclusions from the San Carlos volcanic field, Arizona, bearing on their petrogenesis. J.Petrol. **in press**:

Garcia, M.O., Frey, F.A. and Grooms, D.G. (1986). Petrology of volcanic rocks from Kaula Island, Hawaii, implications for the origin of Hawaaian phonolites. Contrib. Mineral. Petrol. **94**: 461-471.

Gerlach, D.C. (1986). Geochemistry and petrology of recent volcanics of the Puyehue-Cordon Caulle area, Chile (40.5°). Massachusetts Institute of Technology, Cambridge, Massachusetts PhD.

Gill, J.B. (1981). Orogenic andesites and plate tectonics. Berlin, Springer Verlag.

Green, T.H. (1981). Experimental evidence for the role of accessory phases in magma genesis. J. Volc. Geotherm. Res. **10**: 405-422.

Green, T.H. and Pearson, N.J. (1985). Rare earth element partitioning between clinopyroxene and silicate liquid at moderate to high pressure. Contrib. Mineral. Petrol. **91**: 24-36.

Grove, T.L. and Bryan, W.B. (1983). Fractionation of pyroxene phyric MORB at low pressure: An experimental study. Contrib. Mineral. Petrol. **84**: 293-309.

Grutzeck, M., Kridelbaugh, S. and Weill, D. (1974). The distribution of Sr and REE between diopside and silicate liquid. Geophys. Res. Lett. **1**: 273-275.

Hart, S.R. and Zindler, A. (1986). In search for bulk-earth composition. Chem. Geol. **57**: 247-267.

Hart, S.R. and Zindler, A. (1988). Constraints on the nature and developement of chemical heterogeneities in the mantle. Mantle Convection.

Harte, B., Winterburn, P.A. and Gurney, J.J. (1987). Metasomatic and enrichment phenomena in garnet peridotite facies mantle xenoliths from the Matsoku kimberlite pipe], Lesotho. Mantle Metasomatism. London, Academic Press.

Hickey, R.L., Frey, F.A. and Gerlach, D.C. (1986). Multiple sources for basaltic arc rocks from the southern volcanic zone of the Andes (34^{o}-41^{o}S): Trace element and isotopic evidence for contributions from subducted oceanic crust, mantle and continental crust. J. Geophys.Res. **91**: 5963-5983.

Hofmann, A.W. (1988). Chemical differentiation of the Earth: the relationship between mantle, continental crust, and oceanic crust. Earth Plan. Sci. Lett. **90**: 297-314.

Huebner, J.S., Lipin, B.R. and Wiggins, L.B. (1976). Partitioning of chromium between silicate crystals and melts. Proc. Lunar Sci. Conf. **7th**: 1195-1220.

Irving, A.J. and Frey, F.A. (1978). Distribution of trace elements between garnet megacrysts and host volcanic liquids of kimberlitic to rhyolitic composition. Geochim. Cosmochim. Acta. **42**: 771-787.

Irving, A.J. and Frey, F.A. (1984). Trace element abundances in megacrysts and their host basalts: Constaints on partition coefficients and megacryst genesis. Geochim. Cosmochim. Acta. **48**: 1201-1221.

Jagoutz, E., Carlson, R.W. and Lugmair, G.W. (1980). Equilibrated Nd-unequilibrated Sr isotopes in mantle xenoliths. Nature. **286**: 708-710.

Jagoutz, E., Lorentz, V. and Wanke, H. (1979a). Major and trace elements of Al-augite and Cr-diopsides from ultramafic nodules in European alkali basalts. The Mantle sample, inclusions in kimberlites and other volcanics. Washington, D.C., American Geophysical Union.

Jagoutz, E., Palme, H., Baddenhausen, H., Blum, K., Cendales, M., Dreibus, G., Spettel, B., Lorenz, V. and Wanke, H. (1979b). The abundance of major, minor and trace elements in the Earth's mantle as derived from primitive ultramafic nodules. Proc. Lunar. Sci. Conf. **10th**: 2031-2050.

Johnson, K.T.M., Dick, H.J.B. and Shimizu, N. (1989). Melting in the oceanic upper mantle: an ion microprobe study of diopsides in abyssal peridotites. submitted. :

Kato, T., Irifune, T. and Ringwood, A.E. (1987). Majorite partition behavior and petrogenesis of the Earth's upper mantle. Geophys. Res. Lett. **14**: 546-549.

Kato, T., Ringwood, A.E. and Irifune, T. (1988). Constraints on element partition coefficients between $MgSiO_3$ perovskite and liquid determined by direct measurements. Earth Plan. Sci. Lett. **90**: 65-68.

Kay, R.W. (1980). Volcanic arc magmas: Implications of a melting-mixing model for element recycling in the crust-upper mantle system. J.Geol. **88**: 479-552.

Klein, E.M., Langmuir, C.H., Staudigel, H. and Hamelin, B. (1988). The Australian-Antarctic Discordance (AAD); A convective boundary between the Indian and Pacific Ocean isotopic provinces. Abstr. EOS. **69**: 507.

Langmuir, C.H., Bender, J.F. and Batiza, R. (1986). Petrological and tectonic segmentation of the East Pacific Rise, 5°30'-14°30'N. Nature. **322**: 422-429.

Langmuir, C.H., Bender, J.F., Bence, A.E., Hanson, G.N. and Taylor, S.R. (1977). Petrogenesis of basalts from the Famous area: mid-Atlantic ridge. Earth Plan. Sci. Lett. **36**: 133-156.

Lanphere, M.A. and Frey, F.A. (1987). Geochemical evolution of Kohala volcano, Hawaii. Contrib. Mineral. Petrol. **95**: 100-113.

Leeman, W.P., Budahn, J.R., Gerlach, D.C., Smith, D.R. and Powell, D.N. (1980). Origin of Hawaiian tholeiites: Trace element constraints. Am. J. Sci. **280A**: 794-819.

Liotard, J.M., Barsczus, H.G., Dupuy, C. and Dostal, J. (1986). Geochemistry and origin of basaltic lavas from Marquesas Archipelago, French Polynesia. Contrib. Mineral. Petrol. **92**: 260-268.

MacGregor, I.D. (1979). Mafic and ultramafic xenoliths from the Kao kimberlite pipe. The mantle sample: Inclusions in kimberlites and other volcanics. Washington DC, American Geophysical Union.

McCallum, I.S. and Charrette, M.P. (1978). Zr and Nb partition coefficients: Implications for the genesis of mare basalts, KREEP, and sea floor basalts. Geochim. Cosmochim. Acta. **42**: 859-869.

Melson, W.G., Hart, S.R. and Thompson, G. (1972). St. Paul's rocks, equatorial Atlantic: Petrogenesis, radiometric ages, and implications on the sea-floor spreading. Geol. Soc. Am. Mem. **132**: 241-272.

Menzies, M.A. and Hawkesworth, C.J. (1987). Upper mantle processes and composition. Mantle Xenoliths. New York, John Wiley & Sons.

Menzies, M.A., Halliday, A.N., Palcz, Z., Hunter, R.H., Upton, B.G.J., Aspen, P. and Hawkesworth, C.J. (1987a). Evidence from mantle xenoliths for an enriched lithospheric keel under the Outer Hebrides. Nature. **325**: 44-47.

Menzies, M.A., Rogers, N., Tindle, A. and Hawkesworth, C.J. (1987b). Metasomatic and enrichment processes in the lithospheric peridotites, an effect of asthenosphere-lithosphere interaction. Mantle Metasomatism. London, Academic Press.

Morris, J.D. (1984). Enriched geochemical signatures in Aleutian and Indonesian arc lavas: An isotopic and trace element investigation. Massachusetts Institute of Technology, Cambridge PhD.

Morris, J.D. and Hart, S.R. (1983). Isotopic and incompatible element constraints on the genesis of island arc volcanics: Cold Bay and Amak Islands, Aleutians. Geochim. Cosmochim. Acta. **47**: 2015-2030.

Newsom, H.E., White, W.M., Jochum, K.P. and Hofmann, A.W. (1986). Siderophile and chalcophile element abundances in oceanic basalts, Pb isotope evolution and growth of the Earth's core. Earth Plan. Sci. Lett. **80**: 299-313.

Nicholls, I.A. and Harris, K.L. (1980). Experimental rare earth element partition coefficients for garnet, clinopyroxene and amphibole coexisting with andesitic and basaltic liquids. Geochim. Cosmochim. Acta. **44**: 287-308.

Nicholls, I.A. and Ringwood, A.E. (1973). Effect of olivine stability in tholeiites and the production of silica undersaturated magmas in the island arc environment. J.Geol. **81**: 285-300.

Nixon, P.H. and Boyd, F.R. (1979). Garnet bearing lherzolites and discrete nodules from the Malaita alnoite, Solomon Islands, S.W. Pacific, and their bearing on oceanoc mantle composition and geotherm. The mantle sample: Inclusions in kimberlites and other volcanics. Washington, D.C., American Geophysical Union.

Nixon, P.H., Rogers, N.W., Gibson, I.L. and Grey, A. (1981). Depleted and fertile mantle xenoliths from South African kimberlites. Ann. Rev. Earth Plan. Sci. **9**: 285-309.

Ohtani, E., Moriyama, J. and Kawabe, I. (1988). Majorite garnet stability and its implication for genesis of komatiite magmas. Abstr. Chem. Geol. **70**: 147.

Ormerod, D.S., Hawkesworth, C.J., Rogers, N., Leeman, W.P. and Menzies, M.A. (1988). Tectonic and magmatic trabsitions in the Western Great Basin, USA. Nature. **333**: 349-352.

Pearce, J.A. and Cann, J.R. (1973). Tectonic setting of basic volcanic rocks determined using trace element analyses. Earth Plan. Sci. Lett. **19**: 290-300.

Pearce, J.A. and Norry, M.J. (1979). Petrogenetic implications of Ti, Zr, Y and Nb variations in volcanic rocks. Contrib. Mineral. Petrol. **69**: 33-47.

Pearce, J.A., Rogers, N., Tindle, A.J. and S, W.J. (1985). Geochemistry and petrogenesis of Basalts from Deep Sea Drilling Project Leg 92, eastern Pacific. Init. Repts. DSDP. Washington, DC, U>S Govt. Printing Office.

Pegram, W.J. (1986). Geochemical processes in the sub-continental mantle and the nature of crust mantle interaction: Evidence from the Mesozoic Appalachian Tholeiite Province. Massachusetts Institute of Technology, Cambridge, Massachusetts PhD.

Phipps Morgan, J. (1987). Melt migration beneath mid-ocean spreading enters. Geophys. Res. Lett. **14**: 1238-1241.

Phipps Morgan, J. and Forsyth, D.W. (1988). Three-dimensional flow and temperature perturbations due to a transfrom offset: Effects on oceanic crustal and upper mantle structure. J. Geophys. Res. **93**: 2955-2966.

Press, S., Witt, G., Sech, H.E., Eonov, D. and Kovalenko, V.I. (1986). Spinel peridotie xenoliths from the Tariat depression, Mongolia. I: Major element chemistry and mineralogy of a primitive mantle xenolith suite. Geochim. Cosmochim. Acta. **50**: 2587-2599.

Price, R.C., Kennedy, A.K., Riggs-Sneeringer, M. and Frey, F.A. (1986). Geochemistry of basalts from the Indian Ocean triple junction: Implication for the generation and evolution of Indian Ocean ridge basalts. Earth Plan. Sci. Lett. **78**: 279-296.

Prinzhofer, A. and Allegre, C.J. (1985). Residual peridotites and the mechanism of partial melting. Earth Plan. Sci. Lett. **74**: 251-265.

Puchelt, H. and Emmermann, R. (1983). Petrogenetic implications of tholeiitic basalt glasses from the East Pacific Rise and the Galapagos spreading center. Chem. Geol. **38**: 39-56.

Reid, A.M., Donaldson, C.H., Brown, R.W., Ridley, W.I. and Dawson, J.B. (1975). Mineral chemistry of peridotite xenoliths from the Lashaine volcano, Tanzania. Phys. Chem. Earth. **9**: 525-543.

Rhodes, J.M., Blanchard, D.P., Dungan, M.A., Rodgers, K.V. and Brannon, J.C. (1978). Chemistry of Leg 45 basalts. Initial Reports of the Deep Sea Drilling Project. Washington, U.S. Government Printing Office.

Richardson, S.H., Erlank, A.J. and Hart, S.R. (1985). Kimberlite-borne garnet peridotite xenoliths from old enriched subconbtinental lithosphere. Earth Plan. Sci. Lett. **75**: 116-128.

Roden, M.F. (1982). Geochemistry of the earth's mantle, Nunivak Island, Alaska and other areas: evidence from xenolith studies. MIT PhD.

Roden, M.F., Frey, F.A. and Francis, D.M. (1984a). An example of consequent mantle metasomatism in peridotite inclusions from Nunivak, Alaska. J. Petrol. **25**: 546-577.

Roden, M.K., Hart, S.R., Frey, F.A. and Melson, W.G. (1984b). Sr, Nd and Pb isotopic and REE geochemistry of St. Paul's rocks: The metamorfic and metasomatic development of an alkali basalt magma source. Contrib. Mineral. Petrol. **85**: 376-390.

Roden, M.F., Irving, A.J. and Murthy, V.R. (1988). Isotopic and trace element composition of the upper mantle beneath a youn continental rift: Results from Kilbourne Hole, New Mexico. Geochim. Cosmochim. Acta. **52**: 461-473.

Salters, V.J.M. (1987). Characteristics of the mantle beneath the Carpathians, Hungary, as inferred from calc-alkaline volcanics. NATO Adv. Res. Workshop on crust/mantle recycling ar convergence zones. 120-121.

Salters, V.J.M. and Shimizu, N. (1988). World-wide occurrence of HFSE-depleted mantle. Geochim. Cosmochim. Acta. **52**: 2177-2182.

Saunders, A.D. (1987). Geochemistry of basalts from mesozoic pacific ocean crust: Deep Sea Drilling Project Leg 91. Init. Repts. DSDP. U.S. Governement Printing Office.

Schnetzler, C.C. and Philpotts, J.A. (1970). Partition coefficients of rare-earth elements between igneous matrix material and rock-forming mineral phenocrysts- II,. Geochim. Cosmochim. Acta. **34**: 331-340.

Scott, D.R. and Stevenson, D.J. (1989). A self-consistent model of melting, magma migration and buoyancy-driven circulation beneath mid-ocean ridges. J. Geophys. Res. **94**: 2973-2988.

Shee, S.R. and Gurney, J.J. (1979). The mineralogy of xenoliths from Orapa, Botswana. The mantle sample: Inclusions in kimberlites and other volcanics. Washington DC, American Geophysical Union.

Shibata, T. and Thompson, G. (1986). Peridotites from the Mid-Atlantic Ridge at 43^{o}N and their petrogenetic relation to abyssal tholeiites. Contrib. Mineral. Petrol. **93**: 144-159.

Shimizu, H. (1980). Experimental study on rare-earth element partitioning in minerals formed at 20 and 30kb for basaltic systems. Geochem. J. **14**: 185-202.

Shimizu, H., Sangen, K. and Masuda, A. (1982). Experimental study on rare-earth element parttioning in olivine and clinopyroxenes

formed at 10 and 20kb for basaltic systems. Geochem. J. **16**: 107-117.

Shimizu, N. (1975). Rare earth elements in garnets and clinopyroxenes from garnet lherzolite nodules in kimberlites. Earth Plan. Sci. Lett. **25**: 26-32.

Shimizu, N. (1987). Trace element abundance patterns of pyroxenes in spinel lherzolite nodules from Salt Lake Crater, Oahu (abstr.). EOS. **68**: 447.

Shimizu, N. and Allegre, C.J. (1978). Geochemistry of transition elements in garnet lherzolite nodules in kimberlites. Contrib. Mineral. Petrol. **67**: 41-50.

Shimizu, N. and Hart, S.R. (1974). Rare earth elemnt concentrations in clinopyroxenes from an ocean ridge lherzolite. Carnegie Inst. Wash. Yearb. **73**: 964-967.

Shimizu, N. and Hart, S.R. (1982). Appplications of the ion microprobe to geochemistry and cosmochemistry. Ann. Rev. Earth Plan. Sci. **10**: 483-526.

Shimizu, N. and Kushiro, I. (1975). The partitioning of rare-earth elements and barium between garnet and liquid at high pressures: preliminary experiments. Geophys. Res. Lett. **2**: 413-416.

Shimizu, N., Semet, M.P. and Allegre, C.J. (1978). Geochemical applications of quantative ion-microprobe analysis. Geochim. Cosmochim. Acta. **42**: 1321-1334.

Smith, D. and Boyd, F.R. (1987). Compositional heterogeneity in high-temperature lherzolite nodule and implications for mantle processes. Mantle Xenoliths. New York, John Wiley & Sons.

Song, Y. and Frey, F.A. (1989). Geochemistry of peridotite xenoliths in basalt from Hannuoba, Eastern China: Implications for subcontinental mantle heterogeneity. Geochim. Cosmochim. Acta. **53**: 97-113.

Stephenson, P.J., Griffin, T.J. and Sutherland, F.L. (1980). Cainozoic volcanism in Northeastern Australia. The geology and geophysics of northeastern Australia. Sidney, Geological Society of Australia.

Stern, C.R., Saul, S., Futa, K. and Skewes, M.A. (1986). Nature and evolution of the subcontinental mantle lithosphere below southern South America and implications for Andean magmatism. Revista Geologica de Chile. **27**: 41-53.

Stern, C.R., Saul, S., Skewes, M.A. and Futa, K. (1989). Garnet peridotite xenoliths from the Pali-Aike alkali basalts of southernmost South America. Austr. J. Earth Sci. **in press**:

Stosch, H.-. and Lugmair, G.W. (1986). Trace element and Sr and Nd isotope geochemistry of peridotite xenoliths from the Eifel (West Germany) and their bearing on the evolution of the subcontinental lithosphere. Earth Plan. Sci. Lett. **80**: 281-298.

Stosch, H.G., Lugmair, G.W. and Kovalenko, V.I. (1986). Spinel peridotite xenoliths from the Tariat depression, Mongolia. II: Geochemistry and Nd and Sr isotopic composition and their implications for the evolution of the subcontinental lithosphere. Geochim. Cosmochim. Acta. **50**: 2601-2614.

Stosch, H.-. and Seck, S.A. (1980). Geochemistry and mineralogy of two spinel peridotite suites from Dreiser Weiher, West Germany. Geochim. Cosmochim. Acta. **44**: 457-470.

Sun, S., Nesbitt, R.W. and Sharaskin, A.Y. (1979). Geochemical characteristics of mid-ocean ridge basalts. Earth Plan. Sci. Lett. **44**: 119-138.

Tanaka, T. and Nishizawa, O. (1975). Partitioning of REE, Ba and Sr between crystal and liquid phases for a natural silicate system at 20kb pressure. Geochem. J. **9**: 161-166.

Tarney, J., Saunders, A.D., Mattey, D.P., Wood, D.A. and Marsh, N.G. (1981). Geochemical aspects of back-arc spreading in the Scotia Sea and western Pacific. Phil. Trans. Roy. Soc. London. **A 300**: 263-285.

Tatsumoto, M. (1978). Isotopic composition of lead in oceanic basalts and its implication to mantle evolution. Earth Plan. Sci. Lett. **38**: 63-87.

Tera, F., Brown, L., Morris, J.D., Sacks, I.S., Klein, J. and Middleton, R. (1986). Sediment incorporation in island-arc magmas: Inferences from ^{10}Be. Geochim. Cosmochim. Acta. **50**: 535-550.

Thompson, R.N., Morrison, M.A., Dickin, A.P. and Hendry, G.L. (1983). Continental flood basalts...Arachnids rule OK? Continental basalts and mantle xenoliths. Cheshire, U.K., Shiva.

Tormey, D.R., Grove, T.L. and Bryan, W.B. (1987). Experimental petrology of normal MORB near the Kane fracture zone: 22°-25°N, mid-Atlantic ridge. Contrib. Mineral. Petrol. **96**: 121-139.

White, W.M. and Patchett, P.J. (1984). Hf-Nd-Sr isotopes and incompatible element abundances in island arcs: Implications for magma origins and crust-mantle evolution. Earth Plan. Sci. Lett. **67**: 167-185.

White, W.M., Tapia, M.D.M. and Schilling, J.-. (1979). The petrology and geochemistry of the Azores Islands. Contrib. Mineral. Petrol. **69**: 201-213.

Wood, D.A. (1979). A variable veined suboceanic upper mantle-Genetic significance for mid-ocean ridge basalts from geochemical evidence. Geology. 7: 499-503.

Wood, D.A., Tarney, J., Varet, J., Saunders, A.D., Bougault, H., Joron, J.L., Treuil, M. and Cann, J.R. (1979). Geochemistry of basalts drilled in the North Atlantic by IPOD Leg 49: Implications for mantle heterogeneity. Earth Plan. Sci. Lett. **42**: 77-97.

Zindler, A. and Hart, S.R. (1986). Chemical Geodynamics. Ann. Rev. Earth Plan. Sci. **14**: 493-571.

Zindler, A. and Jagoutz, E. (1988). Mantle cryptology. Geochim. Cosmochim. Acta. **52**: 319-333.

Chapter 3:
The Use of Hf-Isotopes to Constrain Magmatic Processes and Mantle Sources

3.1 Introduction

This chapter reports the results of a Hf-isotope study on island arc and oceanic basalts, and the interpretation thereof. The analytical technique for Hf-isotopes is described in the appendix. ^{176}Hf is produced by β-decay of ^{176}Lu. The half life of ^{176}Lu is $3.57\pm0.14 *10^{10}$ a, leading to a decay constant of $1.94\pm0.07*10^{-11}a^{-1}$ (Tatsumoto et al., 1981). The half-life was determined by analyses of Lu/Hf and Hf isotopic composition of meteorites (C-types and eucrites) of well known age (Patchett and Tatsumoto, 1980b; Patchett and Tatsumoto, 1981; Tatsumoto et al., 1981). These studies also yield the initial $^{176}Hf/^{177}Hf$ for Bulk Earth (BE) of 0.27978. The bulk earth Lu/Hf ratio equals 0.2373 ($^{176}Lu/^{177}Hf$=0.0337, conversion factor from atomic to elemental weight ratios equals 7.0415) (Beer et al., 1984), and using the decay equation a present day $^{176}Hf/^{177}Hf$ =0.28289 for BE is obtained. The first successful use of Hf-isotopes to constrain geological processes was reported by Patchett and Tatsumoto (1980a) using chemical techniques described by Patchett and Tatsumoto (1980c).

This chapter consists of 4 parts. The first part is a general introduction and reviews the behavior of Lu and Hf, especially in magmatic processes. The second part, on the mantle taxonomy, presents new data on Hf-isotopic composition of mantle-derived materials and adds the Hf-isotopes to the framework of endmember mantle components as defined by Zindler and Hart (1986). The third part presents and discusses new data on Fiji, and the use of Hf-isotopes in island arc magma generation. The fourth part discusses the Hf-isotope systematics in oceanic basalts and implications for MORB genesis.

The measurement of Hf-isotopic composition is by far more difficult then the analysis for either Nd, Sr or Pb isotopic composition. The similarity in chemical behavior of Hf and Zr makes it difficult to separate pure Hf. Furthermore, the ionization potential of Hf is high, causing a very low ionization efficiency. Therefore, Hf-isotopes should only be used in cases where they have the potential to be complementary to the conventional isotopic systematics. The work

done by Patchett and others, and this work, indicates where Hf-isotopes add to our understanding of geological processes.

3.2 Geochemistry of Lu and Hf

The Lu-Hf systematics will add information to the established isotopic systems in situations where the Lu/Hf fractionation is different and more distinct than other parent-daugther ratios. The behavior of Lu and Hf in geological processes has to be known to make predictions on which rocks can be usefully studied with Lu-Hf. Lu and Hf are both incompatible elements in magmatic processes (<15 GPa) and, as such, always concentrate in the melt relative to crystalline phases. Hf behaves very similarly to Zr, both crustal rocks and mantle-derived rocks have close to chondritic Zr/Hf ratio (Zr/Hf= 38.5) (Anders and Grevesse, 1989). Furthermore, different types of chondrites have identical Zr/Hf ratios. Hf is a so-called High Field Strength Element (HFSE), together with Zr, Ti, Nb and Ta. HFSE are elements with a large charge (4+ for Ti, Zr and Hf; and 4 or 5+ for Nb and Ta) and a small ionic radius (0.42, 0.59 and 0.58Å for Ti(IV), Zr(IV) and Hf(IV) respectively; and 0.68Å for both Ta(VI) and Nb(VI)) (Henderson, 1986).

Zr and Hf are incompatible in most minerals, and in crustal rocks largely concentrated in zircon ($ZrSiO_4$). Zircon can contain 15,000-20,000ppm Hf (Patchett et al., 1981). Lu, on the other hand, by far less compatible in zircon than Hf, and as a consequence the $^{176}Hf/^{177}Hf$ of a zircon is essentially its initial ratio. This has been used to determine the Hf isotope crustal growth curve (Patchett et al., 1981). Zircons are very resistant to weathering and alteration. Therefore, zircons in sediments like placers and sands contain a major parts of the sediment's Zr and Hf budget. Lu on the other hand concentrates in the clay fraction. As a consequence, the Lu/Hf ratio in sediments ranges from an average $^{176}Lu/^{177}Hf \approx 0.01$ in sands and turbidites, to $^{176}Lu/^{177}Hf \approx 0.02$ for shales and clays and $^{176}Lu/^{177}Hf \approx 0.06$ for deep sea red clays and manganese nodules (Patchett et al., 1984). For comparison, the Bulk Earth $^{176}Lu/^{177}Hf = 0.0337$. Different types of sediments can have large differences in $^{176}Hf/^{177}Hf$ ratio,

Figure 3.1

Hofmann diagram for Nd, Sm, and Zr. Both MORB and OIB are plotted. Horizontal lines are the C-1 (or BE) ratios. The square with the lowest trace element concentrations is average N-type MORB (Hofmann, 1988). Other squares are averages for Hawaiian volcanoes (Leeman et al., 1980). Data sources: Clague and Frey (1982), Dupuy et al. (1987), Frey et al. (1974), Frey et al. (1980) Hofmann et al. (1987), Liotard et al. (1986), Pearce et al. (1985), Perfit and Fornari (1986), Price et al. (1986), Puchelt and Emmermann (1983), Rhodes et al. (1978), White et al. (1979), Wood et al. (1979). The Sm/Hf variation is approximately horizontal and the Nd/Hf variation is sligthly positive indicating Nd is more compatible than Hf.

Zr/Hf and Sm/Hf are constant, but somewhat scattered. Sm/Hf variation indicates Sm and Hf are very close in incompatibility during melt processes in the upper mantle.

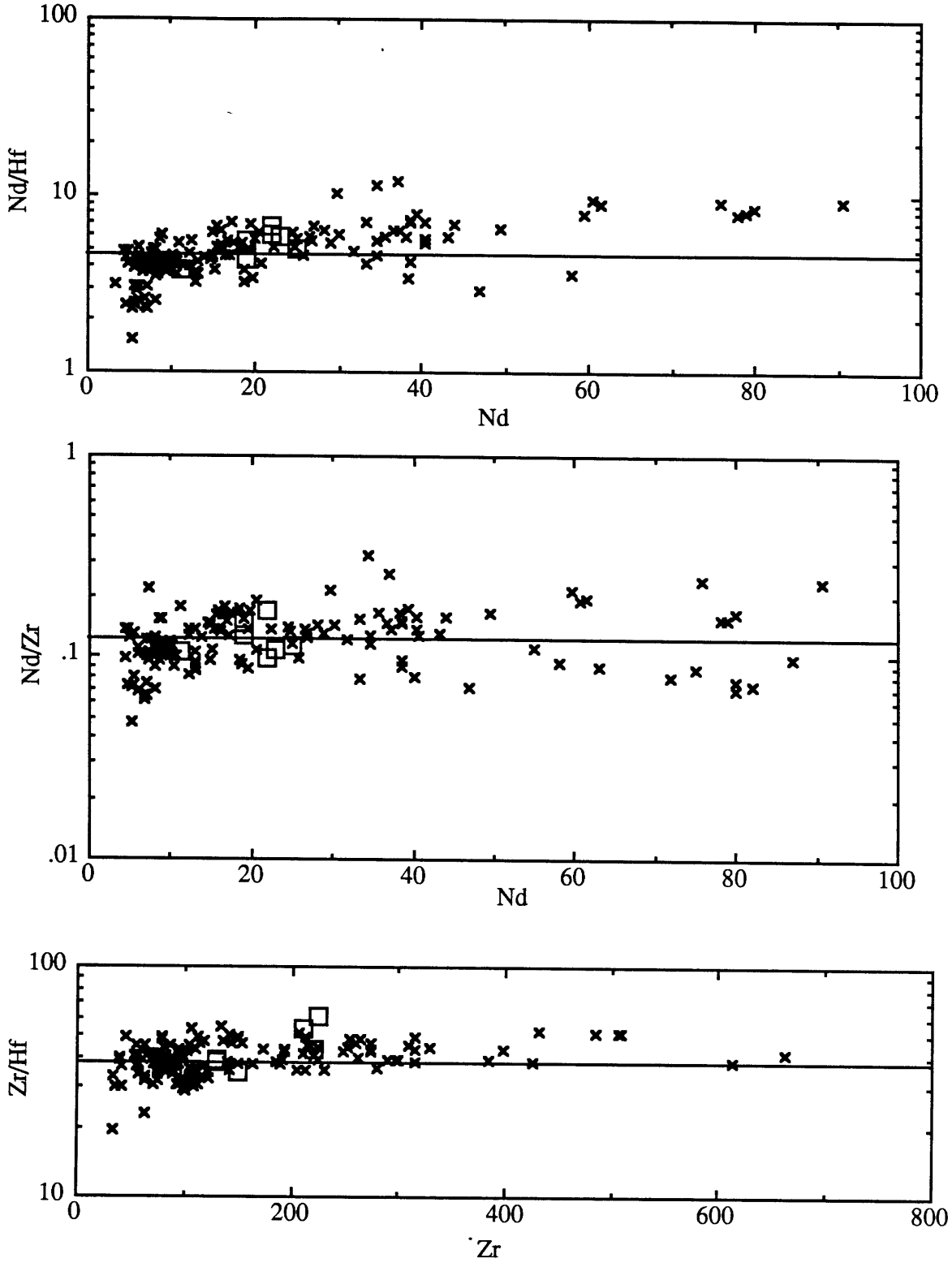
100
10
1
Nd/Hf
0
20
40
60
80
100
Nd
1
.1
.01
Nd/Zr
0
20
40
60
80
100
Nd
100
10
Zr/Hf
0
200
400
600
800
Zr

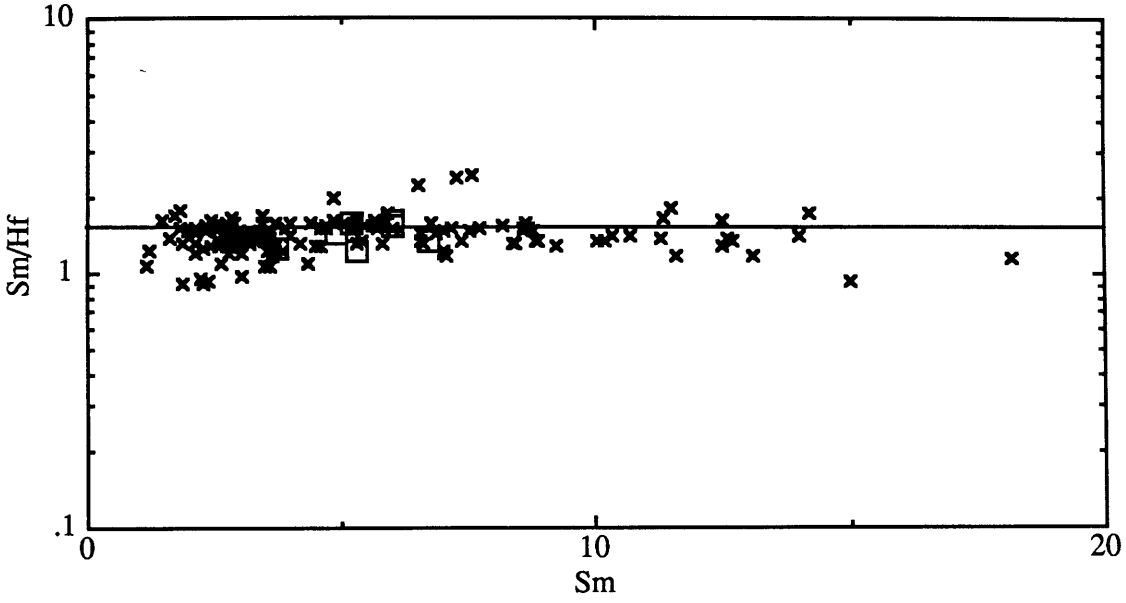
10
1
.1
Sm/Hf
0
10
20
Sm

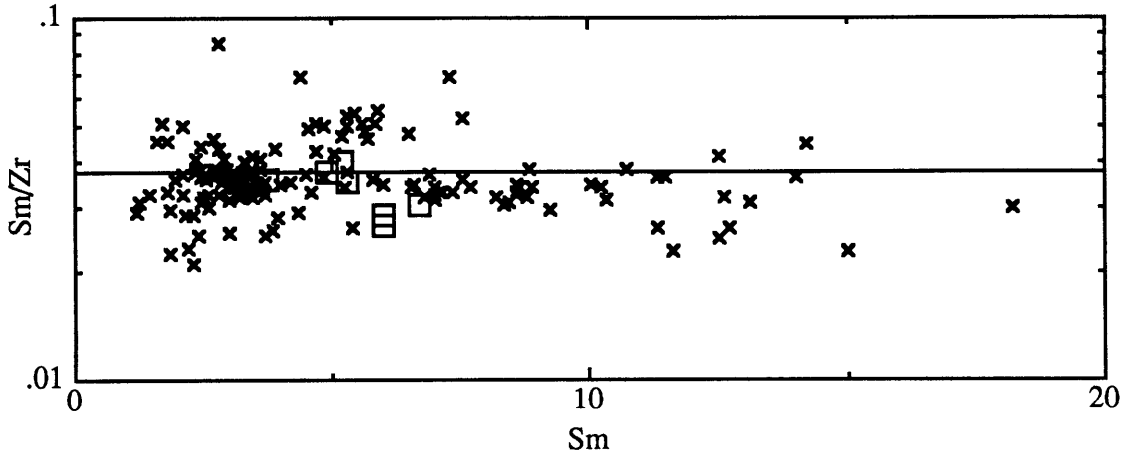
.1
.01
Sm/Zr
0
10
20
Sm

depending upon the age of the hinterland and the age of the sediments. For continental crust, a Lu/Hf=0.10 ($^{176}Lu/^{177}Hf$=0.0142) has been proposed (Taylor and McLennan, 1985). However, Taylor and McLennan (1985) estimated Zr/Hf=33.3, and Hf/Hf*=0.99 and Zr/Zr*=0.86 for the continental crust (definition for HFSE/HFSE* ratios as in Chapter 2). This fractionation of Zr/Hf away from C-1 chondrites is unlikely and their estimate for Zr or Hf is not correct. In general, Lu/Hf ratio in the continental crust is low and fractionation from BE, i.e. 58%. is similar to the fractionation in Sm/Nd ratio (45%). For comparison Lu/Sm and Lu/Nd are respectively 51% and 65% lower than their BE ratios.

Chapter 2 already discussed part of the incompatible trace element behavior, and this part is an addition to the treatise in Chapter 2. Lu is more compatible than Hf in all major mantle minerals existing at pressures below 15GPa. Also, in all these phases Sm is more compatible than Nd, and consequently the Lu/Hf and Sm/Nd systems seem to behave fairly similar. Fig. 3.1 shows the Nd/Hf and Sm/Hf and Zr/Hf variations for oceanic basalts. The trends on these diagrams are close to horizontal indicating the elements are all very similar in compatibility. Sm/Hf behaves as coherently as Zr/Hf. Zr is normally determined by XRF (10% precision 1σ), Hf and Sm are most times determined by INAA on exactly the same sample, which makes the consistency between Zr and Hf even more significant. However, for both Zr/Hf and Sm/Hf there exists considerable scatter. Better determinations for both Zr and Hf are needed to determine whether the scatter indeed exists. Based on charge- radius arguments, it seems remarkable that Zr, Hf and Ti show compatibility in the range of the REE. REE have 3+ charge and range in radius from 1.032Å for La(VI) to 0.861Å for Lu(VI), which is vastly different from the HFSE. The REE and HFSE most likely occupy different sites in minerals, and the similarity in behavior in magmatic processes is more a coincidental than likeness in chemical behavior.

Fig. 3.2 shows a spidergram for average Ocean Island Basalts (OIB), Island Arc Basalts (IAB), N-type MORB and continental crust. The pattern for IAB shows small depletions in Ti, Zr and Hf compared

Figure 3.2

Spider diagram with trace element abundance patterns for average N-type MORB (Hofmann, 1988) and average continental crust (Taylor and McLennan, 1985). Also shown are a typical trace element abundance patterns for ocean island basalts (OIB) and island arc basalts (IAB), data from Basaltic Volcanism Study Project (1981). IAB pattern shows the typical enrichment in Sr and depletion in Zr and Hf, and only a slight depletion in Ti. Continental crust which is thought to be formed from arc volcanics does not show Hf and Zr depletions. Normalizations as in chapter 2.

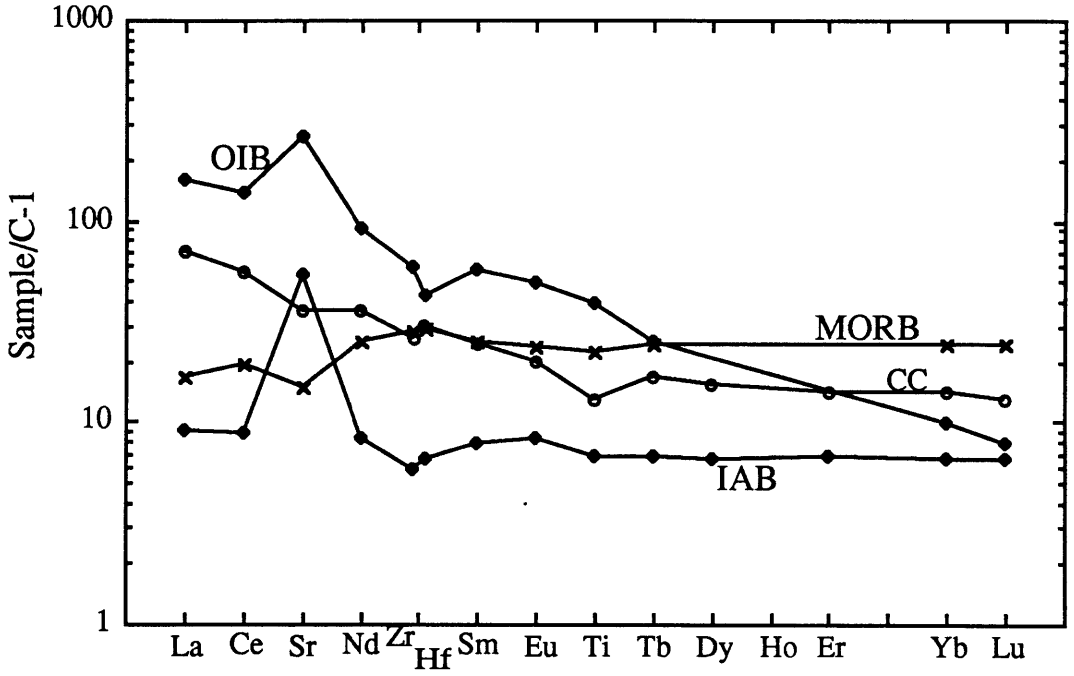
1000
100
10
1
Sample/C-1
OIB
MORB
CC
IAB
La
Ce
Sr
Nd
Zr
Hf
Sm
Eu
Ti
Tb
Dy
Ho
Er
Yb
Lu

Figure 3.3

Sm/Nd vs Lu/Hf for MORB (crosses), OIB (circles) and IAB (plusses). As expected, OIB have lower Lu/Hf than MORB and IAB. Although the variation of OIB and MORB is roughly positive, existence of these ratios over time will lead to large variation in isotopic compositions. Contrary to expectations IAB have similar Lu/Hf than MORB for given Sm/Nd, though they do have higher Lu/Hf than OIB. Data sources as in Fig. 3.1 and Basaltic Volcanism Study Project (1981), Dupuy et al. (1982), Gerlach (1986), Morris and Hart (1983), Nye and Reid (1986), White and Patchett (1984). For IAB only tholeiites and basalts are plotted. Note that the IAB data includes data from Chili, but all these lavas can be considered to be uncontaminated (Gerlach, 1986).

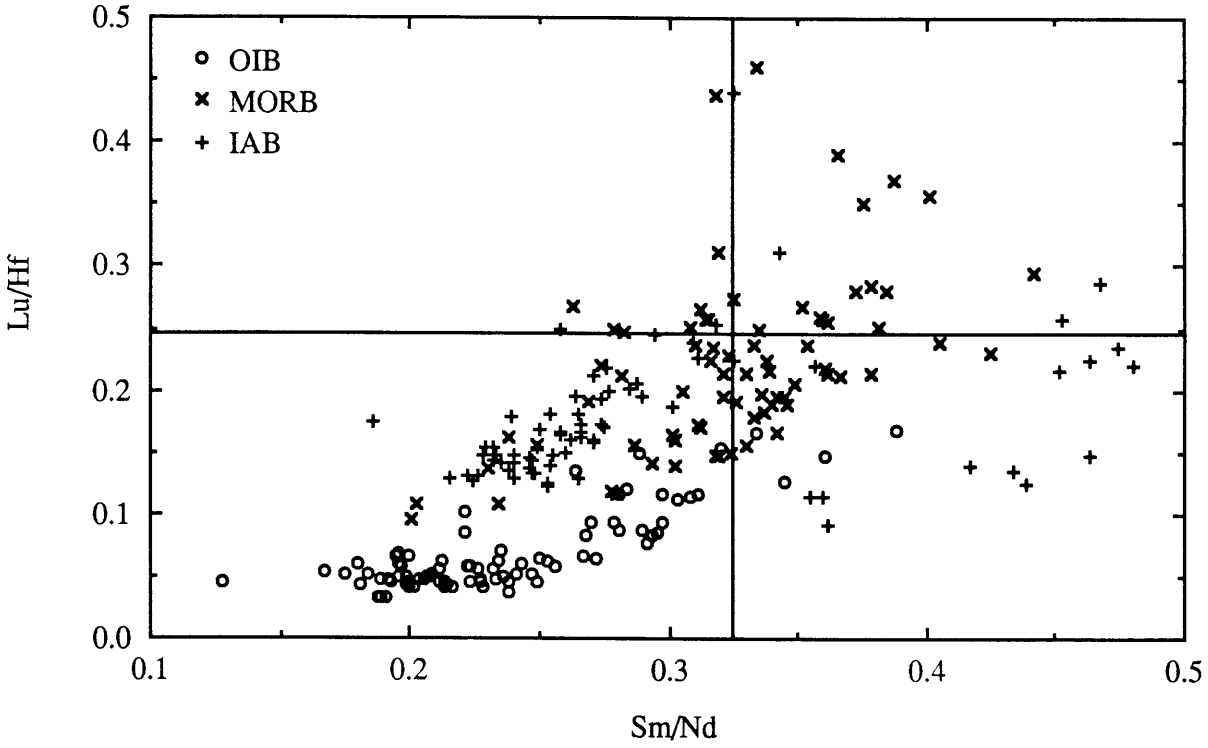
OIB
MORB
IAB
Lu/Hf
Sm/Nd
0.5
0.4
0.3
0.2
0.1
0.0
0.1
0.2
0.3
0.4
0.5

PAGES (S) MISSING FROM ORIGINAL

Page 163 is missing.

with White's data (Hart et al., 1986) the EMII and HIMU mantle components can be characterized. As was noted previously (Patchett, 1983) the variation in Hf-isotopes of MORBs is large. Samples with the most radiogenic Nd (and hence least radiogenic Sr) show a large variation in Hf isotopic composition. The extensive coverage of Kerguelen Island and Walvis Ridge allows characterization of the EMI component. I also analyzed several additional MORBs to attempt to characterize DMM better. Table 3.1 lists the Hf isotope results from this study.

3.3.1 Kerguelen-Heard Plateau and Kerguelen Island

The Kerguelen-Heard Plateau (KHP) with $3x10^6$ km^2 (twice the size of France), is the second largest of submarine features (The Ontong-Java Plateau with $4x10^6$ km^2 is larger). Here I discuss the results of major, trace and isotopic analyses from 4 ODP-drill holes and from some Kerguelen Island samples. Kerguelen Island samples are donated by D. Weis, and were chosen to represent the full range of variation in $^{143}Nd/^{144}Nd$ on Kerguelen Island. D. Weiss also kindly provided the Nd-isotopes on these samples. Given the size of the KHP this study can only be considered as exploratory. Fig. 3.4 shows the bathymetry of the KHP and indicates the holes drilled during Leg 119 and 120 of the Ocean Drilling Program. Based on sea floor magnetics from around the plateau and K-Ar dates on the basement lavaflows, the basement is 110± 15 Ma in age. The occurrence of beach-type deposits, combined with fossil reefs and pieces of wood just above the basement, indicates that the KHP was above sea level during its formation approximately 110 Ma ago. The basalt flow drilled at Site 748 is located in the sediment column and is not as part of the basement. The K-Ar age of this basalt is 80 Ma, indicating that it postdates basement formation. Hole conditions caused premature cessation of the drilling operation at Site 748, and the basement was not reached. The basement is believed to be at least 100m below the intra sediment basalt flow of Site 748. On Kerguelen Island, the oldest lavas are 40 Ma in age, and these lavas are transitional between MORB and OIB in chemical characteristics

Figure 3.4

Map of the Kerguelen Heard Plateau. Numbers 736 through 750 are the Site numbers of Leg 119 and Leg 120 of the Ocean Drilling Program. Site 748 and Site 747-750 recovered basalts. This study reports data for Site 747 to 750.

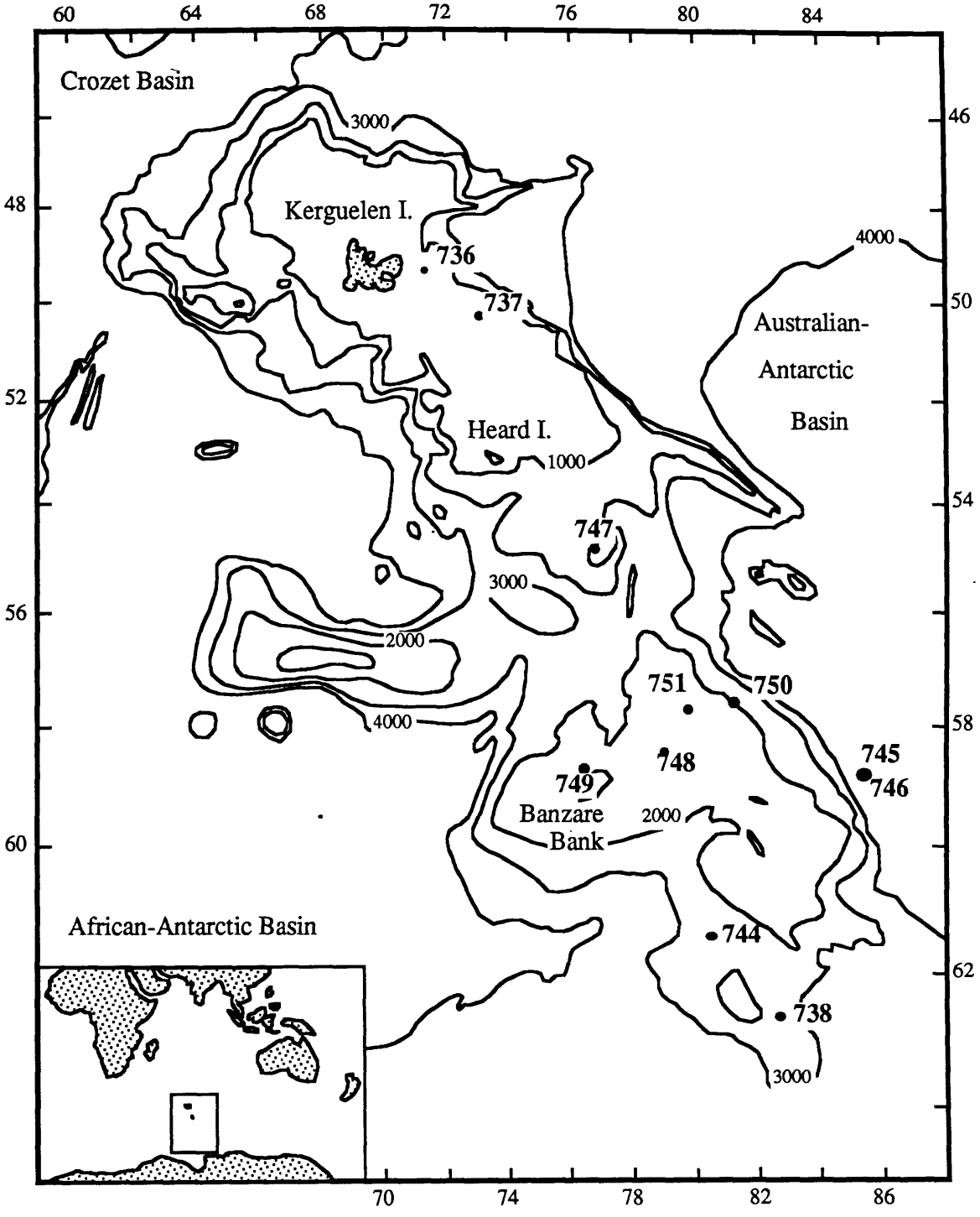
60
64
68
72
76
80
84
Crozet Basin
3000
46
48
Kerguelen I.
736
737
4000
50
Australian-
Antarctic
Basin
52
Heard I.
1000
54
747
3000
56
2000
751
750
4000
58
745
748
746
749
Banzare
Bank
2000
60
African-Antarctic Basin
744
62
738
3000
70
74
78
82
86

(Gautier et al., 1989; Storey et al., 1989). The Kerguelen-Heard Plateau is thought to have formed in a situation analogous to present day Iceland: a ridge centered hot spot (Munschy and Schlich, 1988; Mutter and Cande, 1983), I will call this phase of volcanic activity the ridge-phase. The KHP is thought to be the extension of the Ninetyeast Ridge and was crossed by the spreading ridge about 90-95 Ma ago (Mahoney et al., 1983; Royer and Sandwell, 1989). On the plateau, major volcanic activity leading to the plateau formation stopped about 110 Ma ago. A second stage, the hot-spot-stage, of major activity started ±40 Ma ago and results in the formation of Kerguelen Island first (40 Ma-0.5 Ma) and later Heard Island (1.8 Ma-present). Thus no major volcanic activity occurred between 100 and 40 Ma.

Except for Site 748 basalts the KHP basement basalts are aphyric to sparsely phyric hyperstene normative tholeiites, containing plagioclase and olivine as phenocrysts. The Site 748 basalt has augite, plagioclase, and analcite as crystalline phases, and no olivine. The low CaO/Al_2O_3 ratio of the basalts from Site 748 indicate that this basalt fractionated some augite. The CaO/Al_2O_3 vs. Mg# plot (Fig. 3.5) supports these basic petrographic observations. Since all basalts are at least slightly altered only elements not susceptible to alteration processes are used to determine the chemical characteristics of the basement. Based on the preliminary results reported here the KHP lavas are extremely variable in composition, but the basalts from any one Site show less variation than the total variation. Each of the sites has different chemical characteristics (Fig. 3.5 and 3.6). Table 3.1 lists the trace element characteristics of the Kerguelen Plateau basalts. Based on some incompatible trace element ratios the KHP basalts, except Site 748, are intermediate between MORB and OIB (Fig. 3.7). The southernmost basalts are more MORB-like while the northernmost basalts resemble Kerguelen Island volcanics. Fig. 3.8 shows the REE patterns for KHP basalts, which range from OIB-type LREE enriched at Site 747 to flat to LREE depleted patterns for Site 750.

Sr and Nd isotopic variations for the KHP basalts cover a large part of the range of oceanic volcanics. All samples for which isotope data are reported were leached (48hrs in 6.2N HCl at 75°C). Thus, the

Table 3.1
Trace element contents (in ppm) for KHP basalts

Site	747*	747*	747*	747*	748*	748*	749*	749	749
Core	11R-1	12R-4	16-4	16-5	79-6	84CC	15-5	16-7	16R-7
Interval	6-8.	36-40	50-53	103-106	90-94	0-2	125-127	69-76	75-77
La	13.20	12.50	13.20	12.30	105.00	106.00	6.80	3.20	3.44
Ce	32.00	28.60	28.60	25.50	224.00	297.00	18.80	9.60	8.80
Sr	265.3	243.9	240.4	234.0	1130.0	1045.0	214.0	225.0	240.0
Nd	18.00	17.00	17.00	15.00	103.00	104.00	12.30	6.30	6.70
Zr	159	123	100	97	599	393	91	41	46
Hf	3.80	3.30	2.60	2.20	9.00	6.20	2.00	1.10	1.26
Sm	4.54	4.08	3.47	3.38	13.72	12.36	3.47	2.00	1.95
Eu	1.37	1.32	1.14	0.98	3.61	3.38	1.22	0.83	0.89
Ti	12208	9801	7756	7277	16476	18042	9143	5533	5293
Tb	0.89	0.79	0.78	0.62	1.33	1.30	0.69	0.49	0.44
Yb	2.35	2.83	2.13	1.91	1.77	2.20	2.60	1.39	1.65
Lu	0.30	0.37	0.31	0.28	0.26	0.26	0.39	0.22	0.26

Site	749	749*	750*	750	750	750	750*	750B
Core	15R-5	12R-4	15-2	17-3	14R-1	16R-6	17R-3	15R-5
Interval	127-131	144-148	88-92	23-26	38-40	58-63	26-30	126-130
La	6.30	6.31	2.50	4.00	2.71	2.03	3.15	1.79
Ce	16.60	17.20	5.60	8.90	5.50	5.80	9.30	6.00
Sr	225.0	226.0	113.0	193.0	43.0	130.0	152.0	124.0
Nd	11.00	10.80	4.50	6.10	5.00	3.90	7.30	3.60
Zr	92	93	24	47	33	33	38	32
Hf	2.43	2.43	0.88	1.20	0.92	1.01	1.29	0.86
Sm	3.32	3.52	1.39	2.22	1.51	1.41	2.14	1.33
Eu	1.31	1.32	0.60	0.84	0.54	0.65	0.93	0.63
Ti	8358	8419	4268	7037	5232	4329	5232	4090
Tb	0.70	0.77	0.40	0.58	0.53	0.42	0.59	0.40
Yb	2.65	2.90	2.06	2.57	1.88	2.22	2.39	1.94
Lu	0.40	0.40	0.29	0.34	0.32	0.33	0.43	0.31

Samples where Sites are indicates by a star are analyzed by Storey (Leicester)
Ti and Zr are shipboard XRF analyses, all other elements are INAA

Table 3.2
Sr, Nd and Pb isotopes for the Kerguelen-Heard Plateau basalts collected on Leg 120

Site	Core	Interval	87Sr/86Sr	143Nd/144Nd	206Pb/204Pb	207Pb/204Pb	208Pb/204Pb
747	12R-4	45-46	0.705508	0.512435	17.466	15.461	37.977
747	16R-2	85-87	0.705895	0.512452	18.275	15.643	38.459
747C	12R-2	122-124	0.705660	0.512445	-	-	-
747C	16R-2	81-84	0.705866	0.512410	17.608	15.508	38.072
748	79R-7	65-67	0.705157	0.512491	18.305	15.613	38.495
749	16R-7	107-109	0.703506	-	18.031	15.579	38.222
749	15R-2	35-37	0.704237	0.512763	18.200	15.625	38.435
750	16R-3	134-136	0.705012	0.512902	18.112	15.585	38.405
749C	12R-4	144-148	0.704268	-	17.980	15.587	38.204
749C	15R-5	127-130	0.704306	0.512764	17.978	15.587	38.213
749C	16R-7	75-77	0.703531	-	18.065	15.574	38.028
750B	17R-3	26-30	0.705300	-			

Analytical techniques are described in chapter 1
- means not analyzed

Figure 3.5

CaO/Al_2O_3, and TiO_2 versus Mg#. The different sites overlap in major elements, CaO/Al_2O_3 is given as an example. Minor element contents such as TiO_2, differs from site to site for a given Mg#. Data from Leg 120 preliminary report.

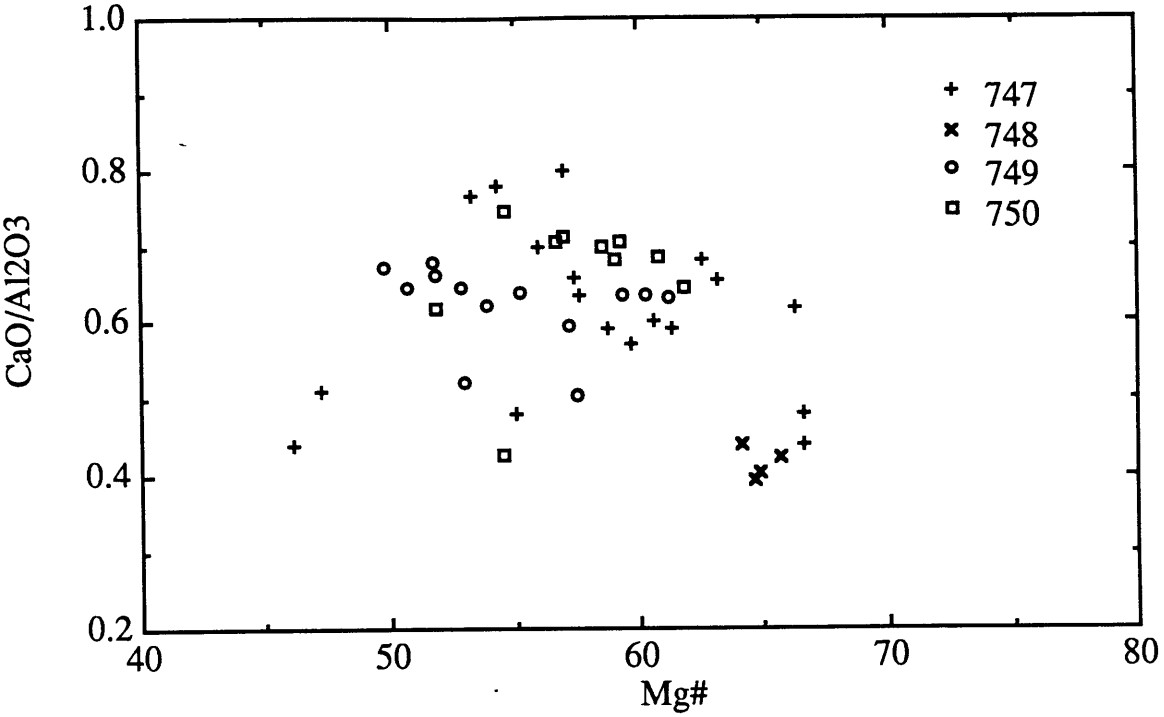
1.0
0.8
0.6
0.4
0.2
CaO/Al2O3
40
50
60
70
80
Mg#
747
748
749
750

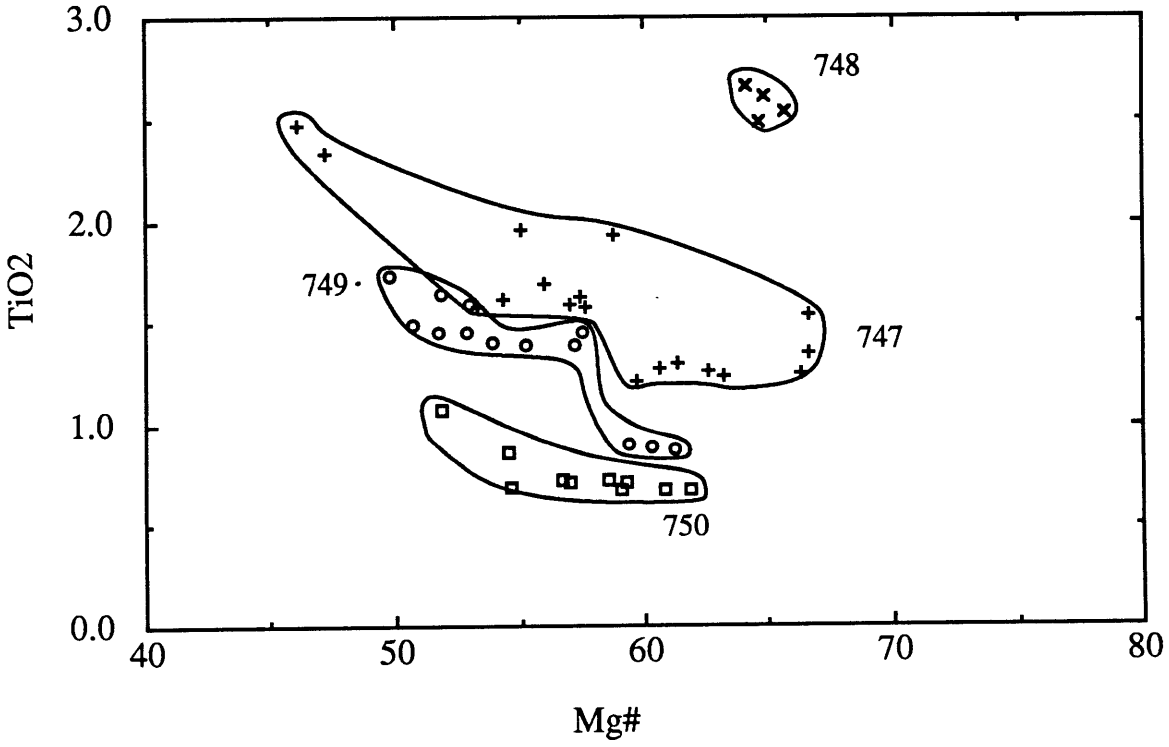
3.0
2.0
1.0
0.0
TiO2
40
50
60
70
80
Mg#
748
749
747
750

Figure 3.6

Zr versus Mg#, and Zr versus Nb for KHP basalts. Site 748 basalts are so enriched that they plot off scale. Different sites have different Zr content for given Mg#. Zr-Nb plot indicates that the difference in trace element characteristics is in degree of enrichment. Incompatible elements appear to be correlated from site to site indicating they could represent different degrees of melting from a similar source. The isotopic compositions however, indicate different source materials for the different sites.

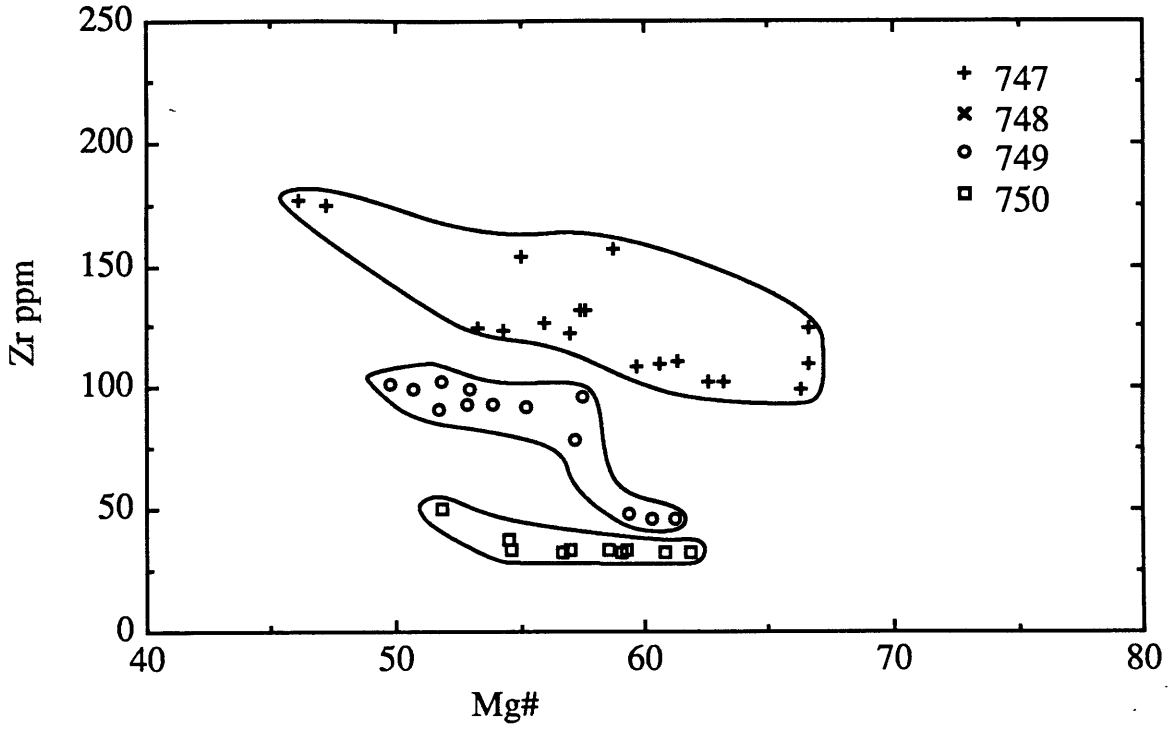
250
200
150
100
50
0
Zr ppm
40
50
60
70
80
Mg#
747
748
749
750

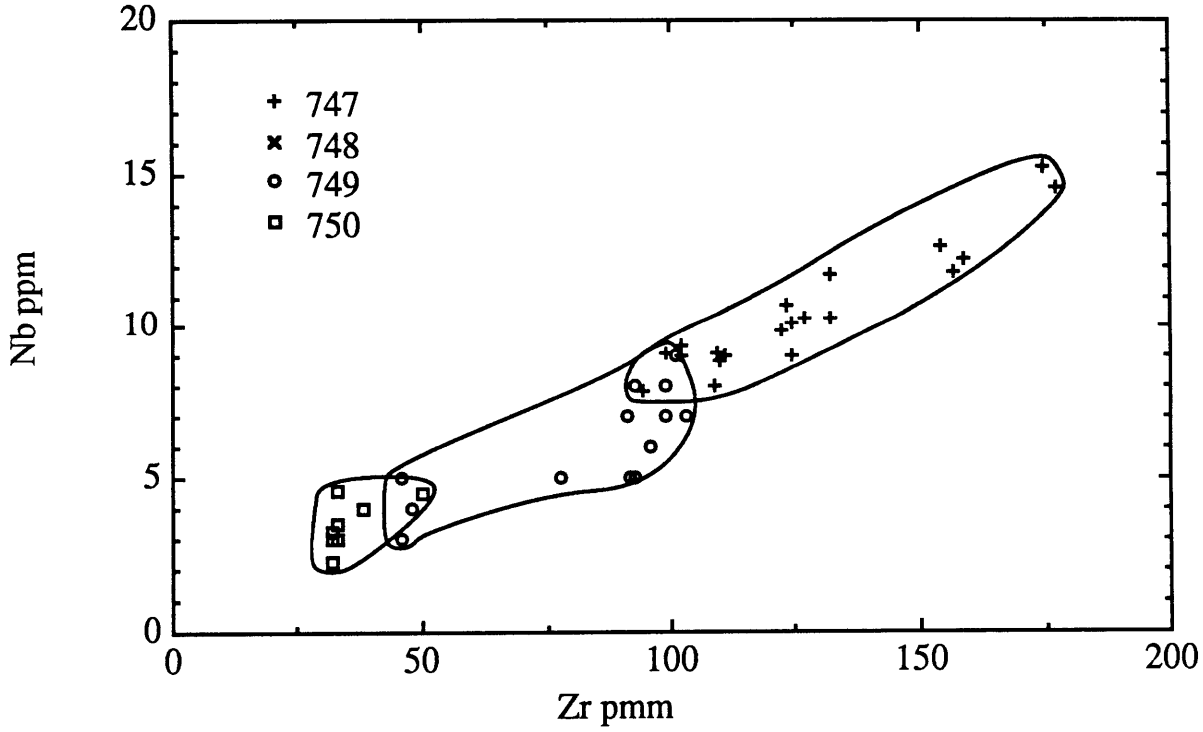
20
15
10
5
0
Nb ppm
0
50
100
150
200
Zr pmm
747
748
749
750

Figure 3.7

Zr/Nb versus P/Y showing the inter-element variation for basalts from all Leg 120 Sites compared to MORB (Price et al., 1986), Transitional MORB (le Roex et al., 1987), plateau basalts from the Nauru Basin (Saunders, 1985) and Kerguelen and Heard Island (Storey, unpublished data).

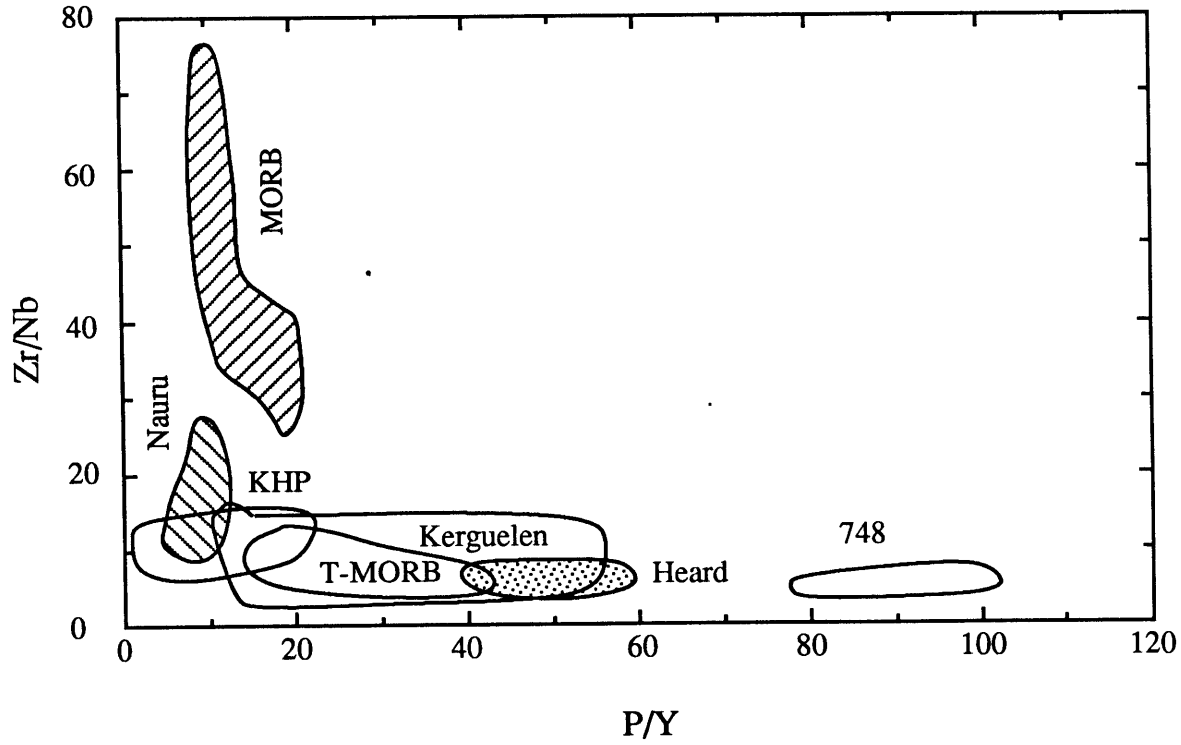
80
60
40
20
0
Zr/Nb
MORB
Nauru
KHP
Kerguelen
T-MORB
Heard
748
0
20
40
60
80
100
120
P/Y

Figure 3.8
Spider diagrams for KHP basalts. Normalizations as in Chapter 2. Note the decrease in LREE enrichment from Site 747- 749- 750.

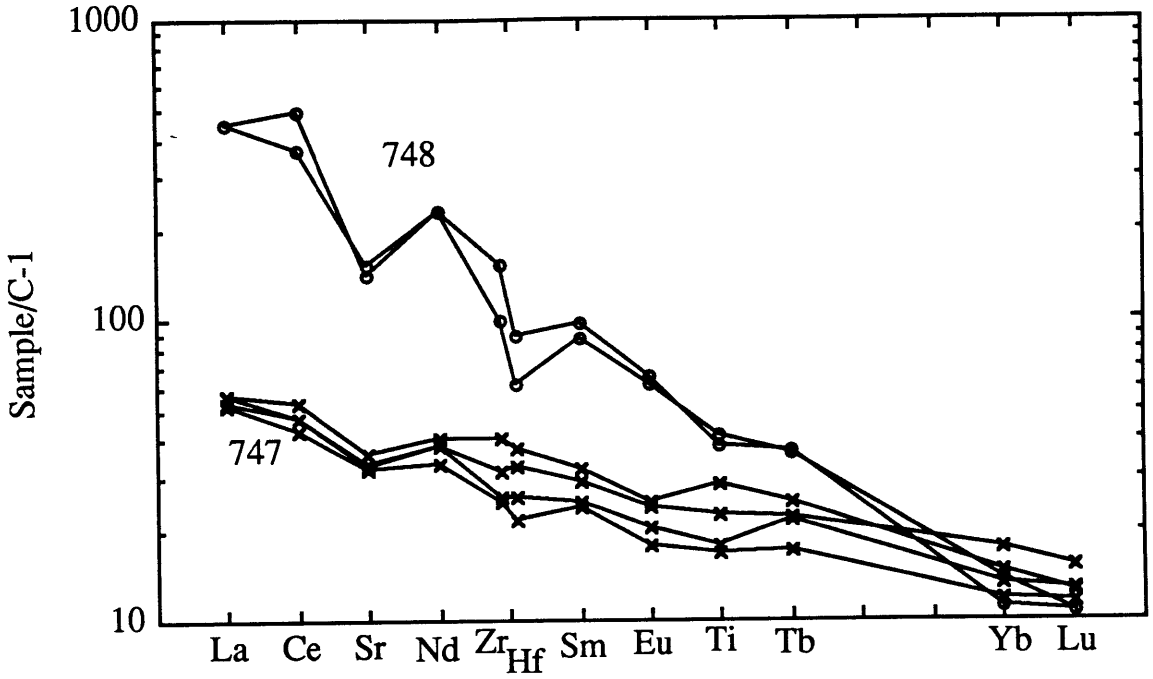
1000
100
10
Sample/C-1
748
747
La
Ce
Sr
Nd
Zr
Hf
Sm
Eu
Ti
Tb
Yb
Lu

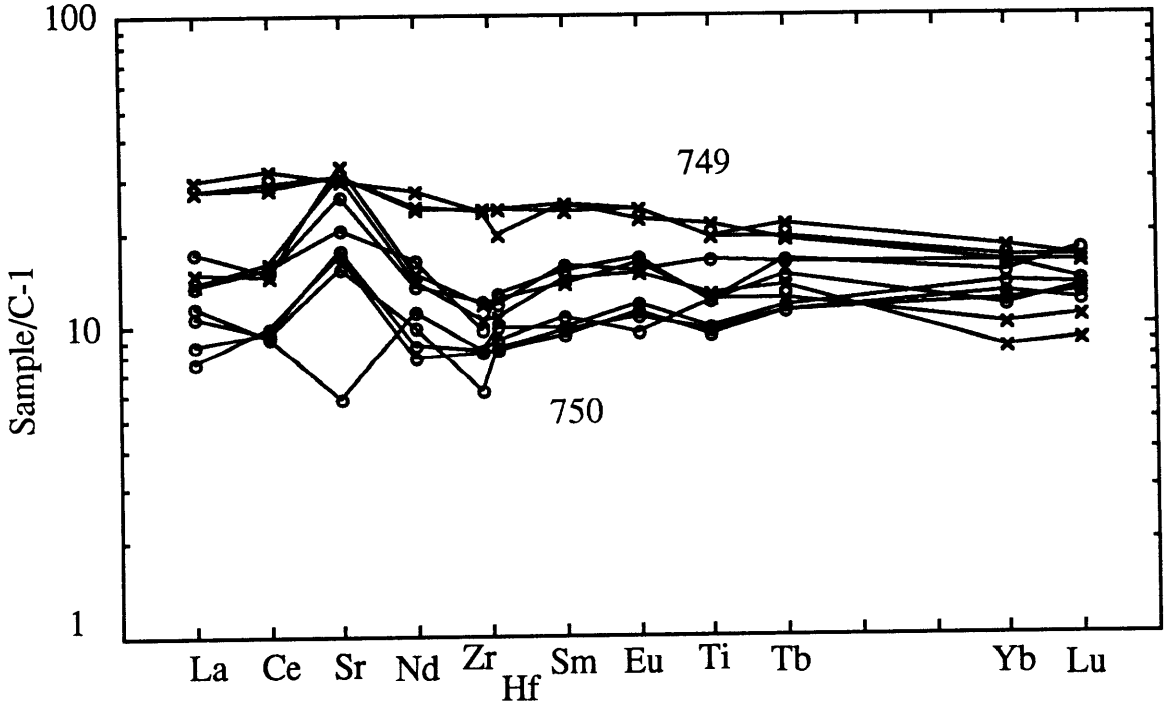
100
10
1
Sample/C-1
749
750
La
Ce
Sr
Nd
Zr
Hf
Sm
Eu
Ti
Tb
Yb
Lu

Figure 3.9

Sr- Nd isotope correlation diagram for the KHP basalts. The four sites occupy different areas on the diagram, indicating different source characteristics for the sites. Insets show the REE patterns for the lavas. Vertical axis for the REE diagrams is from 1-100 for 749 and 750, from 10-100 for 747, and from 10-1000 for 748.

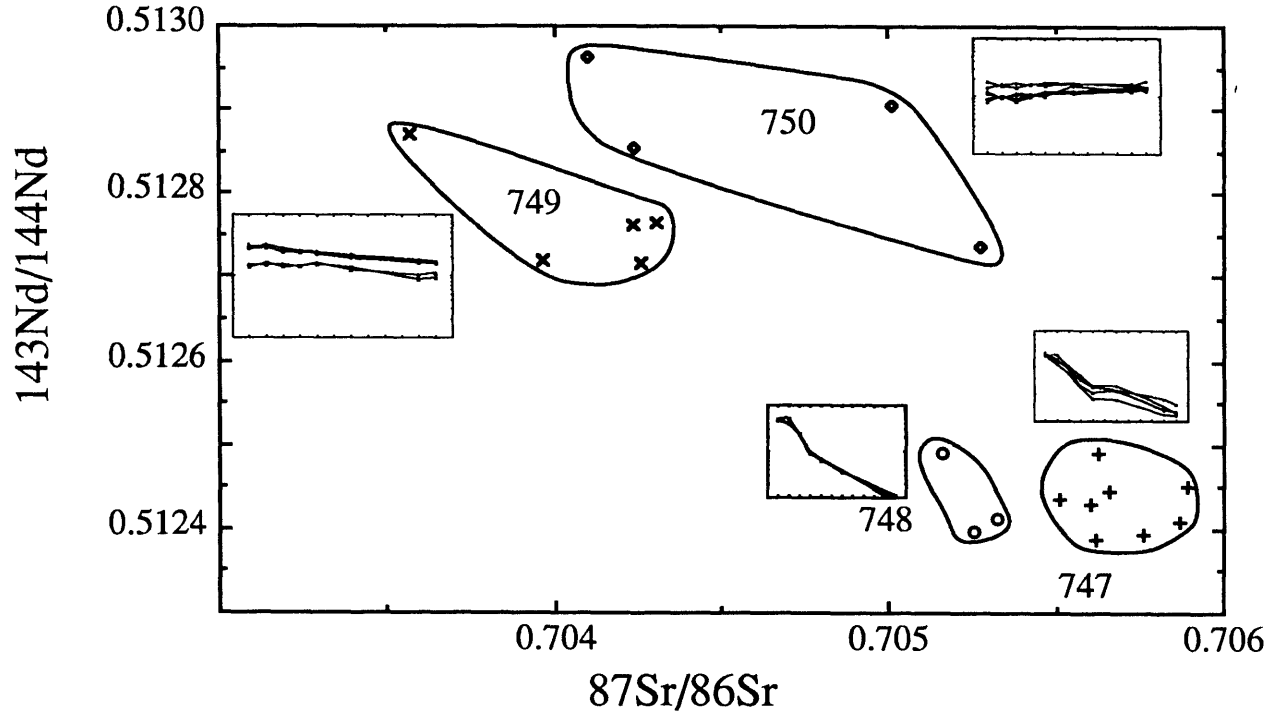
0.5130
0.5128
0.5126
0.5124
143Nd/144Nd
750
749
748
747
0.704
0.705
0.706
87Sr/86Sr

Figure 3.10

$^{87}Sr/^{86}Sr$ versus $^{143}Nd/^{144}Nd$ and $^{206}Pb/^{204}Pb$ versus $^{87}Sr/^{86}Sr$ for the KHP basalts, compared with OIB. The Sr-Nd isotope correlation diagram also shows the unpublished data from Storey. Field for Kerguelen Island, and fields for OIB and MORB from Hart (1988). Solid circles on the Pb-Sr diagram are KHP basalts. The Pb-Sr is not intended to show the available data on oceanic islands. The high $^{87}Sr/^{86}Sr$ KHP basalts overlap with the high $^{87}Sr/^{86}Sr$ basalts from Kerguelen Island. None of the Plateau basalts overlap with Heard Island basalts. Field for Heard Island from Storey et al. (1989), fields for other OIB and MORB from Zindler and Hart (1986). The high $^{87}Sr/^{86}Sr$ basalts of the KHP are clearly part of the EMI endmember.

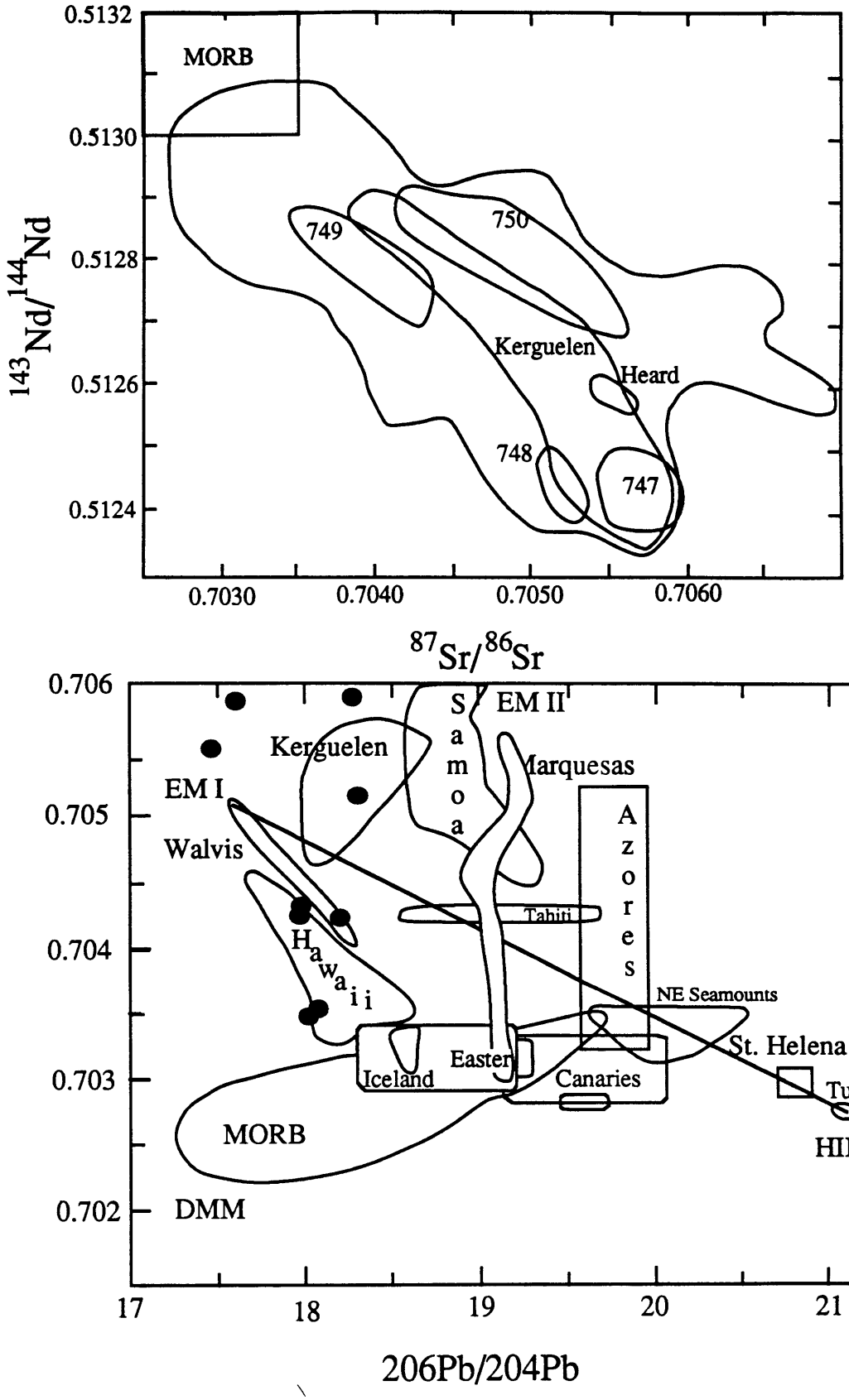
0.5132
0.5130
0.5128
0.5126
0.5124
143Nd/144Nd
MORB
749
750
Kerguelen
Heard
748
747
0.7030
0.7040
0.7050
0.7060
87Sr/86Sr
0.706
0.705
0.704
0.703
0.702
87Sr/86Sr
EM II
Samoa
Kerguelen
Marquesas
EM I
Walvis
Azores
Tahiti
Hawaii
NE Seamounts
St. Helena
Easter
Iceland
Canaries
Tubuaii
MORB
HIMU
DMM
17
18
19
20
21
206Pb/204Pb

observed isotopic variation is thought to be real and not an artifact of alteration. None of the samples are age corrected. Using the trace element concentrations of the leached basalts the age correction is small for Nd and can be up to 0.0001 for $^{87}Sr/^{86}Sr$. Age corrections are insignificant compared with the total variation, and will not significantly affect the discussion presented here. The four different sites occupy different areas on the Nd-Sr isotope correlation diagram, and samples which are most depleted in LREE also have more depleted isotopic signatures, (Fig. 3.9). The large variation in isotopic composition of the basement of the Plateau indicates the existence of significant heterogeneities in the mantle underneath the Plateau. The Plateau data overlaps for a large part with the field for Kerguelen Island volcanics. The northern Site (747) and the alkali basalt (Site 748) overlap with the most enriched end of the Kerguelen Island field, though they are separate from the Heard Island field. The KHP basalts are lower in $^{143}Nd/^{144}Nd$ and higher in $^{87}Sr/^{86}Sr$ than other oceanic plateau volcanics (Cheng et al., 1987; Mahoney, 1987). Furthermore it can be seen from Fig. 3.10 that the Site 747 and Site 748 basalts lie close to the EMI component as defined by (Zindler and Hart, 1986). In Sr-Pb isotopic composition space, the KHP basalts again overlap with the field of Kerguelen Island basalts and basalts from Site 747 and 748 are proximal to the EMI mantle endmember. It can be concluded that KHP basalts have Nd-Sr-Pb (and Hf) isotopic characteristics similar to Kerguelen Island volcanics, and the two different type of volcanics seem to share the same mantle component: EMI. The occurrence of the same mantle components in the 2 types of volcanism, which are 60 Ma apart, suggests these mantle components were continuously present below the Plateau. The EMI component is associated with both the "ridge-phase", and the hot-spot-stage of the plateau, and because it is related to the ridge-phase EMI seems to be spatially related to the MORB (DMM) reservoir. At Kerguelen Island (the hot-spot-stage) the sampling of the EMI reservoir might simply be the re-tapping of this EMI-DMM mantle mix. Analyses of KHP basalts and Kerguelen Island volcanics will allow assessment of the Hf isotopic composition of the EMI component. Hf isotope analyses are listed in Table 3.3a.

Table 3.3a
Hf and Nd isotopes and trace elements for OIB

Sample#	176Hf/177Hf	143Nd/144Nd	147Sm/144Nd	176Lu/177Hf	Del(Lu/Hf)	Del(Sm/Nd)
KERGUELEN						
77-211*	0.282791	0.51262	0.1299	0.0071	0.7739	0.3342
80-135*	0.282774	0.51254	0.1084	0.0056	0.8183	0.4266
81-18*	0.282868	0.51266	0.1400	0.0091	0.7258	0.2933
81-19*	0.282962	0.51274	0.1451	0.0111	0.6864	0.2897
80-71*	0.282719	0.5125	0.1052	0.0037	0.8729	0.4346
2621	0.282828	0.512479	0.1382	0.0069	0.7856	0.2508
3308	0.282836	0.512543	0.1140	0.0049	0.8487	0.3976
3312	0.282811	0.512346	0.1239	0.0063	0.8029	0.2893
3315	0.283033	0.512711	0.1380	0.0096	0.7422	0.3168
3319	0.282857	0.512447	0.1369	0.0086	0.7381	0.2477
KERGUELEN-HEARD PLATEAU						
747C-12R-4,45-47*	0.282722	0.512435	0.1502	0.0159	0.4603	0.1708
747C-16R-2,85-87	0.2826	0.512452	0.1277	0.0169	0.3591	0.2996
748C-79R-7,65-67*	0.282659	0.512491	0.0834	0.0028	0.9013	0.5501
749C-15R-5,0127-130*	0.283009	0.512764	0.1892	0.0232	0.3673	0.0820
747C-12R-4, 41-43*	0.282725	0.512429	0.1502	0.0159	0.4617	0.1687
GALAPAGOS						
Sc-64	0.283215	0.513035	0.1869	0.0220	0.4746	0.1753
E-4	0.283118	0.512877	0.1464	0.0113	0.7141	0.3180
TRISTAN						
T369	0.282848	0.5125	0.1098	0.0052	0.8407	0.4098
T617	0.282882	0.51255	0.0995	0.0052	0.8446	0.4758
BOUVET						
BV-1	0.283092	0.51285	0.1346	0.0088	0.7743	0.3671
BV-2	0.283028	0.51282	0.1334	0.0085	0.7712	0.3657
FIJI						
W253*	0.282767	0.51264	0.1268	0.0115	0.6239	0.3551
ICELAND						
IC58	0.283297	0.513057+	0.1867+	0.0226	0.1696	0.1663
OAHU						
oa3	0.283204	0.513031	0.1336	0.0116	0.7213	0.4098
Oa4	0.283319	0.51306	0.1199	0.0104	0.7659	0.4754
oa5	0.283279	0.51305	0.1375	0.0110	0.7466	0.3965
oa6	0.283245	0.51304	0.1478	0.0119	0.7208	0.3488
oa10	0.283214	0.513049	0.1714	0.0142	0.6614	0.2474
thol4	0.283177	0.51302	0.1629	0.0119	0.7087	0.2777
thol3	0.283147	0.513028	0.1568	0.0099	0.7534	0.3066
MAUNA LOA						
thol-3	0.283136	0.512906	0.1709	0.0178	0.5541	0.2118
thol5	0.283051	0.512706	0.1588	0.0107	0.7160	0.2125
Walvis Ridge						
525A-57-1,119-124*	0.282773	0.512461	0.1368	0.0111	0.6377	0.2527
525A-63-2,63-68*	0.28264	0.512379	0.1277	0.0100	0.6364	0.2777
527-41-4,10-15*	0.282878	0.512694	0.1802	0.0316	0.0535	0.1025
528-42-1,40-45*	0.282892	0.512555	0.1217	0.0130	0.6155	0.3602
528-42-2,145-150*	0.283114	0.512699	0.1638	0.0249	0.3670	0.1854

Stars at the sample numbers indicate samples that were analyzed by me. Other analyses are referenced in figures
Normalizations as in Table 3.3b
+ means analysis by J. Blusztjan

Table 3.3b
Hf and Nd isotopes and trace elements for MORB

SAMPLE#	176Hf/177Hf	143Nd/144Nd	176Lu/177Hf	147Sm/144Nd	Del(Lu/Hf)	Del(Sm/Nd)
AD2-1	0.283125	0.513152+	0.0211	0.1972	0.467	0.163
AD3-3	0.283521	0.513281	0.0261	0.2008	0.475	0.181
AD5-5	0.283194	0.513131	0.0271	0.2147	0.344	0.082
525-2	0.283223	0.513119	0.0325	0.1863	0.229	0.200
.527-6-1	0.283395	0.513098	0.0270	0.1754	0.420	0.242
PD-1-1	0.283159	0.513201	0.0246	0.2057	0.392	0.140
PD-3-a	0.283195	0.513192	0.0270	0.2069	0.348	0.133
PD-4-g	0.283165	0.513153	0.0281	0.1936	0.308	0.178
GS104-25-2*	0.283288	0.513237	0.0287	0.2084	0.343	0.139
GS104 -20-21*	0.283229	0.513204	0.0280	0.2164	0.337	0.096
GS104-25-1*	0.28313	0.513264	0.0280	0.2118	0.295	0.132
D2-SRH-B	0.28336	0.513286+	0.0214	0.192+	0.531	0.219
11327	0.283245	0.51312	0.0266	0.2093	0.376	0.102
Leucite Hills						
NTP8*	0.282389	0.512024				
17460*	0.28249	0.512073				
HM1-4*	0.282379	0.511832				
174033*	0.282478	0.511843				
17434*	0.282352	0.511871				

176Hf/177Hf normalized to JMC 475= 0.2822
143Nd/144Nd normalized to BCR-1=0.51264
Samples with stars are analyzed by me
Plusses are analyses from J. Blusztjan

3.3.2 Walvis Ridge

Samples from Walvis Ridge spanning the entire range of Nd isotopic compositions (Richardson et al., 1982) were analyzed for Hf. Splits of the same samples reported by Richardson were analyzed. Walvis Ridge basalts have the purest EMI signatures of oceanic basalts, which is the reason they were analyzed. The EMI endmember has very low $^{143}Nd/^{144}Nd$ and relatively low $^{87}Sr/^{86}Sr$. Determination of the Hf-isotopes for Walvis Ridge basalts will indicate whether Hf-isotopes correlate with the Nd-isotopes for low $^{143}Nd/^{144}Nd$.

3.3.3 Kane Fracture Zone

Three basalts from the Kane Fracture Zone were analyzed for Nd, Sr and Hf isotopic composition. Patchett's work shows that the expected Nd-Hf correlation breaks down for MORBs (Patchett, 1983; Patchett and Tatsumoto, 1980a). Kane Fracture Zone basalts are MORBs with the most depleted Sr and Nd isotopic characteristics in the ocean basins (Machado et al., 1982). Determination of Hf isotopes will further assess the Nd-Hf correlation in MORB, or the lack thereof. The Kane basalts were also analyzed for Sr and Nd isotopes to check whether these basalts are indeed extreme in $^{143}Nd/^{144}Nd$ and $^{87}Sr/^{86}Sr$. Analyses are listed in Table 3.3b.

3.3.4 Leucite Hills, Wyoming

AS the ultimate pursuit of the EMI component I analyzed some volcanic products from the Leucite Hills, Wyoming. These volcanic products, outcropping as plugs, necks and breccias, belong to a unique group of volcanic products generally referred to as potassium-rich alkaline volcanic products. One K-Ar date indicates an age of 1.1 Ma (MacDowell, 1966). Three distinct rock types are present wyomingite, orendite and madupite. Relative to the wyomingites and the orendites, madupites are poor in SiO_2 and K_2O

Table 3.4
Trace element contents (in ppm) for Leucite Hills volcanics

	NTP-8	HM1-4	17403	17434	17460	Norm
Cs	2.9	2.3	1.8	2.2	3.9	0.005
Rb	238	221	313	323	210	0.220
Ba	8169	8576	5658	5494	8299	2.340
Th	31	32	14	12	42	0.029
Pb	39	41	30	30	45	0.060
U	6.9	8.7	4.0	3.1	11.1	0.008
K	53328	74028	93636	93900	60144	100
Ta	4.8	3.1	2.3	2.4	6.9	0.014
La	255	313	144	115	362	0.235
Ce	542	691	313	260	798	0.603
Sr	2146	3750	2284	1954	5938	7.400
Nd	198	242	127	106	286	0.452
Hf	42	34	13	36	38	0.102
Zr	1540	1400	590	1290	2060	3.940
Sm	23.5	29.0	15.9	13.5	35.1	0.147
Eu	5.0	6.4	3.7	3.1	7.7	0.056
Tb	0.98	1.23	0.83	0.68	1.43	0.036
Yb	0.69	1.05	0.90	0.71	1.03	0.162
Lu	0.09	0.16	0.18	0.09	0.17	0.024

Column Norm contains normalization values used for spiderdiagram

Figure 3.11
Spidergram for the Leucite Hills volcanics showing the extreme enrichments in trace elements. Crosses are wyomingites and orendites, ellipses are madupite. Normalization values given in Table 3.4.

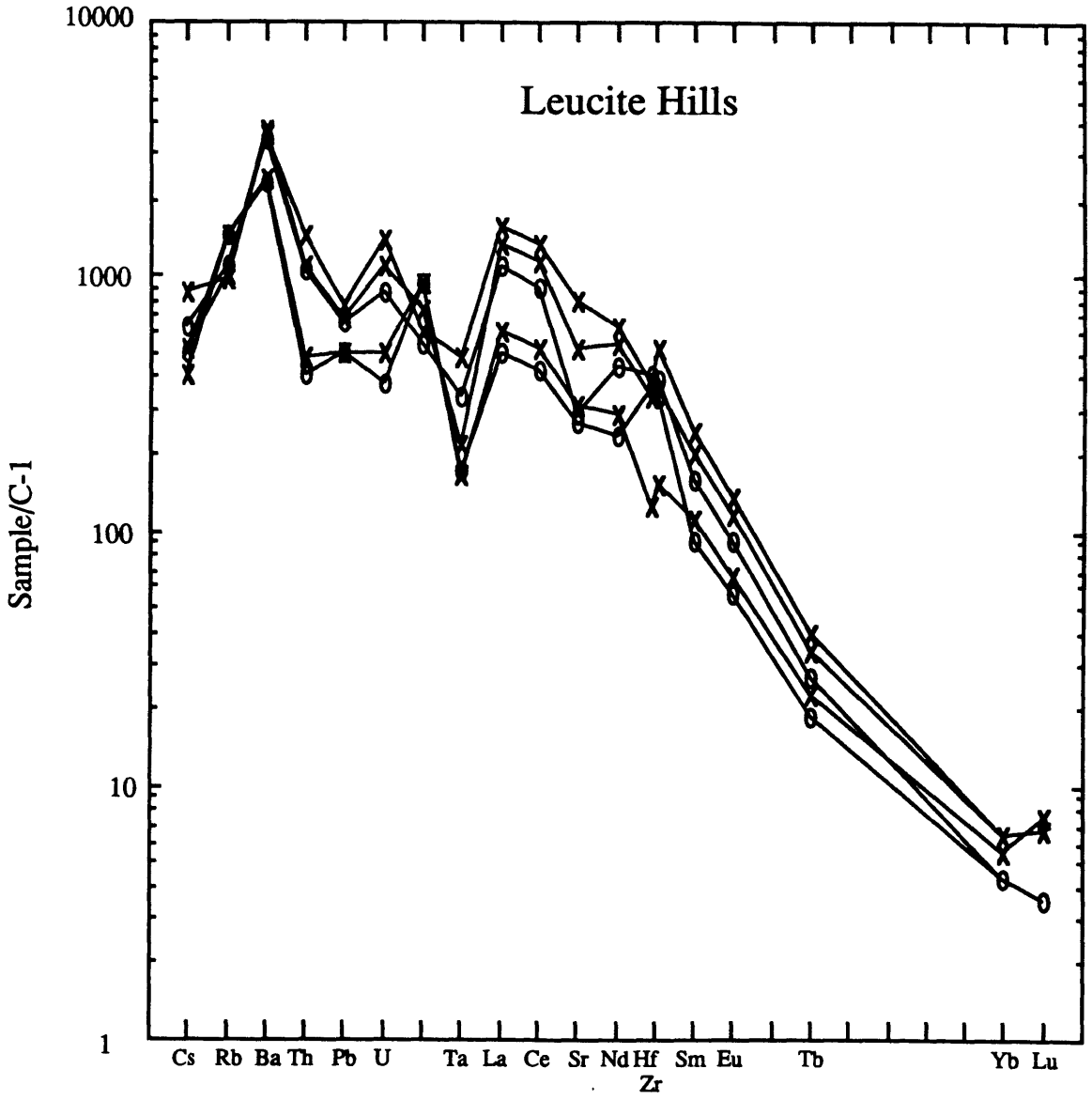
Leucite Hills
10000
1000
100
10
1
Sample/C-1
Cs Rb Ba Th Pb U Ta La Ce Sr Nd Hf Sm Eu Tb Yb Lu
Zr

(Carmichael, 1967). All Leucite Hills volcanic products show extreme enrichments in the incompatible trace elements with La/Yb=755-212, see Table 3.4. and Fig. 3.11. The high Ni and Cr content (160 and 350ppm respectively), and the occurrence of Cr-diopside as xenocrysts indicate a mantle origin for these volcanic products. Furthermore, these extreme incompatible trace element enrichments preclude the possibility of crustal contamination to affect the isotopic compositions. In addition to exhibiting extreme trace element enrichments, the Leucite Hill lavas are one of the rare occurrences in the world which show a definite enrichment in Hf and Zr over the REE. As such, Hf-isotopes on the rocks might reveal a decoupling of Hf and Nd isotopes. The Leucite Hills volcanic products are unique in isotopic composition for mantle material in that they are very low in $^{143}Nd/^{144}Nd$ for given a $^{87}Sr/^{86}Sr$. As can be seen in Fig. 3.12, the Leucite Hills volcanic products are extreme in Nd isotopic composition, which is in accordance with other work (Vollmer et al., 1984).

3.3.5 Hf-Isotope Results

Fig. 3.12 displays all available Hf and Nd isotope data on oceanic volcanic products and Leucite Hills. The elongation of the OIB field indicates that the Lu-Hf and Sm-Nd system behave similarly. For OIB, the total variation in Hf isotopes equals 0.25%, while the total variation in Nd isotopic composition equals 0.17%. To achieve the complete range of isotopic composition for OIB in 2 Ga the parent/daughter ratio fractionation equals 53% for Lu/Hf and 35% for Sm/Nd. To obtain the total range of oceanic volcanics (OIB and MORB) in 2 Ga, 72% fractionation of the Lu/Hf ratio is needed, while for Sm/Nd only 41% fractionation is needed. The distance between Lu and Hf on a spidergram is five times the distance between Sm and Nd, while the fractionation of Lu/Hf is less than twice that of Sm/Nd. This indicates that in the system peridotite melt the K_D pattern on a spidergram flattens towards the HREE. The Leucite Hills samples plot in the extension of the OIB-array. This indicates Lu/Hf and Sm/Nd behave similar, even at extreme mantle compositions. On a smaller

Figure 3.12A and B

Hf- Nd isotope correlation diagrams of volcanics. OIB data from Hart et al. (1986), Patchett and Tatsumoto (1980a), Patchett and Tatsumoto (1980b), and White unpublished data. Kerguelen Island analyses: array formed by the low $^{176}Hf/^{177}Hf$ samples are my data, the high $^{176}Hf/^{177}Hf$ are data from Patchett, combined with $^{143}Nd/^{144}Nd$ from Dosso et al. (1979) for the Patchett data and Gautier et al. (1989) for my data. Mantle endmembers are indicated. Clearly the isotopic variation in MORB cannot be acccomadated by a fixed composition of the DMM endmember. Leucite Hills lavas fall in extension of the OIB field.

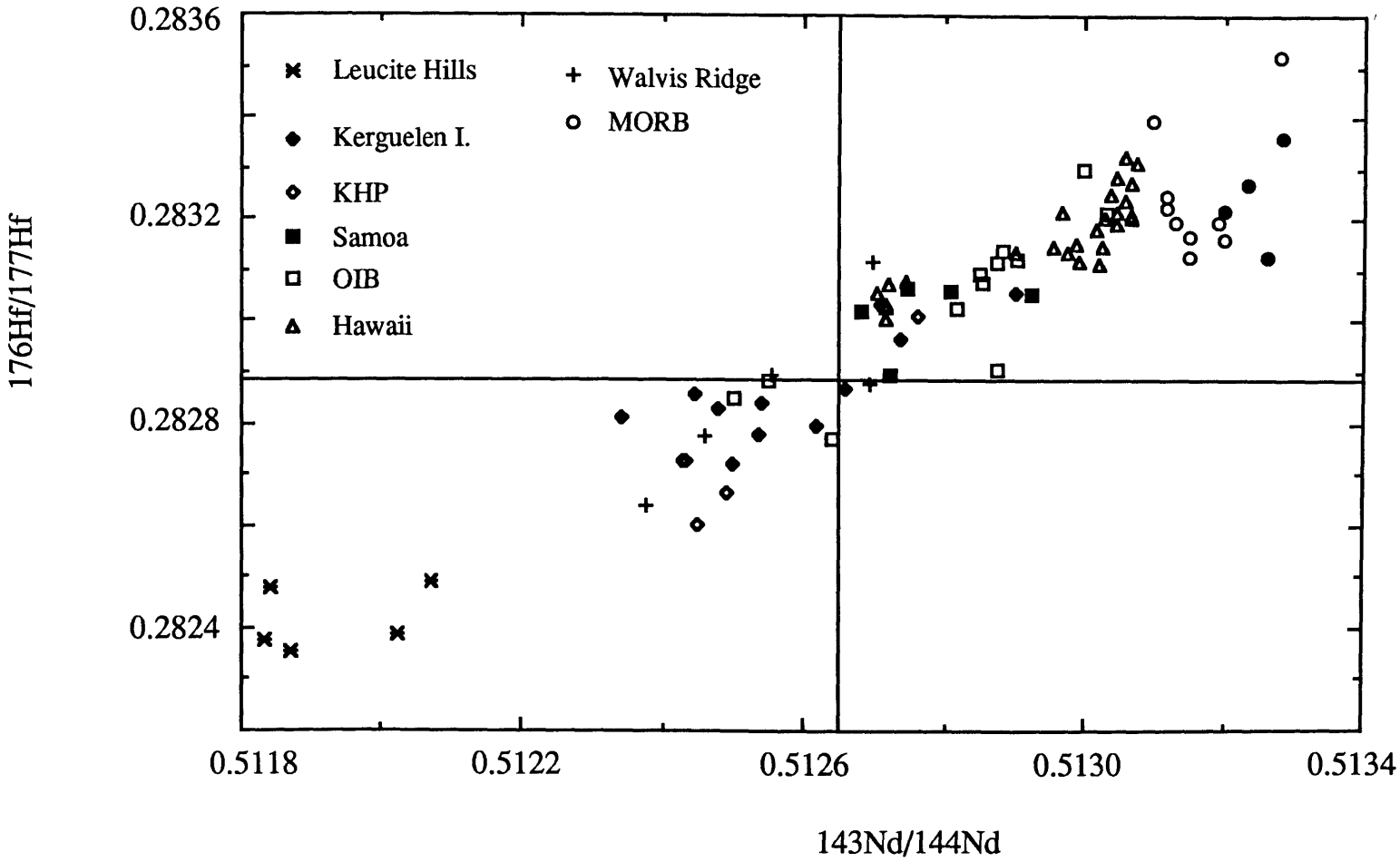
0.2836
0.2832
0.2828
0.2824
176Hf/177Hf
Leucite Hills
Kerguelen I.
KHP
Samoa
OIB
Hawaii
Walvis Ridge
MORB
0.5118
0.5122
0.5126
0.5130
0.5134
143Nd/144Nd

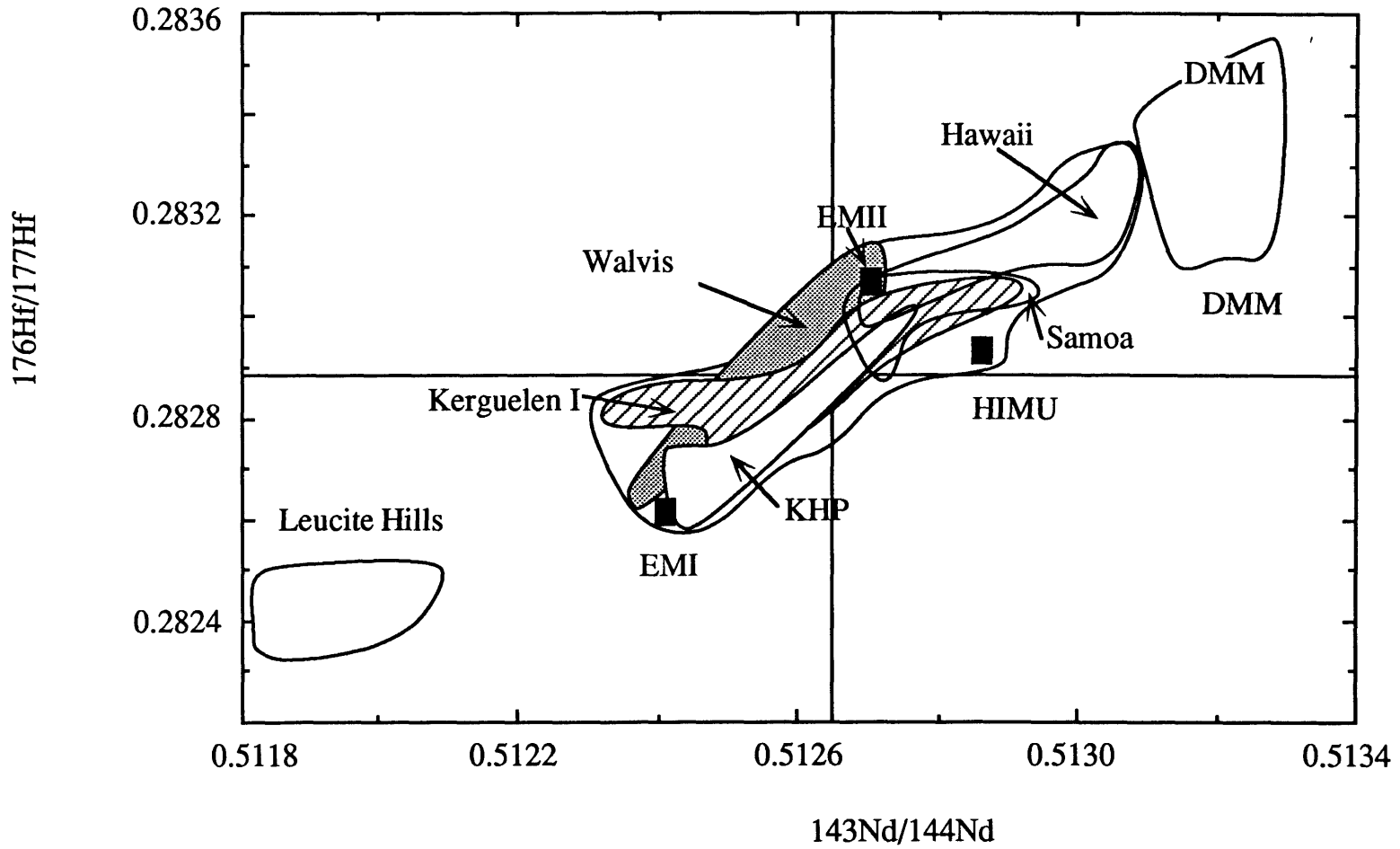
0.2836
0.2832
0.2828
0.2824
176Hf/177Hf
0.5118
0.5122
0.5126
0.5130
0.5134
143Nd/144Nd
DMM
Hawaii
EMII
Walvis
DMM
Samoa
Kerguelen I
HIMU
KHP
Leucite Hills
EMI

data set Patchett calculated that the Lu/Hf fractionation in sub-oceanic mantle is about twice that of Sm/Nd, which is in agreement with the above calculation.

The Hf-isotope analyses of Walvis Ridge, Kerguelen Plateau and Kerguelen Island delineates the EMI endmember quite well. Since EMI is defined on oceanic volcanics Leucite Hill samples are not considered as defining the endmember. The determination by White of St. Helena (Hart et al., 1986) locates the HIMU endmember on the Hf-Nd isotope correlation diagram. The determination of the Hf isotopic composition of the Samoan volcanics indicates the other enriched mantle endmember, EMII. The field outlined by MORB does not delineate a trend and Hf isotopic compositions partly overlap with the OIB field (MORB and OIB do not overlap in $^{143}Nd/^{144}Nd$). The added analyses of the Kane Fracture Zone extends the range of Hf-isotopes to lower $^{176}Hf/^{177}Hf$ at the high $^{143}Nd/^{144}Nd$ end of the MORB range, and further documents the lack of correlation between Nd and Hf isotopes in MORB. The total range in $^{176}Hf/^{177}Hf$ for MORB is from 0.283125- 0.283521 (0.14%). In contrast the range in $^{143}Nd/^{144}Nd$ for MORB, 0.513098- 0.513281 (0.035%), is limited. Although the total number of MORB samples analyzed for Hf isotopes is small, clearly Nd and Hf isotopes are not well correlated. A later part of this chapter will deal with the Nd and Hf isotopic compositions and their parent-daughter ratios in MORB. For the purposes of this section the variable $^{176}Hf/^{177}Hf$ in MORB requires a range of depleted mantle endmembers which range in $^{176}Hf/^{177}Hf$ but with essentially constant $^{143}Nd/^{144}Nd$. The high $^{176}Hf/^{177}Hf$ end of the OIB field requires just one high $^{176}Hf/^{177}Hf$-high $^{143}Nd/^{144}Nd$ depleted mantle component. The Leucite Hills lavas lie on an extension of the OIB field and uphold the general correlation between Sm/Nd and Lu/Hf.

3.4 Island Arc Volcanism

In general, the debate on the origin of the chemical characteristics of calc-alkaline volcanism is centered on the mantle characteristics in a subarc environment and the involvement (and

extent of involvement) of a component from the subducted slab. Apart from their unique tectonic setting, island arc volcanic rocks are distinguishable from other volcanic rocks in that they are:

- low in the so-called HFSE elements (Pearce and Cann, 1973; Pearce and Norry, 1979). Fig. 3.2 demonstrates the low HFSE content of island arc volcanics. The low abundances exhibit themselves best in Nb, Ta, and Ti. Hf and Zr are also lower compared to the neighboring REE, although the effect is not as pronounced as for the other 3 HFSE.
- High in Sr compared to Ce and Nd.
- High concentrations of mobile elements such as Cs, Li, Be, B and Ba compared to other elements with similar incompatibilty in the system melt-peridotite (Leeman, 1987; Morris and Hart, 1983; Tera et al., 1986).
- High $^{207}Pb/^{204}Pb$ for a given $^{206}Pb/^{204}Pb$, leading to high $\Delta 7/4Pb$, but $\Delta 8/4Pb$ close to zero (Hickey et al., 1986; Salters et al., 1988).

Three explanations have been put forward to explain these characteristics. Stern (1982) and Morris and Hart (1983) argue that most island arc magmas are from an OIB-type mantle without significant modification from the slab. The HFSE depletion is then explained by a phase, high in Ti, which is residual after melting (i.e. effectively changing the normal melt-peridotite petrology). Gill (1981), Nicholls and Ringwood (1973), and Tera et al. (1986) all argue that a slab component is an important feature in calc-alkaline volcanic products. The ^{10}Be evidence for the slab component is a very compelling argument in this respect. This slab component is high in alkaline, alkaline earth and rare earth elements and the HFSE depletion is in fact an REE enrichment. The question of whether this slab component is added to an OIB-type mantle (Gill, 1981; Tera et al., 1986) or to a MORB-type mantle (DePaolo and Johnson, 1979; Kay, 1977) is unknown.

As a third explanation Salters and Shimizu (1988), (see also Chapter 2), found that mantle materials characteristically exhibit HFSE depletions. Consequently they argue that the HFSE depletions in island arc volcanics are a reflection of their source and are not created by addition of a slab component or presence of titanates

during melting. Thus, although a slab component must be present (^{10}Be), this slab component does not alter the HFSE/REE ratios significantly.

The Lu-Hf isotope system appears an ideal system to address the question of the age of the HFSE depletion. If the HFSE depletion is a recent characteristic created either during the melting process or by the addition of a slab component just prior to melting, then the Nd and Hf isotopes should still be coupled. However, if the HFSE depletion is long-lived, then this should appear as a radiogenic $^{176}Hf/^{177}Hf$ ratio in islan arc volcanic products (IAV). White and Patchett (1984) concluded and Fig. 3.3 illustrates that the Lu/Hf ratios in island arc basalts are similar to the Lu/Hf in MORB. However, the slope of the trace element pattern on a spidergram can be changed by melting, as can be the Lu/Hf ratio. In the peridotite melt system below 15 GPa Hf is more incompatible than Lu, and thus the Lu/Hf ratio in basalts is not necessarily constant. Although the source of calc-alkaline volcanic products can have Lu/Hf ratios higher than BE, melting can lower this ratio significantly. A better way to determine Hf depletions is by comparing Hf with elements of similar compatibility (like Sm and Nd) and most IAV do have $Hf/Hf^* < 1$. In the system spinel peridotite-melt Hf/Hf^* is constant and should reflect the source ratio (see Chapter 2 for a discussion of the distribution coefficients). If the source of IAB has a smooth trace element pattern on a spidergram then, garnet residual in the IAV source will lower Hf/Hf^* and Zr/Zr^* in the melt, however garnet will also raise Ti/Ti^* compared to the source. Since most IAV have $Ti/Ti^* < 1$, the presence of garnet residual to IAB genesis is not likely, unless the IAV source has even larger Ti/Ti^* than the IAV. Amphibole, a phase often proposed as being important in IAV genesis, will have the opposite effect on the HFSE/REE fractionation as garnet, i.e amphibole will increase Zr/Zr^* and decrease Ti/Ti^*, and thus kaersutite or pargasite do not play an important role in generating HFSE depletions in IAV.

In order to asses the age of the HFSE depletion in island arcs I analyzed samples from Fiji. Fiji was chosen because of the comprehensive body of geochemistry already assembled for Fiji (Gill,

Figure 3.13

Simplified map of the southwest Pacific ocean after Gill (1987). Wallis Island is a small oceanic island east of Viti Levu, the principal island of the Fiji archipelago

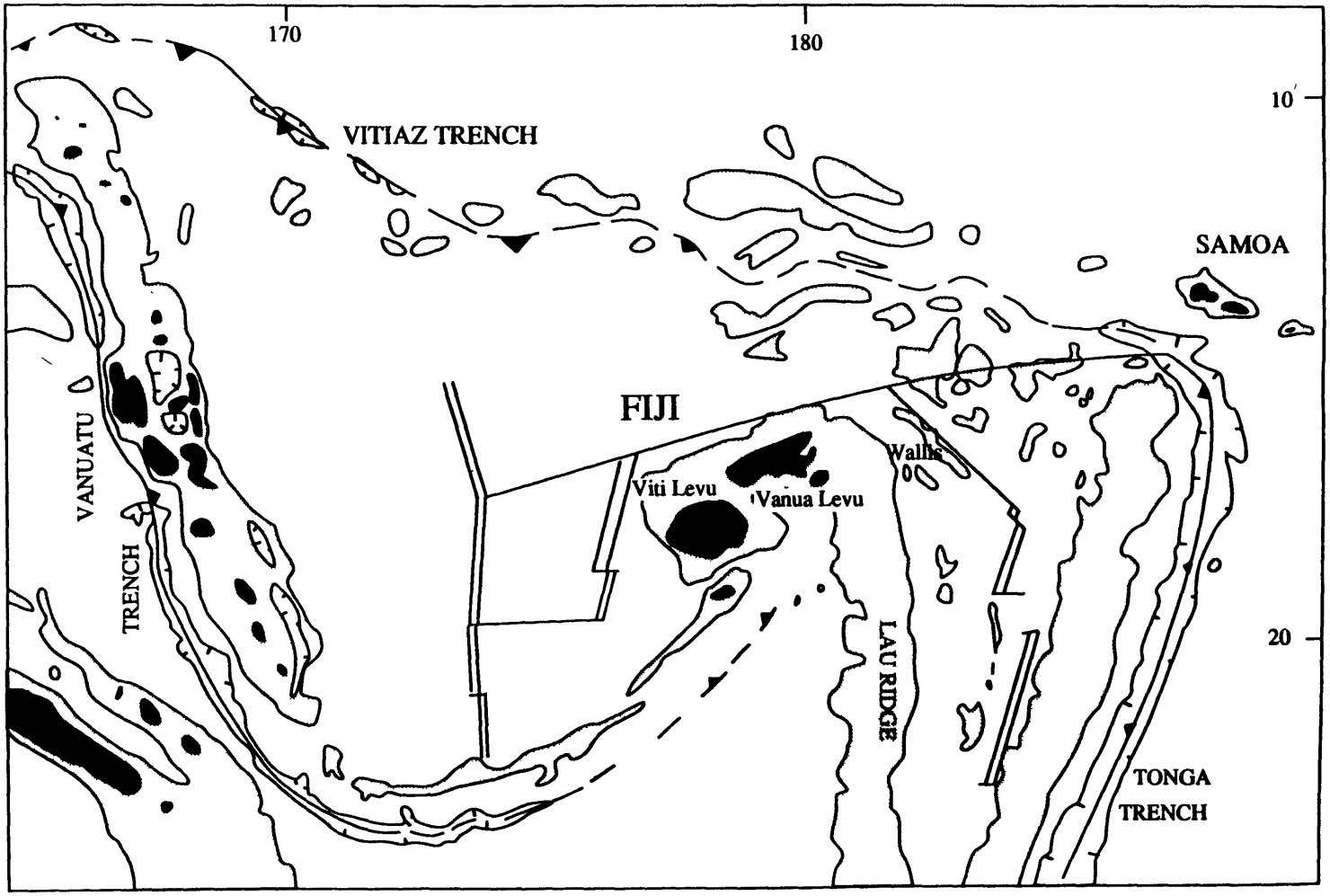
170
180
10
20
VITIAZ TRENCH
SAMOA
FIJI
VANUATU
TRENCH
Viti Levu
Vanua Levu
Wallis
LAU RIDGE
TONGA
TRENCH

Table 3.5
Hf and Nd isopic compositions of Fijian volcanics

Sample #	176Hf/177Hf	143Nd/144Nd	Age	Type	Stage
WA45	0.283198	0.513066	33	High HFSE basalt	I
WA2	0.283116	0.513089	M. Miocene	Medium HFSE, basalt	I
69-851	0.283284	0.51306	M. Miocene	Low HFSE, Px andesite	I
WA4	0.283089	0.5131	10	High HFSE, basalt	I
71-374	0.283116	0.51307	6-9.	Mature arc thol.	II
68-66	0.283187	0.51301	5.7	Mature arc	II
W10	0.283194	0.51297	3.9	Early rifting,shoshonite	III
71-372	0.283296	0.513074	3.9	Early Rifting	III
W253	0.283101	0.512804	<0.1	Alk.Bas.	IV
69-829	0.283038	0.51284	<0.1	Alk.Bas.	IV
4-1.	0.282918	0.512783	recent	Wallis Island	
4/2.	0.283047	0.51277	recent	Wallis Island	
164-1	0.283259	0.51305+	recent	Back arc basalt	
133/1A	0.283302	0.51298+	recent	Back arc basalt	

Normalizations as in Table 3.3
Nd-data either from Gill(1984) or my data
Nd-data from K. Johnson

1984; Gill, 1987; Gill et al., 1984; Gill and Whelan, 1989a; Gill and Whelan, 1989b), and in an attempt to minimize the importance of other processes (especially crustal contamination) and thus maximize the chance of finding high $^{176}Hf/^{177}Hf$.

Fig. 3.13 shows a schematic map of the Fijian archipelago and the main features of the ocean basin around Fiji. The Fiji island group is a complex of calc-alkaline volcanoes built on an oceanic plate, and has the longest period of volcanism in an island arc type setting (>30 Ma). Furthermore, because the subducted plate is also oceanic, continental crustal contamination can be ruled out as a process causing the major chemical trends. The Pb-isotopic characteristics of Fijian volcanics (Gill, 1984) indicate minimal contribution from a subducted slab component ($\Delta 7/4Pb \approx 0$). As a consequence the mantle beneath Fiji had the longest possible period of time to develop a Hf isotope signature, and the Fijian lavas are an as pure as possible melt of sub-arc mantle.

Gill (1984), Gill (1987), Gill et al. (1984) divide the volcanism of the Fijian archipelago into four different stages. The first stage (>33 Ma to 10 Ma) is the early arc stage. During this stage, Fiji was part of the Vitiaz arc, which stretched from New Britain to the Fiji and Vanuatu island group. Volcanics from this stage are mainly tholeiitic and basaltic, and all volcanism was submarine. The second stage (10-5 Ma) is called the mature arc stage. Samples from this stage range from basalt to andesite. About 5 Ma ago the Vitiaz Arc broke up, by faulting between Viti Levu and Vanuatu, which moved the Fiji archipelago away from the trench. In the third, early rifting, stage (5-3 Ma) the movement away from the trench coincided with a change in eruptive products towards more alkalic compositions ranging from tholeiites, to shoshonites and calc alkaline andesites. The present stage is the Late rifting stage. The Fiji archipelago is now well removed from the trench, but a hot spot is active beneath Fiji producing mainly alkali olivine basalts and hawaiites. Results of the analyses on all four stages of volcanism are listed in Table 3.5. Furthermore, I analyzed lavas which are possible representatives of the OIB and MORB mantle source near Fiji. OIB mantle source is analyzed with the fourth stage of Fijian magmatism and with Wallis

Figure 3.14

$^{176}Hf/^{177}Hf$ versus $^{143}Nd/^{144}Nd$ for the three different basalt types from the Fiji region. Crosses are Island Arc Volcanics and are related to subduction. Circles are 2 alkali basalts from the Fijian archipelago related to the Late stage rifting and 2 basalts from Wallis Island. Plusses are 2 dredge basalts from the ridge of the back arc basin.

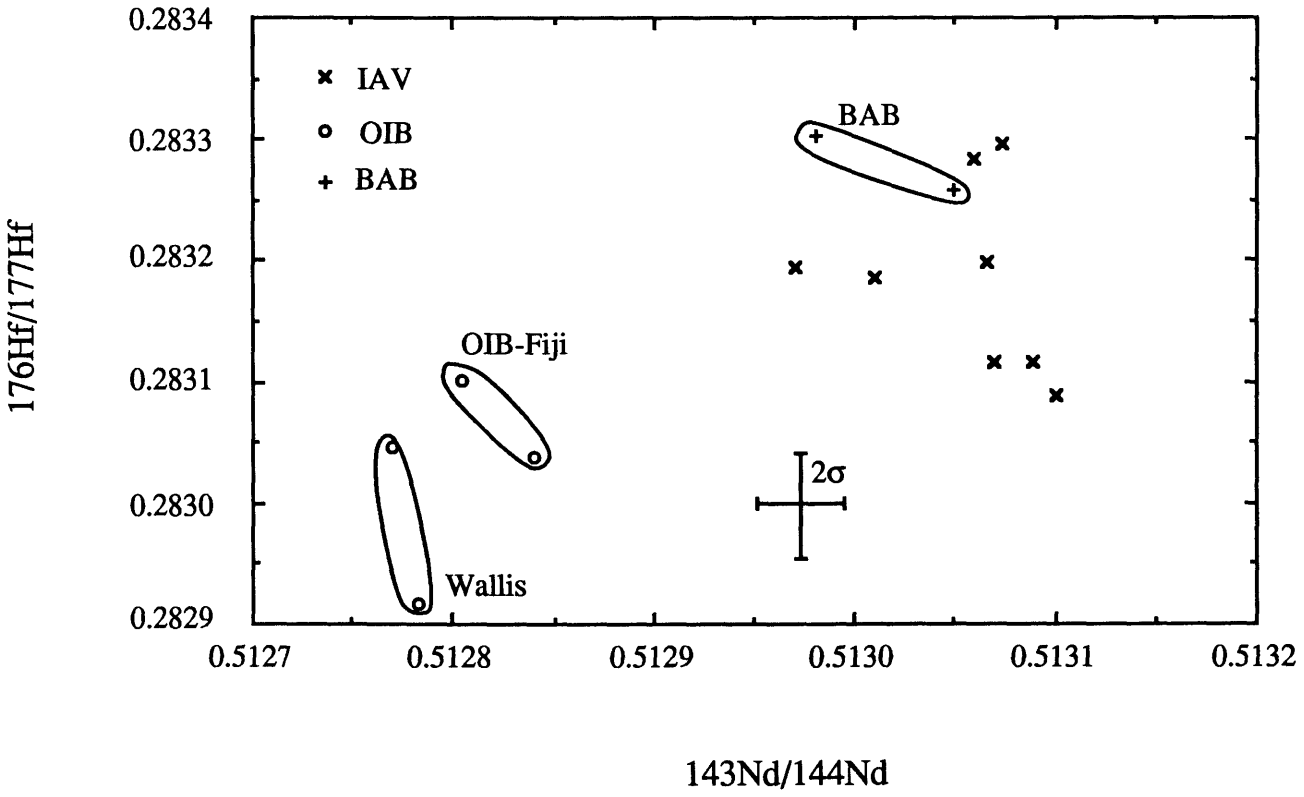
0.2834
0.2833
0.2832
0.2831
0.2830
0.2829
0.5127
0.5128
0.5129
0.5130
0.5131
0.5132
176Hf/177Hf
143Nd/144Nd
IAV
OIB
BAB
BAB
OIB-Fiji
Wallis
2σ

Figure 3.15

Spider diagram for the Fijian volcanics. Representative of the different stages of magmatic activity in the Fijian archipelago. Data from Gill (1984), Gill (1987), Gill et al. (1984), Gill and Whelan (1989a), Gill and Whelan (1989b).

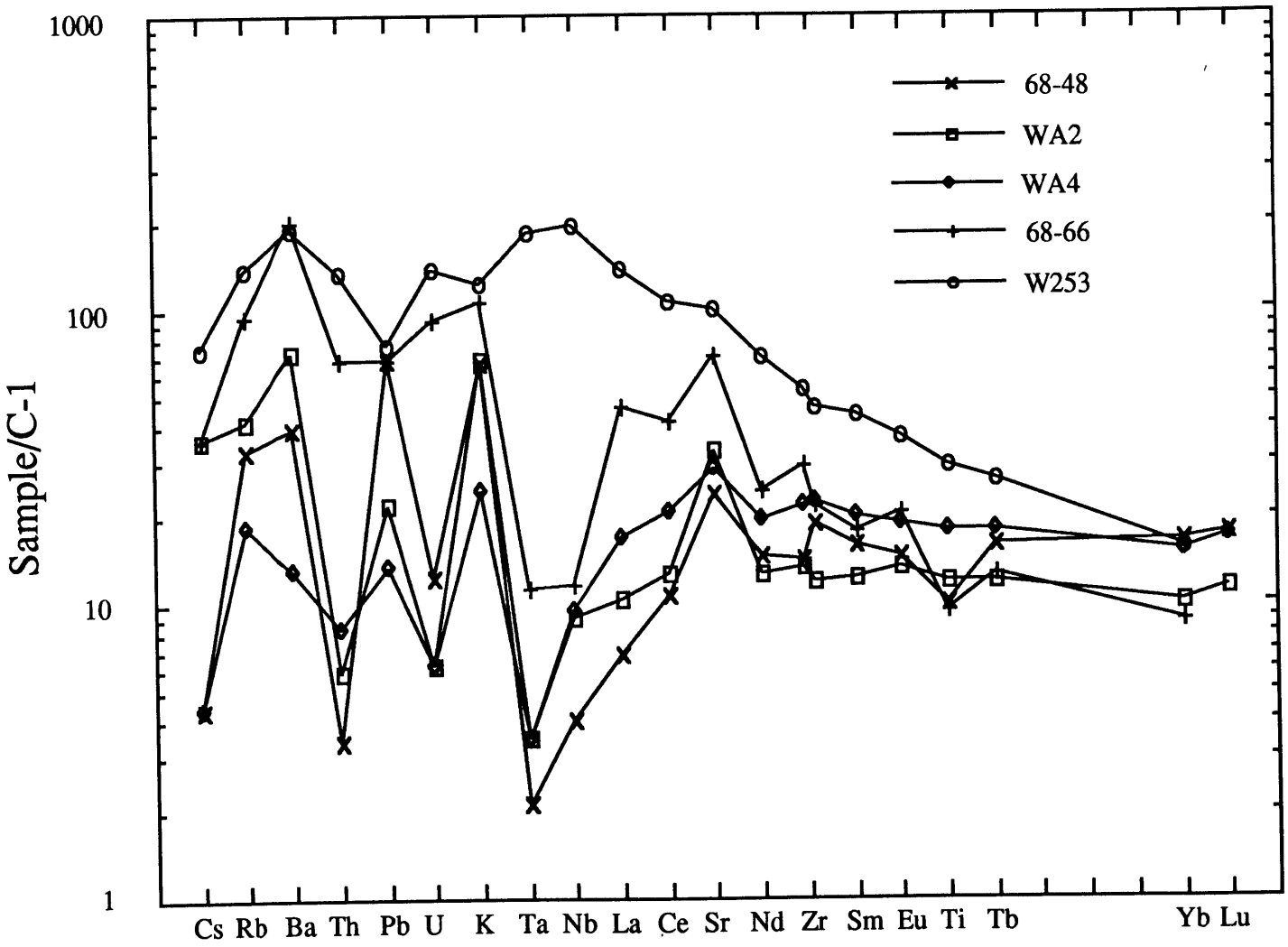
1000
100
10
1
Sample/C-1
68-48
WA2
WA4
68-66
W253
Cs Rb Ba Th Pb U K Ta Nb La Ce Sr Nd Zr Sm Eu Ti Tb Yb Lu

Figure 3.16

$^{176}Hf/^{177}Hf$ versus $^{143}Nd/^{144}Nd$ for Island Arc Volcanic rocks compared with oceanic volcanic rocks. Fields for OIB and MORB from Fig. 3.12. IAV are devided into 2 groups. Group II (circles) are IAV which have demonstrable amounts of crustal component added. Group I (crosses) are thought to be more or less unaffected by crustal contamination. Most of the "uncontaminated" basalts fall clearly above the regression line through the OIB field. Data from White and Patchett (1984) and this study.

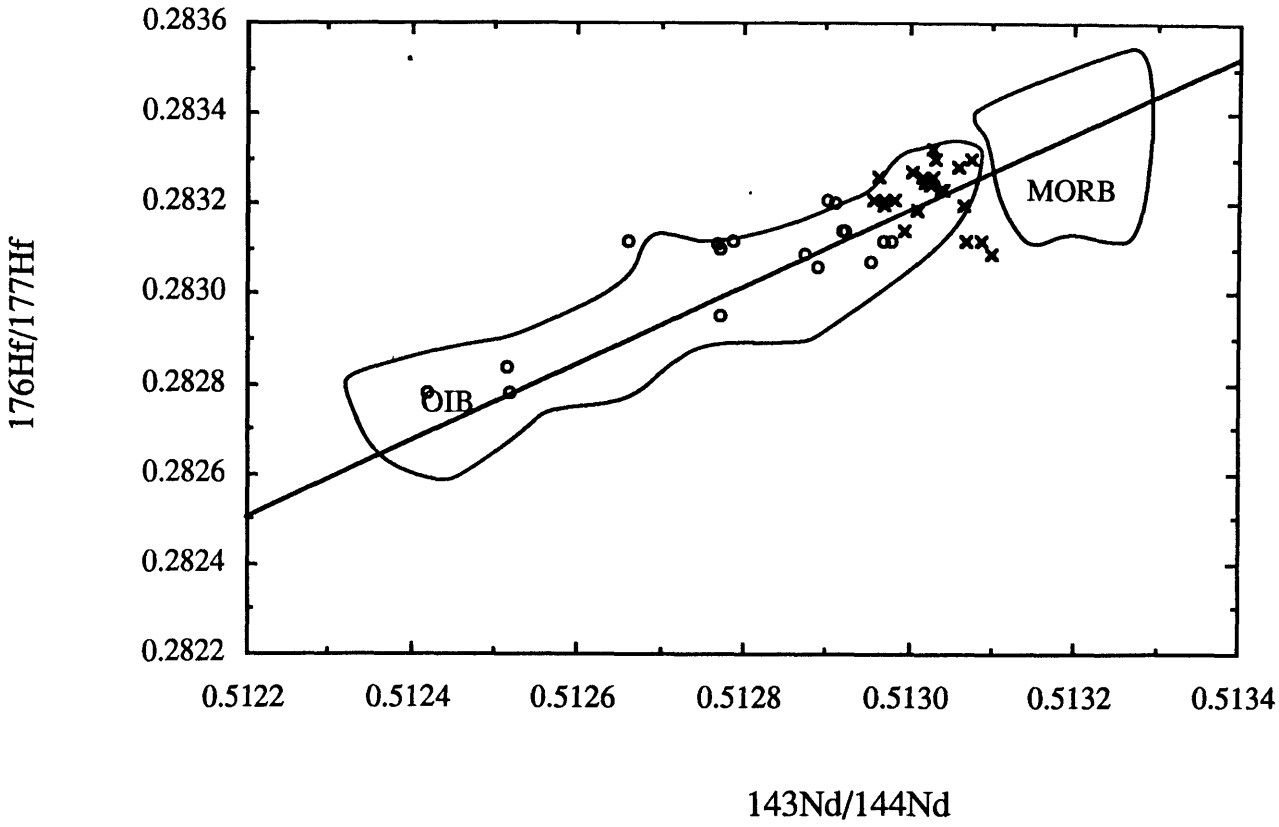
0.2836
0.2834
0.2832
0.2830
0.2828
0.2826
0.2824
0.2822
176Hf/177Hf
0.5122
0.5124
0.5126
0.5128
0.5130
0.5132
0.5134
143Nd/144Nd
MORB
OIB

Island samples. Only two sample, possibly of MORB source origin, are represented by analyses of a back arc basin basalts.

Fig. 3.14 shows the Hf-Nd isotope correlation diagram for Fijian lavas and basalts nearby. The results are listed in Table 3.5. The range in $^{176}Hf/^{177}Hf$ for the Fijian arc lavas is slightly higher than, although within analytical precision, of the range of the OIB-type basalts at Fiji. The average $^{176}Hf/^{177}Hf$ and $^{143}Nd/^{144}Nd$ of the Fijian arc lavas is clearly higher than the averages for the possible OIB source. The total variation within the Fijian arc lavas (i.e. the first three stages only) is relatively small and almost within analytical precision. The arc lavas also overlap in $^{176}Hf/^{177}Hf$ with possible MORB sources (Fig. 3.12). The Fijian case indicates that $^{176}Hf/^{177}Hf$ are similar, but different in $^{143}Nd/^{144}Nd$ from the nearby OIB sources. Fig. 3.15 shows the trace element patterns on a spidergram for the 5 different volcanic stages. Fijian island-arc lavas are generally depleted in the incompatible trace elements. Only small depletions in Ti, compared to the REE are observed, and the depletions are absent for Hf and Zr; Nb and Ta depletions are prominently present. Fig. 3.16 shows the Hf-Nd isotope variation for IAV as compared to OIB and MORB. The IAV should be split in to 2 groups based on the possibility that some IAV are contaminated by continental crustal material. The Marianas, Izu, Aleutians, Fiji and New Britain are considered as being the least contaminated with continental crustal material (Gill et al., 1984; Meijer, 1976; Nye and Reid, 1986; Stern and Bibee, 1984), and they can be considered a window into the subarc mantle. The Lesser Antilles, Sunda and Banda are considered to be contaminated with continental crustal material (Davidson, 1983; Morris, 1984; White and Dupre, 1986), and as a consequence the isotopic characteristics may be changed towards crustal characteristics. Except for 3 Fiji samples, the field for the least contaminated IAV is slightly offset to higher $^{176}Hf/^{177}Hf$ for a given $^{143}Nd/^{144}Nd$ compared to OIB. Calculating an age for the Hf-depletion is hampered by the lack knowledge of the parent-daugther ratios. Furthermore, the lack of correlation between Hf/Hf* and $^{176}Hf/^{177}Hf$ (Fig. 3.17) makes it difficult to estimate Lu/Hf ratios of the source. The difference between the $^{176}Hf/^{177}Hf$ of the OIB

Figure 3.17

$^{176}Hf/^{177}Hf$ versus Hf/Hf* for island arc volcanics. plusses represent the Lesser Antilles, crosses Fiji, circles Mariana, open squares New Britain, filled squares Aleutians, triangles Banda, and stars represent Sunda. Data sources as in Fig. 3.16, and 3.15.

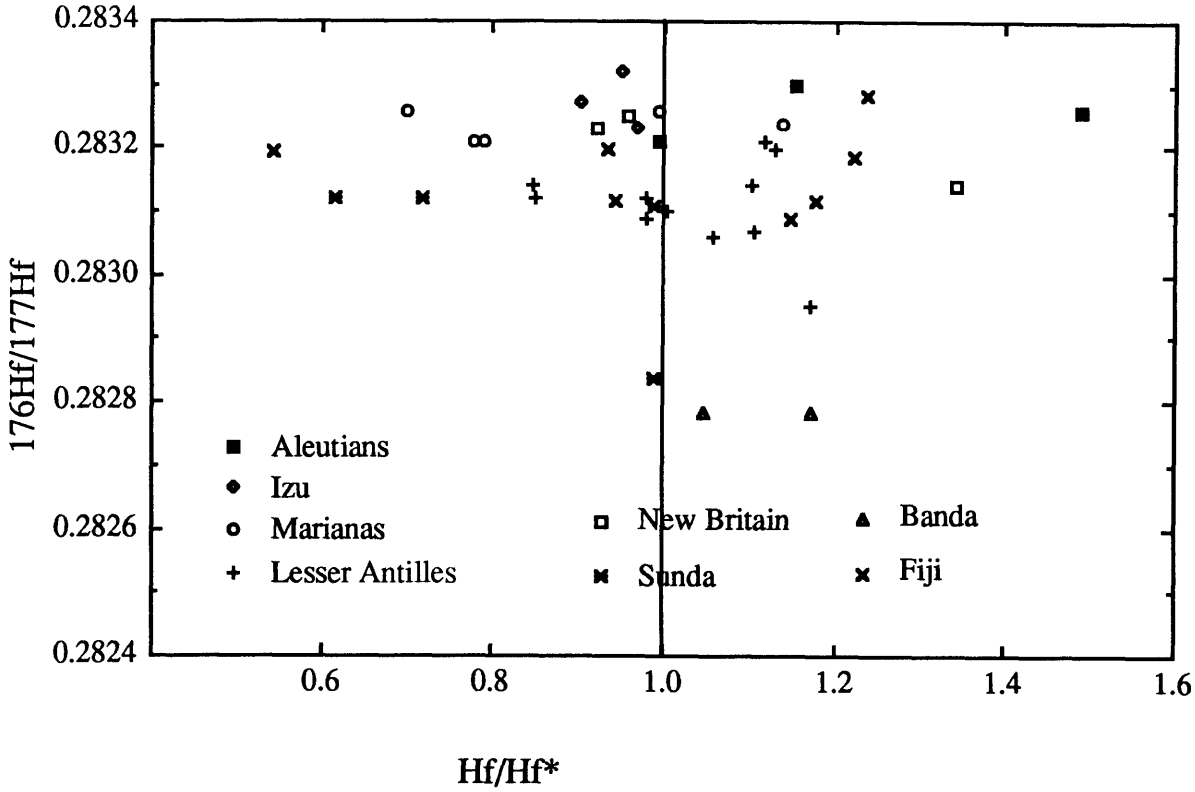
0.2834
0.2832
0.2830
0.2828
0.2826
0.2824
176Hf/177Hf
0.6
0.8
1.0
1.2
1.4
1.6
Hf/Hf*
Aleutians
Izu
Marianas
Lesser Antilles
New Britain
Sunda
Banda
Fiji

Figure 3.18

Hf/Hf* versus Sr/Nd for mafic subduction related volcanics. Data sources as in Fig. 3.3. If the Hf depletion in island arcs is generated at the same time as the Sr-enrichment than a positive correlation is expected. However, no correlation is observed. To calculate the Hf-depletions for New Hebrides the Nd content of the basalts was derived from the REE pattern.

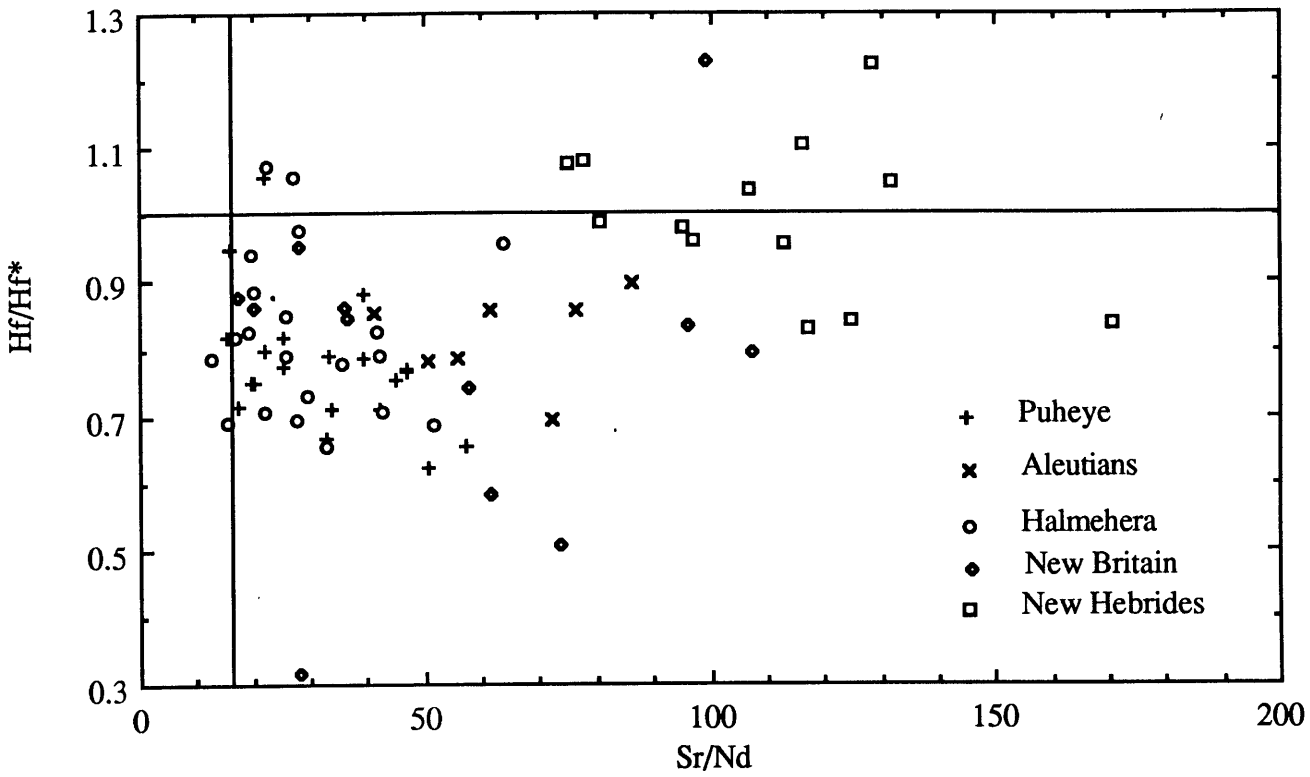
1.3
1.1
0.9
0.7
0.5
0.3
Hf/Hf*
0
50
100
150
200
Sr/Nd
Puheye
Aleutians
Halmehera
New Britain
New Hebrides

Figure 3.19

Hf/Hf* versus Ce/Yb and Ti/Ti* for calc-alkaline volcanics. Data sources as in Fig. 3.3. Except for the New Hebrides volcanics of a given arc show a very weak positive correlation between Ce/Yb and Hf/Hf*, indicating the possibility of increase in Hf-depletion with increasing LREE enrichment. No correlation exists between the Hf and Ti depletion.

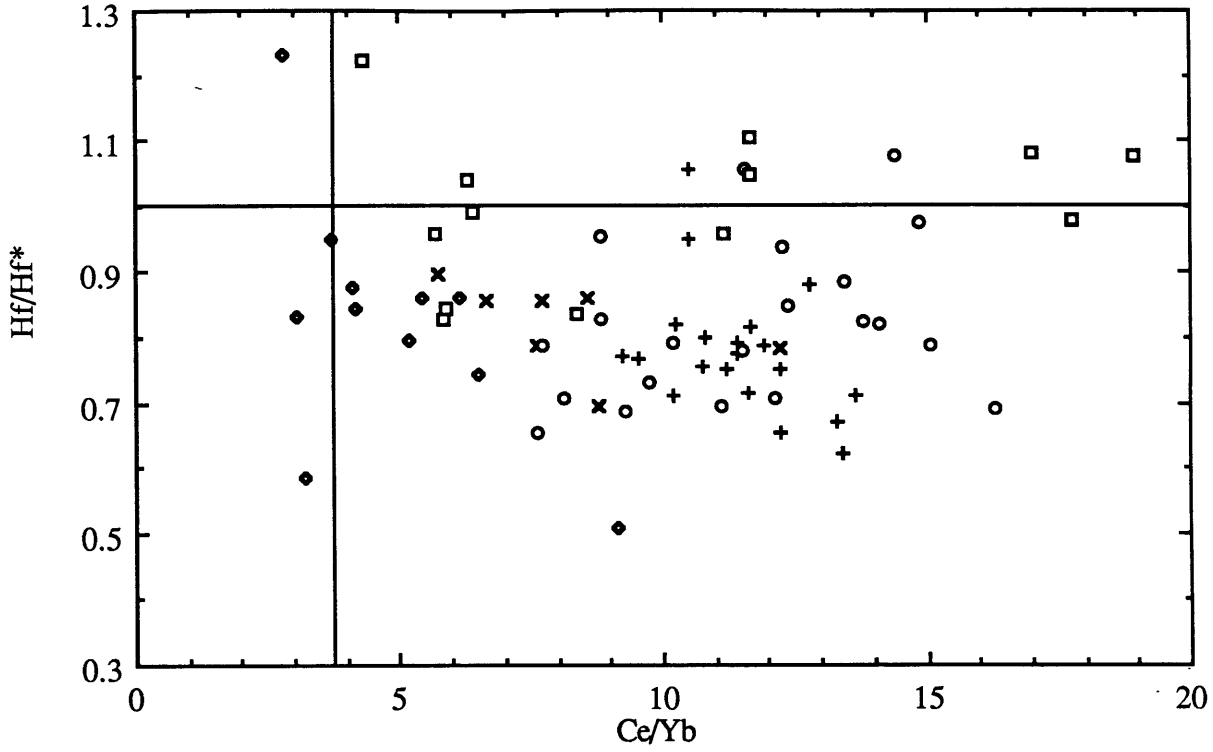
1.3
1.1
0.9
0.7
0.5
0.3
Hf/Hf*
0
5
10
15
20
Ce/Yb

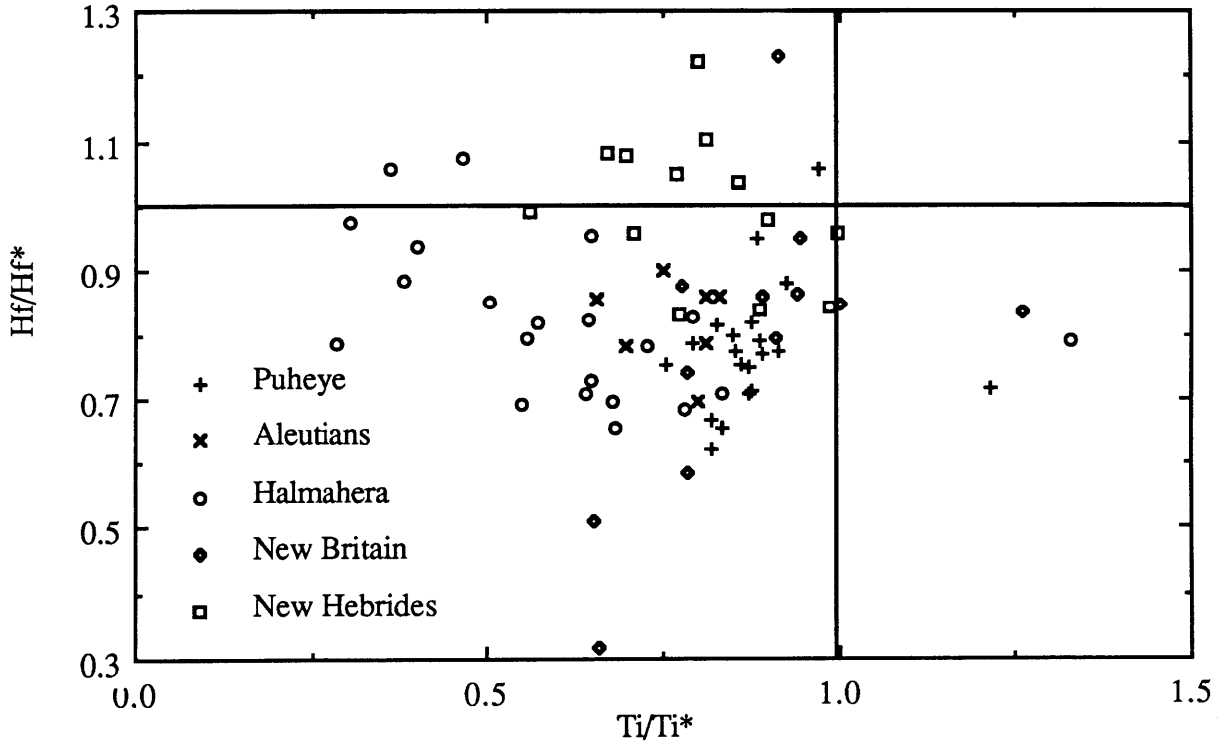
1.3
1.1
0.9
0.7
0.5
0.3
Hf/Hf*
Puheye
Aleutians
Halmahera
New Britain
New Hebrides
0.0
0.5
1.0
1.5
Ti/Ti*

regression line in Fig. 3.16 and the average IAV is small. Assuming a Hf/Hf*=0.8, and a flat REE pattern in the source, this high Lu/Hf ratio has to exist for 250 Ma to achieve the shift in $^{176}Hf/^{177}Hf$. But basically the shift is small and can be caused by insufficient analyses on IAV. Thus, the Hf-isotope evidence for a long lived HFSE depleted source for IAV is inconclusive.

Fig. 3.18 and 3.19 plots trace element data of subduction-related volcanic products, tholeiites, basalts and basaltic andesites. In order to minimize low level fractionation processes, and to concentrate on mantle variations only mafic IAV were used. Hf/Hf* or Zr and Ti are not correlated with the other characteristics of IAV, such as Sr/Nd (Fig. 3.18). Assuming high Sr/Nd in IAV is related to a slab component, then the lack of correlation between Hf/Hf* and Sr/Nd ratio indicates the HFSE depletion is not related to a slab component. The Sr/Nd and HFSE/REE variation in peridotites supports a different origin for the Sr enrichments and HFSE depletions (see Chapter 2). Chapter 2 also discusses the lack of coherent behavior of the different HFSE. Fig. 3.19 shows that in mafic calc-alkaline volcanics variations Ti and Hf are independent from each other, and that Hf depletion is not simply related to LREE enrichment, i.e. Ce/Yb ratio. Furthermore, the Hf, Zr and Ti depletions are not as prominent as expected in the mafic IAV. A review of the literature indicates the HFSE depletions are not related to Mg#, other major elements, Ce/Yb ratio, K/Rb or other geochemical parameters. This suggests the Hf/Hf* variations are not created by a late stage process, but by some process that is now overprinted by processes such as melting and addition of a slab component, and crystal fractionation, etc. It must be noted that volcanics that lack Hf or Zr depletions invariably do show Nb or Ta depletions (if Nb or Ta are measured).

Fig. 3.20 and 3.21 show the parent-daugther variations and their corresponding isotope ratios for MORB, OIB and IAV. Clearly, the IAV do not fall on a simple bulk earth derived isochron. The field for IAV is intermediate between the MORB and OIB field, and the position to the left of even a 3 Ga isochron indicates a recent decrease in Lu/Hf and Sm/Nd. The deviation of MORB from any of the isochrons in Fig. 3.20 and 3.21 is caused by the melting process with garnet and

Figure 3.20

$^{176}Lu/^{177}Hf$ versus $^{176}Hf/^{177}Hf$ for island arc basalts. Fields for MORB and OIB are indicated but will be discussed later. I=Izu, M=Marianas, LA=Lesser Antilles, B=Banda, S=Sunda, F=Fiji, A=Aleutians, and NB indicates New Britain. Straight lines are 1, 2, and 3 Ga isochrons through BE. IAB are clearly enriched in Hf over Lu compared to BE, while having isotopic characteristics depleted compared to BE. The deviation for IAB from isochrons is similar to OIB and MORB and indicates a recent enrichment in Hf over Lu. Data sources from Fig. 3.16, 3.23 an 3.24.

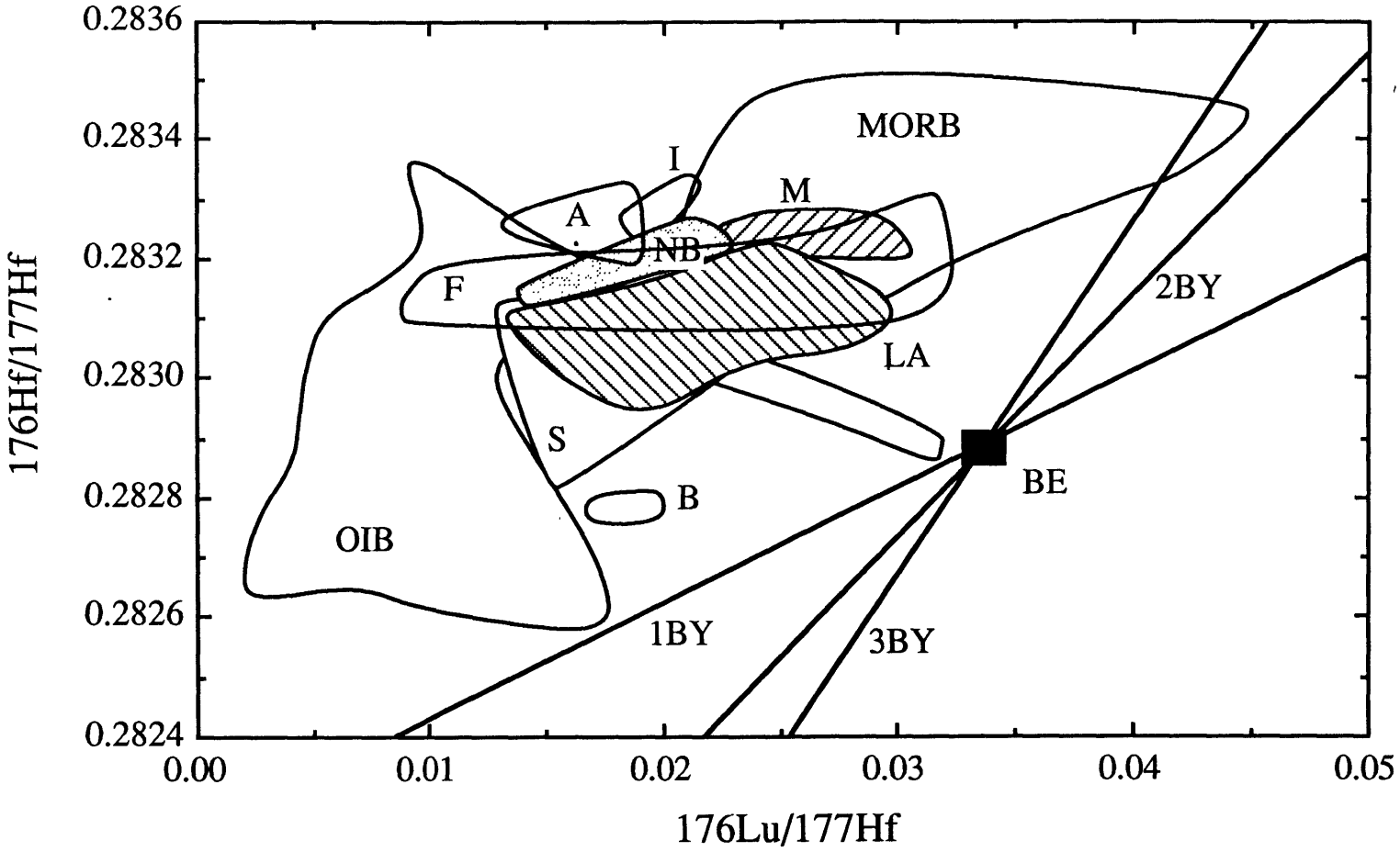
0.2836
0.2834
0.2832
0.2830
0.2828
0.2826
0.2824
176Hf/177Hf
0.00
0.01
0.02
0.03
0.04
0.05
176Lu/177Hf
MORB
I
M
A
NB
F
LA
2BY
S
BE
B
OIB
1BY
3BY

Figure 3.21

$^{147}Sm/^{144}Nd$ $^{143}Nd/^{144}Nd$ for island arc basalts. Fields for MORB and OIB are indicated but will be discussed later. I=Izu, M=Marianas, LA=Lesser Antilles, B=Banda, S=Sunda, F=Fiji, A=Aleutians, and NB indicates New Britain. Straight lines are 1, 2, and 3 Ga isochrons through BE. The deviation for IAB from isochrons is similar to OIB and MORB and indicates a recent enrichment in Nd over Sm. Data sources from Fig. 3.16, 3.23 an 3.24.

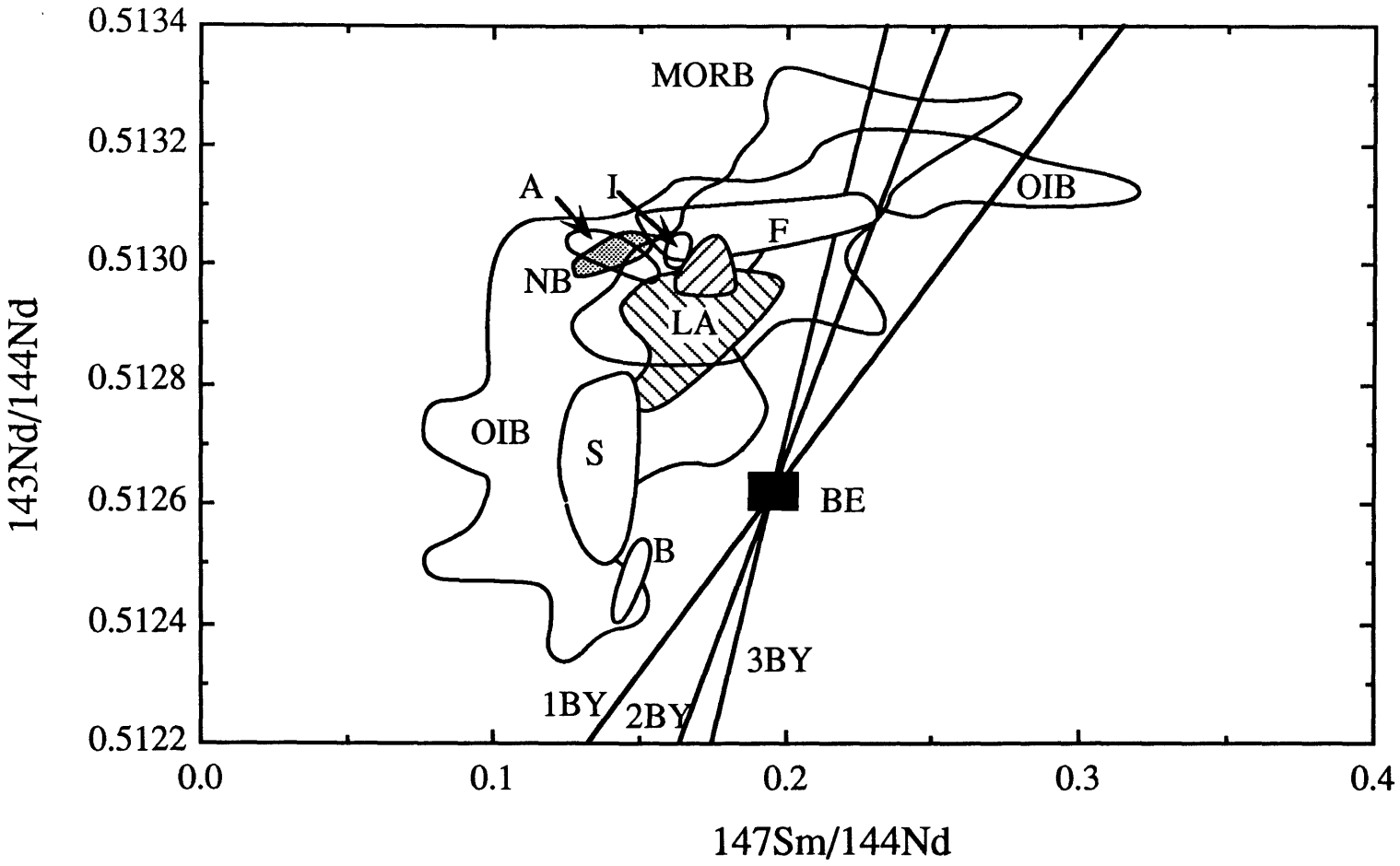
0.5134
0.5132
0.5130
0.5128
0.5126
0.5124
0.5122
143Nd/144Nd
0.0
0.1
0.2
0.3
0.4
147Sm/144Nd
MORB
OIB
A
I
F
NB
LA
OIB
S
BE
B
3BY
1BY
2BY

clinopyroxene as two important residual phases, as discussed in the next section. Similarly, the position of the IAV data, and the lack of correlation between Hf/Hf* and $^{176}Hf/^{177}Hf$ indicates a recent disturbance of the Hf-isotope systematics, which is of the same order as the MORB and OIB variation. However, part of the difficulty in characterizing the source of IAV is that the melting process is not well constrained. Island arc volcanics are in general volatile rich (Gill, 1981) and as such, amphibole can be a residual phase after melting. Both amphibole and garnet are able to fractionate the HFSE from the REE, see Chapter 2 for distribution coefficients. The lack of our knowledge of the chemical composition of the subarc mantle, and the possible existence of amphibole in the source makes it difficult to model the melting process. However, based on the available data the following generalizations can be made:

- $^{176}Hf/^{177}Hf$ indicate that "uncontaminated" IAV show a long term Lu/Hf higher than bulk earth.
- Nb and Ta depletions are a more prevalent characteristic in IAV than Zr, Hf and Ti depletions.
- the behavior of Hf, Zr and Ti is not correlated.
- HFSE depleted mantle is a ubiquitous component in the shallow mantle (<100km).
- Melting with amphibole as a residual phase will lead to $(Hf/Hf^*)_{melt}>(Hf/Hf^*)_{source}$ and $(Zr/Zr^*)_{melt}>(Zr/Zr^*)_{source}$, and $(Ti/Ti^*)_{melt}<(Ti/Ti^*)_{source}$, i.e. will reduce Hf and Zr depletions compared to the REE. Garnet residual after melting has the opposite effect on the partitioning of Hf, Zr and Ti than amphibole.

Melting of HFSE-depleted mantle, with amphibole and/or garnet residual and thus enhancing or reducing the HFSE depletions, can explain the observations based on the HFSE and REE. The persistence of the Nb and Ta depletions indicate the melting process has less influence on these elements, and incorporating these elements into genetic scenarios for IAV is an important future step. Chapter 2 discussed the likely origin for the HFSE-depleted mantle. This origin implies the occurrence of HFSE-depleted mantle in depleted MORB mantle, and in the mantle residual to MORB genesis. Furthermore, at localities with paired alkaline and calc-alkaline volcanism, (Fiji,

Carpathians, Patagonia, Turkey), the two types of volcanism are not simply related to each other, indicating the existence of heterogeneous mantle. Generating IAV from HFSE depleted mantle which is residual after MORB genesis is a likely and most simple explanation for the HFSE depletions. However, this mantle has to be later enriched in some 'mobile' elements, Cs, ^{10}Be, and Sr specifically. Addition of a slab component is the most likely enrichment process. This slab component can "flux" the depleted mantle and cause the melting leading to calc-alkaline volcanics. This could also explain the relation between HFSE depleted magmas and subduction. The mantle residual after MORB genesis is too residual to melt in the shallow mantle (i.e. always below its solidus), except when it is fluxed with a slab component, which effectively lowers the solidus.

3.5 The Hf-paradox, and the role of garnet in the MORB source

3.5.1. Introduction

This part of the Chapter is a slightly extended version of a paper recently submitted to Nature. As a consequence, some parts of this section may overlap with previous sections, but I think and hope this will present the arguments in a more coherent fashion. Mid-Ocean Ridge Basalts have ^{176}Hf/^{177}Hf ratios indicating derivation from a mantle reservoir with a long term Lu/Hf ratio greater than Bulk Earth. However, the measured Lu/Hf in MORB are lower than Bulk Earth. We call this the Hf-paradox (Salters and Hart, 1989). The purpose of this section is to solve the Hf-paradox in terms of a melting model and to examine the model in light of petrological and geophysical constraints on mid-ocean ridge magmatism.

Patchett and co-workers published a series of papers using Hf-isotopes to constrain geological processes (Patchett, 1983; Patchett et al., 1981; Patchett and Tatsumoto, 1980a; Patchett and Tatsumoto, 1980b; Stille et al., 1983; White and Patchett, 1984). In general they concluded that Hf-isotopes in oceanic volcanics (MORB and OIB) are well correlated with Nd-isotopes (Patchett, 1983), and

Figure 3.22

Lu/Hf, Sm/Nd and Hf/Hf* versus Mg# for MOR volcanics. Circles are Pacific, crosses are Atlantic, and diamonds are Indian Ocean MORB. Clearly there is no systematic variation between any of the trace element ratios and Mg# indicating fractionation has no effect on these trace element ratios. Data sources Clague and Frey (1982), Dupuy et al. (1987), Frey et al. (1974), Frey et al. (1980), Hofmann et al. (1987), Liotard et al. (1986), Pearce et al. (1985), Perfit and Fornari (1986), Price et al. (1986), Puchelt and Emmermann (1983), Rhodes et al. (1978), White et al. (1979), Wood et al. (1979). Horizontal line marked BE is Bulk Earth Lu/Hf ratio. Lines marked 2 Ga and 3 Ga indicates the Lu/Hf (or Sm/Nd) ratio that leads to the $^{176}Hf/^{177}Hf$ (or $^{143}Nd/^{144}Nd$) of average MORB in 2 or 3 Ga age.

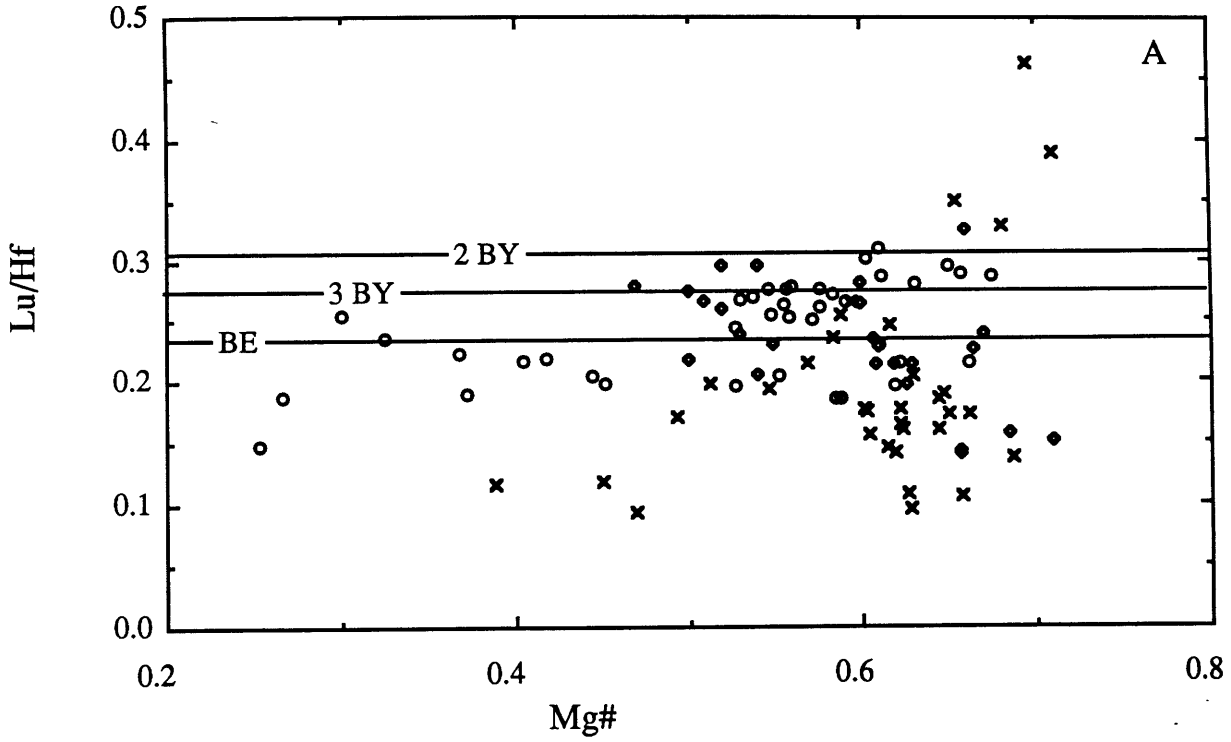
A
Lu/Hf
Mg#
2 BY
3 BY
BE
0.0
0.1
0.2
0.3
0.4
0.5
0.2
0.4
0.6
0.8

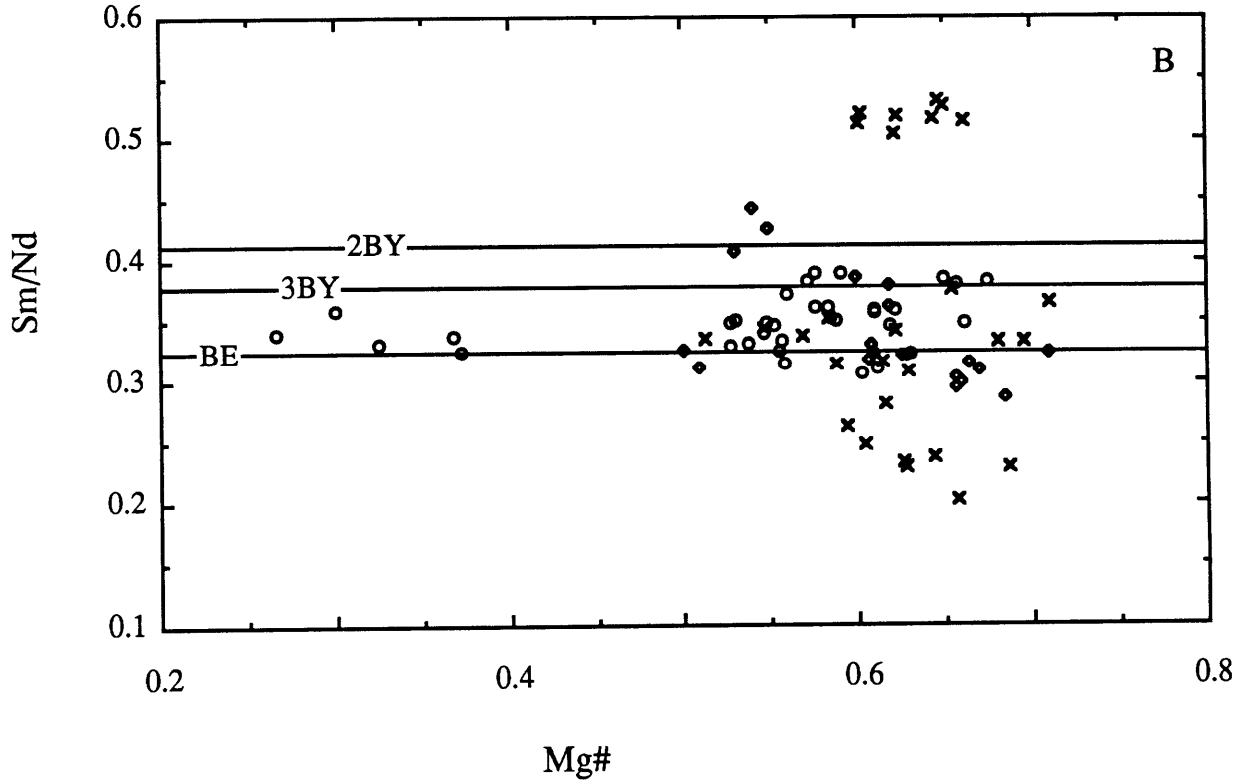
B
Sm/Nd
Mg#
2BY
3BY
BE
0.1
0.2
0.3
0.4
0.5
0.6
0.2
0.4
0.6
0.8

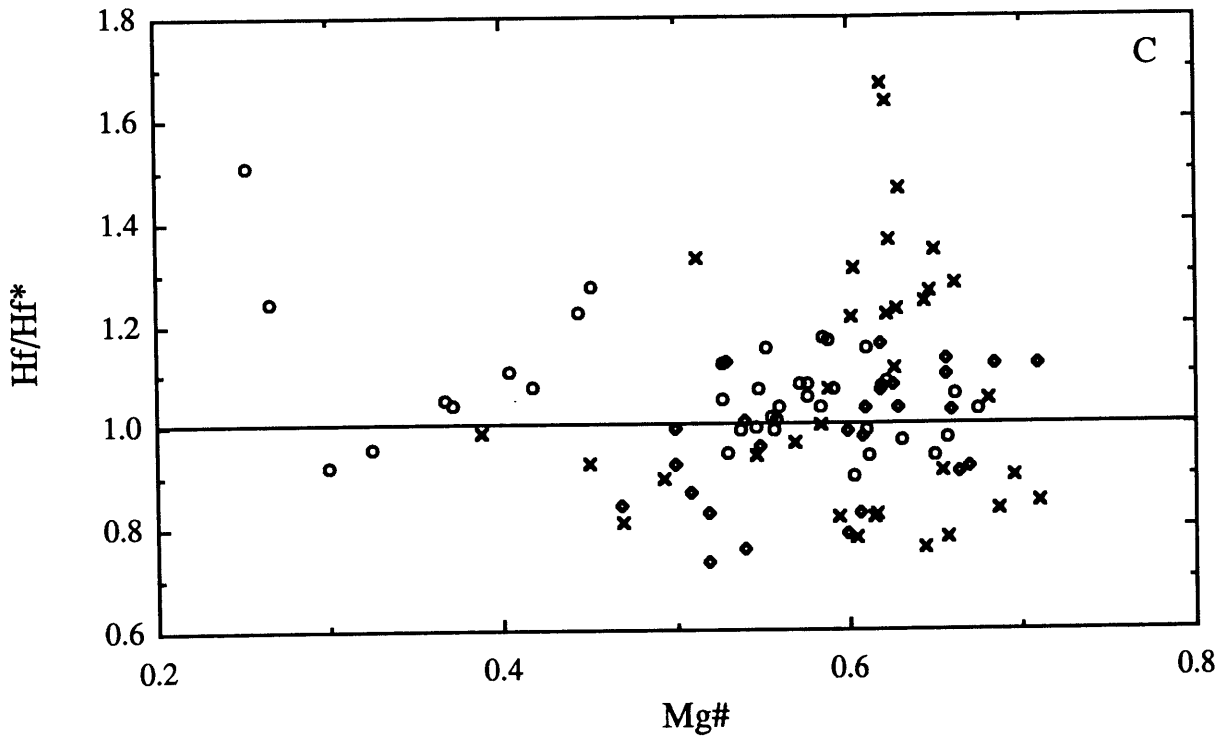
C
1.8
1.6
1.4
1.2
1.0
0.8
0.6
Hf/Hf*
0.2
0.4
0.6
0.8
Mg#

as a consequence the Lu-Hf isotope system has received only very limited attention in mantle studies. The good correlation between the Nd and Hf isotope systematics is believed to reflect similar behavior of parent/daughter ratios during mantle differentiation processes. We can use this similarity in behavior and any deviation thereof to constrain the MORB melting process.

During anhydrous melting of spinel peridotite the partition coefficients increase in the order Nd, Hf, Sm, Lu; this element order is used in constructing spidergrams (Thompson et al., 1983; Wood, 1979). The knowledge of the solid-melt distribution coefficients allows coupling of the isotopes, i.e parent/daughter ratios in the source to their parent/daughter ratios in the melt. This paper is the first to couple Nd and Hf systematics and to quantatively model the difference between source and melt parent/daughter ratios for both systems. MORBs form a fairly smooth pattern on spidergrams, indicating possible derivation from an anhydrous spinel lherzolite. However, MORBs do show a slight but systematic 'hump' for Hf and Zr, and a slight 'valley' for Ti, see Fig. 3.2. This slight deviation from a smooth pattern on a spidergram will be discussed later. Fig. 3.22 shows the variation of Lu/Hf and Sm/Nd with Mg#. From Fig. 3.22 it can be concluded that Sm/Nd and Lu/Hf in MORB are not sensitive to shallow level crystal fractionation effects, so these ratios reflect the original ratios in the source as modified by the melting process. The $^{176}Hf/^{177}Hf$ and $^{143}Nd/^{144}Nd$ ratios yield information on the long-term Lu/Hf and Sm/Nd ratios in the source. As with the Th-isotope systematics, the Hf and Nd systematics give information in a direct way about long term and present day parent-daughter ratios. The difference between the long term and present day parent daughter ratios has to be explained, and this is the focus of this paper.

Fig. 3.23 and 3.24 show the Lu/Hf and Sm/Nd ratios in MORB and hypothetical isochrons for a MORB mantle source. All MORB fall to the left of the 1-3 Ga mantle isochrons, i.e. the Lu/Hf and Sm/Nd ratios in MORB are too low for the observed $^{176}Hf/^{177}Hf$ and $^{143}Nd/^{144}Nd$. This indicates that the MORB melting/eruption process has produced significant fractionation (decrease of the Lu/Hf and Sm/Nd ratios).

Figure 3.23 and 3.24

$^{176}Lu/^{177}Hf$ and $^{147}Sm/^{144}Nd$ versus $^{176}Hf/^{177}Hf$ and $^{143}Nd/^{144}Nd$ for oceanic volcanics. Squares are MORBs, and circles are OIBs. Solid symbols are for those samples where both the Lu-Hf and Sm-Nd systematics are known. The 1 Ga, 2 Ga and 3 Ga lines are isochrons through BE. The geochron is a near vertical line through BE (not shown). Sample falling to the left of the isochrons must have undergone a recent decrease in parent/daughter ratio. $\delta_{(Lu/Hf)}$ and $\delta_{(Sm/Nd)}$ are the difference in percent between parent/daughter measured in the basalt and the calculated parent/daughter ratio if this sample would fall on the 2by isochron. Data from Dupuy et al. (1987), Gerlach et al. (1988), Nakamura and Tatsumoto (1988), Patchett (1983), Patchett and Tatsumoto (1980a), Taras and Hart (1987), White (1979), White and Hofman (1982), Wright and White (1987), Zindler et al. (1979), Zindler et al. (1984) and White unpublished data, and MIT unpublished data.

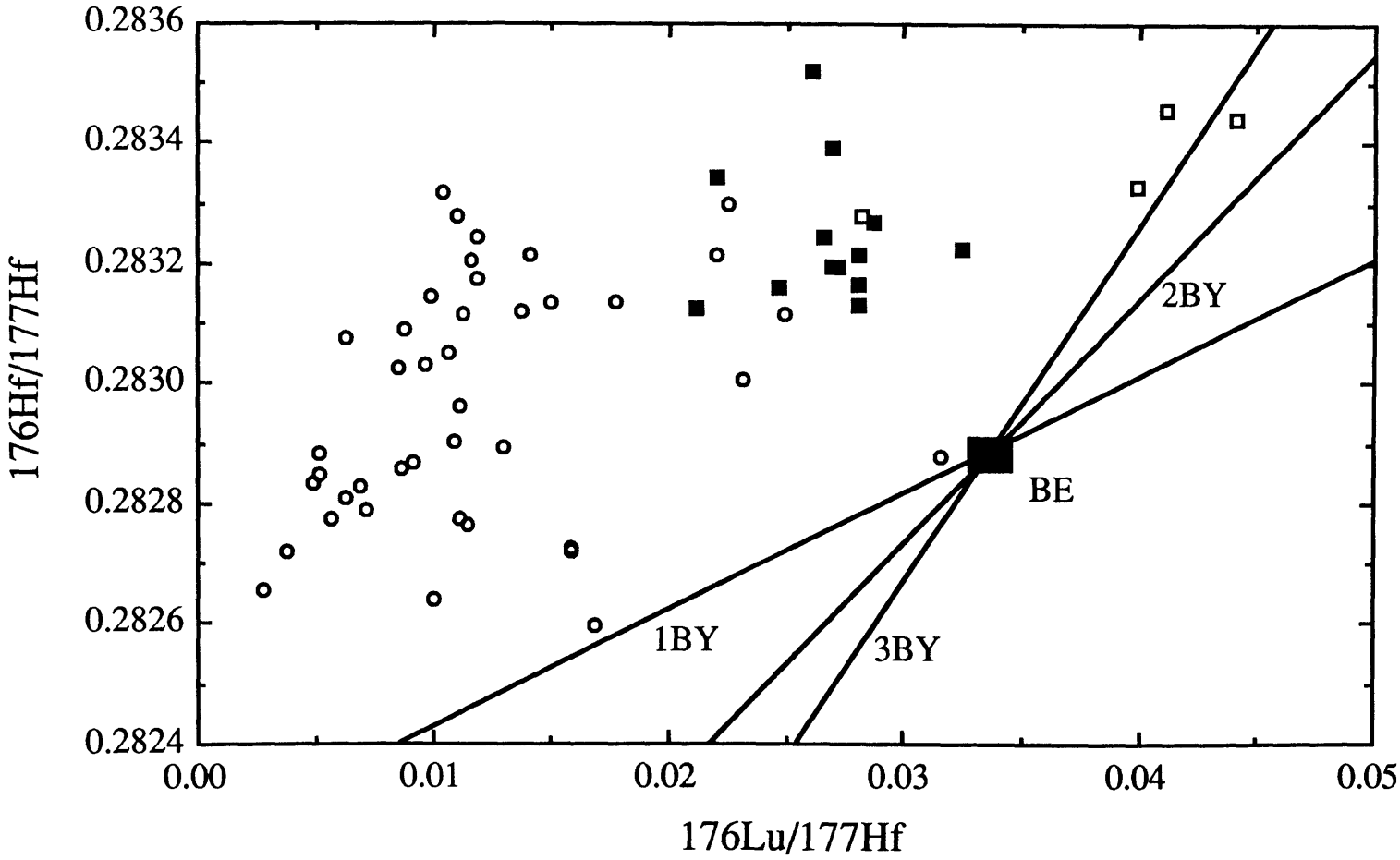
0.2836
0.2834
0.2832
0.2830
0.2828
0.2826
0.2824
176Hf/177Hf
0.00
0.01
0.02
0.03
0.04
0.05
176Lu/177Hf
BE
1BY
2BY
3BY

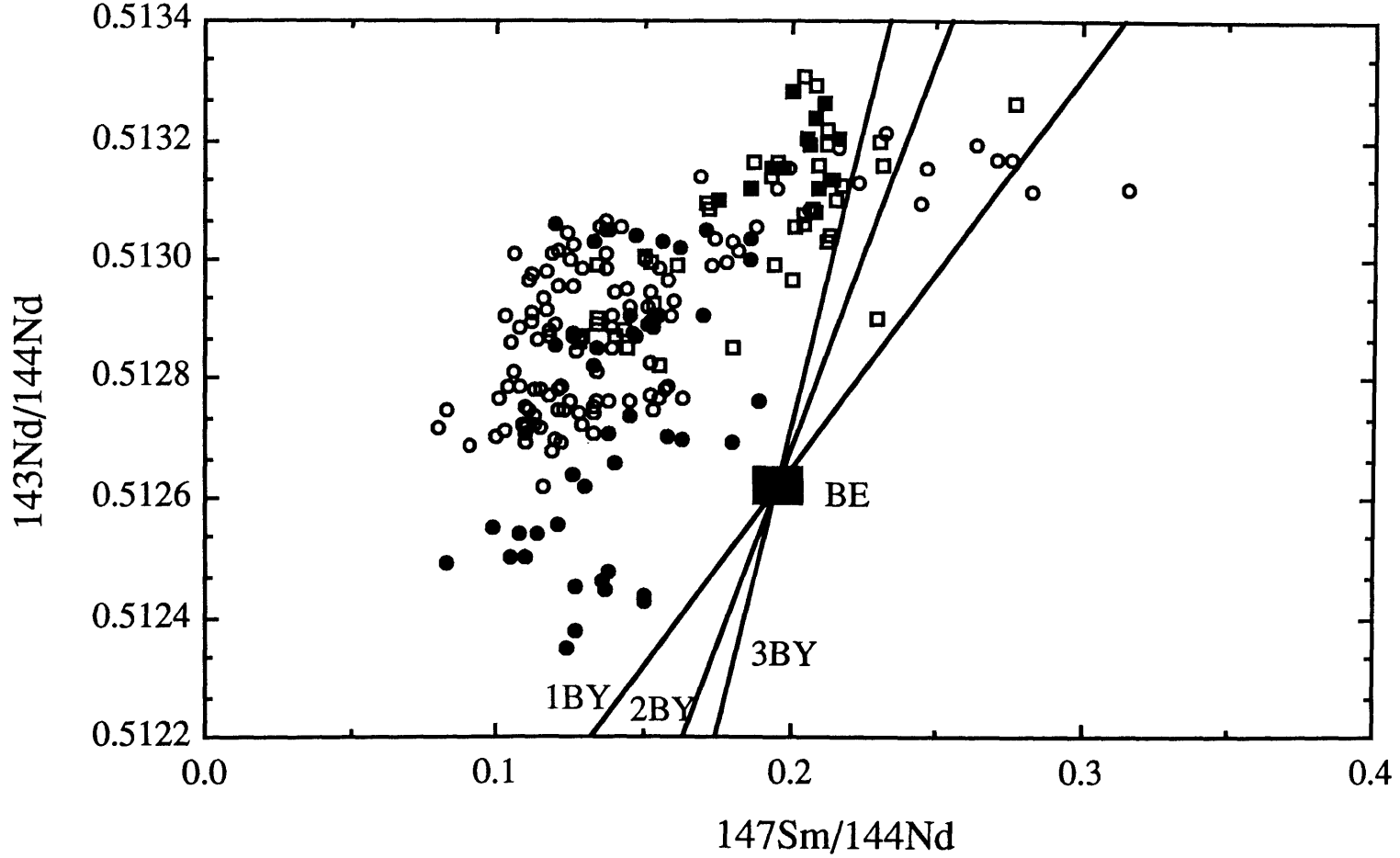
0.5134
0.5132
0.5130
0.5128
0.5126
0.5124
0.5122
143Nd/144Nd
0.0
0.1
0.2
0.3
0.4
147Sm/144Nd
BE
1BY
2BY
3BY

This observation is the Hf-paradox, in that the Lu/Hf in MORB is lower than Bulk Earth, while $^{176}Hf/^{177}Hf$ indicates a long term Lu/Hf higher then BE (Salters and Hart, 1989).

To quantify these parent-daughter fractionations, we will choose a 2 Ga model age for the MORB source (Allegre et al., 1983; Zindler and Hart, 1986); a choice of 1.0 or 3.0 Ga would not alter the arguments below. The difference between the mantle isochron value and the measured MORB value can be expressed as $\delta_{(Sm/Nd)} = ((Sm/Nd)_{2Ga}-(Sm/Nd)_m)/(Sm/Nd)_{2Ga}$; where $(Sm/Nd)_{2Ga}$ is the calculated Sm/Nd based on the measured present day $^{143}Nd/^{144}Nd$ of a basalt and $(Sm/Nd)_m$ is the measured Sm/Nd in this basalt. $\delta_{(Lu/Hf)}$ is defined in the same way, and $\delta_{(Lu/Hf)}$ and $\delta_{(Sm/Nd)}$ for MORB and OIB are plotted in Fig 3.25. A δ value of zero means that the sample falls on a 2 Ga isochron through BE. The observation that $\delta_{(Lu/Hf)}$ is by far larger than zero, and $\delta_{(Lu/Hf)} > \delta_{(Sm/Nd)}$, is part of the Hf-paradox. A recent process has to account for the δ values. Using a younger age to calculate the δ-values will result in higher δ values for MORBs while decreasing the δ values for some OIB. Using a 3 Ga reference isochron will lower the δ-values, but a 3 Ga average age for the mantle is inconsistent with Pb-isotope data (Tatsumoto, 1978) and recent "chemical geodynamics models (Zindler and Hart, 1986, Allegre et al., 1983).

The high $\delta_{(Sm/Nd)}$ in OIB was recognized early on (DePaolo and Wasserburg, 1976), and this phenomenon was shown to be more pronounced in the Lu-Hf system, extending to MORB as well as OIB (Patchett and Tatsumoto, 1980a). The high $\delta_{(Sm/Nd)}$ in OIB is thought to be caused by either recent metasomatism or by extremely small degrees of melting of a garnet lherzolite (Basaltic Volcanism Study Project, 1981). For MORB, metasomatism is a viable though ad hoc explanation for the low Sm/Nd and Lu/Hf in the basalts; we will explore the more likely case that melting has decreased Lu/Hf and Sm/Nd in MORB, and has led to the observed $\delta_{(Lu/Hf)}$ and $\delta_{(Sm/Nd)}$.

MORBs are generally perceived to form by decompression melting of a spinel lherzolite, followed by fractionation in a magma chamber prior to eruption.

Figure 3.25

$\delta_{(Lu/Hf)}$ versus $\delta_{(Sm/Nd)}$ for OIB and MORB. $\delta_{(Lu/Hf)}$ and $\delta_{(Sm/Nd)}$ are the deviations in Lu/Hf and Sm/Nd from the 2 Ga isochron in Fig. 3.23 and 3.24. Symbols for basalts, and data sources as in Fig.3.23 and3.24. Non-modal sequential batch equilibrium melting model, curves are for different degrees of melting and for varying amounts of melting in the garnet stability field. Numbers on the right of the diagram, decreasing in the y-direction are the different degrees of melting at the ridge axis, i.e the maximum degree of melting ((a+b) in Fig. 3.26). Numbers across at the bottom of the diagram are percents of melt of the total amount of melt on-axis melting that is generated in the garnet stability field. Numbers in the field, i.e. 19, 36, 49, 64, 84 and 96, are the percentages of the total amount of melt collected that was generated in the garnet stability field.

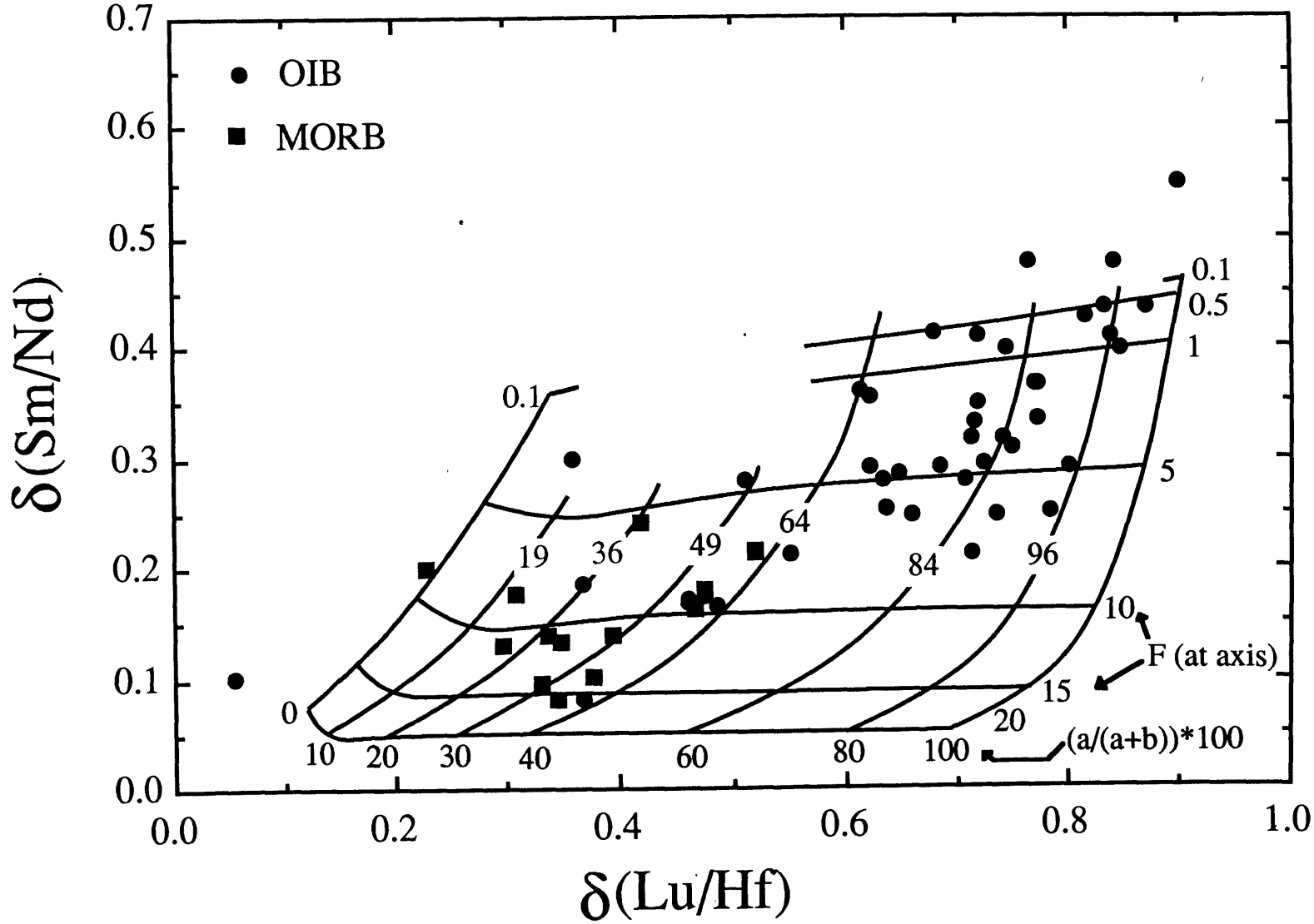
OIB
MORB
δ(Sm/Nd)
δ(Lu/Hf)
0.0
0.1
0.2
0.3
0.4
0.5
0.6
0.7
0.8
1.0
0.1
0.5
1
5
10
15
20
0
19
36
49
64
84
96
10
20
30
40
60
80
100
F (at axis)
(a/(a+b))*100

This scenario implies that the mantle residual to MORB genesis consists of olivine, orthopyroxene and probably some Cr-diopside (Dick et al., 1984). Estimates for the degree of melting of MORB range from 1- 25% (Bender et al., 1984; Dick et al., 1984; Klein and Langmuir, 1987). In general the bulk of MORBs are believed to be generated at pressures of at least 8-10 kbars, since MORB is not in equilibrium with orthopyroxene below this pressure (Elthon, 1988; Falloon and Green, 1987; Stolper, 1980).

3.5.2 Modelling and discussion.

The melting equation for equilibrium non modal partial melting (Allegre and Minster, 1978) is used to calculate the trace element ratios in the melt. The proportions in which the phases enter the melt are taken such that the major element composition of the melt is basaltic. The first conclusion is that simple one stage melting models with anhydrous spinel lherzolite as a source material cannot create the observed $\delta_{(Lu/Hf)}$ in MORB, unless extremely small amounts of melt are extracted (<0.1%). In the spinel stability field clinopyroxene is the phase that dominates Lu/Hf and Sm/Nd fractionation of a four phase lherzolite. The combined $\delta_{(Sm/Nd)}$ and $\delta_{(Lu/Hf)}$ systematics cannot be satisfied with any degree of melting in the spinel stability field using either a batch equilibrium melting or any of the more complicated melting models (Langmuir et al., 1977; Maaloe, 1982; McKenzie and Bickle, 1988; Navon and Stolper, 1987; O'Hara, 1985; Prinzhofer and Allegre, 1985). The Sm-Nd and Lu-Hf systematics cannot be simultaneously satisfied even by using an extreme set of partition coefficients for clinopyroxene. Increasing D_{Lu} to 1.00 (D_{Lu}/D_{Hf}=3.06, well outside experimental values, although a D_{Lu}= 1.00 is still viable), will not satisfy both the Sm-Nd and Lu-Hf isotope systematics.

What is needed is a phase with D_{Lu}/D_{Hf} larger than clinopyroxene, while changing the bulk K_ds of Sm and Nd to a lesser extent. Garnet fits this bill, since the bulk K_d ratios in the initial solid change from 1.42 to 1.90 for Sm/Nd and from 1.28 to

9.79 for Lu/Hf. D_{Sm}/D_{Nd} equals 1.42 for clinopyroxene and 5.12 for garnet, while D_{Lu}/D_{Hf} equals 1.22 and 2.39 for clinopyroxene and garnet respectively. For garnet-melt distribution coefficients we used published data (Fujimaki et al., 1984) combined with our unpublished data on garnet/diopside partitioning in garnet lherzolites xenoliths, from 19-27 kbar, from Pali-Aike, Chile (Stern et al., 1989). A more comprehensive discussion of the garnet distribution coefficients is given in Chapter 2. Garnet plays an important role in OIB genesis, furthermore garnet has been proposed as a residual phase in MORB genesis (Bender et al., 1984; Johnson et al., 1989; O'Hara, 1968), and as an important phase controlling the trace element contents in both alpine peridotites (Loubet et al., 1975), and abyssal peridotites (Johnson et al., 1989).

In our melting model, that satisfies the Sm/Nd and Lu/Hf systematics, melting starts in the garnet stability field. Attempting to make the model as realistic as possible, the following observations were taken into account. Recent calculations on melt extraction indicates that small degrees of melt (0.1-1%) are able to separate from the solid and ascend towards the surface (McKenzie and Bickle, 1988). We modelled this sequentially such that when the peridotite reaches this critical degree of melting(0.1-1%), the melt escapes and is accumulated at the top. The next batch is generated at shallower depth, with slightly different mineralogy (and mineral chemistry) and from a source already depleted by prior melt extraction. While this process is perhaps continuous, we treat it as a sequential batch process for numerical simplicity. Extracting melt only above a certain threshold, as in the critical melting model of Maaloe (1982), would not substantially change the results.

The importance of the shape of the melting regime has been eloquently argued (O'Hara, 1985); as the mantle material rises towards the surface, the material right at the ridge axis will end up higher than its neighboring material somewhat off-axis (Phipps Morgan, 1987). As a consequence, the on-axis peridotite will melt to a larger degree than the off-axis peridotite, which will stop

Figure 3.26

A: Representation of the melting model. The vertical axis is the degree of melting in a column of mantle, i.e. the total amount of melt generated in a unit volume of peridotite. a/(a+b) is the fraction of melt in a melt column generated in the garnet field; this number appears as the bottom row of numbers below the melting curves in Fig. 3.25. (Initial garnet/diopside ratio in the peridotite =1). The area within the triangle and below the spinel-garnet transition as a percent of the total area of the triangle, is the fraction of melt generated in the garnet stability field. These numbers appear horizontally within the model field in Fig. 3.25. The breakdown of 1% garnet produces 0.5% diopside. Our preferred set of Ds for olivine, orthopyroxene and clinopyroxene are originated from those listed by Irving and Frey (1984), and Frey et al. (1978) Fujimaki et al. (1984) and Grutzeck et al. (1974). For diopside the distribution coefficients for Sm, Nd, Lu, Hf are 0.37, 0.26, 0.45, and 0.37 respectively. For garnet the Ds for Sm, Nd, Lu, Hf are 0.13, 0.03, 5.5, and 0.23 respectively. Although the absolute Ds of the elements might not be known accurately we think that the D-ratios are better constrained for the REE and Hf. Therefore our modelling only involves of trace element ratios without emphasis on the trace element abundances. In the garnet stabilty field the weight fraction of phases in the melt are 0.45, 0.45 and 0.1, garnet, diopside and olivine+orthopyroxene respectively. In the spinel stability, field the mode in the melt for clinopyroxene and olivine+orthopyroxene are 0.7 and 0.3 respectively.

B: The possible more realistic physical situation under a mid-ocean ridge. The isotherms are not completely horizontal under a segment of the ocean crust that includes a ridge (Phipps Morgan , 1987; Scott and Stevenson, 1989). Consequently the garnet spinel transition is not a horizontal line. Modelling of the garnet-spinel transition as a hortizontal line is a first order approximation of the melting regime. The diagram is drawn as a cartoon and no actual scale is implied.

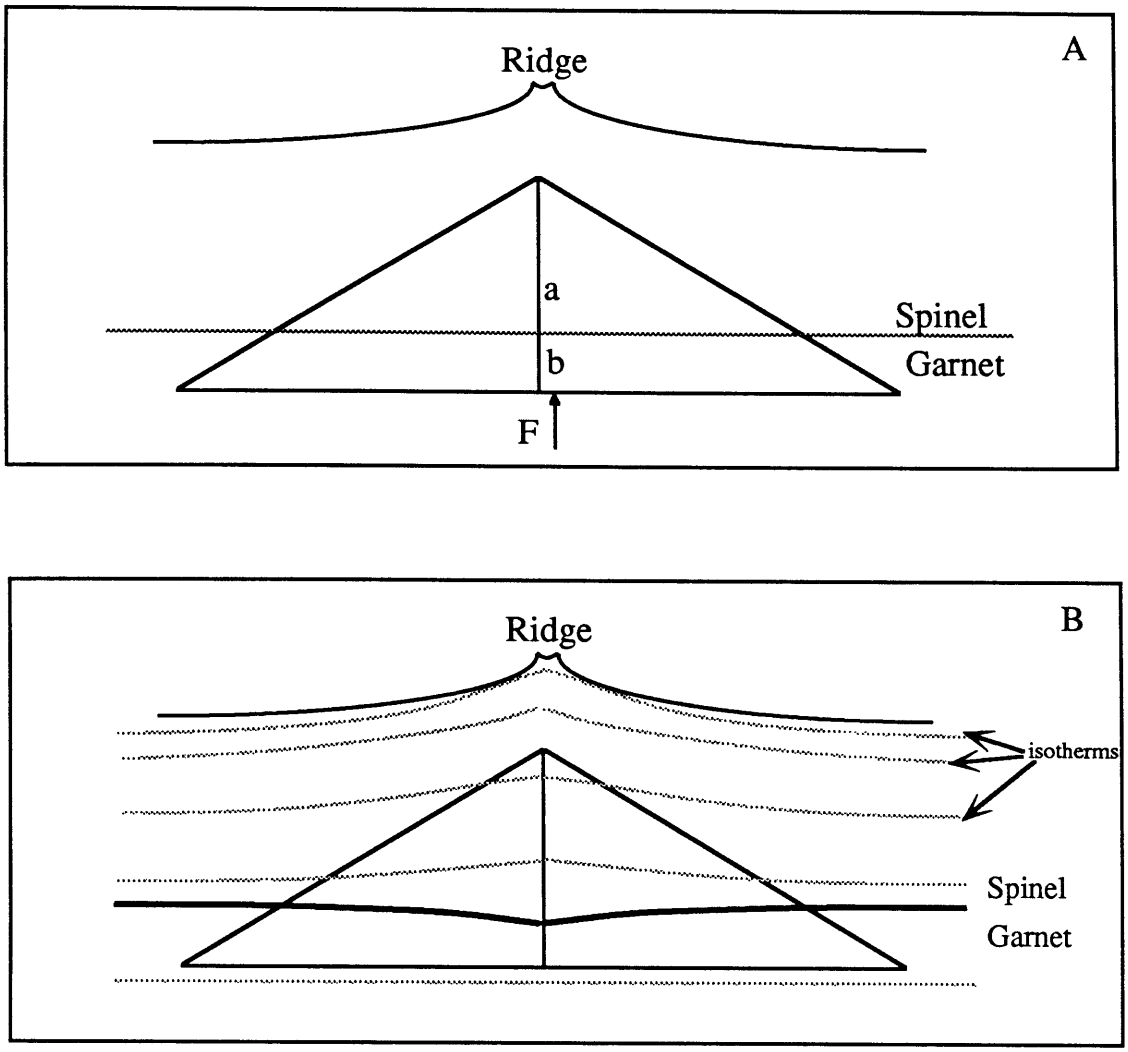

Figure 3.26

rising and 'turn the corner' at greater depth. Furthermore, the isotherm at the bottom of the plate is undisturbed and a ridge is not dynamically compensated (McKenzie and Bickle, 1988; Richter and McKenzie, 1981). Consequently, material right under the ridge and material slightly off-axis will start melting at the same depth. In our model, the melt generated off-axis is funnelled and collected at the center. The decrease in degree of melting away from the ridge is assumed to be linear (Phipps Morgan, 1987; Scott and Stevenson, 1989), (Fig 3.26).

Amphibole is another phase that can change the K_ds appropriately (15-20% of modal amphibole would be needed to change the K_ds for the trace elements enough). However, MORBs are undersaturated in H_2O, and thus amphibole cannot be a residual phase during the majority of the melting in MORB genesis

The modelling to obtain the trace element ratios in the melt is forward and presented as a cartoon in Fig 3.26A. The details of the model are as follows: first for a box of mantle directly beneath the ridge, this box of mantle melts as it rises towards the surface. The initial mineralogy of the box is 80% combined olivine, plus orthopyroxene and spinel, 10% of clinopyroxene and 10% of garnet. The minerals are grouped this way since the modelling involves the REE and Hf only, and garnet and clinopyroxene are the only two phases controlling the distribution of these elements The 80% of other phases is just a dilution factor. 0.5% of melt is formed, and all the melt is allowed to escape, and collected at the top. The collected melt fractions are mixed. Melt components are 45% garnet, 45% clinopyroxene and 10% of other phases. The melt does not change its trace element composition during ascent to the surface. After extraction of the melt, the mineral modes and concentrations for the next batch of melt are recalculated. At an arbitrary point in the ascent, i.e. after a set percentage of melt is generated, garnet breaks down and produces equal amounts of clinopyroxene and other components. New modes are calculated and the composition for the next batch is calculated. All melt batches are collected at the top and the melt is averaged. Each individual batch of melt is given a weight factor dependent on

where it is generated. The next column slightly of axis is calculated the same way, with 1% of melt taken away from the previous column. The last column is calculated is for 1% of melting. Since melting starts at the same depth, for the case that the on-axis column generates 5% melt in the garnet field, than the off-axis column that generates only 5% of melt, melts only in the garnet stability field.

Fig. 3.25 illustrates the effect of garnet on the Sm/Nd and Lu/Hf ratios using the above equilibrium sequential batch melting model. Garnet is residual in the deeper part of the melting column. The middle of the MORB field in Fig. 3.25 can be reached with 10-15% total melting on-axis with only 1/5 of the melting occurring in the garnet stability field. The low $\delta_{(Sm/Nd)}$, high $\delta_{(Lu/Hf)}$ MORBs can be generated by 15% of melting on-axis with 1/3 of the melt generated in the garnet field. Simpler melting models with residual garnet are also able to generate the observed variations, but smaller degrees of melting are required. Whatever melting model is chosen, garnet is always needed to some extent. Fig. 3.25 also illustrates the conventional wisdom that many OIBs can only be generated by small degrees of melting, mostly in the garnet stability field.

The dynamic melting model proposed by Langmuir et al. (1977), or the model proposed by Johnson et al. (1989) is also capable of explaining the $\delta_{(Sm/Nd)}$ and $\delta_{(Lu/Hf)}$, however smaller degrees of melting are necessary. The models proposed by McKenzie and Bickle (1988), or Prinzhofer and Allegre (1985) are not able to generate the observed $\delta_{(Sm/Nd)}$ and $\delta_{(Lu/Hf)}$.

The model in Fig. 3.26 uses individual melt batches of 0.5%, and a garnet/diopside ratio of 1. If 0.1% of melt is allowed to escape, then slightly less total melt is needed, 14-3%, to obtain the full range of $\delta_{(Lu/Hf)}$ and $\delta_{(Sm/Nd)}$ in MORB. A maximum amount of total melt (between 7-20%) can be obtained by extracting individual batches of 1%. The lower degrees of total melting needed with small (0.1%) individual batches is a consequence of the efficiency of this process, i.e. larger degrees of total melting lead to over-fractionation.

Based upon literature data (Boyd, 1987; Cox et al., 1987; Ehrenberg, 1982) and the Pali Aike xenoliths, it can be seen that a garnet/diopside ratio of 1 is a very reasonable first approximation. Decrease of this ratio will tend to increase the amount of melting needed in the garnet field (require melt to start deeper) and decrease the total amount of melting, which is apparently contradictory.

The correlation between $\delta_{(Lu/Hf)}$ and other indicators of degree of melting, like $Na_{8.0}$ (Klein and Langmuir, 1987), confirms the notion that $\delta_{(Lu/Hf)}$ can be used as an indicator for the degree of melting. Furthermore, our estimates of the degree of melting, 5-17% agrees with the estimates of Klein and Langmuir (1987).

The onset of melting in the garnet stability field places the geotherm under the ridge on the solidus at 1450°C ±50°C and 80-90km (Basaltic Volcanism Study Project, 1981; Scarfe and Takahashi, 1986; Takahashi and Kushiro, 1983). This estimate is within error of the Parsons and Sclater, (1977) estimate of 1350°C ±275°C at 125km for the base of the lithosphere, though suggesting that their estimate is somewhat on the low side. Attempts to calculate whether the total amount of melt produced is realistic fails because of the lack of knowledge of the behavior of the solidus as a function of melt depletion of the peridotite. Experiments on peridotites (Green et al., 1979; Scarfe and Brearley, 1987) indicate an increase in the solidus by ≈50°C for 20% batch melting of a fertile peridotite; this is a minimum estimate for a sequentially melted source. In our model, the peridotite is sequentially depleted, and only a small degree of the melt might stay behind. In order to assess the validity of our model, the solidus of a depleted peridotite needs to be known. Assuming the increase in the solidus is 75°C, and using heat of fusion data from (Ghiorso, 1985), then the magma reaches 1300-1320°C at 20km depth with 15% of adiabatic batch melting. High Mg# MORBs have maximum liquidus temperatures at 1atm of ≈1250°C. There is disagreement as to whether the high MgO (10-11 wt% MgO) MORBs as observed at the ocean floor are indeed 'primary' magmas. If these high MgO MORBs are primary, then this fixes the melt

liquidus at ≈1250°C. However, if the primary MORB magmas contain approximately 15 wt% MgO, then the liquidus temperature will be 1300-1350°C at 1atm (Basaltic Volcanism Study Project, 1981; Green et al., 1979). Given the uncertainties involved, our model is not in contradiction with the available petrological information. Assuming an onset of melting at 90km and ≈1450°C, adiabatic melting over the whole interval, ≈150cal/gr for heat of fusion, and ≈ 0.3°C/Km for the adiabat then MORB represent 30-40% of melting. Clearly this is not the case, and melting must stop earlier. Experimental evidence on MORBs indicates that MORBs are in equilibrium with a four phase spinel lherzolites at minimum pressures of 8-10kbars, ≈30km (Elthon, 1988; Falloon and Green, 1987). However, MORBs are mixtures of melts generated at different depth, and it is unclear if the shallowest melt that contributed to MORB had to be derived from depths in excess of 30 km. Thus, the amount of melt produced between 90 and 30 km is not known, since this is also dependent on the solidus of the peridotite as a function of the degree of depletion (remember, all or almost all the melt is sequentially extracted, thereby rapidly depleting the peridotite). At 1350°C and 10kbar orthopyroxene will dissolve up to 5% normative clinopyroxene (Lindsley, 1983). Thus a depleted peridotite can still contain Ca even though clinopyroxene is not present. I thus propose that melting stops because the clinopyroxene is exhausted and it becomes in effect 3 phase melting instead of 4 phase melting. Furthermore, to limit the amount of melting, the effect of the change from 4 to 3 phases has to significantly steepen the solidus. Melting experiments on depleted peridotites will be needed to confirm these assertions.

Assuming an onset of melting at 90km depth, then the relatively large degree of melting in the garnet stability field can be explained by the effect of increased amounts of melt generated at a cusp of the solidus (Presnall and Hoover, 1987) at the garnet spinel transition.

The $\delta_{(Lu/Hf)}$ and $\delta_{(Sm/Nd)}$ calculated above assumed 2 Ga as the depletion age for the MORB mantle. However, an average age of 600my for the MORB reservoir has been suggested, based on U-Th-

Pb trace element and isotope systematics (Galer and O'Nions, 1985). Decreasing the age of the MORB reservoir to 600 my will increase the $\delta_{(Lu/Hf)}$ and $\delta_{(Sm/Nd)}$; this will require an increase in the amount of melting in the garnet field. On the other hand, the U-Th-Pb arguments are partly based on the partitioning behavior of these trace elements, and this is unknown in the presence of garnet. Partition studies for U-Th and Pb between garnet and melt are necessary in order to evaluate the Th-isotope constraints on MORB mantle.

In summary, the Hf-Nd isotope and trace element characteristics of MORBs provide strong constraints on the depth of origin of MORB and unquestionably require garnet as a residual phase during the early stages of melting.

In general, however, MORB petrogenesis has a number of unexplained features: Fig. 3.2 shows that MORB has a slight, but consistent enrichment in Hf, and Zr over the REE; MORB also has consistent depletion in Ti over the REE. Chapter 2, Fig. 2.2, gives the distribution coefficients for the REE and Ti and Zr for garnet. Assuming a smooth source pattern, it can be seen from the Ds that melting in the presence of garnet will produce a melt depleted in Zr and Hf and enriched in Ti compared to the REE, i.e. Zr and Hf are kept in the source. This pattern is opposite as what is observed in MORB.

To complicate matters abyssal peridotites show depletions in both Ti and Zr, with REE characteristics that requires melting in the garnet stability field (Johnson et al., 1989). If MORB is in equilibrium with the clinopyroxenes in the abyssal peridotites then MORB should be depleted in Zr and Hf and enriched in Ti. If the clinopyroxenes in abyssal peridotites are the products of the breakdown of garnet, and if MORB (with a smooth pattern) was extracted in the garnet stability field then the clinopyroxenes should have Zr enrichments and Ti depletions. In a general sense Fig. 3.1 shows that Nd is clearly more incompatible than Hf or Zr, and that Sm, Zr and Hf have similar incompatibilty. With garnet, and clinopyroxene as the only phases available to generate the trace element characteristics in MORB the source of MORB has to have Zr and Hf enrichment and Ti depletion. This enrichment in Hf and Zr plus depletion in Ti indicates a previous

depletion in the presence of garnet, and a non-smooth trace element pattern for the MORB source. Thus, it is indicated that the crust extraction which led to the formation, approximately 2 Ga ago of the depleted MORB mantle, took place in the garnet stability field.

The next problem is the decoupling between Hf and Nd isotopes in MORB. If the Hf-isotopes are just the reflection of different degrees of depletion (2 Ga ago) in the garnet stability field then $^{176}Hf/^{177}Hf$ in MORB should still correlate with $^{143}Nd/^{144}Nd$. The lack of correlation between the two isotopic systematics indicate there exists a process that fractionate Lu/Hf different from Sm/Nd. Evidence for a process that decreases Lu/Hf while increasing Sm/Nd is also indicated by the HFSE depletions in peridotites. If this depletion is old and does contribute in a small amount to the MORB source then an isotopic signatures can observed without a clear trace element signature. Assuming a MORB source which is LREE depleted and has Hf/Hf*>1 and Ti/Ti*<1, and using the proposed sequential melting model (Fig 3.26) the calculated melts are similar to observed trace element patterns of MORB. This assumes that the contribution of the HFSE depleted mantle to MORB is small and swamped by the large degree (5-10%) of melting of MORB mantle. The reason why HFSE depleted peridotite is abundantly available on the ocean floor while hardly present in the magma then needs to be addressed.

As a last point to ponder; it seems that the MORB field on a Hf-Nd isotope correlation diagram plots largely below the OIB regression line. Assuming the OIB regression line indicates the Hf-Nd evolution line with a smooth source spidergram and realizing that MORB probably have a high Lu/Hf component, then MORB should plot mostly above the OIB regression line instead of below this line. An explanation could be that the HFSE depletion is originated from material that has a long term HFSE enrichment, the complement of the peridotites. This material will have a long term low Lu/Hf and thus have low $^{176}Hf/^{177}Hf$. Determining Hf isotopes in depleted peridotites can answer some of these questions, and I will hopefully report on this in the future. At the moment, however, the trace element characteristics of MORB and abyssal peridotites are not yet fully explained and reconciled.

3.6 Conclusions

1) The Kergùelen Heard Plateau basalts have a strong EMI signature
2) The space and time relationships of the basalts from the Kerguelen Heard Plateau and Kerguelen Island indicate the EMI and DMM component in the mantle are spatially closely related.
3) "Uncontaminated" island arc volcanics have slightly higher $^{176}Hf/^{177}Hf$ than OIB for given $^{143}Nd/^{144}Nd$ indicating the possible existence of HFSE depleted material for some time.
4) It seems more likely that IAV are generated from mantle that has undergone melt depletion to generate MORB and re-enrichment to flux this mantle and allow generation of IAV.
5) The onset of melting to generate MORB is in the garnet stability field.
6) The melt depletion event that created the MORB reservoir has trace element characteristics indicating that this event took place in the garnet stability field.
7) For OIB, the Hf-Nd isotope composition are strongly correlated.
8) Hf and Nd isotopes in MORB are not correlated.

3.7 References

Allegre, C.J., Hart, S.R. and Minster, J.F. (1983). Chemical structure and evolution of the mantle and the continents determined by inversion of Nd and Sr isotopic data, II. Numerical experiments and discussion. Earth Plan. Sci. Lett. **66**: 191-213.

Allegre, C.J. and Minster, J.-. (1978). Quantative models of trace element behavior in magmatic processes. Earth Plan. Sci. Lett. **38**: 1-25.

Anders, E. and Grevesse, N. (1989). Abundances of the elements: Meteoritic and solar. Geochim. Cosmochim. Acta. **53**: 197-214.

Basaltic Volcanism Study Project. (1981). Basaltic Volcanism on the terrestrial planets. New York, Pergamon Press.

Beer, H., Walter, G., Macklin, R.L. and Patchett, P.J. (1984). Neutro capture cross sections and solar abundances of ^{160,161}Dy, ^{170,171}Yb, ^{175,176}Lu and ^{176,177}Hf for the *s*-process analysis of the radionuclide ^{176}Lu. Phys. Rev. **C30**: 464-478.

Bender, J.F., Langmuir, C.H. and Hanson, G.N. (1984). Petrogenesis of basalt glasses from the Tamayo region, East Pacific Rise. J. Petrol. **25**: 213-254.

Boyd, F.R. (1987). High- and low temperature garnet peridotite xenoliths and their possible relation to the lithosphere-asthenosphere boundary beneath souther Africa. Mantle Xenoliths. New York, John Wiley & Sons.

Carmichael, I.S.E. (1967). The mineralogy and petrology of the volcanic rocks from the Leucite Hills, Wyoming. Contrib. Mineral. Petrol. **15**: 24-66.

Cheng, Q., Park, K., Macdougall, J.D., Lugmair, G.W., Staudigel, H., Hawkins, J. and Lonsdale, P. (1987). Isotopic evidence for a hotspot origin of the Loisville seamount chain. Seamounts, Islands, and Atolls. Washington, DC, American Geophysical Union.

Clague, D.A. and Frey, F.A. (1982). Petrology and trace element chemistry of the Honolulu volcanics, Oahu: Implication for the oceanic mantle below Hawaii. J. Petrol. **23**: 447-504.

Cox, K.G., Smith, M.R. and Beswetherick, S. (1987). Textural studies of garnet lherzolites: evidence from high-temperature harzburgites. Mantle Xenoliths. New York, John Wiley & Sons.

Davidson, J.P. (1983). Lesser Antilles isotopic evidence of the role of subducted sediment in island arc magma genesis. Nature. **306**: 253-256.

DePaolo, D.J. and Johnson, D.W. (1979). Magma genesis in the New Britain island-arc: Constraints from Nd and Sr isotopes and trace element patterns. Contrib. Mineral. Petrol. **70**: 367-379.

DePaolo, D.J. and Wasserburg, G.J. (1976). Inferences about magma sources and mantle structure from variations of $^{143}Nd/^{144}Nd$. Geophys. Res. Lett. **3**: 743-746.

Dick, H.J.B., Fisher, R.L. and Bryan, W.B. (1984). Mineralogical variability of the uppermost mantle along mid-ocean ridges. Earth Plan. Sci. Lett. **69**: 88-106.

Dosso, L., Vidal, P., Cantagrel, J.M., Lameyre, J., Marot, A. and Zimine, S. (1979). "Kerguelen: continental fragment or oceanic island?"; petrology and isotopic geochemistry evidence. Earth Plan. Sci. Lett. **43**: 46-60.

Dupuy, C., Dostal, J., Marcelot, G., Bougault, H., Joron, J.L. and Treuil, M. (1982). Geochemistry of basalts from central and southern New

Hebridesarc: Implication for their source rock composition. Earth Plan. Sci. Lett. **60**: 207-225.

Dupuy, C., Vidal, P., Barsczus, H.G. and Chauvel, C. (1987). Origin of basalts from the Marquesas Archipelago (south central Pacific Ocean); isotope and trace elemnt constraints. Earth Plan. Sci. Lett. **82**: 145-152.

Ehrenberg, S.N. (1982). Rare earth element geochemistry of garnet lherzolite and megacrystalline nodules from minette of the Colorado Plateau province. Earth Plan. Sci. Lett. **57**: 191-210.

Elthon, D. (1988). The petrogenesis of primary mid-ocean ridge basalts. Critical. Rev. Marine Sci. **in press**:

Falloon, T.J. and Green, D.H. (1987). Anhydrous partial melting of MORB pyrolite and other peridotite compositions at 10 kbar: Implications for the origin of primitive MORB glasses. Min. Petrol. **37**: 181-219.

Frey, F.A., Bryan, W.B. and Thompson, G. (1974). Atlantic Ocean floor: geochemistry and petrology of basalts from Legs 2 and 3 of the Deep-Sea Drilling Project. J. Geophys. Res. **79**: 5507-5527.

Frey, F.A., Dickey, J.S., Thompson, G., Bryan, W.B. and Davies, H.L. (1980). Evidence for heterogeneous primary MORB and mantle sources, NW Indian ocean. Contrib. Mineral. Petrol. **74**: 387-402.

Frey, F.A., Green, D.H. and Roy, S.D. (1978). Integrated models for basalt petrogenesis: a study of quartz tholeiites to olivine melilitites from south eastern Australia utilizing geochemical and experimental petrological data. J. Petrol. **19**: 463-513.

Fujimaki, H., Tatsumoto, M. and Aoki, K. (1984). Partition coefficients of Hf, Zr and REE between phenocrysts and groundmasses. J. Geophys.Res. **89**: 662-672.

Galer, S.J.G. and O'Nions, R.K. (1985). Residence time of thorium, uranium and lead in the mantle with implications for mantle convection. Nature. **316**: 778-782.

Gautier, I., Giret, A., Vidal, P., Di Donato, G. and Weis, D. (1989). Petrology and geochemistry of Kerguelen basalts (south Indian Ocean): evolution of an hotspot from a ridge to an intraplate position. preprint. :

Gerlach, D.C. (1986). Geochemistry and petrology of recent volcanics of the Puyehue-Cordon Caulle area, Chile (40.5^{o}). Massachusetts Institute of Technology, Cambridge, Massachusetts PhD.

Gerlach, D.C., Cliff, R.A., Davies, G.R., Norry, M. and Hodgson, N. (1988). Magma sources of the Cape Verdes archipelago: Isotopic and trace element constraints. Geochim. Cosmochim. Acta. **52**: 2979-2992.

Ghiorso, M.S. (1985). Chemical mass transfer in magamtic processes I. Thermodynamic relations and numerical algorithms. Contrib. Mineral. Petrol. **90**: 107-120.

Gill, J.B. (1981). Orogenic andesites and plate tectonics. Berlin, Springer Verlag.

Gill, J.B. (1984). Sr-Pb-Nd isotopic evidence that both MORB and OIB sources contribute to oceanic island arc magmas in Fiji. Earth Plan. Sci. Lett. **68**: 443-458.

Gill, J.B. (1987). Early geochemical evolution of an oceanic island arc and backarc: Fiji and the south Fiji basin. J. Geol. **95**: 589-615.

Gill, J.B., Stork, A.L. and Whelan, P.M. (1984). Volcanism accompanying back-arc basin development in the southwest Pacific. Tectonophysics. **102**: 207-224.

Gill, J. and Whelan, P. (1989a). Early rifting of an oceanic island arc (Fiji) produced shoshonitic to tholeiitic basalts. J. Geophys. Res. **94**: 4561-4578.

Gill, J. and Whelan, P. (1989b). Postsubduction ocean island alkali basalts in Fiji. J. Geophys. Res. **94**: 4579-4588.

Green, D.H., Hibberson, W.O. and Jaques, A.L. (1979). Petrogenesis of mid-ocean ridge basalts. The earth: Its origin structure and evolution. London, Academic Press.

Grutzeck, M., Kridelbaugh, S. and Weill, D. (1974). The distribution of Sr and REE between diopside and silicate liquid. Geophys. Res. Lett. **1**: 273-275.

Hart, S.R. (1988). Heterogeneous mantle domains: signatures, genesis and mixing chronologies. Earth Plan. Sci. Lett. **90**: 273-296.

Hart, S.R., Gerlach, D.C. and White, W.M. (1986). A possible new Sr-Nd-Pb mantle array and consequences for mantle mixing. Geochim. Cosmochim. Acta. **50**: 1551-1557.

Henderson, P. (1986). Inorganic geochemistry. Oxford, Pergamon Press.

Hickey, R.L., Frey, F.A. and Gerlach, D.C. (1986). Multiple sources for basaltic arc rocks from the southern volcanic zone of the Andes (34^{o}-41^{o}S): Trace element and isotopic evidence for contributions from subducted oceanic crust, mantle and continental crust. J. Geophys.Res. **91**: 5963-5983.

Hofmann, A.W. (1988). Chemical differentiation of the Earth: the relationship between mantle, continental crust, and oceanic crust. Earth Plan. Sci. Lett. **90**: 297-314.

Hofmann, A.W., Feigenson, M.D. and Raczek, I. (1987). Kohala revisited. Contrib. Mineral. Petrol. **95**: 114-122.

Irving, A.J. and Frey, F.A. (1984). Trace element abundances in megacrysts and their host basalts: Constaints on partition coefficients and megacryst genesis. Geochim. Cosmochim. Acta. **48**: 1201-1221.

Johnson, K.T.M., Dick, H.J.B. and Shimizu, N. (1989). Melting in the oceanic upper mantle: an ion microprobe study of diopsides in abyssal peridotites. submitted. :

Kay, R. (1977). Geochemical constraints on the origin of Aleutian magmas. Island Arcs, Deep Sea Trenches and Back Arc Basins. Washington, DC, American Geophysical Union.

Klein, E.M. and Langmuir, C.H. (1987). Ocean ridge basalt chemistry, axial depth, crustal thickness and temperature variations in the mantle. J. Geophys. Res. **92**: 8089-8115.

Langmuir, C.H., Bender, J.F., Bence, A.E., Hanson, G.N. and Taylor, S.R. (1977). Petrogenesis of basalts from the Famous area: mid-Atlantic ridge. Earth Plan. Sci. Lett. **36**: 133-156.

le Roex, A.P., Dick, H.J.B., Gulen, L., Reid, A.M. and Erlank, A.J. (1987). Local and regional heterogeneity in MORB from the mid-Atlantic ridge between 54.5°S and 51°S: evidence for geochemical enrichment. Geochim. Cosmochim. Acta. **51**: 541-556.

Leeman, W.P. (1987). Boron geochemistry of volcanic arc magmas: evidence for recycling of subducted oceanic lithosphere. EOS, Abstr. **68**: 462.

Leeman, W.P., Budahn, J.R., Gerlach, D.C., Smith, D.R. and Powell, D.N. (1980). Origin of Hawaiian tholeiites: Trace element constraints. Am. J. Sci. **280A**: 794-819.

Lindsley, D.H. (1983). Pyroxene thermometry. Am Min. **68**: 477-493.

Liotard, J.M., Barsczus, H.G., Dupuy, C. and Dostal, J. (1986). Geochemistry and origin of basaltic lavas from Marquesas Archipelago, French Polynesia. Contrib. Mineral. Petrol. **92**: 260-268.

Loubet, M., Shimizu, N. and Allegre, C.J. (1975). Rare earth elements in alpine peridotites. Contrib. Mineral. Petrol. **53**: 1-12.

Maaloe. (1982). Geochemical aspects of permeability controlled partial melting and fractional crystallization. Geochim. Cosmochim. Acta. **46**: 43-57.

MacDowell, F.W. (1966). Potassium-argon dating of Cordilleran intrusives. Columbia Unversity PhD.

Machado, N., Ludden, J.N., Brooks, C. and Thompson, G. (1982). Fine-scale isotopic heterogeneity in the sub-Atlantic mantle. Nature. **295**: 226-228.

Mahoney, J.J. (1987). An isotopic study of Pacific oceanic plateaus: implications for their nature and origin. Seamounts, Islands, and Atolls. Washington, DC, American Geophysical Union.

Mahoney, J.J., McDougall, J.D., Lugmair, G.W. and Gopalan, K. (1983). Kerguelen hot spot source for the Rajmahal traps and Ninetyeast Ridge. Nature. **303**: 385-389.

McKenzie, D. and Bickle, M.J. (1988). The volume and composition of melt generated by extension of the lithosphere. J. Petrol. **29**: 625-679.

Meijer, A. (1976). Pb and Sr isotopic data bearing on the origin of volcanic rocks from the Mariana island-arc system. Geol. Soc. Am. Bull. **87**: 1358-1369.

Morris, J.D. (1984). Enriched geochemical signatures in Aleutian and Indonesian arc lavas: An isotopic and trace element investigation. Massachusetts Institute of Technology, Cambridge PhD.

Morris, J.D. and Hart, S.R. (1983). Isotopic and incompatible element constraints on the genesis of island arc volcanics: Cold Bay and Amak Islands, Aleutians. Geochim. Cosmochim. Acta. **47**: 2015-2030.

Munschy, M. and Schlich, R. (1988). Structure and evolution of the Kergueln-Heard Plateau (Indian Ocean) deduced from seismic stratigraphy studies. Mar. Geol. **76**: 131-152.

Mutter, J.C. and Cande, S.C. (1983). The early opnening between Broken Ridge and Kerguelen Plateau. Earth Plan. Sci. Lett. **65**: 369-376.

Nakamura, Y. and Tatsumoto, M. (1988). Pb, Nd, and Sr isotopic evidence for a multicomponent source for rocks of Cook-Austral Islands and heterogeneities of mantle plumes. Geochim. Cosmochim. Acta. **52**: 2909-2924.

Navon, O. and Stolper, E. (1987). Geochemical consequences of melt percolation: the upper mantle as a chromatographic column. J.Geol. **95**: 285-307.

Nicholls, I.A. and Ringwood, A.E. (1973). Effect of olivine stability in tholeiites and the production of silica undersaturated magmas in the island arc environment. J.Geol. **81**: 285-300.

Nye, C.J. and Reid, M.R. (1986). Geochemistry of primary and least fractionated lavas from Okmok volcano, Central Aleutians,

implications for arc magma genesis. J. Geophys. Res. **91B**: 10271-10287.

O'Hara, M.J. (1968). The bearing of phase equilibria studies on the origin and evolution of basic and ultrabasic rocks. Earth. Sci. Rev. **4**: 69-133.

O'Hara, M.J. (1985). Importance of the 'shape' of the melting regime during partial melting of the mantle. Nature. **314**: 58-62.

Parsons, B. and Sclater, J.G. (1977). An analysis of the variation of ocean floor bathymetry and heat flow with age. J. Geophys. Res. **82**: 803-827.

Patchett, P.J. (1983). Importance of the Lu-Hf isotopic system in studies of planetary chronology and chemical evolution. Geochim. Cosmochim. Acta. **47**: 81-91.

Patchett, P.J., Kouvo, O., Hedge, C.E. and Tatsumoto, M. (1981). Evolution of continental crust and mantle heterogeneity: evidence from Hf isotopes. Contrib. Mineral. Petrol. **78**: 279-297.

Patchett, P.J. and Tatsumoto, M. (1980a). Hafnium isotope variations in oceanic basalts. Geophys. Res. Lett. **7**: 1077-1080.

Patchett, P.J. and Tatsumoto, M. (1980b). Lu-Hf total-rock isochron for the eucrite meteorites. Nature. **288**: 571-574.

Patchett, P.J. and Tatsumoto, M. (1980c). A routine high-precision method for Lu-Hf isotope geochemistry and chronology. Contrib. Mineral. Petrol. **75**: 263-267.

Patchett, P.J. and Tatsumoto, M. (1981). Lu/Hf in chondrites and definition of a chondritic hafnium growth curve. Lunar and Planetary Science. Houston, Lunar and Planetary Inst.

Patchett, P.J., White, W.M., Feldmann, H., Kielinczuk, S. and Hofmann, A.W. (1984). Hafnium/rare earth element fractionation in the sedimentary system and crustal recycling into the Earth's mantle. Earth Plan. Sci. Lett. **69**: 365-378.

Pearce, J.A. and Cann, J.R. (1973). Tectonic setting of basic volcanic rocks determined using trace element analyses. Earth Plan. Sci. Lett. **19**: 290-300.

Pearce, J.A. and Norry, M.J. (1979). Petrogenetic implications of Ti, Zr, Y and Nb variations in volcanic rocks. Contrib. Mineral. Petrol. **69**: 33-47.

Pearce, J.A., Rogers, N., Tindle, A.J. and S, W.J. (1985). Geochemistry and petrogenesis of Basalts from Deep Sea Drilling Project Leg 92, eastern Pacific. Init. Repts. DSDP. Washington, DC, U>S Govt. Printing Office.

Perfit, M.R. and Fornari, D.J. (1986). Geochemical studies of abyssal lavas recovered by DSRV Alvin from the eastern Galapagos rift, Inca transform and Ecuador rift 3. Trace element abundances. J. Geophys. Res. **88B**: 10551-10572.

Phipps Morgan, J. (1987). Melt migration beneath mid-ocean spreading enters. Geophys. Res. Lett. **14**: 1238-1241.

Presnall, D.C. and Hoover, J.D. (1987). High pressure phase equilibrium constraints on the origin of mid-ocean ridge basalts. Magmatic processes: Physiochemical principles. The Geochemical Society.

Price, R.C., Kennedy, A.K., Riggs-Sneeringer, M. and Frey, F.A. (1986). Geochemistry of basalts from the Indian Ocean triple junction: Implication for the generation and evolution of Indian Ocean ridge basalts. Earth Plan. Sci. Lett. **78**: 279-296.

Prinzhofer, A. and Allegre, C.J. (1985). Residual peridotites and the mechanism of partial melting. Earth Plan. Sci. Lett. **74**: 251-265.

Puchelt, H. and Emmermann, R. (1983). Petrogenetic implications of tholeiitic basalt glasses from the East Pacific Rise and the Galapagos spreading center. Chem. Geol. **38**: 39-56.

Rhodes, J.M., Blanchard, D.P., Dungan, M.A., Rodgers, K.V. and Brannon, J.C. (1978). Chemistry of Leg 45 basalts. Initial Reports of the Deep Sea Drilling Project. Washington, U.S. Government Printing Office.

Richardson, S.H., Erlank, A.J., Duncan, A.R. and Reid, D.L. (1982). Correlated Nd, Sr, and Pb isotopic variation in Walvis Ridge basalts and implications for the evolution of their mantle source. Earth Plan. Sci. Lett. **59**: 327-342.

Richter, F.M. and McKenzie, D. (1981). Parameterizations for the horizontally averaged temperature of infinite Prandtl number convection. J. Geophys. Res. **86**: 1738-1744.

Royer, J. and Sandwell, D.T. (1989). Evolution of the Eastern Indian Ocean since the Late Cretaceous: constraints from GEOSAT altimetry. submitted to JGR. :

Salters, V.J.M. and Hart, S.R. (1989). Hf isotopes in oceanic volcanics; the Hf Paradox. Trans. AGU. **70**: 510.

Salters, V.J.M., Hart, S.R. and Panto, G. (1988). Origin of late Cenozoic volcanic rocks from the Carpathian Arc, Hungary, Ch. 19. Pannonian Basin: a study in basin evolution. Tulsa, Oklahoma, AAPG and Hungarian Geol. Soc.

Salters, V.J.M. and Shimizu, N. (1988). World-wide occurrence of HFSE-depleted mantle. Geochim. Cosmochim. Acta. **52**: 2177-2182.

Saunders, A.D. (1985). Geochemistry of basalts from the Nauru Basin, Deep Sea Drilling Project Legs 61 and 89: implications for the origin of oceanic flood basalts. Init. Repts. DSDP. U.S. Governement Printing Office.

Scarfe, C.M. and Brearley, M. (1987). Mantle xenoliths: melting and dissolution studies under volatile free conditions. Mantle xenoliths. New York, Wiley and Sons.

Scarfe, C.M. and Takahashi, E. (1986). Melting of garnet peridotite to 13 GPa and the early history of the upper mantle. Nature. **322**: 354-356.

Scott, D.R. and Stevenson, D.J. (1989). A self-consistent model of melting, magma migration and buoyancy-driven circulation beneath mid-ocean ridges. J. Geophys. Res. **94**: 2973-2988.

Stern, C.R., Saul, S., Skewes, M.A. and Futa, K. (1989). Garnet peridotite xenoliths from the Pali-Aike alkali basalts of southernmost South America. Austr. J. Earth Sci. **in press**:

Stern, R.J. (1982). Strontium isotopes from circum-pacific intra-oceanic island arcs and marginal basins:Regional variations and implications for magma genesis in island arcs. Geol. Soc. Am. Bull. **93**: 477-486.

Stern, R.J. and Bibee, L.D. (1984). Esmeralda Bank: geochemistry of an active submarine volcano in the Mariana Island Arc. Contrib. Mineral. Petrol. **86**: 159-169.

Stille, P., Unruh, D.M. and Tatsumoto, M. (1983). Pb, Sr, Nd and Hf istopic evidence of multiple sources for Oahu, Hawaii basalts. Nature. **304**: 25-29.

Stolper, E. (1980). A phase diagram for mid-ocean ridge basalts: preliminary results and implications for petrogenesis. Contrib. Mineral. Petrol. **74**: 13-27.

Storey, M., Saunders, A.D., Tarney, J., Gibson, I.L., Norry, M.J., Thirwall, M.F., Leat, P., Thompson, R.N. and Menzies, M.A. (1989). Contamination of Indian Ocean asthenosphere by the Kerguelen-Heard mantle plume. Nature. **338**: 574-576.

Takahashi, E. and Kushiro, I. (1983). Melting of a dry peridotite at high pressures and basalt magma genesis. Am. Min. **68**: 859-879.

Taras, B.D. and Hart, S.R. (1987). Geochemical evolution of the New England seamount chain: isotopic and trace-element constraints. Chem. Geol. **64**: 35-54.

Tatsumoto, M., Unruh, D.M. and Patchett, P.J. (1981). U-Pb and Lu-Hf systematics of Antarctic meteorites. Mem. Nat. Inst. Polar. Res. Tokyo, Spec. Issue. **20**: 237-249.

Taylor, S.R. and McLennan, S.M. (1985). The continental crust: its composition and evolution. Oxford, Blackwell Scientific Publications.

Tera, F., Brown, L., Morris, J.D., Sacks, I.S., Klein, J. and Middleton, R. (1986). Sediment incorporation in island-arc magmas: Inferences from ^{10}Be. Geochim. Cosmochim. Acta. **50**: 535-550.

Thompson, R.N., Morrison, M.A., Dickin, A.P. and Hendry, G.L. (1983). Continental flood basalts...Arachnids rule OK? Continental basalts and mantle xenoliths. Cheshire, U.K., Shiva.

Vollmer, R., Ogden, P., Schilling, J., Kingsley, R.H. and Waggoner, D.G. (1984). Nd and Sr isotopes in ultrapotassic volcanic rocks from the Leucite Hills, Wyoming. Contrib. Mineral. Petrol. **87**: 359-368.

White, W.M. (1979). Geochemistry of basalts from the FAMOUS area: a reexamination. Carnegie Inst. Wash. Yearb. **78**: 325-331.

White, W.M. and Dupre, B. (1986). Sediment subduction and magma genesis in the Lesser Antilles: Isotopic and trace element constraints. J. Geophys. Res. **91B**: 5927-5941.

White, W.M. and Hofman, A.W. (1982). Sr and Nd isotope geochemistry of oceanic basalts and mantle evolution. Nature. **296**: 821-825.

White, W.M. and Patchett, P.J. (1984). Hf-Nd-Sr isotopes and incompatible element abundances in island arcs: Implications for magma origins and crust-mantle evolution. Earth Plan. Sci. Lett. **67**: 167-185.

White, W.M., Tapia, M.D.M. and Schilling, J.-. (1979). The petrology and geochemistry of the Azores Islands. Contrib. Mineral. Petrol. **69**: 201-213.

Wood, D.A. (1979). A variable veined suboceanic upper mantle-Genetic significance for mid-ocean ridge basalts from geochemical evidence. Geology. **7**: 499-503.

Wood, D.A., Tarney, J., Varet, J., Saunders, A.D., Bougault, H., Joron, J.L., Treuil, M. and Cann, J.R. (1979). Geochemistry of basalts drilled in the North Atlantic by IPOD Leg 49: Implications for mantle heterogeneity. Earth Plan. Sci. Lett. **42**: 77-97.

Wright, E. and White, W.M. (1987). The origin of Samoa: new evidence from Sr, Nd and Pb isotopes. Earth Plan. Sci. Lett. **81**: 151-162.

Zindler, A. and Hart, S.R. (1986). Chemical Geodynamics. Ann. Rev. Earth Plan. Sci. **14**: 493-571.

Zindler, A., Hart, S.R., Frey, F.A. and Jakobsson, S.P. (1979). Nd and Sr isotope ratios and rare earth element abundances in Rekjanes peninsula basalts: evidence for mantle heterogeneity beneath Iceland. Earth Plan Sci Lett. **45**: 249-262.

Zindler, A., Staudigel, H. and Batizza, R. (1984). Isotope and trace element geochemistry of young Pacific seamounts: implications for the scale of upper mantle heterogeneity. Earth Plan. Sci. Lett. **70**: 175-195.

APPENDIX A:
ANALYTICAL TECNIQUE FOR HF-ISOTOPES

Introduction

The following is the result of trial and error for a couple of years to try to improve on the Hf-separation chemistry and mass spectrometry. I experimented with and tried a large number of 'things'. The tracking of the Hf was almost always done with hot ^{181}Hf, which was made by neutron bombardment of ^{180}Hf at the MIT nuclear reactor. This is by far the best and easiest technique to detect and track Hf in both solid and solution. The half-life of ^{181}Hf is 35 days, which makes it ideal for this purpose

In general, Hf is hard to keep in solution unless HF is present in the solvent. Even in a dilute form, 0.1N HF, the dissolution of Hf-salts is easily accomplished. However, Hf in solution is strongly complexed by F-ions or groups. HF is used to dissolve the rock and thereby vast quantaties of F are introduced. In the first 2 chemistry steps, my samples are too large to assure removal of F by evaporating with perchloric or sulfuric acid. Thus as a consequence I always have HF present. However, I tried to keep the normality of HF as low as possible in all the column steps. The highest normality used in the column chemistry is 4.0N.

A.2 Hf separation chemistry.

0.5 to 1.0 gr of rock powder is weighed out into a 60ml Savilex beaker (vial #561). Some H_2O (4ml) is added, and slurried with the rock powder to reduce static charge. In a clean air flow box on a hot plate about 15-20ml of concentrated HF is added. This is allowed to sit in the open beaker for 10-12 hours at room temperature. After this time, the hot plate is turned up to 100°C. The sample is dissolved and dried down at this temperature, which takes about 36 hours. During dissolution the beaker is kept open. The dried, mostly white material is allowed to cool to room temperature. Then 2ml of 4N HF is added and allowed to sit for at least 2 hours. The 2ml of HF plus all the residue is poured into a centrifuge tube. The centrifuge tube is ultrasoned for 30 minutes, centrifuged and the solute is poured in a second centrifuge tube. To the residue 1ml of 4N HF is

added, ultrasoned for at least 30 minutes, centrifuged and poured of (decanted) in the solute tube. This is done till 6 ml of solute are collected. The last ml of 4N HF which is added to the residue is allowed to sit for at least 12 hrs after which it is ultrasoned (30 min) and centrifuged. Not all the Hf will come in solution when the temperature of the hot plate was higher than 100°C during the dry down stage.

The total 6ml of solute is centrifuged again and loaded on 6ml, 1 cm diameter, Dowex1-X8 (200-400 mesh) anion exchange column. The separation on this column is essentially a batch process. The sample is rinsed on the column with another 3ml of 4N HF. The matrix of the sample is removed by elution with 250ml of 4N HF. The column should have a reservoir of at least 250 ml for ease of use. The reservoir is made of a 250ml Teflon FEP separatory funnel with plug and tap removed. The funnel is connected to the column (a 12ml liquid transfer pipet (polypropylene)with frit) by shrinkable teflon tubing. After the 250 ml 4.0N HF are drained (about 8hrs) 30 ml of 1.0N HF/1.0N HCl is added and drained. Then, 55ml of 1.0N HF/1.0N HCl is added and collected in a 60 ml Savillex beaker. The column is cleaned by 50ml of concentrated HF (28N), 20ml of H_2O, 100ml of 8N HNO_3, 10ml of H_2O and conditioned with $3x25$ml of 4N HF. The eluted sample is dried down at 100°C in a clean air flow box, 1ml of 4N HF is added and dried down again. The sample is cooled to room temperature after which 0.3ml of 4N HF are added and the sample is allowed to sit overnight to dissolve. The dissolution of the sample is almost always completes. If not, another 0.5ml of 4N HF is added, the sample is dried down again, and again dissolved in 0.3ml 4N HF at room temperature. After this column the sample consists essentially out of Ti, Zr and Hf, some impurities, Fe and Ca in small quantities, are left.

The second column is 19cm long and 0.5cm in diameter, and is used in part as a purification column and in part as a separation column. The sample is purified from what was left in the.batch process in the first column step plus Hf and Zr are partly separated from Ti. The column material is Dowex1-X8 (200-400 mesh) anion resin. The sample is loaded in 0.3ml 4N HF and rinsed 3 times with

0.2ml of 4N HF. First 20ml of 4N HF is washed through after which 20ml of 1.0N HF/1.0N HCl is washed trough. The sample, now mostly Hf, Zr and some Ti, is eluted and collected with 10ml of 1.0N HF/1.0N HCl, and dried down on a hot plate at 100°C. The column is cleaned with 6ml of concentrated HF, 3ml of H_2O, 12ml of 8N HNO_3, and 4ml of H_2O, after which it is backwashed with 8ml with 4N HF, and rinsed once with 4ml of 4N HF.

The third column's dimensions are 12cm long and 0.5cm in diameter. The colomn has a long stem ensuring a pressure head of at least 20cm. The pressure is kept relatively constant by a reservoir at the top of the column. A hole, approximately 1cm above the resin level, is used to drain the excess acid out of the pressure head. The column material is HDEHP (Di(2-ethylhexyl) orthophosphoric acid) adhered to teflon beads. A better description of this material can be found in A. Zindlers thesis (Zindler, 1980). The column is packed to a flow rate of 10ml of H_2O per hour with a filled pressure head. The dried sample from column 2 is dissolved in 0.3 ml of 6.2N HCl/0.14N HF. If the sample does not dissolve completely, it is dried down with 4N HF, slowly, and again dissolved with 0.3 ml of 6.2N HCl/0.14N HF. Ultrasoning can sometimes help. After the sample is loaded on the column it is rinsed 3 times with 0.2 ml 6.2NHCl/0.14N HF and 40 ml of 6.2NHCl/0.14N HF is loaded. The sample is eluted till just before the Hf comes off, in my case after 3.5 to 4 hours. The exccess acid is drained through the hole above the resin and the hole is closed by wrapping teflon tape around the column. Hf is collected in 60 minutes using 2.5N HCl/0.3N HF as elutant. The column is cleaned with 10ml of concentrated HF and 2 times 10ml of 6.2N HCl. The exact HF normality is not important here. The normality of the HF should be tuned in such a way that it takes at least 3 hrs before the Hf begins to come off the column. The behavior of Hf on this column is very sensitive to the flowrate, and the particular batch of column material. However, Zr and Ti, the only two other elements loaded, are equally sensitive, so it is just a matter of careful calibration. The calibration stays the same for a long time, and is robust. After collection the sample is dried down at 100°C.

The 3rd column of the column procedure described here is partly adapted from Fujimaki et al. (1984). The technique described by Patchett and Tatsumoto (1980) (P&T from now on) has been tried but was found to result in erratic yields. The principal difference between this technique and the P&T technique is that the complexing of Hf with fluoride is accepted and used in the separation, instead of being avoided as in the other technique. The third column of the P&T method requires complete removal of all the fluoride present in the separate. Since Hf strongly complexes with F, this is very hard achieve, and sometimes fails. If a trace of F is loaded on the third P&T column the distribution coefficient for Hf is 0 and Hf will be removed from the column in the first 2ml instead of after 15ml, which reduces the yield of thiscolumn to zero. Every chemistry step in my new technique uses HF. This ensures that Hf is continously in solution and that Hf is not left as a residue in some beaker or vial. The first and second column separate Zr, Hf and Ti from the rest of the sample (Faix et al., 1981). Also on the second column,the Zr-Hf fraction is cleaned up and partially separated from Ti (Nelson et al., 1960). The third column was partly described by Fujimaki et al. (1984). The disadvantage of this new procedure is the fact that Ti is not completely separated from Hf. Ti will evaporate before Hf in the mass spectrometer, but this is a time-intensive way to separate Ti. Separation of Hf and Zr as a mandelic acid complex (Belcher et al., 1954; Kumins, 1947), directly from the dissolved rock was tried, but proven unsuccesful. If the rock is dissolved in HF, traces of F will inhibit the formation of the mandelic acid complex. If the rock is fluxed and dissolved in HCl, too much HCl is needed to dissolve the sample and consequently the concentration Hf is too low for quantative removal. Fluoride complexes of Hf are in fact too strong to be able to break in a quantitative and reproducible manner in a rock matrix. This new technique was developed under the principle 'if you can not beat them, join them".

Each column is cleaned with HF after use, as I suspect this is necessary in order to dissolve any of the Hf that may have precipitated. The HF cleaning is done as a first cleaning step. Very high blank levels are measured if this HF cleaning is omitted. The

total procedural blank is measured between 0.5 and 1 ngr, which is still somewhat on the high side; this may be caused in part by low yields on the blank chemistries. The reagant blanks add up to ≈300pgr, and based on the experience with the radioactive Hf, less than 10^{-6} of the loaded sample Hf is present after the first stage of cleaning.

A.3 Hf mass spectrometry

Hf is run on double Re filaments using zone refined Re 0.0012 inches thick and 0.030 inches wide. The length of the ionization filament has to be at least 1.5 cm to avoid burn-out of the filament before the Hf ion beam deteriorates. The loading procedures is as follows:

- Hf is dissolved in a tiny drop of 0.15N HF.
- 2 thin stripes of polyethelyene are melted onto the filament about 2mm apart,
- a droplet of 0.5N HNO_3 is dried down,
- the Hf sample is loaded in the 0.15N HF solution,
- before the Hf-solution dries down, a drop of 0.25-0.3N H_3PO_4 is added, dried after that another couple of drops of H_3PO_4 are added,
- a drop (≈1μl)of colloidal B-metal in H_2O is added. Boron metal is obtained as >99.5% pure B, <0.28μm in size, form Cerac, inc. (407 North 13th Street, Milwaukee, Wisconsin, 53233). Approximately 15mgr of B-metal is slurried in ≈1ml of H_2O.
- the sample is dried down slowly, i.e. 5.minutes at 1.7A, 5. minutes at 2.0A, and 5 minutes at 2.3A. After which the current is turned up slowly till the filament is glowing red. The temperature of the filament is not increased when fumes are visible from the filaments. The sample is dried till the filament is red glowing (3-3.5A) and no fumes are released. In order to avoid burning of the filament during loading the dry down can be done in a N_2 atmosphere.

The sample is run with a typical ^{180}Hf signal of at least 1.5x 10^{-11}A and most times around 2.5-3.0x 10^{-11}A ^{187}Re. A precision of better

than 0.015% for $^{176}Hf/^{177}Hf$ is normally achieved by collecting 100 to 150 ratios. Sample is brought to running temperature slowly, over the course of 1 hour in order to achieve stable signals. ^{187}Re current is typically between $1\text{-}3x10^{-10}A$ during the run A first group of samples was analyzed at MIT using TIMER, a 12" NBS type machine, which has been refurbished with Cary 401 VRE and Hewlett Packard multimeter and computer. The rest of the samples were run at UC Santa Barbara (in G. Tiltons lab) using a multicollector (5) Finnigan-MAT 260. Both machines are able to keep the low pressure vacuum in the source of the mass spectrometer by use of a cold finger. The temperature of the ionization filament is so high ($\approx 2300^{o}C$) that the source will overheat without the cold finger. Filament currents during a run are typically $\approx 5.8A$ for the ionization and 4.8-5.2A for the evaporation filament.

Attempts were made to run Hf while the Hf was complexed on the filament as a chloride, fluoride, nitrate, phosphate, carbide and nitride. The different filament materials which were experimented with were non-zone refined Re, Ta, W, Re/W alloy, Pt, carburized Re and carburized W. Zone-refined Re resulted in the best running characteristics. Non-zone refined Re is equally good except it contain traces of W, causing ^{180}W isobaric interferences. Hf runs this well with the boron present, apparently because Hf and B combine to form Hf-boride. This boride is refractory enough to evaporate slowly at the high temperatures, and it achieves the most stable emission of Hf-ions. Hf is too refractory as a carbide, and as a consequence the filament will burn out before the Hf is evaporated. Carburized Re as an ionizing filament was tried, but the Re-C filament material is very brittle, and many filaments break on the way from the carburizer to the mass spectrometer.

Table A1 reports all Hf isotope analyses obtained during this study. Betwee. 50 and 200 ratios were collected for each sample. the first group of samples was analyzed at MIT. During the period of a year, the Hf-standard was measured at MIT and the average is given in the table. The three groups of data collected at Santa Barbara warrent different corrections (dependent on the measured value of the JMC 475 standard) since each group of data was obtained in such

a short time interval (within two weeks). Standard values for Nd also changed for the three time periods in a similar way. Replicates on a number of samples (see table A.2) suggest that the in-run statistics give a reasonable estimate of precision. The average reproducibilty of the 6 replicates was 0.021%.

The part of the analytical technique that can be most improved is the mass spectrometry in that increase in the ionization efficiency will improve the precision. In my chemistry samples, if samples fail, it is because of Ti-impurities in the sample. A somewhat better separation from Ti would eliminate that and will increase the success rate.

Table A1
Hf isotope ratios as measured

1st Group, analyzed at MIT between March-Nov. 1987

Sample #	176Hf/177Hf	2 sigma	corrected
NTP 8	0.282272	0.0175	0.282364
NTP 8	0.282322	0.0098	0.282414
17460	0.282398	0.0159	0.282490
17434	0.28226	0.0131	0.282352
17403	0.282386	0.0189	0.282478
HM1-4	0.282287	0.0073	0.282379
17651	0.282307	0.0155	0.282399
W253	0.283052	0.0389	0.283144
W 253	0.282985	0.0101	0.283077
GS 104 20-21	0.283137	0.0131	0.283229
GS 104 25-2	0.283196	0.0261	0.283288
164-1	0.283191	0.031	0.283283
69-851	0.283199	0.027	0.283291
JMC 475	0.282108	Average of 15 runs	

2nd Group analyzed Dec 1987 in S. Barbara

Sample #	176Hf/177Hf	2 sigma	corrected
4- 2	0.283047	0.007	0.283082
W 253	0.283046	0.0078	0.283081
68-66	0.283152	0.0177	0.283187
69-851	0.283241	0.0118	0.283276
71-372	0.283261	0.0145	0.283296
W 10	0.283159	0.0109	0.283194
77-211	0.282756	0.0066	0.282791
80-135	0.282739	0.0122	0.282774
81-18	0.282833	0.0101	0.282868
81-19	0.282927	0.009	0.282962
133/1A	0.283235	0.0092	0.283270
JMC 475	0.282122	0.0079	
JMC 475	0.282209	0.0135	
JMC 475	0.282152	0.0089	
JMC 475	0.282217	0.0185	
JMC 475	0.282127	0.0075	
Average	0.282165		

Table A1 continued
Hf isotope ratios as measured
3rd Group Nov 1988 S. Barbara

Sample #	176Hf/177Hf	2 sigma
525A-57-1,119-124	0.282744	0.0239
525A-63-2,63-68	0.282744	0.0149
133/1A	0.283333	0.0119
164-1	0.283326	0.0249
GS 104 25-1	0.28313	0.0192
4-1.	0.282918	0.0231
71-374	0.283116	0.011
80-71	0.282719	0.0201
747C-12R-4,45-47	0.282722	0.0246
747C-16R-2,85-87	0.2826	0.0142
748C-79R-7-65-67	0.282659	0.0076
WA-2	0.283116	0.0103
WA-4	0.283089	0.0194
JMC 475	0.282205	0.0111
JMC 475	0.282171	0.0061
JMC 475	0.282192	0.0087
JMC 475	0.282219	0.0096
JMC 475	0.282177	0.0082
Average	0.282193	

4th Group of samples March-April 1989 S. Barbara

Sample #	176Hf/177Hf	2 sigma	corrected
749C-12R-4,144-148	0.282854	0.0239	0.282883
749C-15R-5,127-130	0.28298	0.0242	0.283009
747C-12R-4,41-43	0.282696	0.0137	0.282725
69-829	0.283009	0.0165	0.283038
525A-57-1,119-124	0.282744	0.0083	0.282773
WA45	0.283169	0.0362	0.283198
525A-63-2,63-68	0.282611	0.0081	0.282640
527-41-4,10-15	0.282849	0.0248	0.282878
528-42-1,40-45	0.282863	0.0111	0.282892
528-42-2,145-150	0.283085	0.042	0.283114
JMC 475	0.282166	0.009	
JMC 475	0.282162	0.0063	
JMC 475	0.282167	0.0088	
JMC 475	0.282184	0.0053	
JMC 475	0.282174	0.0078	
Average	0.282171		

2 sigmas are given in %

Table A2
Duplicates for Hf isotopes

Sample	176Hf/177Hf	2 sigma	where? when?
NTP-8	0.28236	0.0175	MIT 87
NTP-8	0.28241	0.0098	MIT 87
W253	0.28314	0.0389	MIT 87
W253	0.28308	0.0101	MIT 87
W253	0.28308	0.0078	SB 88
164-1	0.28328	0.031	MIT 87
164-1	0.28333	0.0249	SB 88
133/1A	0.28327	0.0092	SB 87
133/1A	0.28333	0.0119	SB 88
525A-57-1,119-124	0.28274	0.0239	SB 88
525A-57-1,119-124	0.28277	0.0083	SB 89
525A-63-2,63-68	0.28274	0.0149	SB 88
525A-63-2,63-68	0.28264	0.0081	SB 89

A.4 References.

Belcher, R., Sykes, A. and Tatlow, J.C. (1954). Mandelic acid and halogen-substituted mandelic acids as reagents for the determination of zirconium. Anal. Chim. Acta. **10**: 34-47.

Faix, W.G., Caletka, R. and Krivan, V. (1981). Element distribution coefficients for hydrofluoric acid/nitric acid solutions and the anion exchange resin Dowex 1-X8. Anal. Chem. **53**: 1719-1721.

Fujimaki, H., Tatsumoto, M. and Aoki, K. (1984). Partition coefficients of Hf, Zr and REE between phenocrysts and groundmasses. J. Geophys.Res. **89**: 662-672.

Kumins, C.A. (1947). Zirconium determination in the presence of interfering elements. Anal. Chem. **19**: 376-377.

Nelson, F., Rush, R.M. and Kraus, K.U. (1960). Anion-exchange studies. XXVII. Adsorbability of a number of elements in HCl-HF solutions. :

Patchett, P.J. and Tatsumoto, M. (1980). A routine high-precision method for Lu-Hf isotope geochemistry and chronology. Contrib. Mineral. Petrol. **75**: 263-267.

Zindler, A. (1980). Geochemical processes in the earth's mantle and the nature of crust-mantle interactions: Evidence from studies of Nd and Sr isotope ratios in mantle derived igneous rocks and lherzolite nodules. Massachusetts Institute of Technology, Cambridge, Massachusetts PhD.